

**Titre:** Characterization of Hydrodynamics and Solids Mixing in Fluidized  
Title: Beds Involving Biomass

**Auteur:** Farzam Fotovat  
Author:

**Date:** 2013

**Type:** Mémoire ou thèse / Dissertation or Thesis

**Référence:** Fotovat, F. (2013). Characterization of Hydrodynamics and Solids Mixing in  
Citation: Fluidized Beds Involving Biomass [Thèse de doctorat, École Polytechnique de  
Montréal]. PolyPublie. <https://publications.polymtl.ca/1295/>

 **Document en libre accès dans PolyPublie**  
Open Access document in PolyPublie

**URL de PolyPublie:** <https://publications.polymtl.ca/1295/>  
PolyPublie URL:

**Directeurs de  
recherche:** Jamal Chaouki, & Jeffrey M. Bergthorson  
Advisors:

**Programme:** Génie chimique  
Program:

UNIVERSITÉ DE MONTRÉAL

CHARACTERIZATION OF HYDRODYNAMICS AND SOLIDS MIXING  
IN FLUIDIZED BEDS INVOLVING BIOMASS

FARZAM FOTOVAT

DÉPARTEMENT DE GÉNIE CHIMIQUE  
ÉCOLE POLYTECHNIQUE DE MONTRÉAL

THÈSE PRÉSENTÉE EN VUE DE L'OBTENTION

DU DIPLÔME DE PHILOSOPHIAE DOCTOR

(GÉNIE CHIMIQUE)

DÉCEMBRE 2013

UNIVERSITÉ DE MONTRÉAL

ÉCOLE POLYTECHNIQUE DE MONTRÉAL

Cette thèse intitulée:

CHARACTERIZATION OF HYDRODYNAMICS AND SOLIDS MIXING  
IN FLUIDIZED BEDS INVOLVING BIOMASS

présentée par: FOTOVAT Farzam

en vue de l'obtention du diplôme de : Philosophiae Doctor

a été dûment acceptée par le jury d'examen constitué de :

M. LEGROS Robert, Ph.D., président

M. CHAOUKI Jamal, Ph.D., membre et directeur de recherche

M. BERGTHORSON Jeffrey M., Ph.D., membre et codirecteur de recherche

M. TAVARES Jason-Robert, Ph.D., membre

M. MACCHI Arturo, Ph.D., membre

*In the name of GOD the beneficent, the merciful*

**DEDICATION**

*Dedicated to*

***My Beloved Parents***

## ACKNOWLEDGEMENT

First and foremost, I wish to express my gratitude to my advisor Professor J. Chaouki for his solid support and the freedom he gave me to conduct research during my PhD. He continually and convincingly conveyed a spirit of adventure in regard to research.

I greatly appreciate all precious comments and efforts made by Professor J. Bergthorson for the improvement of the quality of the papers. I acknowledge the expert guidance provided by Dr. D. Bai which was very helpful to tackle the technical problems with regard to the waste separation project.

I would like to show my gratitude to my committee members, Professor A. Macchi, Professor R. Legros, Professor J. Tavares and Professor L. Saydy whose guidance and comments are greatly valuable.

I am so thankful to Dr. A. Abbasi for his knowledge and efforts to conduct the numerical simulation of biomass fluidization. I would like to thank Dr. P. Sauriol, Dr. M. Latifi, Dr. B. Esmaeili, Dr. J-P. Laviolette and Dr. R. Jafari for their expert help with some aspects of this study. I am also grateful for assistance of Mr. G. Baptiste and Ms. L. Griffon who helped me during their internships with a few series of elutriation and fluidization experiments.

I thank all staff of the Chemical Engineering department, particularly Mr. R. Delisle, Mr. J. Huard, Mr. S. Simard Fluery, Mr. G. Robin, Ms. M. Lamarche and Mr. G. Lessard for their technical assistantship. My especial thank goes to Mr. Y. Belkhir for building the new fluidization column and his availability to do ad hoc unenviable jobs.

I am deeply grateful to Mr. J. Shabanian, whose friendly attitude and effective collaboration in making the optical probes and conducting the primary RPT experiments was really valuable.

I would like to appreciate the kindness of Ms. S. Benzennou, who proofread the Résumé of this thesis. I am very thankful for the cooperative manner of all my colleagues in our research group, particularly, the friendly supports lent by Mr. O. Ebrahimpour and Mr. M. Aghabarannejad.

I deeply thank unforgettable kindness of Dr. R. Rezavani and Ms. S. Lotfi, who sincerely supported me to settle down in Montréal. I am so grateful to Mr. M. Kheiri, who generously

accommodated me for about one month after my arrival in Montréal and was a close and true friend of mine during these years.

I genuinely express my profound gratefulness to my lovely brother, Farshad, as I owe my success in my lifetime to his heartfelt sympathy and supports.

Finally, from the very bottommost part of my heart; I would like to express my eternal gratitude towards my devoted parents for their everlasting unconditional love and support, for their spiritual encouragement and for keeping hope alive in every single day of my life; however, it will never be a right word to reflect my feeling of appreciation about their self-sacrifice and altruism.

## RÉSUMÉ

L'intérêt croissant pour l'utilisation de la biomasse comme source renouvelable d'énergie propre a entraîné l'application vaste d'unités de traitement thermique de la biomasse à travers le monde. Ces unités, qui sont principalement basées sur la fluidisation gaz-solide, souffrent de certains obstacles hydrodynamiques tels que la ségrégation du lit. En outre, les aspects d'écoulement multiphasiques complexes de ces unités ont toujours demeuré largement inconnus. Par conséquent, la réalisation d'une recherche approfondie sur ce domaine est cruciale pour le design et l'optimisation du fonctionnement des unités de biomasse à lit fluidisé. Cette thèse se concentre donc sur la caractérisation de l'hydrodynamique et les phénomènes de mélange dans les lits fluidisés contenant des mélanges de sable et de particules irrégulières de biomasse.

Le premier objectif de cette étude est de comprendre l'effet des grosses particules de biomasse sur les caractéristiques des bulles et le type de distribution de gaz dans les lits fluidisés de sable. Cela est essentiel pour atteindre le deuxième objectif qui est la caractérisation de mélange/ségrégation de la biomasse et des particules de sable dans les conditions de fluidisation. Explorer les paramètres régissant le mélange/ségrégation est utile pour ajuster les conditions d'exploitation afin d'améliorer ce phénomène bénéfique pour le système. En conséquence, la ségrégation est exploitée dans le dernier chapitre de cette thèse afin de séparer les composants combustibles des déchets solides municipaux par un processus par étapes.

Une variété de techniques expérimentales est utilisée pour étudier le comportement des deux phases constituant un lit fluidisé, soit phase diluée (bulle) et dense (émulsion). L'exploration des vitesses de fluidisation pour les mélanges de sable et de biomasse dévoile que l'apparition des bulles dans ce système se produit à une vitesse de gaz plus élevée par rapport à la vitesse de fluidisation initiale de fluidisation ( $U_{if}$ ). La vitesse initiale de bullage ( $U_{ib}$ ), la vitesse de fluidisation finale ( $U_{ff}$ ), et la vitesse du gaz de transition du régime de bullage au régime turbulent ( $U_c$ ) augmentent avec l'augmentation de la fraction de la biomasse dans le mélange. Les fluctuations locales des signaux de pression et de porosité sont mesurées dans des positions différentes du lit à l'aide de capteurs de pression absolue et différentielle et des sondes à fibre optique. L'analyse statistique du signal de pression au dessus du lit révèle que l'augmentation de la charge de la biomasse empêche l'évolution des bulles à faible vitesse de gaz ( $U < 0,6$  m/s),

tandis qu'à des vitesses élevées, la tendance de propagation de lits contenant différentes fractions de la biomasse est comparable. L'ajout de particules de biomasse à un lit de sable conduit à augmenter la porosité moyenne du lit, mais le degré de vide de chaque phase reste inchangé. On observe que les grandes particules de biomasse déclenchent l'éclatement de bulles, ce qui mène à l'augmentation de la fréquence de bullage. La fraction de bulles au centre du lit augmente avec la charge de biomasse. Cependant, en ajoutant 2% en masse de la biomasse au sable pur, cette fraction diminue à la paroi puis augmente à l'addition de biomasse supplémentaire.

La technique de suivi des particules radioactives (RPT) est mise en œuvre dans la deuxième partie de ce travail pour étudier le mouvement et la distribution des particules de biomasse à  $U=0,36$  m/s et  $U=0,64$  m/s. À cet égard, une particule active de biomasse est suivie pour une longue période de temps et sa position instantanée est enregistrée. Les données acquises sont ensuite traitées pour obtenir le profil de concentration moyenne temporelle des particules de biomasse. Ce profil représente la ségrégation des particules de biomasse qui ont tendance à s'accumuler dans les niveaux supérieurs du lit. Les variations de la fraction de la biomasse avec la vitesse de la fluidisation sont déduites des changements locaux des valeurs de perte de charge moyenne temporelle au dessus du lit. Pour déterminer les paramètres affectant le mouvement et la ségrégation des particules de biomasse, le mouvement circulaire de la biomasse est également examiné en utilisant les données RPT. A  $U=0,36$  m/s, La circulation de la biomasse est empêchée lorsque la charge de biomasse monte, ce qui entraîne une ségrégation plus prononcée du sable et de la biomasse. Une tendance inverse est observée à  $U=0,64$  m/s, lorsque la charge de la biomasse augmente de 2% à 16% en masse. C'est à dire, plus de particules de biomasse peuvent compléter leur circulation tout en coulant dans les parties les plus profondes du lit. Cela provoque une répartition plus uniforme de particules le long du lit et amène un plus haut degré de mélangeage. Ces phénomènes pourraient être directement liés à l'activité de bullage du lit qui est influencée par la vitesse du gaz et de la composition du lit, comme indiqué dans la première partie de cette étude. Sur la base des résultats RPT, la vitesse d'augmentation moyenne de la biomasse est de 0,2 fois la vitesse de bulle, indépendamment de la charge de biomasse ou de la vitesse de fluidisation. Un modèle unidimensionnel est proposé afin de prévoir la fraction volumique de la biomasse le long du lit. Certains des termes de ce modèle sont liés au comportement de fluidisation des particules de biomasse, déduits par RPT. Les résultats de ce modèle pourraient prédire avec succès les valeurs expérimentales correspondantes.

La fluidisation du sable et des particules de biomasse cylindriques est aussi simulé à l'aide du logiciel BARRACUDA CPFD, qui est basé sur la méthode Lagrange-Eulérienne. Les résultats des simulations et des expériences sont comparés dans le but d'évaluer la capacité de l'approche numérique pour prédire les caractéristiques de propagation du mélange sable-biomasse pour les systèmes différents en termes de composition et de vitesse de fluidisation. L'approche numérique choisie pourrait prédire avec succès la mesure de l'expansion du lit pour chaque espèce (sable ou biomasse). En outre, les propriétés statistiques de la distribution de la taille et la vitesse des bulles –telles que la moyenne, l'écart-type et l'asymétrie –obtenues à partir de la simulation sont comparables avec les valeurs expérimentales correspondantes.

La dernière partie de cette thèse est consacrée à la séparation des principaux composants des déchets encombrants déchiquetés. Le motif derrière cela est la nécessité du contrôle de la composition des combustibles dérivés de déchets solides pour promouvoir l'efficacité de la combustion et de réduire le niveau des émissions qui en résultent. À cet effet, les écoulements presque purs des éléments combustibles dérivés des déchets solides sont exigés de fabriquer un combustible souhaitable.

À cet égard, un processus par étapes est développé sur la base des phénomènes d'élutriation et de ségrégation. Après élimination des espèces légères et entrelacées de déchets déchiquetés par élutriation, les matériaux non élutriés sont en outre séparés dans deux colonnes successives de fluidisation. Polypropylène et perles de verre sont introduits comme les médias de fluidification dans ces colonnes afin de rendre la ségrégation des composants cible et non-cibles possibles. Par conséquent, les matériaux combustibles indésirables et les particules de plastique dur sont séparés comme le trop-plein de la première et la deuxième étape de fluidification. Une deuxième colonne d'élutriation est également conçue pour séparer la fibre et le plastique mou. Les pourcentages de recouvrement et la pureté des étapes constituant le processus global sont respectivement de 95% et 47% dans les conditions de fonctionnement optimales. Pour déterminer ces conditions, plusieurs paramètres d'influence tels que la vitesse d'élutriation, la durée de l'élutriation, la taille et la densité des médias de fluidisation et de la configuration initiale du déchet et les matières du lit sont explorés. La cinétique de ségrégation est également dérivée pour les deux étapes de fluidification.

## ABSTRACT

Growing interest in the use of biomass materials as a clean and renewable source of energy has resulted in the widespread application of thermal biomass processing units across the world. These units, which are mainly based on gas-solid fluidization, suffer from some hydrodynamic hurdles, such as the segregation of bed inventory. In addition, the complex multiphase flow aspects of these units have still remained largely unknown. Hence, conducting comprehensive research in this field is crucial for the optimal design and operation of fluidized bed biomass units. This thesis, therefore, focuses on the characterization of hydrodynamics and mixing phenomena in fluidized beds containing mixtures of sand and irregular biomass particles.

In the first two chapters of this thesis the principal aspects of the hydrodynamic phenomena in fluidized beds involving biomass are briefly discussed and the most significant relevant findings are reviewed. The first objective of this study is understanding the effect of the large biomass particles on the bubbling characteristics and gas distribution pattern of sand fluidized beds. In this regard, the third chapter of this thesis is devoted to studying the local and global pattern of gas distribution between the dilute (bubble) and dense (emulsion) phases of a fluidized bed composed of sand and different weight fractions of biomass (2–16%). This is essential for achieving the second objective, which is the characterization of mixing/segregation of biomass and sand particles under fluidization conditions. It is the subject of the fourth chapter of the present thesis in which the axial distribution of large biomass particles in a sand-biomass fluidized bed is discussed. In view of the growing importance of the numerical simulations in optimal design and operation of biomass fluidized bed units, the fifth chapter of this thesis focuses on the experimental validation of a Lagrangian-Eulerian numerical approach simulating fluidization of both sand and biomass particles. Exploring the parameters governing mixing/segregation is helpful to adjust the operating conditions to enhance either phenomenon that is beneficial. Accordingly, segregation is exploited in the sixth chapter of this thesis to separate the main combustible components of the shredded bulky waste through a step-wise process.

A variety of experimental techniques are employed to study the behavior of two constituting phases of a fluidized bed, i.e., dilute (bubble) and dense (emulsion) phases. Exploring the characteristic fluidization velocities of sand-biomass mixtures unveils that the onset of bubbling

in these systems occurs at a higher gas velocity compared to that of the initial fluidization velocity ( $U_{if}$ ). The initial bubbling velocity ( $U_{ib}$ ), the final fluidization velocity ( $U_{ff}$ ), and the transition gas velocity from bubbling to turbulent regime ( $U_c$ ) rise by increasing the fraction of biomass in the mixture. The local fluctuations of the pressure and voidage signals are measured in different positions of the bed using absolute and differential pressure transducers and optical fiber probes. Statistical analysis of the pressure signal at top of the bed reveals that increasing the biomass load hinders the evolution of bubbles at a low gas velocity ( $U < 0.6$  m/s), while at high velocities, the bubbling trend of beds containing different fractions of biomass is comparable. The addition of biomass particles to a bed of sand leads to an increase in the mean voidage of the bed; however, the voidage of each phase remains unaffected. It is observed that large biomass particles trigger a break-up of the bubbles, which results in boosting bubbling frequency. The fraction of bubbles at the center of the bed increases with the load of biomass. At the wall region, however, it starts to decrease by adding 2% wt. biomass to pure sand and then increases with the further addition of biomass.

The Radioactive Particle Tracking (RPT) technique is implemented in the second section of this work to study the motion and distribution of biomass particles at  $U=0.36$  m/s and  $U=0.64$  m/s. In this regard, an active biomass particle is tracked for a long period of time and its instantaneous position is recorded. The acquired data is then processed to achieve the time-averaged concentration profile of biomass particles. This profile represents the segregation of biomass particles, which tend to accumulate in the upper levels of the bed. Changes in the fraction of biomass with increasing gas velocity are inferred from the local changes of the time-averaged pressure drop values at the top of the bed. To determine the parameters affecting the movement and segregation of biomass particles, their circulatory motion is also scrutinized using the RPT data. The circulation of biomass is impeded when the load of biomass rises at  $U=0.36$  m/s, resulting in a more pronounced segregation of sand and biomass. The opposite trend is observed at  $U=0.64$  m/s, i.e., when the biomass load increases from 2% to 16% wt., more biomass particles can successfully complete their circulation while sinking to the deeper parts of the bed. This prompts a more uniform distribution of particles along the bed and brings about a higher degree of mixing. These phenomena could be directly related to the bed bubbling activity which is influenced by the gas velocity and the composition of the bed inventory as noted in the first part of this study. Based on the RPT results, the average rise velocity of biomass is 0.2 times the

bubble velocity, regardless of the biomass load or fluidization velocity. A one-dimensional model is proposed to predict the volume fraction of biomass along the bed. Some of the terms of this model are linked to the fluidizing behavior of biomass particles as deduced from the RPT findings. The model's results could successfully predict the corresponding experimental values.

The fluidization of sand and cylindrical biomass particles is also simulated using the BARRACUDA CPFD software, which is based on the Lagrangian-Eulerian approach. Simulation and experimental results are compared in order to evaluate the capability of the numerical approach to predict the bubbling characteristics of the sand-biomass mixture for systems differing in composition and fluidization velocity. The chosen numerical approach could successfully predict the extent of bed expansion for each species (sand or biomass particles). Moreover, the statistical properties of the distribution of both bubble size and velocity such as mean, standard deviation and skewness, obtained from the simulation are fairly comparable with the corresponding experimental values.

The last part of this thesis is devoted to the separation of the main components of the shredded bulky waste. The motive behind this is the necessity of controlling the composition of the solid waste-based Engineered Fuel (EF) to promote combustion efficiency and lower the level of the resulting emissions. For this purpose, nearly pure streams of the combustible components derived from the municipal solid waste (MSW) are required to make a tailored EF. Therefore, a step-wise process has been developed based on the elutriation and density segregation techniques. After removal of the light and interwoven species of the shredded waste by elutriation, the non-elutriated materials are further separated into two successive fluidization columns. Polypropylene and glass beads are introduced as the fluidization media in these columns in order to make density segregation of the target and not-target components possible. Hence, undesirable combustible matters and hard plastic are separated as the overflow of the first and second fluidization steps. A second elutriation column is also devised to separate and recover fiber and soft plastic. The recovery and purity percentages of the steps of the overall process are respectively over 95% and 47% under optimal operating conditions. To determine these conditions, several influential parameters, such as the elutriation velocity and time, the size and density of the fluidization media, and the initial configuration of the feedstock and bed material, are explored. The kinetics of segregation is also derived for both fluidization steps.

## TABLE OF CONTENTS

DEDICATION .....	III
ACKNOWLEDGEMENT .....	IV
RÉSUMÉ.....	VI
ABSTRACT .....	IX
TABLE OF CONTENTS .....	XII
LIST OF TABLES .....	XV
LIST OF FIGURES.....	XVII
NOMENCLATURE.....	XXI
LIST OF ABBREVIATIONS .....	XXVII
CHAPTER 1 INTRODUCTION.....	1
CHAPTER 2 LITERATURE REVIEW .....	8
2.1 Thermal processing of biomass.....	8
2.2 Multiphase flow aspects of biomass fluidization .....	11
2.2.1 Characteristic fluidization velocities.....	11
2.2.2 Gas distribution and bubble characteristics.....	14
2.3 Mixing and segregation phenomena .....	16
2.3.1 Mixing and segregation in binary mixtures.....	16
2.3.2 Mixing and segregation in systems containing biomass .....	22
2.4 Numerical modeling of gas-solid fluidized beds.....	25
2.4.1 Eulerian-Eulerian approach.....	27
2.4.2 Eulerian-Lagrangian approach .....	30
2.4.3 Numerical modeling of biomass fluidization .....	34

CHAPTER 3	ARTICLE 1: THE EFFECT OF BIOMASS PARTICLES ON THE GAS DISTRIBUTION AND DILUTE PHASE CHARACTERISTICS OF SAND-BIOMASS MIXTURES FLUIDIZED IN THE BUBBLING REGIME.....	37
3.1	Introduction.....	39
3.2	Experimental.....	41
3.3	Results and discussion.....	45
3.3.1	Characteristic fluidization velocities.....	45
3.3.2	Gas distribution pattern and bubble characterization.....	47
3.3.3	Visual bed expansion and mixing/segregation patterns.....	57
3.4	Conclusion.....	60
CHAPTER 4	ARTICLE 2: DISTRIBUTION OF LARGE BIOMASS PARTICLES IN A SAND-BIOMASS FLUIDIZED BED: EXPERIMENTS AND MODELING.....	61
4.1	Introduction.....	63
4.2	Experimental.....	66
4.3	Results and discussion.....	68
4.3.1	Characterization of biomass fluidization.....	68
4.3.2	Quantification and modeling the axial distribution of the volume fraction of biomass.....	78
4.4	Conclusion.....	90
CHAPTER 5	BUBBLE BEHAVIOR IN A BIOMASS-SAND FLUIDIZED BED: VALIDATION OF CFPD-BASED MODEL.....	91
5.1	Introduction.....	92
5.2	Experimental.....	94
5.3	The Hybrid Mathematical Model.....	96
5.4	Simulation Parameters.....	99

5.5	Results and Discussion.....	102
5.6	Conclusion.....	112
CHAPTER 6 ARTICLE 3: THE SEPARATION OF THE MAIN COMBUSTIBLE COMPONENTS OF MUNICIPAL SOLID WASTE THROUGH A DRY STEP-WISE PROCESS .....		113
6.1	Introduction.....	115
6.2	Experimental .....	121
6.2.1	Characteristics of SBW .....	121
6.2.2	Experimental apparatus and procedure .....	123
6.3	Results and discussion.....	126
6.3.1	The overall process.....	126
6.3.2	Shredded bulky waste (SBW) elutriation.....	127
6.3.3	Dry density separation.....	132
6.3.4	Effect of bed material size.....	136
6.3.5	Effect of bed dimensions.....	137
6.3.6	Effect of feed (non-elutriated SBW) properties .....	137
6.3.7	Kinetics of segregation in dry density separation .....	138
6.4	Conclusion.....	141
CHAPTER 7 GENERAL DISCUSSION.....		145
CHAPTER 8 CONCLUSIONS AND RECOMMENDATIONS.....		149
8.1	Conclusions.....	149
8.2	Original contributions .....	150
8.3	Future work and recommendations.....	151
BIBLIOGRAPHY .....		154

## LIST OF TABLES

Table 2.1: Powder groups and their key characteristics (Crowe, 2010) .....	10
Table 2.2: Summary of representative experimental work on segregation (Joseph et al., 2007) ..	19
Table 3.1: Properties of materials used .....	43
Table 3.2: Properties of systems studied.....	43
Table 3.3: Summary of the effect of increasing the mass fraction of biomass on bed characteristics .....	59
Table 4.1: Properties of materials used .....	67
Table 4.2: Properties of systems studied.....	67
Table 4.3: Comparing the values of $X_{Be0}$ obtained from the fitting of experimental data and Eq. (4.13) ( $k=2$ ).....	84
Table 5.1: Properties of materials used .....	96
Table 5.2: Properties of systems studied.....	96
Table 5.3: The input parameters for the simulation .....	101
Table 5.4: Comparisons of the mean, standard deviation and skewness of the experimentally and corresponding numerically obtained bubble size distributions. ....	109
Table 5.5: Comparisons of the mean, standard deviation and skewness of the experimentally and corresponding numerically obtained bubble velocity distributions. ....	109
Table 6.1: High heating value (HHV), elemental analysis and moisture content of the main combustible components of SBW used in this study .....	118
Table 6.2: True and bulk densities of the waste, its main constituents and their respective weight fractions.....	122
Table 6.3: Properties of bed materials used in density segregation experiments.....	125
Table 6.4: Details of experiments conducted to examine the effect of some operating conditions on the performance of the fluidization column I.....	134

Table 6.5: Details of experiments conducted to examine the effect of the fluidization medium properties on the performance of the fluidization column II .....	136
Table 6.6: List of components whose segregation kinetics are studied in the density separation steps and the equations and respective parameters describing the kinetics .....	140
Table 6.7: Specifications of each separation unit.....	142

## LIST OF FIGURES

Fig. 2.1: Schematic representation of the model describing segregation in fluidized bed.....	21
Fig. 2.2: Pattern of mixing and segregation for different initial conditions (Yong Zhang et al., 2008).....	25
Fig. 2.3: Graphic representation of the multi-level modeling scheme. (Van der Hoef et al., 2006) .....	26
Fig. 3.1: Sketch of the fluidization column equipped with pressure transducers and optical fiber probes .....	43
Fig. 3.2: The calibration curve used to calibrate the optical fiber probe and the mean values of solid holdup obtained using the calibration equation.....	45
Fig. 3.3: Variation of $U_{if}$ , $U_{ib}$ , $U_{ff}$ , and $U_c$ with the load of biomass.....	47
Fig. 3.4: Variation of parameter $\beta$ as one of the two curve fitting parameters of Student's distribution .....	49
Fig. 3.5: The probability density function of the local voidages registered at $h=175$ mm at a) $U=0.30$ m/s, $r/R=0$ , b) $U=0.80$ m/s, $r/R=0$ , c) $U=0.30$ m/s, $r/R=0.87$ , d) $U=0.80$ m/s, $r/R=0.87$ .....	50
Fig. 3.6: a) The time-mean dilute phase fraction, b) the mean gas holdup, and c) the mean voidage of dilute and dense phases of beds comprising sand and biomass in a bubbling fluidization regime. ( $r/R=0$ , $h=175$ mm).....	51
Fig. 3.7: a) The time-averaged dilute phase fraction, b) the mean gas holdup, and c) the mean voidage of dilute and dense phases of beds comprised of sand and biomass in a bubbling fluidization regime. ( $r/R=0.87$ , $h=175$ mm).....	53
Fig. 3.8: The ratio of the bed voidage of the dense phase to that of the dilute phase at $h=175$ mm at a) $U=0.30$ m/s, b) $U=0.80$ m/s.....	54
Fig. 3.9: A comparison of mean bubble size for a bed of sand alone and mixtures containing biomass at different fluidization velocities at $r/R=0$ .....	56
Fig. 3.10: Void frequency at $h=175$ mm and a) $r/R=0$ , b) $r/R=0.87$ .....	56

Fig. 3.11: Experimental and estimated values of $H/H_{mf}$ vs. superficial gas velocity.....	59
Fig. 4.1: a) Profile of the difference between the local pressure drop gradients of mixtures of sand and biomass and that of a similar bed composed of sand alone in a bubbling regime b) Variation of parameter $\beta$ as one of the two curve fitting parameters of Student's distribution used to fit the PDF of pressure increments. ....	70
Fig. 4.2: Time-averaged concentration (occupancy) profile of biomass particles of mixtures containing a) 2%, b) 16% biomass, fluidized at $U=0.64$ m/s.....	71
Fig. 4.3: Probability density function of the normalized gross cycle length for systems fluidized at a) $U=0.36$ m/s b) $U=0.64$ m/s.....	72
Fig. 4.4: Occurrence percentage of jumps in gross cycles of systems fluidized at a) $U=0.36$ m/s, b) $U=0.64$ m/s.....	73
Fig. 4.5: Probability density profile of the maximum attainable depth of biomass particles for systems fluidized at $U=0.64$ m/s. ....	74
Fig. 4.6: a) The mean cycle time and b) the cycle frequency of systems fluidized at $U=0.36$ and $U=0.64$ m/s.....	75
Fig. 4.7: The time-averaged concentration (occupancy) profiles of the biomass particles involved in gross cycles at $U=0.64$ m/s for mixtures composed of (a) 2% (b) 16% biomass. The most probable pathway of the biomass gross cycle has been illustrated by the black curves. ....	78
Fig. 4.8: The experimental normalized volume fraction of biomass ( $X_B/X_{B,total}$ ) vs. the dimensionless height at a) $U=0.36$ m/s b) $U=0.64$ m/s.....	79
Fig. 4.9: Diagram of the model.....	80
Fig. 4.10: Mean rising velocities of biomass particles along the bed compared with the mean velocity of bubbles.....	82
Fig. 4.11: The experimental and modeled volume fraction of biomass ( $X_B$ ) vs. the dimensionless height of the mixtures containing 2, 8, and 16% biomass fluidized at a) $U=0.36$ m/s b) $U=0.64$ m/s. $X_{Be0}$ is the single adjustable parameter in the model used determined by data fitting. ....	85

- Fig. 4.12: The experimental and modeled volume fraction of biomass ( $X_B$ ) vs. the dimensionless height of the mixtures containing 2, 8, and 16% biomass fluidized at a)  $U=0.36$  m/s b)  $U=0.64$  m/s when Eq. (4.13) is used to estimate  $X_{Be0}$ .....85
- Fig. 4.13: Sensitivity of the model proposed with respect to  $U_{bm}U_b$ , as applied to the experimental data of Bilbao et al. (R. Bilbao et al., 1988), (fluidization of straw-sand mixtures at  $U=0.14$  m/s,  $x_{straw}=0.08$ ,  $d_{sand}=158$   $\mu\text{m}$ ,  $d_{straw}=794$   $\mu\text{m}$ ,  $\rho_{sand}=2000$   $\text{kg/m}^3$ ,  $\rho_{straw}=350$   $\text{kg/m}^3$ ).....87
- Fig. 4.14: The values predicted by the proposed model when  $U_{bm}U_b=0.2$  (white symbols) and  $U_{bm}U_b=0.3$  (black symbols) vs. the corresponding experimental data reported by Bilbao et al. (R. Bilbao et al., 1988), ( $U=0.17$  m/s,  $d_{sand}=158$   $\mu\text{m}$ ,  $d_{straw}=1265$   $\mu\text{m}$ ,  $\rho_{sand}=2000$   $\text{kg/m}^3$ ,  $\rho_{straw}=350$   $\text{kg/m}^3$ ).....88
- Fig. 4.15: The values predicted by the proposed model when  $U_{bm}U_b=0.2$  (white symbols) and  $U_{bm}U_b=0.3$  (black symbols) vs. the corresponding experimental data reported by Bilbao et al. (R. Bilbao et al., 1988), ( $x_{straw}=0.08$ ,  $d_{sand}=158$   $\mu\text{m}$ ,  $d_{straw}=794$   $\mu\text{m}$ ,  $\rho_{sand}=2000$   $\text{kg/m}^3$ ,  $\rho_{straw}=350$   $\text{kg/m}^3$ ).....89
- Fig. 5.1: Sketch of the fluidization column equipped with optical fiber probes used for the experiments. ....95
- Fig. 5.2: Particles volume fraction during the first 1s fluidization of a sand-biomass mixture at  $U=0.64$  m/s, (biomass load= 8% wt., initially well-mixed mixture).....104
- Fig. 5.3: Simulation of sand fluidization in a bed constituted by sand and biomass particles.  $U=0.64$  m/s, (biomass load= 8% wt., initially well-mixed mixture).....105
- Fig. 5.4: Simulation of biomass fluidization in a bed constituted by sand and biomass particles.  $U=0.64$  m/s, (biomass load= 8% wt., initially well-mixed mixture).....106
- Fig. 5.5: Comparison of the experimentally measured and numerically calculated a) bubble size distribution b) bubble rise velocity distribution as a function of superficial gas velocity for a mixture containing 8% wt biomass. Red lines indicate the mean value of each graph. ....107
- Fig. 5.6: Comparison of the experimentally measured and numerically calculated a) bubble size distribution b) bubble rise velocity distribution as a function of superficial gas velocity for a mixture containing 16% wt biomass. Red lines indicate the mean value of each graph. ....108

Fig. 5.7: Comparison of the experimentally obtained and corresponding numerical values of the mean a) bubble size, b) bubble velocity distribution .....	110
Fig. 5.8: Comparison of the experimentally obtained and corresponding numerical values of the standard deviation of a) bubble size, b) bubble velocity distribution .....	110
Fig. 5.9: Comparison of the experimentally obtained and corresponding numerical values of the skewness of a) bubble size, b) bubble velocity distribution.....	111
Fig. 6.1: a) NO <sub>x</sub> b) SO <sub>2</sub> emission rate of some of the US power plants combusting coal .....	117
Fig. 6.2: Total MSW generation (by material), 2011 (Agency, 2013).....	118
Fig. 6.3: Particle size distribution of the SBW used in the experiments and its main constituents .....	123
Fig. 6.4: Elutriation yield vs. time for four different gas velocities .....	128
Fig. 6.5: Effectiveness of the separation of fiber, soft plastic and hard plastic via the elutriation technique in step 1.....	130
Fig. 6.6: Weight fraction of main constituents of waste in the non-elutriated materials of step 1 .....	131
Fig. 6.7: Percentage distribution of feed components along the bed in the second density segregation step when the fluidization medium is a) glass beads b) PVDF beads .....	136
Fig. 6.8: Concentration of the intended components vs. time for the density separation step a) I b, c) II .....	140
Fig. 6.9: Schematic presentation of the whole process proposed for the separation of the MSW components and mass balance calculated for 100 g of the SBW based on the separation efficiency of each unit. ....	143
Fig. 6.10: Ternary diagram of the EF composition, which can be produced by mixing fiber, soft and hard plastic on the basis of the separation efficiencies of the proposed process.....	144

## NOMENCLATURE

### Symbols

$A$ : Cross-sectional area of the bed [ $\text{m}^2$ ]

$A_c$ : Catchment area of a single distributor hole [ $\text{m}^2$ ]

$Ar$ : Archimedes number [-]

$C_d$ : Drag coefficient [-]

$d_p$ : Sauter mean diameter [-]

$D$ : Bed diameter [m]

$d_b$ : Bubble diameter [m]

$D_f$ : A positive constant [ $\text{kgm}^{-1}\text{s}^{-2}$ ]

$d_m$ : Minimum moving zone diameter [m]

$D_p$ : Interphase drag coefficient [-]

$d_p$ : Particle size [mm]

$d_{\text{sand}}$ : Mean size of sand particles [m]

$d_{\text{straw}}$ : Mean size of straw particles [m]

$e$ : Overall separation efficiency of density segregation method [-]

$e_n$ : A positive constant [ $\text{kgm}^{-1}\text{s}^{-2}$ ]

$e_t$ : A positive constant [ $\text{kgm}^{-1}\text{s}^{-2}$ ]

$F$ : Momentum exchange rate per unit volume between the fluid and particle phases

$F_w$ : Ratio of bubble wake volume to bubble volume, 0.185 [-]

$g$ : Gravitational acceleration [ $\text{ms}^{-2}$ ]

$h$ : Height from the distributor [-]

$H_0$ : Initial height of the dense bed [m]

$H_{\text{eff}}$ : Effective height of the bed up to which 95% of all tracer occurrences takes place [m]

$H_{\text{mf}}$ : Height of the bed under complete fluidization conditions,  $U_{\text{mf}}$  or  $U_{\text{ff}}$  [m]

$I_{\text{p}}$ : Maximum iterations for pressure calculations []

$I_{\text{u}}$ : Maximum iterations for velocity calculations []

$I_{\text{v}}$ : Maximum iterations for volume calculations []

$k$ : Segregation rate constant [ $\text{s}^{-1}$ ]

$K_{\text{w}}$ : Exchange coefficient between the dilute and dense phases [ $\text{s}^{-1}$ ]

$L$ : Height of the dense bed in segregation density tests [mm]

$L_{\text{max}}$ : Maximum attainable depth of biomass particles

**MI**: Mixing index

$m_{\text{p}}$ : Mass of an individual particle in the cloud [kg]

$N(\alpha, \beta)$ : Normalization factors of the Student's and Gamma distributions [-]

$N_{\text{c}}$ : Number of the clouds in the computational cell [-]

$n_{\text{c}}$ : Number of the particles in the clouds [-]

$P$ : Fluid pressure (Chapter 5) [ $\text{kgm}^{-1}\text{s}^{-2}$ ]

$P$ : Purity percentage of target material in density segregation tests (Chapter 6) [-]

$P_{\text{s}}$ : A positive constant (Chapter 5) [-]

$q$ : Bubble-emulsion exchange rate for sand [ $\text{m}^2\text{s}^{-1}$ ]

$r$ : An arbitrary radial position in the bed [m]

**R**: Bed radius [m]

$R$ : Recovery percentage of target material in density segregation tests (Chapter 6) [-]

$Re$ : Reynolds [-]

$Re_{\text{ff}}$ : Reynolds number at final fluidization velocity [-]

$r_{\text{p}}$ : Residual for pressure [ $\text{kgm}^{-1}\text{s}^{-2}$ ]

$r_u$ : Residual for velocity [ $\text{ms}^{-1}$ ]

$r_v$ : Residual for volume [ $\text{m}^3$ ]

$S_{ij}$ : Deformation rate [-]

$t$ : Time/duration [min]

$t_e$ : Elutriation duration [min]

$U$ : Superficial gas velocity [ $\text{ms}^{-1}$ ]

$U_b$ : Bubble rise velocity [ $\text{ms}^{-1}$ ]

$\bar{U}_b$ : Mean bubble rise velocity [ $\text{ms}^{-1}$ ]

$\bar{U}_{bm}$ : Mean rise velocity of biomass particles [ $\text{ms}^{-1}$ ]

$U_c$ : Transition gas velocity from a bubbling to turbulent regime [ $\text{ms}^{-1}$ ]

$U_e$ : Elutriation velocity [m/s]

$U_f$ : Fluidization velocity [m/s]

$U_{ff}$ : Final fluidization velocity [ $\text{ms}^{-1}$ ]

$U_{ib}$ : Initial bubbling velocity [ $\text{ms}^{-1}$ ]

$U_{if}$ : Initial fluidization velocity [ $\text{ms}^{-1}$ ]

$U_{mf}$ : Minimum fluidization velocity [ $\text{ms}^{-1}$ ]

$V$ : Voltage [V]

$V$ : Volume of computational cell (Chapter 5) [ $\text{m}^3$ ]

$V_0$ : Voltage at empty column [V]

$v_f$ : Fluid velocity [ $\text{ms}^{-1}$ ]

$V_{mf}$ : Voltage at the minimum fluidization velocity [V]

$v_p$ : Particle velocity [ $\text{ms}^{-1}$ ]

$V_p$ : Particle volume [ $\text{m}^3$ ]

$W_{if}$ : Mass of target components in the feedstock [g]

$W_{it}$ : Mass of target components in the target stream elucidated in Fig. 6.9 [g]

$W_{jf}$ : Mass of non-target components in the feedstock [g]

$W_{jt}$ : Mass of non-target components in the target stream elucidated in Fig. 6.9 [g]

$W_{Tt}$ : Total mass of the target stream [g]

$x$ : Mass concentration at a specific part of the bed [-]

$x_0$ : Initial mass concentration at a specific part of the bed [-]

$x_\infty$ : Equilibrium mass concentration at a specific part of the bed [-]

$X_{B, total}$ : Total volume fraction of biomass along the bed [-]

$X_B$ : Volume fraction of biomass in a specific layer [-]

$X_{Be}$ : Volume fraction of biomass in the emulsion phase of a specific layer [-]

$X_{Be0}$ : Volume fraction of biomass in the emulsion phase at  $Z=0$  [-]

$x_{Bm}$ : Weight fraction of biomass in the mixture [-]

$X_{fe}$ : Volume fraction of fluidization medium in the emulsion phase of a specific layer [-]

$x_{straw}$ : Weight fraction of straw in the mixture [-]

$x_T$ : Weight fraction of jetsam in the whole bed [-]

$x_U$ : Weight fraction of jetsam in the upper region of the bed [-]

$Y$ : Deviation factor from two-phase theory of fluidization [-]

$z$ : Generic random variable [-]

$Z$ : Height above the distributor plate [m]

### Greek letters

$\alpha, \beta$ : Curve-fitting parameters for Student's distribution [-]

$\beta$ : A constant (Chapter 5) [-]

$\beta_g$ : Ratio of the bed voidage of the dense phase to that of the dilute phase [-]

$\delta_b$ : Volume fraction of bubbles in bed [-]

$\delta_{ij}$ : Kronecker delta [-]

$\delta_{ij}$ : Kronecker delta [-]

$\varepsilon$ : A constant (Chapter 5) [-]

$\varepsilon$ : Void fraction [-]

$\varepsilon_b$ : Mean voidage of dilute phase [-]

$\varepsilon_B$ : Void fraction of a bed of biomass alone [-]

$\varepsilon_e$ : Void fraction of emulsion phase in a biomass-fluidization medium mixture [-]

$\varepsilon_F$ : Void fraction of a bed of fluidization medium alone [-]

$\varepsilon_{mf}$ : Void fraction at the minimum fluidization velocity [-]

$\varepsilon_r$ : Gas holdup [-]

$\zeta$ : A parameter representing an elastic restitution factor [-]

$\eta_i$ : Effectiveness of separation of component i via elutriation [-]

$\theta_{cp}$ : Particle volume fraction at close packing [-]

$\theta_f$ : Fluid volume fraction [-]

$\theta_p$ : Particle volume fraction

$\mu_f$ : Fluid viscosity coefficient [ $\text{kgm}^{-1}\text{s}^{-1}$ ]

$\mu_g$ : Dynamic viscosity of gas [ $\text{kgm}^{-1}\text{s}^{-1}$ ]

$\rho$ : Probability density function (PDF) [-]

$\rho_f$ : Fluid density [ $\text{kgm}^{-3}$ ]

$\rho_g$ : Density of gas [ $\text{kgm}^{-3}$ ]

$\rho_p$ : Density of particle [ $\text{kgm}^{-3}$ ]

$\rho_p$ : Particle density [ $\text{kgm}^{-3}$ ]

$\rho_{sand}$ : Density of sand [ $\text{kgm}^{-3}$ ]

$\rho_{\text{straw}}$ : Density of straw [ $\text{kgm}^{-3}$ ]

$\tau_f$ : Fluid stress tensor [ $\text{kgm}^{-1}\text{s}^{-2}$ ]

$\tau_p$ : Particle stress tensor [ $\text{kgm}^{-1}\text{s}^{-2}$ ]

$\phi$ : Sphericity [-]

$\Psi^b_F$ : Volumetric flow rate of fluidization medium in the bubble phase [ $\text{m}^3\text{s}^{-1}$ ]

$\Psi^e_B$ : Volumetric flow rate of biomass in the emulsion phase [ $\text{m}^3\text{s}^{-1}$ ]

## LIST OF ABBREVIATIONS

**ABS:** Acrylonitrile butadiene styrene

**CFD:** Computational fluid dynamics

**CPFD:** Computational particle fluid dynamics

**CSWD:** Chittenden solid waste district

**CT:** Computed tomography

**EF:** Engineered fuel

**EJ:** Exa joule

**F:** Fiber

**FFT:** Fast Fourier transform

**GHG:** Greenhouse gas

**G-R:** Gibilaro-Rowe

**HHV:** High heating value

**HP:** Hard plastic

**I.D.:** Internal diameter

**MSW:** Municipal solid waste

**NC:** Noncombustible materials

**OC:** Other combustible materials

**PC:** Polycarbonate

**PDF:** Probability density function

**PE:** Polyethylene

**PEPT:** Positron emission particle tracking

**PP:** Polypropylene

**PS:** Polystyrene

**PSD:** Particle size distribution

**PT:** Pressure transducer

**PVC:** Polyvinyl chloride

**RDF:** Refused-drive fuel

**RPT:** Radioactive particle tracking

**RT:** Residence time

**SBW:** Shredded bulky waste

**SP:** Soft plastic

**SRF:** Solid recovered fuel

**TSV:** Terminal settling velocity

**WTE:** Waste to energy

## CHAPTER 1

### INTRODUCTION

Energy is considered a prime agent in the generation of wealth and a significant factor in economic development. The importance of energy in economic development is universally recognized and historical data verify the strong relationship between the availability of energy and economic activity (Kalogirou, 2004). Energy resources are split into three categories: fossil, nuclear, and renewable resources. Policy makers take into account a combination of economic, social, environmental and safety considerations to decide which types of energy source should be utilized.

Climate change is one of the most serious environmental problems. Increased levels of greenhouse gases (GHGs) in the atmosphere lead to warmer temperatures on the earth's surface. CO<sub>2</sub> is the main greenhouse gas associated with global warming. At the present time, about 98% of carbon emissions result from fossil fuel (coal, oil, and natural gas) combustion and coal is responsible for 30–40% of global CO<sub>2</sub> emissions from fossil fuels. Concentration of CO<sub>2</sub> in the atmosphere will continue rising unless major changes are made in the way fossil fuels are used to provide energy services (Hoffert et al., 1998).

Renewable energy technologies produce marketable energy by converting natural phenomena into useful forms of energy. These technologies use the sun's energy and its direct and indirect effects on the earth (solar radiation, wind, falling water and various plants, i.e., biomass), gravitational forces (tides), and the heat of the earth's core (geothermal) as the resources from which energy is produced (Kalogirou, 2004). By applying a renewable energy intensive scenario, the global consumption of renewable sources by 2050 would reach 318 EJ (1 EJ=10<sup>18</sup> J) (Johansson, Kelly, Reddy, & Williams, 1993). Renewable energy resources that use domestic resources have the potential to provide energy services with zero or almost zero emissions of both air pollutants and greenhouse gases.

Biomass has the potential to become one of the major global primary renewable energy sources during the next century. The term biomass could include organic matter produced as a result of

photosynthesis as well as municipal, industrial and animal waste material. The modernized bioenergy systems are recommended as important contributors to future sustainable energy systems and to sustainable development in both developed and developing countries (Berndes, Hoogwijk, & van den Broek, 2003). The components of biomass include cellulose, hemicelluloses, lignin, extractives, lipids, proteins, simple sugars, starches, water, hydrocarbons, ash, and other compounds. Two larger carbohydrate categories that have significant value are cellulose and hemi-cellulose. The lignin fraction consists of non-sugar type molecules (Ayhan Demirbas, 2005). The average majority of biomass energy is produced from wood and wood wastes (64%), followed by solid waste (24%), agricultural waste (5%) and landfill gases (5%) (A Demirbas, 2000). Biomass materials are abundant and rapidly replenished by a natural process. It can take 2 to 100 years for different sources of plant energy to regrow, such as the difference between fast growing switch grass and slow growing trees. Biomass can be economically produced with minimal or even positive environmental impacts through perennial crops. The CO<sub>2</sub> emitted from the thermal conversion of biomass material is naturally sequestered by photosynthesis. Biomass-based energy sources cover around 12% of total world energy consumption.

Biomass energy can be recovered by burning biomass as a fuel; however, the biomass-to-electricity systems based on gasification have been proven to be a promising conversion technology and have certain advantages over combustion. Gasification is a thermal process that converts solid fuels to combustible gaseous fuel through partial oxidation in the presence of air and/or steam. The efficiency of gasification is higher than direct combustion. Moreover, due to the higher efficiency of gas turbines compared to steam turbines, power generation via biomass gasification in an Integrated Gasification Combined Cycle (IGCC) increases the electrical efficiency by 22-37%. Product gas from a biomass gasifier, however, must be cleaned to remove the tar and particulate matter before entering the gas turbine (Radmanesh, 2006).

Combustion and gasification of biomass are realized in bubbling or circulating fluidized bed reactors. Fluidization is usually achieved by the introduction of pressurized fluid through the particulate medium. This results in the medium then having many properties and characteristics of normal fluids. Due to its unique features, such as the effective contact of solid and gas phases, efficient and uniform heat transfer, and suitability for processing a wide range of feedstocks, fluidized bed reactors are extensively utilized for biomass thermal processing.

The irregular nature of biomass particles in terms of physical properties, such as size and density, makes their fluidization difficult or even impossible. Therefore, the addition of an inert granular material, such as sand or alumina, to biomass is necessary to facilitate the fluidization process. Considering the significant difference between the physical properties of the biomass and the inert material particles, a complex multiphase flow is associated with fluidizing a mixture of these particles.

Due to the limited understanding of the multiphase flow aspects of the irregular particles, the design and operation of the current biomass fluidized bed units are based on the conventional knowledge of fluidization, which is mainly developed on the basis of regular particles. Accordingly, the impact of physical irregularities on the hydrodynamic features of fluidization is ignored or underestimated.

Upon feeding into a hot fluidized bed, a fuel particle undergoes a series of stages from the initial release of the moisture to the final transformation into ashes (Miccio, Russo, & Silvestri, 2013). The size of biomass particles used as feedstock in biomass combustors or gasifiers is usually much larger than the coal particles fed to the coal processing units. Therefore, despite the intense heat transfer process, biomass particles remain at their original size for a considerable period of time (several tens of seconds) before being fractured as a result of thermal degradation. Proportionally, devolatilization of biomass particles and burning of the residual char lasts longer, depending on the type of fuel particles. These characteristic times are much longer than the corresponding times for the coal particles. The existence of irregular particles for a long period of time inside the reactor affects the hydrodynamic features of the bed. As explained, it is more noticeable in the case of biomass processing compared to the widely used coal units. This signifies that the current knowledge of the hydrodynamic phenomena in the fluidized bed combustors or gasifiers, mainly based on coal processing, is not sufficient for the design and optimization of units dealing with biomass materials. Therefore, extensive research on the fluidization of biomass is essential.

One of the critical hydrodynamic aspects in either biomass combustors or gasifiers is the gas distribution between the dilute and dense phases of fluidization. The extent of effective contact between gas and solid particles governs the performance of reactions taking place in the reactor. For instance, in the case of biomass combustion, the inert material particles interfere with the

process of O<sub>2</sub> diffusion, namely the approach of oxygen molecules to the fuel particle surface. The mass transfer process towards the fuel particle is hindered in the fluidized bed, as opposed to heat transfer for which the conditions in a fluidized bed and the presence of inert material particles are favorable. While the temperature field is homogenous in fluidized beds, the concentration field, i.e., oxygen distribution, is very heterogeneous. Fuel particles inhabit the emulsion phase of the bed and consume all or most of the oxygen available in the emulsion phase. Furthermore, a large amount of air, i.e., oxygen, is moving in bubbles and can pass through the bed without reacting with fuel particles. The concentration differences of O<sub>2</sub>, CO and CO<sub>2</sub> between bubbles and emulsion can be considerable, and the process of mass transfer from bubbles to emulsion can be a limiting factor for fluidized bed combustion (Oka, 2010). On the other hand, the mixing of solids in a gas fluidized bed is induced by bubbles. Bubbles carry solids up in their wake. When bubbles rise, it also causes solids to drift in the bed. This upward movement of solids is known as a bubble-induced drift of solids. A downward movement of solids also takes place to compensate for the upward movement of solids. These ascending and descending phases are responsible for the mixing in the bed. All of these features confirm the importance of the accurate assessment of the dilute phase behavior, which is subject to change in the presence of biomass particles.

A combination of pressure and optical fiber probes are deployed in this study to scrutinize the global and local behavior of bubbles and the gas distribution pattern for mixtures of sand and biomass particles. Through these techniques, some vital parameters, such as the characteristic fluidization velocities, bubble evolution pattern, local gas holdup, mean voidage of the dilute and dense phases, bed expansion, and bubble size, velocity and frequency changes, are investigated. Knowledge of these parameters is pivotal for the successful design and operation of bubbling fluidized beds.

Another major issue for the biomass processing units, where biomass is co-fluidized with much denser and smaller inert material particles, is the interaction and mixing of the species. Under fluidization conditions, lighter/smaller particles tend to move to the upper sections of the bed (flotsam behavior), whereas denser/larger species remain in the lower parts (jetsam behavior). This results in the segregation of the bed components, which negatively affects the reactor performance. In view of the very low density of biomass particles, they usually congregate at the top of the bed. On the other hand, the bubbles issuing from a fuel particle during devolatilization,

climb up the bed and erupt at the surface where they burn-off. The volatile release is also responsible for fast and stable fuel particle segregation at the bed surface, at least under the conditions of the incipient bubbling regime (Bruni et al., 2002). Some consequences of biomass segregation in the bed are the release of volatiles into the freeboard, the ineffective heat transfer along the bed, the deterioration of the activity of the tar decomposition reaction and the heterogeneous distribution of the gas reactants and products (L. Shen, Xiao, Niklasson, & Johnsson, 2007).

The bed materials employed in the majority of the studies performed on the mixing/segregation issues are limited to the conventional binary mixtures, in which each species has its own minimum fluidization velocity. Compared with the conventional binary mixtures, the extent of dissimilarity between the properties of typical biomass and inert materials is much more substantial. A profound knowledge of the mixing/segregation phenomena in such systems is greatly lacking. Most of the studies on biomass mixing are devoted to the quantification of the extent of mixing under different operating conditions. In addition, the techniques implemented for this purpose have not been able to provide information on mixing/segregation mechanisms, particularly in the three-dimensional (3D) units. Therefore, the results obtained are limited to ad hoc situations, which cannot reliably be generalized to the practical biomass fluidization beds.

Radioactive particle tracking (RPT) is a powerful technique used in this work to provide more detailed phenomenological information on the hydrodynamic behavior of fluidized biomass particles. This technique is based on the principle of tracking the motion of a single particle as a marker of the phase, which is under consideration in a flow vessel (Roy, Larachi, Al-Dahhan, & Duduković, 2002). It is clear that the tracer should be a representative of the typical particles and mimic their behavior perfectly. Thus, in the case of tracking the solid particulates, the tracer particle is designed to have the same dimensions and effective density of the intended solid particles. The local position of a single tracer, which is placed in a bed consisting of sand and biomass, is provided in a non-intrusive manner. The instantaneous position of the tracer obtained in a Lagrangian framework gains a deep insight into the motion of irregular biomass particles. The time-averaged concentration and velocity profiles of the biomass particles in the bed are also obtainable after processing the RPT data.

Modeling the axial distribution of biomass along the bed is useful to assess the heat and mass transfer profiles and evaluate the yield of reactions taking place in combustors or gasifiers. Gibilaro and Rowe (Gibilaro & Rowe, 1974) constructed a simple equilibrium model to predict jetsam volume concentration versus bed height, based on a one-dimensional system consisting of bulk and wake phases, where jetsam was preferentially discharged by rising bubbles. A one-dimensional model has been developed in the current study based on the Gibilaro and Rowe (G-R) model to predict the volume fraction of biomass along the axis of the bed. To develop this model, the RPT based findings have been adopted to modify the terms of the G-R model in a way that would also be useful to predict the distribution of flotsam (biomass) particles. The predicted values of the model are compared with the corresponding RPT results.

In spite of significant progress in developing the experimental techniques employed to characterize multiphase flow aspects of fluidized beds, lack of sufficient information on particle-scale impedes the development of a viable method to scale-up, design, control, and optimize mixing/segregation behaviors. Computational fluid dynamics (CFD) provides valuable tools to model fluidized bed dynamics and plays a central role in the future design and operation of large scale fluidized beds. The Computational Particle Fluid Dynamics (CPFD) numerical scheme has some unique advantages, which makes it suitable for studying the fluidization phenomena in large commercial systems containing billions of particles. In this regard, the transient flow structure as well as the bubble properties of the systems studied experimentally in this work are also explored numerically using the BARRACUDA CPFD software. The acceptable consistency of bubble characteristics obtained from the experimental and numerical approaches corroborates the suitability of the CPFD numerical scheme to closely simulate the fluidized bed units involving biomass.

Municipal solid waste (MSW) is an abundant, renewable, sustainable and low cost source of energy. It earns second place in terms of the magnitude of energy produced from different types of biomass materials. In the United States alone, over 100 million tons of combustible materials, including paper, paperboard and plastic waste, are produced per year (Agency, 2013). The thermo-chemical treatment process of solid waste has several advantages such as the significant reduction of waste in mass (about 70-80%) and in volume (about 80-90%) resulting in drastic savings of land required for landfilling, the destruction of organic contaminants, and the environmentally compatible exploitation of the renewable energy of the waste (Arena, 2012).

There are two main categories of waste-to-energy (WTE) plants. In mass-burn plants, the MSW is fed as collected into large furnaces. In refuse-derived fuel (RDF) plants, the MSW is first shredded into small pieces and most of the metals are recovered before combustion (Psomopoulos, Bourka, & Themelis, 2009). In fact, several successive treatment stages of screening, shredding, size reduction, classification, separation, drying and densification are required to obtain a RDF of certain characteristics (Hernandez-Atonal, Ryu, Sharifi, & Swithenbank, 2007). In spite of these pretreatments, RDF combustion suffers from problems stemming from the improper and uncontrolled composition of the RDF. For example, the significant ash content could be problematic if the percentage of paper in the RDF is high. Moreover, corrosion of the facilities is a serious challenge when chlorine-containing plastics, such as Polyvinyl chloride (PVC), are burnt in the bed. In light of these drawbacks, it is extremely important to produce a novel solid waste-based fuel whose composition is controllable. To make such a fuel, which has been recently patented as “Engineered Fuel, EF” (Calabrese & Bai, 2010), effective separation techniques must be implemented to recover the main combustible materials of MSW.

In spite of the aforementioned detrimental impact of segregation on the operation of biomass combustors or gasifiers, segregation could be effectively exploited to separate and classify the matters differing in size, density or even shape. Based on one of the objectives of this work, which is exploring the segregation-related phenomena in fluidized beds, a dry step-wise process is introduced to separate the combustible components of the solid municipal waste by exploiting the density separation technique. The combustible components, i.e., fiber, and soft and hard plastic materials, which are obtained from the MSW through the proposed process, can be mixed in predetermined ratios in order to reach the favorable EF composition.

## CHAPTER 2

### LITERATURE REVIEW

#### 2.1 Thermal processing of biomass

Renewable energy is one of growing importance in satisfying environmental concerns over fossil fuel usage. Biomass is considered the renewable energy source with the highest potential to contribute to the energy needs of modern society for both the developed and developing economies world-wide (Bridgwater, 2003). The potential of biomass energy derived from forest and agriculture residues worldwide is estimated at about 30 EJ/year (Gallucci, 2012). Moreover, if bio-residues or waste-biomass are considered, its potential could provide as much as 330 GW of electric power, if utilized efficiently. The power generation cycles based on the biomass derived from short rotation forestry and other energy crops are characterized by near-zero contribution to the accumulation of green house gases which makes them a clean substitute of the fossil fuels. There are three main thermal processes available for converting biomass to a more useful energy form, i.e. pyrolysis, combustion and gasification.

Pyrolysis is a thermal decomposition process converting biomass into liquid (bio-oil), gaseous and solid fractions, in the absence of oxygen. It is always the first step in combustion and gasification, starting at 200-300 °C, before oxidation of the primary pyrolysis products.

In presence of oxygen a combustion process takes place at 800- 900 °C, the product of which is heat, to be used either directly or for power generation (steam turbine). The technology is widely available commercially and there are many successful working examples throughout North America and Europe, frequently using forestry, agriculture and industrial wastes (Bridgwater, 2003).

Gasification is a thermo-chemical conversion process utilizing air, oxygen and/or steam as gasification agents, which converts biomass at  $T > 800$  °C into gases, such as hydrogen, carbon monoxide, carbon dioxide and methane (Syngas), together with organic vapors which condense

under ambient conditions known collectively as tar. Gasification occurs in a number of sequential steps:

- Drying to evaporate moisture
- Pyrolysis to give gas, vaporized tars or oils and a solid char residue
- Gasification or partial oxidation of the solid char, pyrolysis tars and pyrolysis gases

When a solid fuel is heated to 300-500 °C in the absence of an oxidizing agent, it pyrolyses to solid char, condensable hydrocarbons or tar, and gases. The relative yields of gas, liquid and char depend mostly on the rate of heating and the final temperature. Generally in gasification, pyrolysis proceeds at a much quicker rate than gasification and the latter is thus the rate controlling step. The gas, liquid and solid products of pyrolysis then react with the oxidizing agent to give permanent gases of CO, CO<sub>2</sub>, H<sub>2</sub>, and lesser quantities of hydrocarbon gases. Char gasification is the interactive combination of several gas-solid and gas-gas reactions in which solid carbon is oxidized to CO, CO<sub>2</sub> and H<sub>2</sub> is generated through the water-gas shift reaction. The gas-solid reactions of char oxidation are the slowest and limit the overall rate of the gasification process. The gas composition is influenced by many factors such as feed composition, waster content, reaction temperature, and the extent of oxidation of the pyrolysis products.

Bubbling and circulating fluidized beds are among the most reliable systems of biomass processing with high market attractiveness for respectively medium and large scale applications.

The primary features of bubbling fluidized beds are as follow:

- High reliability with a variety of feedstocks
- Favorable gas-solid contacting
- Uniform and controllable temperature and high reaction rates
- High particulates in the product gas and moderate tar levels in product gas
- Good scale-up potential to 10-15 dry t/h with high specific capacity
- Great tolerance to particle size range
- Feasibility of adding tar cracking catalysts to bed
- Also economic for small to medium range capacities

Geldart (D. Geldart, 1973) proposed a popular classification scheme for particles fluidized in air under atmospheric conditions. Four powder groups were suggested in order to distinguish broad

types of behavior. These four groups (A, B, C, and D) are frequently referred to in the literature. The characteristics of the four groups and criteria to distinguish them are summarized in Table 2.1. Group C particles are usually inappropriate for fluidization due to excessive interparticle forces, whereas groups A, B, and D can be fluidized, and used in practical applications.

Fluidization of biomass particles is a difficult or even impossible task due to their peculiar shape, size and density. To overcome this difficulty and also improve the heat transfer in the bed, an inert solid is often added to biomass particles. Silica sand, alumina, calcite, and olivine are some types of such inert materials. Biomass particles in the bed are in continuous motion and in collision with inert material particles, and also in constant contact with the gas phase.

At the moment when a cold biomass (fuel) particle enters a fluidized bed of hot inert material particles ( $T \approx 800-900$  °C), the heating process begins due to continuous collision with hot particles. Despite the intense heat transfer process, the fuel particle in a fluidized bed is heated at a rate of 100 °C/s for fuel particles whose sizes range from 5 to 50 mm. Devolatilization lasts from 10 to 100 s, depending on the type and size of biomass particles, while residual char burning (in the case of fluidized bed combustion) takes much longer time, 100-2000 s (Oka, 2010).

Table 2.1: Powder groups and their key characteristics (Crowe, 2010)

Group	Mnemonic	Example	Key features	Interparticle forces relative to weight-buoyancy	Typical particle size ( $\mu\text{m}$ )
C	Cohesive	Flour	Fluidize poorly due to strong interparticle forces; show channeling	Dominant	<30
A	Aeratable	Fluid cracking catalyst	Excellent fluidization; small bubbles; deaerate slowly when gas flow stopped; high bed expansion, rapid particle mixing	Appreciable	~30-100
B	Bubble readily	Normal sand	Deaerate quickly when gas is shut off; large bubbles ; intermediate solids mixing	Negligible	~100-800
D	Dominantly inertial	Peas	Deaerate quickly when gas is shut off; large bubbles; relatively poor solids mixing	Negligible	>800

## 2.2 Multiphase flow aspects of biomass fluidization

The biomass particles or pieces are commonly large in size, extreme in shape (e.g. long and thin as with stem or fibers), wet and pliable which make them irregular with respect to normal particulate matter handled in chemical, mineral and pharmaceutical operations. These differences are often critical, making it difficult, or even impossible, to handle, feed or process biomass particles requiring addition of inert materials. Hence, their multiphase flow characteristics are of special interest. Understanding and managing multiphase flows are critical to design new and to improve the existing biomass processing units. However, most fundamental work on particulate processes has focused on dry spherical particles of narrow size distribution, with limited extension to other regular shapes. When coupled with the complexity of characterizing the properties and behavior of non-standard materials, general methods of handling irregular particles are not very reliable. Biomass particles are commonly so extreme in nature that their flow characteristics are not readily predictable (Cui & Grace, 2007). Characteristic fluidization velocities, fluidization quality and mixing/segregation phenomena are the subjects which have been investigated more widely compared to other multiphase flow features of biomass fluidization.

### 2.2.1 Characteristic fluidization velocities

Unlike the ideal mono-component systems, where fluidization of the whole bed inventory occurs at a certain superficial gas velocity called minimum fluidization velocity ( $U_{mf}$ ), fluidization of all components constituting a multi-component mixture is achieved in a range of fluidization velocity. In fact, fluidization starts at the “initial” fluidization velocity,  $U_{if}$ , and reaches the “final” state at  $U_{ff}$ , when all particles are fully fluidized.

There are several parameters that determine the fluidization pattern of the two-solid bed, as their variations are clearly reflected by a change of either  $U_{if}$  or  $U_{ff}$ . These parameters include solid properties, i.e. particle density, size and shape factors as well as mixture properties, i.e. composition, bed voidage and packed bed distribution (Formisani, Girimonte, & Vivacqua, 2011).

In view of the importance of onset of full fluidization of bed inventory at  $U_{ff}$ , most researchers have focused on measurement and prediction of this velocity for systems involving biomass. Based on the terminology of the mono-component systems,  $U_{ff}$  is usually called minimum fluidization velocity in the literature, i.e. ( $U_{mf}=U_{ff}$ ). In addition to the importance of minimum fluidization velocity due to indicating the amount of drag force needed to attain solid suspension, it is regarded as a reference for the evaluation of the intensity of the fluidization regime at higher velocity levels.

In spite of extensive studies performed on determination and prediction of the minimum fluidization velocity of inert particles such as sand, glass beads, and alumina, the biomass related studies are relatively new and limited and there is no consensus on the correlation for prediction of the  $U_{mf}$  of biomass or the mixture of biomass and inert particles (Paudel & Feng, 2013).

Aznar et al. (Aznar, Gracia-Gorria, & Corella, 1992) studied the fluidization behavior of sawdust alone and found that it does not fluidize well and it exhibits channeling and Geldart C fluidization behavior. After examining  $U_{mf}$  of biomass-sand mixtures, they suggested that the minimum fluidization velocity of such mixtures should be estimated from the mixture properties, such as composition, particle density, and particle diameter, instead of measuring the minimum fluidization velocity of each component.

Conducting some experiments on binary mixtures of moist saw dust and glass spheres in a large cylindrical fluidized bed, with an inner diameter of 139 cm, Clarke et al. (Clarke, Pugsley, & Hill, 2005) reported that as the moisture content of the biomass is increased, the minimum fluidization velocity for the binary mixture also increases. They indicated that the existing correlations were unsuccessful to predict  $U_{mf}$  for sawdust-glass mixtures.

Noda et al. (Noda, Uchida, Makino, & Kamo, 1986) and Bilbao et al. (R Bilbao, Lezaun, & Abanades, 1987) proposed some correlations based on different definitions of minimum fluidization velocity. These correlations may strongly depend on the characteristics of particles used in their experiments (Paudel & Feng, 2013).

Si and Guo (Si & Guo, 2008) varied the weight percentage of biomass from 20 to 50% in biomass-sand mixtures fluidized in Perspex column with an inner diameter of 5.3 cm and studied the effect of mass percentage of biomass on the minimum fluidization velocity. The minimum fluidization velocity of the mixtures increased with increasing biomass content in the mixtures.

They found that when the weight percentage of biomass was greater than 50%, there were large relative errors on minimum fluidization velocity between predicted values and experimental data.

Rao and Ram Bheemarasetti (T. Rao & Ram Bheemarasetti, 2001) studied fluidization of mixtures of biomass materials such as rice husk, sawdust and groundnut shell powder and two samples of sand differing in densities and particle sizes. The percentage of biomass materials in the mixtures studied was 2, 5, 10 and 15% by weight. They developed some equations based on effective density and effective diameter for predicting  $U_{mf}$  values of these mixtures which could successfully predict the experimental  $U_{mf}$  values up to 10% weight of biomass particles in mixtures. Rao and Reddy (K. V. N. S. Rao & Reddy, 2010) estimated the fluidization characteristics of the above-mentioned biomass materials in the presence of sand bed. They observed that, for good mixing and uniform distribution of biomass fuel with bed material, size of sand particles play a vital role. They also compared the experimental and theoretical  $U_{mf}$  values obtained from the literature correlations for these binary mixtures. They determined that the most suitable correlation to predict minimum fluidization velocities for three studied biomass fuels is that proposed by Todes (Todes, 1965).

Zhong et al. (Zhong, Jin, Zhang, Wang, & Xiao, 2008) studied the  $U_{mf}$  of a variety of biomass-inert material mixtures. The biomass particles included wood chips, mung beans, millet, and cotton stalk, and inert particles included silica sand, CFB cinder, and aluminum oxide. They determined that increasing diameter and length-to-diameter of long thin biomass types such as corn stalk and cotton stalk increases the minimum fluidization velocity of the mixture. Furthermore, increasing the weight percentage of biomass as well as the diameter and density of the inert particles leads to increasing the minimum fluidization velocity of binary mixtures. Studies of Ramakers et al. (Ramakers, de Ridder, & Kerkhof, 2004) on the fluidization behavior of wood/sand mixtures showed that correlations reported in the literature did not predict the minimum fluidization velocity very well for these mixtures.

Paudel and Feng (Paudel & Feng, 2013) determined experimentally  $U_{mf}$  of several biomass and inert materials as well as the binary mixtures of biomass (corn cob or walnut) and sand particles at biomass weight percentage ranging from 10 to 90% at 10% increment. They also developed new correlations to predict  $U_{mf}$  of inert particles, biomass particles, and biomass and sand mixtures in terms of biomass weight percentage. They found that the  $U_{mf}$ -based Reynolds number

for the mixture of biomass and inert particles depends on the weight percentage of biomass particles other than the Archimedes number. Accordingly, they proposed a new correlation including the weight percentage as an additional variable for the mixture of biomass and sand particles. This unified correlation could successfully predict the minimum fluidization velocity of the biomass-sand mixtures differing in composition.

### **2.2.2 Gas distribution and bubble characteristics**

The bubbles, also often called “voids”, form in gas-fluidized beds because a homogenous bed is unstable to perturbations once the fluidization velocity exceeds the minimum bubbling velocity ( $U_{mb}$ ). For particles in group B and D of the Geldart Classification e.g., sand and typical biomass particles,  $U_{mb}$  coincides with  $U_{mf}$ , which is then considered as the onset of bubbling (Crowe, 2010). The bubbles are surrounded by a “dense phase” or “emulsion” phase composed of particles and interstitial gas. The bubbles, originating in the immediate vicinity of the distribution plate, rise through the bed and, due to bubble coalescence, larger bubbles are formed. Alternatively, large bubbles break up and split into smaller ones. On the bed surface bubbles burst eruptively ejecting the particles far above the bed surface. The motion of bubbles produces very intensive particle circulation in fluidized bed. Behind the bubbles, in their “wake”, particles move upwards, and around the bubbles, among them and especially near walls, the particles move downwards. The motion of bubbles contributes to axial mixing of particles and gas in fluidized bed (Oka, 2010).

The particles presented in the bubbles and the amount of gas in the emulsion phase greatly influence the practical operations. Heat and mass transfer and reaction exist not only at the bubble-emulsion interface, but also inside the two phases. The dynamic structure of each phase and the dispersion of gas and solids into the two phases are matters of importance to effectively quantify the actual transfer and reaction rates in the fluidized beds (Heping Cui, N. Mostoufi, & J. Chaouki, 2001b).

The dynamic behavior of the two-phase flow structures in gas-solid fluidized have extensively been studied for mono-components systems containing conventional fluidization materials such as sand and FCC (D. Bai, Issangya, & Grace, 1999; Buyevich & Kapbasov, 1994; Cui, Li, et al.,

2000; Cui, Mostoufi, & Chaouki, 2000; Li, Wen, Ge, Cui, & Ren, 1998; Antonio Marzocchella, Zijerveld, Schouten, & van den Bleek, 1997; Musmarra, Poletto, Vaccaro, & Clift, 1995), while little attention has been devoted to that of multi-component systems. In practical fluidized beds containing biomass and inert material, the mass percentage of biomass is typically about 1-5%. Thus, the probable impact of irregular biomass particles on the bubbling features of the bed material, e.g. sand, is usually ignored. Very little work has carried out on the dynamics of the gas distribution between the dilute and dense phases of fluidization and characterization of bubbles in the presence of irregular particles.

Studying the amplitude of pressure fluctuations of a bed of sand and thin-long cylindrical cotton stalk particles, Zhang et al. (Yong Zhang, Jin, Zhong, Ren, & Xiao, 2009) found that biomass particles trigger bubble eruption which is more pronounced when the load of biomass increases. In other words, increasing the biomass concentration reduces the probability of bubble growth and coalescence (Y. Zhang, Jin, & Zhong, 2010).

Some researchers have shown that the bed density that is determined by the type and ratio of the components of the bed inventory, can affect gas holdup of the bed. Escudero and Heindel (Escudero & Heindel, 2011) fluidized different materials, i.e., glass beads, ground corncob, and ground walnut shell whose sizes varied between 500-600  $\mu\text{m}$ , and observed that the gas holdup in the bed increased by decreasing the bed density. Gas or solid holdup parameters are important for optimizing fluidization hydrodynamics and process efficiency. In a similar work performed in cold flow fluidized beds of 10.2 cm and 15.2 cm in diameter, Darke and Heindel (Drake & Heindel, 2012) concluded that bed mixing and uniformity is enhanced in both reactors when a lighter material was fluidized. All of these findings demonstrate that the presence of irregular particles impacts the gas distribution circumstances and bubbling behavior of the bed, though the biomass content is relatively low compared to fluidization medium. In view of the role of bubbles as the “mixing agents”, changes in the bubble characteristics can affect the extent of solids mixing in the bed which is crucially important from the design and operation point of view.

## 2.3 Mixing and segregation phenomena

### 2.3.1 Mixing and segregation in binary mixtures

Segregation of solids may take place when particles with different shapes, sizes, and/or densities are fluidized. Apart from cause of segregation, the component tending to sink to the bottom of the bed is referred to as “jetsam”, while that migrating to the fluidized bed surface is referred to as “flotsam”.

Segregation occurrence may be detrimental or beneficial, depending on specific applications. Operations like coal or biomass combustion, gasification and pyrolysis as well as waste incineration and catalytic polymerization all are samples of the simultaneous presence of two or more types of particles of different density and size in which good solid mixing is desired. Poor homogeneity of the particles can lower the overall process efficiency and complicates its thermal control. On the other hand, segregation is needed to separate one solid from the other in fluidized bed separators or classifiers which can be applied for coal cleaning, ore processing drying and waste separation. The knowledge of the fundamentals governing segregation or mixing is important for better using these phenomena to enhance the performance of operations. Therefore it has been a continuous subject of a large number of studies. In general, the concept of numerous papers published in connection to mixing and segregation can be categorized into three groups (Yong Zhang, Jin, & Zhong, 2008).

- Understanding the mechanism of mixing and segregation and providing empirical models based on the relationship between the fluidization gas velocity and the equilibrium concentration profile (Formisani, Girimonte, & Longo, 2008a; A. Nienow, Rowe, & Cheung, 1978; Tanimoto, Chiba, Chiba, & Kobayashi, 1980).
- Examining the equilibrium fluidization curves of binary mixtures to predict the fluidization behavior on the basis of the particle characteristics. (Formisani, Cristofaro, & Girimonte, 2001; A. Marzocchella, Salatino, Di Pastena, & Lirer, 2000; Noda et al., 1986; Olivieri, Marzocchella, & Salatino, 2004).
- Studying the dynamics of mixing and segregation. (T. Chiba, Chiba, & Nienow, 1986; M. C. Leaper, Seville, Hilal, Kingman, & Burbidge, 2004; A. Nienow & Naimer, 2011).

On the basis of these studies, many variables affect the mixing/segregation behavior, including particle properties such as particle size, density, and shape and operating conditions such as superficial gas velocity, particle concentration, initial packing condition, and bed aspect ratio (Feng, Xu, Zhang, Yu, & Zulli, 2004).

Joseph et al. have recently summarized main prior experimental studies performed on size, density and both size and density segregation (Joseph, Leboeiro, Hrenya, & Stevens, 2007). This summary (Table 2.2) covers diverse experimental conditions including various geometries of the employed fluidization columns and different Geldart groups of the used particles.

Differences in particle diameter or density are the two principal driving forces of segregation. Either factor is at work in situations of practical interests, where the solid charge is generally made of solids of different average sizes (e.g. sand and coal in fluidized bed combustors), so that assessing its role on segregation dynamics is an objective of great importance for devising criteria for process design and control. To accomplish this goal, literature studies have generally addressed the two mechanisms of segregation separately.

In the case of segregation only by size, usually larger particles tend to act as jetsam (M. J. V. Goldschmidt, Link, Mellema, & Kuipers, 2003; Wu & Baeyens, 1998). It is shown that increase in the bed height and mean size as well as decrease in the size of fines increases the segregation in such systems (D Geldart, Baeyens, Pope, & Van De Wijer, 1981). A layer inversion phenomenon, in which the role of species acting as flotsam and jetsam changes, may occur for such kind of segregation due to the increase in gas velocity, depending on the composition of components (M. G. Rasul, Rudolph, & Carsky, 1999).

In comparison with those devoted to size-segregating beds, papers that have specifically been focused on the mixing/segregation properties of density-segregating mixtures are much fewer, possibly because these have been judged easier. Very little is known also on the behavior of mixtures of fully dissimilar solids, in which the effects of density and size segregation overlap (Di Renzo, Di Maio, Girimonte, & Formisani, 2008). It is known that density difference is more significant than size difference (Rowe, Nienow, & Agbim, 1972).

Rowe et al. (Rowe et al., 1972), who used the jetsam and flotsam terms for the first time, attributed the component separation to the motion of bubbles in bed. In this regard, it is observed as the bubbles travel up through the bed, particles are drawn into a stagnant zone trailing the

bubble called the wake. Consequently, axial mixing occurs as the new particles from dense surrounding region (emulsion phase) are substituted for particles sloughed off (Hoffmann, Janssen, & Prins, 1993). The particles accompanying wakes are deposited at the bed surface as the bubble reaches the top of the bed so particles from the bottom of the bed may be mixed with those at the top. The void left behind the bubble during its rising is filled by particles falling down around the bubble. According to this mechanism, jetsam particles tend to fall just a little further while flotsam particles fall less quickly. At equilibrium, occurrence of these processes as the cause of simultaneous mixing and segregation results in a concentration gradient in the axial direction.

In systems like biomass fluidization, in which both density and size differ between two fractions which are present in the bed, density would have the dominating effect and the denser component act as jetsam except in very special cases (S. Chiba, Nienow, Chiba, & Kobayashi, 1980). Segregation as a bulk behavior results from the collective interactions among the individual particles, in addition to the interactions between gas and particle. Therefore, analysis on a particle scale based on information such as the trajectories of, and forces acting on, individual particles are critical to the elucidation of the governing mechanisms of mixing/segregation. Gas fluidization involves strong coupling between discrete particles and continuum gas, and is a very complicated dynamic process with vigorous temporal and spatial variation (Feng et al., 2004).

Table 2.2: Summary of representative experimental work on segregation (Joseph et al., 2007)

Reference	Species Differentiation			Conditions			Geometry			Geldart Group			
	$d_R$	$\rho_R$	$S:DL$	$S:DH$	$L:D$	$SS$	$Dyn.$	$2D$	$3D$	$C$	$A$	$B$	$D$
<i>A</i> : (Naimer, Chiba, & Nienow, 1982; A. Nienow, Naimer, & Chiba, 1987; Rowe & Nienow, 1976; Rowe et al., 1972)	✓	✓	-	✓	-	✓	-	✓	✓	-	✓	✓	✓
<i>B</i> : (D Geldart et al., 1981)	✓	✓	-	✓	-	✓	-	-	✓	-	-	✓	✓
<i>C</i> : (Wu & Baeyens, 1998)	✓	✓	-	✓	-	✓	-	-	✓	-	✓	✓	✓
<i>D</i> : (M. Rasul & Rudolph, 2000; M. G. Rasul et al., 1999)	-	✓	-	✓	-	✓	-	-	✓	✓	✓	✓	-
<i>E</i> : (A. Marzocchella et al., 2000; Olivieri et al., 2004).	✓	✓	✓	✓	✓	✓	✓	-	✓	-	-	✓	-
<i>F</i> : (M. J. V. Goldschmidt et al., 2003)	✓	✓	✓	✓	✓	✓	✓	✓	-	-	-	-	✓
<i>G</i> : (Huilin, Yurong, Gidaspow, Lidan, & Yukun, 2003)	✓	✓	-	✓	-	✓	-	-	✓	-	-	-	✓
<i>H</i> : (Joseph et al., 2007)	✓	✓	-	✓	-	✓	-	-	✓	-	-	✓	-

Ref.	Parameters	Principal Measurements	Reported		
			C.P.	M.I.	Trends
<i>A</i>	$U, x, d_R, H_R$	Frozen bed sieving	few	✓	Size-difference systems easiest to mix; jetsam: large particles. Mixing ↑ with presence of standpipe or perforated distributors. M.I. a logistic function of $U$ .
<i>B</i>	$U, d_R$	Frozen bed sieving	few	few	Size segregation ↑ when $d_{\text{fines}} \downarrow$ , $d_{\text{mean}} \uparrow$ , or $U \rightarrow U_{mf}$ . Jetsam: large particles.
<i>C</i>	$U, d_R$	Frozen bed sieving	few	✓	Segregation ↑ when $H_R \downarrow$ ( $H_R < 0.8$ ) or visible bubble flow rate ↓. Jetsam: large particles.
<i>D</i>	$U, x, d_R$	Visual observation of layers	-	-	Segregation ↑ when visible bubble flow rate ↓. Whatever component maximizes bulk density will act as jetsam.
<i>E</i>	$U$	Pressure time-trace analysis	few	✓	Concentration of fluidized top layer and defluidized bottom layer independent of initial mixture concentration.
<i>F</i>	$U, x, H_R$	Digital image analysis	-	✓	Segregation ↑ and segregation rate ↑ when $H_R \downarrow$ or $x \uparrow$ . Jetsam: large particles.
<i>G</i>	$x, d_R$	Frozen bed sieving	✓	✓	Segregation ↑ as $U \downarrow$ . Jetsam: large particles.
<i>H</i>	$U, x, d_R, H_R$	Frozen bed sieving	✓	-	

**Segregation focus nomenclature:**  $d_R$  / different size, same density;  $\rho_R$  / different density, same size  
**S:DL** / small is denser and lighter; **S:DH** / small is denser and heavier; **L:D** / large is denser  
**Conditions:** **SS** / steady-state segregation; **dyn** / dynamic segregation.  
**Reported results:** **C.P.** / concentration profiles; **M.I.** / mixing indices.  
**Parameters varied:**  $U$  / gas velocity;  $x$  / jetsam concentration;  $d_R$  / particle size ratio;  $\rho_R$  / particle density ratio;  $H_R$  / bed aspect ratio.

A common approach for assessing the extent of mixing/segregation is defining an index usually called “mixing index”. The mixing index is traditionally calculated on the basis of mass fraction of jetsam particles, i.e., those particles that, in general, should be found in the bottom of the bed. It compares the mass fraction of jetsam particles found in the upper region of the bed ( $x_U$ ), a region which is user defined, with the overall mass fraction of jetsam particles in the whole bed ( $x_T$ ). It assumes that the jetsam particles are evenly distributed in the upper region. Hence, the mixing index is calculated as

$$MI = \frac{x_U}{x_T} \quad (2.1)$$

For  $MI=0$ , the bed is completely segregated about a horizontal plane and for  $MI=1$ , the bed is perfectly mixed.

This definition of mixing index is subject to some restrictions such as assuming an even distribution of jetsam in the upper region of the bed and getting influenced by what is defined as the upper region which results in producing values outside a commonly acceptable range of 0–1. Moreover, the maximum values are a function of particle density and bed mixture volume or mass ratio. This makes it challenging when comparing mixing levels for different particle types and different overall volume fractions (Keller, Bai, Fox, & Heindel, 2013).

The mixing index is conventionally obtained via the following steps in the experimental set-ups: (a) ‘freezing’ the bed by a sudden stop of the gas supply, (b) dividing the ‘frozen’ bed into several sections, (c) removing the particles of each section, and (d) analyzing the size or density distribution of the particles. This procedure is very laborious and suffers a great deal of uncertainty due to the stochastic nature of solids mixing in fluidized beds. In addition, the results may be distorted during the bed slumping transients for rapid solids mixing rates. Thus, more accurate techniques are required to assess the “*in situ*” distribution of biomass or inert material particles in the bed.

Gibilaro and Rowe (Gibilaro & Rowe, 1974) constructed a simple equilibrium model to predict jetsam volume concentration against bed height. This model has been widely adopted by many investigators to interpret the steady and transient concentration profiles in segregating fluidized beds (K. Lim, Zhu, & Grace, 1995). The Gibilaro-Rowe (G-R) model is based on the counter-current back-mixing (CCBM) model used usually for description of axial solids mixing in

bubbling fluidized bed. According to the CCBM, the movement of solids in the fluidized bed can be described in terms of two separate phases; i.e., a phase consisting of upward moving gas and particles (bubble wake and cloud regions in the dilute or bubble phase) and a phase of downward moving particles and interstitial gas (dense or emulsion phase) (Kok S Lim, Gururajan, & Agarwal, 1993). Accordingly, solids flows in the Gibilaro-Rowe model are controlled by four mechanisms of particles transport: 1) gross solids circulation, 2) exchange between bubble and emulsion phases, 3) axial drift-dispersion mixing, and 4) segregation. Gross circulation is the movement of solids from the bottom of the bed to the surface via the wake phase and also their return to the bottom through the downward motion of the dense phase. The exchange mechanism is the movement of solids between the dense and dilute phase as a result of bubble wake shedding proportional to the concentration difference between the two phases. Axial mixing represents the rising motion of jetsam particles in a pseudo-diffusion mechanism as a side effect of bubble movement. It has been shown that this term could safely be dropped from the mass balance due to its small impact compared to the other mechanisms (Cooper & Coronella, 2005). Finally, as Gibilaro and Rowe assumed, segregation is representative of the tendency for jetsam to percolate through the emulsion phase as compared with its tendency to be mixed by bubbles (Mark C. Leaper, King, & Burbidge, 2007). However, Yoshida et al. attributed this mechanism to the bubble wakes (K. Yoshida, Kameyana, & Shimizu, 1977). Fig. 2.1 elucidates the interaction of these mechanisms when applied to a slice of a fluidized bed.

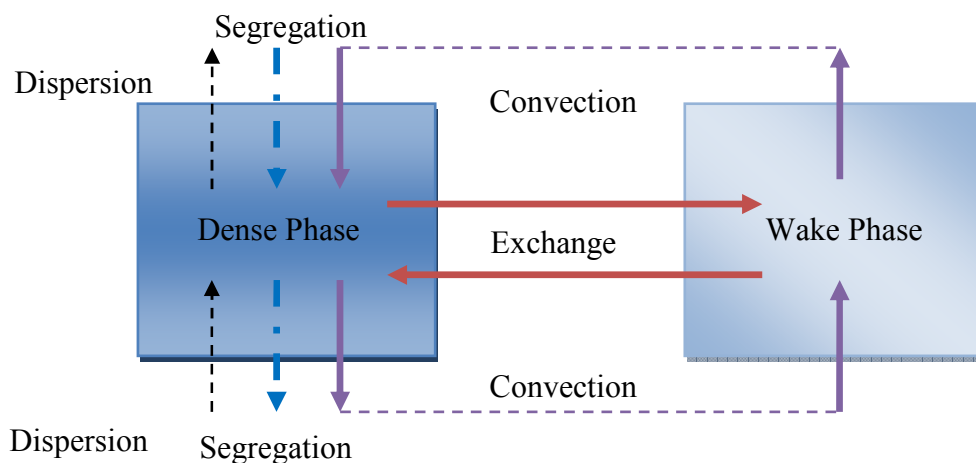


Fig. 2.1: Schematic representation of the model describing segregation in fluidized bed

The G-R model has limited use beyond indicating trends and comparing the relative influence of the different mechanisms involved, since linking the model parameters to real values such as fluidizing velocity and particle size is not straightforward (Naimer et al., 1982). However, some researchers have attempted to relate some of the model parameters to the tangible fluidization parameters (Mark C. Leaper et al., 2007).

### **2.3.2 Mixing and segregation in systems containing biomass**

In biomass fluidized bed combustors or gasifiers large differences in size and density between fuel and inert particles lead to a non-uniform distribution of fuel within the bed. If the vertical mixing between fuel and sand particles is low, and the fuel particles tend to float in the upper regions of the bed, volatiles are released into the freeboard which results in maldistribution of the gas reactants and products. For instance, non-uniform distribution of oxygen across the bed influences the combustion of fuel particles leading to the occurrence of hot/cold spots and ash softening.

In spite of its crucial importance, few studies carried out on mixing/segregation phenomena of biomass fluidization. It should be noted that mixing/segregation behavior of typically studied binary mixtures may not successfully be generalized to systems containing biomass because of the peculiar characteristics of biomass particles, which make them very different from the conventional fluidization materials.

Hemati et al. (Hemati, Spieker, Laguérie, Alvarez, & Riera, 1990) studied mixing and segregation of wood sawdust ( $d_p=345-400 \mu\text{m}$ ,  $\rho_p=500 \text{ kg/m}^3$ ) and coal ( $d_p=425-1000/1700-1800/1000-2360 \mu\text{m}$ ,  $\rho_p=1300 \text{ kg/m}^3$ ) in a bed of sand and alumina particles. Adopting the “*frozen-bed*” technique, they quantified the degree of mixing in bed via defining a mixing index for a vast range of fluidization velocity. On the basis of their findings, strong segregation occurred between sawdust and sand particles for  $U/U_{mf}$  less than 2.5, while uniformity of mixing increased with an increase in the fluidization velocity.

Mourad et al. (Mourad, Hemati, & Laguerie, 1994) scrutinized the hydrodynamic behavior of a fluidized bed dryer containing corn kernels and sand with a size ratio of 25 and density ratio about 0.45. For corn-to-sand weight ratio above 0.14, the pressure drop vs. gas velocity curve of the system showed four regions, corresponding to fixed bed, fully segregated, partially segregated

and completely fluidized beds, respectively. This result was confirmed by the measure of the axial concentration profiles of corn in the bed.

Wirsum et al. (Wirsum, Fett, Iwanowa, & Lukjanow, 2001) studied mixing and segregation behavior of biomass-like spherical solids, 20 to 40 mm in diameter, in a bubbling fluidized bed of quartz sand. They utilized a novel detection technique to obtain single large particle trajectories and consequently the time average segregation patterns of the solid mixtures. The method was based on interactions between a magnetic field imposed on the fluidized bed chamber and a single metal covered tracer particle, which was moving inside the bed, so position of the tracer could be determined at sample rates up to 50 Hz inside a space of approximately 50×50×50 cm. They understood that segregation strongly depends on the excess gas velocity, average diameter of the fluidized sand (jetsam) and flotsam size and density. They concluded that, in general, smaller and denser flotsams could improve vertical mixing as well as smaller sand particles and higher superficial gas velocities.

Shen et al. (L. Shen et al., 2007) developed a digital image processing technique to investigate the biomass mixing in a 2D fluidized bed operating at  $U=0.52$  to 1.22 m/s. They used red wooden balls as the tracer particles injected by gravity into the splash zone of a bed of glass beads in about 0.2 second. The experimental results showed a high degree of biomass mixing in the vertical direction in the bed, whereas horizontal mixing in the bottom zone was found to be relatively limited. Surprisingly, Shen et al. reported that along the vertical direction of the bed, a more uniform distribution of biomass particles was found at a low superficial velocity than at a high superficial velocity: the biomass concentration in the bottom region decreased with the superficial velocity, but increased in the upper region of the bed. Studying the lateral mixing behavior of the particles, they observed that the biomass concentration in the center increased with the superficial velocity, whereas it decreased in the wall region.

Zhang et al. (Yong Zhang, Jin, Zhong, et al., 2009) conducted extensive research on fluidization, mixing, and segregation of biomass containing systems. They carried out pressure fluctuation analysis and employed “*frozen-bed*” method to characterize the fluidization and segregation of the mixtures of sand and cotton stalk particles differing in the load of biomass. Furthermore, applying image processing technique, they could follow the alteration of bubble size and population and visualize a set of mixing/segregation patterns as gas velocity increased. As

reported, at  $U$  slightly larger than  $U_{mf}$ , there is a continuous passage of small bubbles through the bed for the system initiated from the well-mixed conditions. These bubbles move up a part of biomass particles to the top part of the bed. Large exploding bubbles occur at high gas velocity at which segregation takes place more rapidly. Consequently, a nearly pure layer of biomass particles forms floating at the top layer of the bed. Due to the vigorous motion of bubbles at gas velocities about the transition velocity from bubbling to turbulent regime of fluidization ( $U_c$ ), the floating biomass layer is completely involved in mixing, so the strong fluidization brings about the spreading of biomass particles throughout the bed. When gas velocity is further increased, the size of bubbles become much smaller compared with the previous states, as a result, more biomass particles are observed again at the upper part of the bed.

Zhang et al. (Yong Zhang et al., 2008) also studied the effect of the initial packing state of the bed components on their mixing behavior. Accordingly, three initial conditions were considered, i.e. completely segregated state with biomass over the sand (case 1), perfectly mixed (case 2), and completely segregated with biomass beneath the sand (case 3), all representing different feeding strategies of commercial biomass units. It was realized that at low gas velocities, i.e.  $U_{if} < U < U_{ff}$ , the mutual hydrodynamic behavior of biomass and sand particles is greatly influenced by the initial packing states. For instance, for the case 3 and at low gas velocity, the bubbles formed in the bed are too small to lift the biomass particles to the bed surface. Thus, the bottom layer acts as a porous plate gas distributor for the sand located over it. As gas velocity increases, fractions of biomass are transported to the bed surface as a consequence of bubble growth. Once the force exerted by gas is sufficient to break the cohesion and liaison forces between biomass particles, channeling phenomenon appears accelerating rise of biomass particles to the bed surface. Finally, compared with the initial state, an inverse bed could be observed at  $U = U_{ff}$ , where sand particles are mainly located beneath the biomass. Fig. 2.2 shows the evolution of mixing/segregation vs. superficial gas velocity for different initial conditions. Zhang et al. observed that at  $U > U_{ff}$ , the extent of segregation decreased and then slightly increased with gas velocity. They concluded that there is a specific velocity at which the systems studied reach the maximum degree of mixing. As examined for the different mixing ratios of biomass, this velocity is a function of load of biomass.

In addition to the aforementioned findings, Zhang et al. (Yong Zhang et al., 2008) compared the rate and extent of segregation of sand and biomass particles for three cases differing in initial

packing state (the ternary above-mentioned cases). As reported, the degree of segregation is not affected by the initial conditions; however, the segregation rate decreases from case 1 to case 3. It was remarked that the time needed to reach the steady state is proportional to the extent to which the initial system conditions deviate from the equilibrium. Furthermore, it was noted that for all cases this time is inversely proportional to gas velocity. The positive influence of gas velocity on enhancement of the mixing state of the bed was also observed for all cases, regardless of the initial packing conditions.

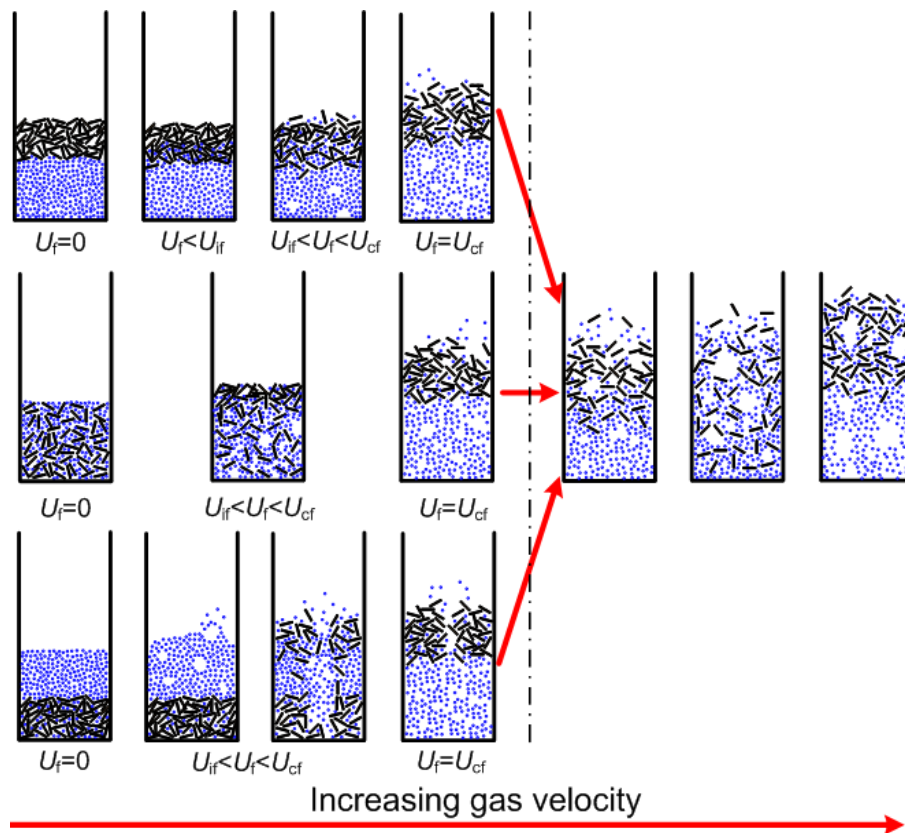


Fig. 2.2: Pattern of mixing and segregation for different initial conditions (Yong Zhang et al., 2008)

## 2.4 Numerical modeling of gas-solid fluidized beds

Lack of sufficient information on particle-scale impedes the development of a viable method to scale-up, design, control, and optimize mixing/segregation behaviors (Shoushtati, Hosseini, & Soleimani, 2013). In spite of significant progress in developing the experimental techniques

adopted to study the characteristics of gas-solid flows, these approaches are not capable enough to extract the dynamic information on transient flow structure and the forces exerted on the particles. Several numerical methods developed in the past two decades have enabled researchers to virtually realize simultaneous measurement of some key parameters. Despite these achievements, the construction of reliable models for large-scale gas-solid fluidized beds is seriously hindered by lack of understanding of the fundamental of dense gas-particle flows. In particular, the phenomena which can be related to the effective gas-particle interaction (drag forces), particle-particle interactions (collision forces), and particle-wall interaction, are not well understood. The prime difficulty is the large separation of scales: the largest flow structures can be of the order of meters; yet these structures are influenced by details of the particle-particle and particle-gas interactions, which take place on the scale of millimeters, or even micrometers (Deen, Van Sint Annaland, Van der Hoef, & Kuipers, 2007) (see Fig. 2.3).

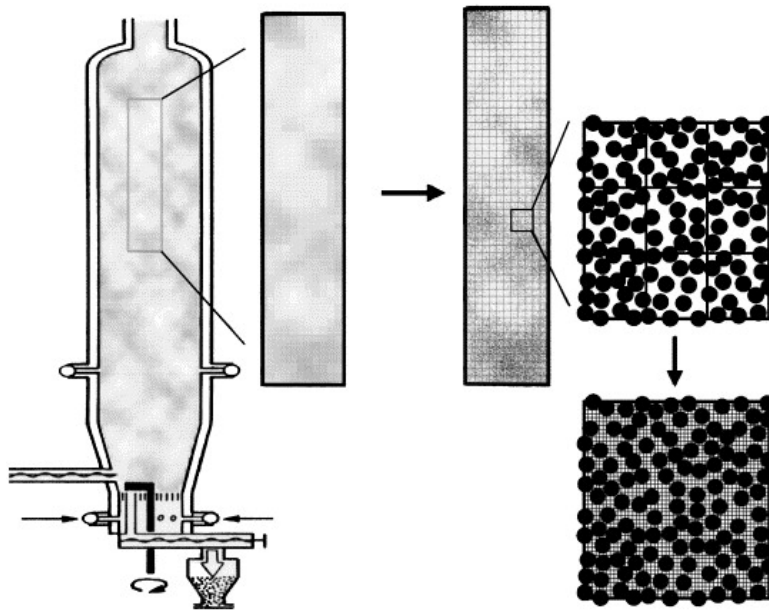


Fig. 2.3: Graphic representation of the multi-level modeling scheme. (Van der Hoef et al., 2006)

Numerical approaches used in the literature for modeling particle-fluid flow can be divided into two categories: continuum-continuum (Eulerian-Eulerian) and continuum-discrete (Eulerian-Lagrangian) models. These models are discussed in details.

### 2.4.1 Eulerian-Eulerian approach

Continuum or Eulerian-Eulerian models assume that the dispersed phase behaves as a fluid and collections of particle are modeled using continuous medium mechanics. The fluid and solid phases are treated as interpenetrating continuum phases. Accordingly, the integral balances of continuity, momentum and energy are constructed for both phases, with appropriate boundary conditions as well as the jump conditions for phase interfaces. Two-fluid model (TFM) regarded as a continuum-continuum is the most commonly used approach for predicting the dynamic behavior of fluid-particle systems (Pain, Mansoorzadeh, & De Oliveira, 2001). The formation, rise and eruption of a single bubble in a two-dimensional fluidized bed has been simulated by Gidaspow (Dimitri Gidaspow, 1986) and Kuipers et al. (J. Kuipers, Van Duin, Van Beckum, & Van Swaaij, 1992; J. A. M. Kuipers, Prins, & Van Swaaij, 1992) using the TFM.

There are many ways, depending on the averaging procedure and the closure laws adopted, to formulate a two-fluid model. The general idea is to first formulate the integral balances for mass, momentum and energy for a fixed control volume containing both phases. This balance must be satisfied at any time and at any point in space, and thus reduces into two types of local equations, one being the local instantaneous equations for each phase and the other an expression of the local instantaneous jump conditions, i.e. the interactions between the phases at the interface. In principle, this set of equations could be solved by direct simulation, i.e. using a numerical mesh finer than the smallest length scales of the flow and a time step shorter than the time scales of the fastest fluctuations (Enwald, Peirano, & Almstedt, 1996).

For the Eulerian-Eulerian approach, the local instantaneous equations must be averaged in a suitable way, either in space, in time or as an ensemble. This allows a coarser mesh and a longer time step to be used in the numerical simulation, but introduces more unknowns than the number of equations into the system, and thus necessitates the inclusion of additional expressions to close the set of equations. The closure laws are of three types: topological, constitutive and transfer laws, where the first type describes the spatial distribution of phase-specific quantities, the second type describes physical properties of the phases and the third type describes different interactions between the phases. As most of these expressions are empirical, experimental data are needed in order to develop and verify the laws (Enwald et al., 1996).

Most of two-fluid models used in the literature suffer from uncertainties in prescribing the viscosity and normal stress of the solid phase. Various non-Newtonian models for the internal stresses of the solid phase have been proposed. These viscosities have been correlated with the experimental observations. However, the need for a more systematic way of prescribing viscosity has led to the popularity of the granular temperature model, which is based on an analogy between kinetic theory of gases and binary particle-particle collisions. The granular temperature (defined as one-third times the fluctuating velocity squared) is introduced to represent the specific kinetic energy of the velocity fluctuations or the translational fluctuation energy resulting from the particle velocity fluctuations. In granular flow, particle velocity fluctuations about the mean are assumed to result in collisions between particles being swept along together by the mean flow. The granular particle temperature equation can be expressed in terms of production of fluctuations by shear, dissipation by kinetic and collisional heat flow, dissipation due to inelastic collisions, production due to fluid turbulence or due to collisions with molecules, and dissipation due to interaction with the fluid (D. Gidaspow, 1994). Use of granular temperature provides a means of calculating the internal stresses without resorting to correlations (Pain et al., 2001).

In TFM, the solid particles are generally considered to be identical having a representative diameter and density. Therefore, the constitutive or closure relations used for momentum exchange between the solid phases, especially in case of a particulate system with particle size distribution, play an important role in the success of the two-fluid model. The population balance-based methods are used to describe the particle size distribution in these systems (Shoushtati et al., 2013).

Most models reported in the literature are based on a two-phase description, one gas and one solid phase, where all the particles are assumed to have identical diameter, density and restitution coefficient. However, the concept of TFM has been generalized to multi-fluid model (MFM) in which  $M$  phases are considered. Each solid phase is uniquely defined by a diameter, density and restitution coefficient. The presence of each phase is described by a volume fraction, varying from zero to one (Vidar Mathiesen, Tron Solberg, & Bjørn H Hjertager, 2000).

Jenkins and Mancini (J. T. Jenkins & Mancini, 1987) extended the kinetic theory for granular flow to binary mixtures. Some research groups have performed computational studies of bi-disperse mixtures, still characterized by particles of constant diameter, trying to predict particle

mixing and segregation (Mazzei, 2011). Mathiesen et al. (Vidar Mathiesen et al., 2000) developed a multiphase gas/solids flow model and performed simulations with one gas and three solid phases. The model predicted segregation effects fairly well and a good agreement with experimental data was demonstrated. A modified multiphase gas/particle flow model was also proposed that was generalized and made consistent for one gas phase and  $N$  number of solid phases to enable description of realistic particle size distribution (V. Mathiesen, T. Solberg, & B. H. Hjertager, 2000). The laws of conservation of mass, momentum and granular temperature are satisfied for each phase individually. The dependent variables, i.e. the volume fraction and the momentum, are solved for each phase. All the phases share a fluid pressure. A conservation equation for granular temperature is solved for each solid phase.

On the basis of the multi-fluid model, it is assumed that the disperse phase is constituted of classes of particles with equal and constant diameters. Real multiphase systems are instead characterized by wide particle size distributions (PSDs) that change continuously owing to fluid-particle and particle-particle interactions. Predicting their evolution is important to describe realistically fluidized suspensions, since the PSDs affect product quality, mixing and segregation patterns, chemical reaction rates, heat transfer rates, loss of non-reacted materials and many other parameters. The constant particle size assumption limits the model flexibility: solids can mix and segregate, but variations in their diameters are not allowed for (Mazzei, 2011). In reality, though, particles can grow, shrink, aggregate, break and nucleate; consequently, their size distribution changes continuously in time and space. Predicting this evolution, which depends on the local conditions wherein the system operates, is essential for a reliable description of the mixture behavior. It can be achieved by solving a population balance equation (PBE). Few attempts to implement the PBE into multiphase CFD codes can be found in the literature to model dense gas-solid systems (Fan & Fox, 2008; Fan, Marchisio, & Fox, 2004; Mazzei, Marchisio, & Lettieri, 2009).

Gera et al. (Gera, Syamlal, & O'Brien, 2004) performed 2D Eulerian-Eulerian simulations validated by experimental work on a mixture of particles having same density but differing in size (1.5 and 2.5 mm glass beads). They showed that segregation took place when the fluidization velocity ( $U$ ) was set between the minimum fluidization velocities ( $U_{mf}$ ) of the small and large glass beads. For superficial gas velocities higher than  $U_{mf}$  of the large particles, segregation disappeared in favor of robust mixing. Studying a similar mixture, Fan et al. (Fan & Fox, 2008)

used 2D Eulerian-Eulerian approach for modeling segregation of dissimilar particles. They validated their calculations via the experiments conducted by Goldshmidt et al (M. Goldschmidt, Kuipers, & Swaaij, 2001). On the basis of the simulation and experiment results, the large particles accumulated at the lower parts of the bed. The mixing state improved by raising the excess gas velocity ( $U - U_{mf}$ ).

Huilin et al. (Huilin, Yurong, & Gidaspow, 2003) carried out some experiments on a binary mixture of particles differing in size or density in a 3D cylindrical column; however their Eulerian-Eulerian calculations were done in a 2D system. Based on the experiment and simulation results, the larger/heavier particles showed jetsam behavior and mixing was enhanced by increasing superficial gas velocity, regardless of the type of particles mixed. Despite the reported agreement between the results of the 3D experiment and 2D simulations, it is worth pointing out that 2D calculations do not always represent correctly the hydrodynamics of cylindrical fluidized beds (Detournay, 2011).

Gao et al. (Gao, Chang, Lu, & Xu, 2008) performed an experimental study and 3D Eulerian-Eulerian simulations on a binary mixture composed of particles having similar densities. In the studied range of gas velocity, segregation was enhanced by increasing  $U$  and reduced when the weight fraction of the fine particles increased in the mixture. Furthermore, the calculations showed the occurrence of radial segregation: higher concentration of fine particles close to the wall in comparison with the center of the bed.

## 2.4.2 Eulerian-Lagrangian approach

In the Lagrangian approach of modeling multiphase flow systems, particles are modeled as discrete elements and the Newtonian equations of motion for each individual particle are solved with inclusion of the effects of particle collisions and forces acting on the particles by the gas. In this approach, the flow of fluid which is considered as a continuum phase is described by the local averaged Navier-Stokes equation. Thus this approach is a coupling of computational fluid dynamics and discrete particle method (CFD-DPM). Discrete particle models or DPMs have been used for a wide range of applications involving particles ever since it was first proposed by Cundall and Strack (Cundall & Strack, 1979). The coupling of the DPM with a finite volume

description of the gas-phase based on the Navier–Stokes equations was first reported in the open literature by Tsuji et al. (Tsuji, Kawaguchi, & Tanaka, 1993) and Hoomans et al. (Hoomans, Kuipers, Briels, & van Swaaij, 1996) for the particle-particle collisions modeled by the soft-sphere and hard-sphere approaches, respectively.

In a hard-sphere system the trajectories of the particles are determined by momentum-conserving binary collisions. The interactions between particles are assumed to be pair-wise additive and instantaneous. In the simulation, the collisions are processed one by one according to the order in which the events occur and the possible occurrence of multiple collisions at the same instant cannot be accounted for. For not too dense systems, the hard-sphere models are considerably faster than the soft-sphere models. At high particle number densities or low coefficients of normal restitution, the collisions will lead to a considerable decrease in kinetic energy. This is the so-called inelastic collapse, in which regime the collision frequencies diverge as relative velocities vanish. Clearly in that case, the hard-sphere method becomes useless (Deen et al., 2007).

In more complex situations, the particles may interact via short- or long-range forces, and the trajectories are determined by integrating the Newtonian equations of motion. Soft-sphere models use a fixed time step and consequently the particles are allowed to overlap slightly. The contact forces are subsequently calculated from the deformation history of the contact using a contact force scheme. The soft-sphere models allow for multiple particle overlap although the net contact force is obtained from the addition of all pair-wise interactions. The soft-sphere models are essentially time driven, where the time step should be carefully chosen in the calculation of the contact forces. The soft-sphere models that can be found in literature mainly differ from each other with respect to the contact force scheme that is used (Deen et al., 2007).

The coefficient of restitution quantifies the elasticity of particle collisions between 1, for fully elastic collisions, and 0 for fully inelastic collisions (Taghipour, Ellis, & Wong, 2005). It was utilized by Jenkins and Savage (J. Jenkins & Savage, 1983) to account for the loss of energy due to collision of particles, which is not considered in the classical kinetic theory. The energy dissipated as a result of collisions of granular inelastic particles has been calculated to obtain the ratio of the velocity fluctuations to the mean flow as a function of the coefficient of restitution (Lun, 1991). A decrease in the coefficient of restitution results in less elastic collisions generating

more fluctuating kinetic energy (M. Goldschmidt et al., 2001). In dense two-phase flows, the particle interaction time may be much larger than the particle mean free flight time. Thus, the assumption that a pair of particles completes its interaction before interacting with another particle may be invalid as the solids concentration increases (D. Zhang & Rauenzahn, 2000).

Since no pre-defined assumption is considered for describing the rheological behavior of solid phase in the CFD-DPM model, it provides a way for conducting more fundamental studies on the multiphase flows as well as directly studying the hydrodynamics of fluidized beds. The CFD-DPM approach provides elaborate information on the trajectories of particles and the transient forces existing between the particles with each other and the particles with the fluid. Therefore, this method gives a reliable way of investigating the underlying physics of gas–solid flow (A. B. Yu & Xu, 2003). Furthermore, the CFD-DPM results provide velocity, contact time of particles at any moment of the simulation, which are not easily accessible through the experimental techniques. These unique capabilities enable researchers to deeply investigate mixing, segregation, agglomeration and the aggregation of particles and formation, growth, coalescence and breakage of bubbles in fluidized beds (Norouzi, Mostoufi, & Sotudeh-Gharebagh, 2012).

In the two-fluid approach, assumptions need to be made concerning the solids rheology where often Newtonian behavior is assumed in absence of a more detailed knowledge. In DPM these assumptions do not need to be made since the motion of each single particle is directly calculated while accounting for interactions with other particles and the continuous phase. In fact, these simulations enable the calculation of transport coefficient like effective viscosity and self-diffusion as it is done in molecular dynamics (MD) since all information is readily available (Chiesa, Mathiesen, Melheim, & Halvorsen, 2005). However, the CFD–DPM simulation has a disadvantage in comparison to the TFM model. The CFD–DPM simulation requires more computational resources and in case of large fluidized beds with millions of particles the computation demands is considerable and, often, limiting. Thus, the application of CFD–DEM method is limited to the lab-scale fluidized bed.

The distinct element method, DEM, is one of the trajectory models, which can calculate the particle velocity and the corresponding particle trajectory to examine interactions, such as those due to multi-body collisions (Kaneko, Shiojima, & Horio, 1999). Trajectory models are applied

to multiphase flows for dilute systems where a continuum model for the particle is not appropriate.

In recent years, CFD-DEM has been more and more widely used to elucidate the mechanisms governing mixing/ segregation (Zhu, Zhou, Yang, & Yu, 2008). Feng et al. (Feng & Yu, 2007) used an Eulerian-Lagrangian approach to model mixing and segregation of particles having identical density but different sizes (1 and 2 mm). They also analyzed the mechanisms of mixing/segregation from the information about the interaction forces between particles and between particles and fluid. The simulation results showed that increasing the weight percentage of the small particles led to decreasing the full fluidization velocity. The dynamic equilibrium between mixing and segregation was established fairly rapidly (in order of some tens of seconds), which reduced by raising superficial gas velocity (Feng et al., 2004). The difference in the upward drag force on flotsam and jetsam particles produces separation in the loose regions. Feng and Yu (Feng & Yu, 2008) also showed that the drag law used for modeling and the interaction between particles play a key role in determining the phenomena governing segregation in fluidized beds. These results were confirmed through the studies of Leboireiro et al. (Leboireiro et al., 2008) by adopting different drag laws for mono and polydisperse systems.

Taking a two dimensional Eulerian-Lagrangian approach, Di Renzo et al. (Di Renzo et al., 2008) modeled a mixture of glass and steel particles differing in density but similar in size (around 440  $\mu\text{m}$ ). Their model could successfully predict the flotsam (jetsam) behavior of the glass (steel) particles at two gas velocities studied.

CFD-DEM simulations show that the mixing is affected by initial packing structure, gas velocity and particle properties. The final equilibrium state is not significantly affected by the initial packing of particles (Bokkers, van Sint Annaland, & Kuipers, 2004; Feng et al., 2004; Rhodes, Wang, Nguyen, Stewart, & Liffman, 2001). The rate and the degree of mixing increase with gas velocity for fluidized beds, but decrease with the increase of particle diameter. Dahl and Hrenya (Dahl & Hrenya, 2005) further examined the effect of size distribution on segregation, and showed that the degree of segregation increases with an increase in the width of particle size distribution, and segregation is attenuated as bubbling becomes more vigorous.

In spite of the capability of the DEM method to provide analysis of flows with a wide range of particle types, sizes, and shapes, computational complexities arise when the particles population

in the system surpasses a quantity (e.g.,  $2 \times 10^5$  particles). Indeed, the high collision frequencies with particle volume fractions above 5% and the computational complexity of analyzing dense particle–particle interactions limit the number of particles in current Lagrangian calculations (Chen, Werther, Heinrich, Qi, & Hartge, 2012). Another crucial point when using the DEM model, even for the two-dimensional (2D), is the CPU-time consumption of detections of particle collisions. When the particles are densely packed in the flow or in regions of the flow, an effective algorithm for collision detection is necessary (Chiesa et al., 2005).

The Computational Particle Fluid Dynamics (CPFD) numerical scheme is an Eulerian–Lagrangian model for gas–solids flows that incorporates the multiphase-particle-in-cell (MP-PIC) method to describe the solid phase. The MP-PIC method calculates the fluid phase using an Eulerian computational grid and the solid phase using Lagrangian computational particles. In MP-PIC, a particle stress gradient term is added to the equation of motion of particles. In the computation, the stress gradient on the grid is first calculated and then interpolated to discrete particles. In CPFD, a “numerical particle” is identified as an ensemble of particles with close properties such as species, size, and density (D. M. Snider, 2007). The “numerical particle” provides a numerical approximation for the solid phase, similarly as the numerical control volume provides for the fluid phase, where its properties are considered essentially identical (Abbasi, Islam, Ege, & de Lasa, 2013). With these computational particles, large commercial systems containing billions of particles can be analyzed using millions of computational particles. The CPFD scheme then allows for extremely efficient calculations of gas–solids fluidization in industrial units. With these attractive advantages, the CPFD scheme has been used for analyzing the fluidized beds (P. Zhao, O’Rourke, & Snider, 2009), bubbling beds (Karimipour & Pugsley, 2012; Dale Snider & Banerjee, 2010) and a fast fluidized bed steam coal gasifier feeding section (Abbasi, Ege, & De Lasa, 2011) in recent years.

### **2.4.3 Numerical modeling of biomass fluidization**

The interest in numerical modeling and simulating fluidization of multi-component mixtures, whose components differ in size or density, is markedly growing; however, number of works done on the hydrodynamics aspects of biomass fluidization units is comparatively few due to the

great complexity of such systems. Compared to the experimental attempts, the computational approaches have received even much less attention.

Yin et al. (Yin, Rosendahl, K Kær, & J Condra, 2004) modeled co-firing biomass with natural gas in 10 m long wall-fired burners in which the particle phase equations were formulated in a Lagrangian frame. Instead of the common assumption of the spherical shape of biomass particles, they assumed solid or hollow biomass cylinders. Accordingly, the particle force balance was modified by considering the shape effect on the drag and lift forces. The shape factor-dependent parameters were also considered in the reaction of biomass particles. The simulation results indicated the shape of the biomass is a key parameter to accurately model the motion and the reaction of the biomass particles.

Qiaoqun et al. (Qiaoqun et al., 2005) investigated experimentally the fluidization behavior of a binary mixture of sand and rice husk particles. They also simulated the experimented systems via a multi-fluid model based on the kinetic theory of granular flow in which transport equations are used for each individual particle phase and momentum exchanges between different particle phases and between particle and gas phases are taken into account. They could predict the distributions of the mass fraction of rice husk particles and the mean particle diameter of mixtures of sands with various sizes and rice husk particles.

Deza et al. (Deza, Franka, Heindel, & Battaglia, 2009) validated the computational simulations of a fluidized bed in a multi-fluid Eulerian-Eulerian framework through X-ray imaging measurements. Like Yin et al. (Yin et al., 2004), they affirmed that the hydrodynamics of the bed is sensitive to the biomass particle sphericity variations; however, the coefficient of restitution does not affect it meaningfully.

Min et al. (Min, Drake, Heindel, & Fox, 2010) simulated a lab-scale fluidized bed reactor with and without side-gas injection. Full Eulerian-Eulerian 3D simulations with different drag models in a fluidized bed without side-gas injection were compared with 3D X-ray computed tomography measurements. Experimental and computational fluid dynamic (CFD) simulation results, when no side-gas was injected, confirmed the occurrence of two large off-center symmetric regions in which the gas holdup was larger than in the center of the fluidized bed. The immediate volatilization of biomass was simulated by side-gas injection and the pertinent experimental and computational results were acceptably in agreement.

Bai et al. (W. Bai, Keller, Heindel, & Fox, 2012) studied segregation of bed species in a cylindrical fluidized bed containing varying volume fractions of ground walnut shell particles and glass beads, both of which belong to Geldart B type particles. A 2D multi-fluid model based on the kinetic theory of granular flow was chosen to carry out the simulations. Increasing the ratio of biomass at  $U=U_{mf}$  increased the extent of segregation. However, the tendency of mixing of biomass and glass beads rose by increasing gas velocity, regardless of the ratio of the two components in the mixture, thus the extent of segregation in different mixtures became comparable at high superficial gas velocities. Both experimental and computational results showed that small and light particles do not mix well with large and heavy particles, whereas large and light particles mix well with small and heavy particles.

## CHAPTER 3

### **ARTICLE 1: THE EFFECT OF BIOMASS PARTICLES ON THE GAS DISTRIBUTION AND DILUTE PHASE CHARACTERISTICS OF SAND-BIOMASS MIXTURES FLUIDIZED IN THE BUBBLING REGIME**

Farzam Fotovat<sup>1</sup>, Jamal Chaouki<sup>1</sup>, Jeffrey Berghorson<sup>2</sup>

<sup>1</sup>Department of Chemical Engineering, École Polytechnique de Montréal, C.P. 6079, Succursale Centre Ville, Montreal, QC, Canada, H3C 3A7

<sup>2</sup>Department of Mechanical Engineering, McGill University, Macdonald Engineering Building, 817 Sherbrooke Street West, Montreal, QC, Canada, H3A 2K6

**Abstract**

The gas distribution between the dilute (bubble) and dense (emulsion) phases of a fluidized bed is studied locally and globally in the bubbling regime for mixtures composed of sand and different weight fractions of biomass (2-16%). The dilute phase has been characterized by analyzing the pressure and voidage signals. A suite of pressure transducers was used to measure pressure fluctuations at different locations along the bed. A reflective optical probe measured local voidage signals and was placed at different radii ( $0 < r/R < 0.87$ ) at a height of  $h=175$  mm above the distributor plate. The mean voidage of the bed is increased with higher biomass loading, primarily because of dilution of the emulsion phase. Changing the quantity of biomass in the bed does not significantly affect the voidage of the bubble and emulsion phases. The void (bubble) fraction increases at the center of the bed, whereas it decreases and then increases at the wall region with increasing weight fraction of biomass. Higher quantities of biomass reduce the mean bubble size and boost the bubble frequency at the center of the bed. The core-annulus structure of the bed is intensified for mixtures with relatively low quantities of biomass, while increasing the biomass load leads to a more uniform distribution of small bubbles across the bed improving the fluidization quality.

**Keywords:** Biomass, Multiphase reactors, Hydrodynamics, Fluidization, Voidage, Gas distribution

### 3.1 Introduction

Use of biomass has the very important benefits of contribution to the security of fuel supply, lower greenhouse gas emissions, and support for agriculture (Lior, 2010). It is presently estimated to contribute ~10-14% of the world's energy supply (Cui & Grace, 2007).

Thermo-chemical processes, such as combustion, pyrolysis or gasification, are currently the most widespread techniques for producing energy or value-added products from biomass. Fluidized bed reactors are often the best systems for carrying out these processes since they offer multiple advantages over other types of reactors. These advantages include: the ability to handle a variety of fuels with different physical properties, effective gas-solid contact and heat transfer, and economic operation at relatively small scales. However, fluidization of large and light objects, such as biomass particles, is a cumbersome task, which only becomes feasible by mixing a small amount of biomass within a bed composed of conventional fluidization materials, such as sand. The mass content of fuel, e.g., coal or biomass, as a percentage of the total bed mass in bubbling bed combustion or gasification conditions is typically about 1-5%, depending on the fuel type, size and reactivity. Accordingly, it is usually envisaged that one fuel particle is surrounded by many particles of fluidization medium and the effect of biomass content on the bed properties is ignored. However, several multiphase flow complexities arise in practice when fluidizing mixtures composed of dissimilar materials. These complexities cannot be estimated by the hydrodynamic behavior of constitutive substances when being fluidized distinctly (Cui & Grace, 2007). Segregation of biomass particles, which tend to migrate to the top of the bed, is one of the most adverse phenomena giving rise to the ineffective heat transfer along the bed, release of volatiles into the freeboard, and deterioration of the activity of the tar decomposition reaction (L. Shen et al., 2007). Misdistribution of fuel particles along the bed can also bring about very heterogeneous distribution of the gas reactants and products. For instance, non-uniform distribution of oxygen across the bed influences the combustion of fuel particles, which results in the occurrence of hot/ cold spots and ash softening.

Larger sized fuel particles will remain at their original size for much longer in the bed before they reach the high temperatures needed for thermal degradation. For instance, on the basis of the energy balance for a single particle, it can be calculated that obtaining 800 °C under fluidization conditions requires tens of seconds for a 10 mm wood particle. This illustrates that the multiphase

flow aspects of the bed could be influenced by the particles, which remain in their original state for a considerable period of bed operation.

Among the limited studies on the multiphase flow aspects of biomass fluidization, determination of characteristic fluidization velocities (Abdullah, Husain, & Pong, 2003; K. V. N. S. Rao & Reddy, 2010; T. Rao & Ram Bheemarasetti, 2001; Yong Zhang, Zhong, & Jin, 2011), and the distribution and mixing pattern of biomass-inert materials (Berruti, Liden, & Scott, 1988; Dos Santos & Goldstein, 2008; L. Shen et al., 2007; Y. H. Yu, Oh, Lee, & Choi, 2003) have been of particular interest to researchers. The impact of irregularly-shaped particles on the characteristics of the dilute and dense phases has received comparatively little attention, and it has generally been assumed that, due to the typically low ratio of biomass to sand in biomass processing units, the gas holdup in the bed is comparable to that of a bed of sand alone. In view of this, gas holdup or void fraction has mostly been studied in bubbling beds containing only relatively small biomass particles. The void fraction and its distribution in a two phase flow system are important in determining the interfacial area available for heat and mass transfer between the phases (Kiared, Larachi, Cassanello, & Chaouki, 1997). In addition, gas or solid holdup parameters are important for optimizing fluidization hydrodynamics and process efficiency (Franka & Heindel, 2009).

Using different materials, i.e., glass beads, ground corncob, and ground walnut shell whose sizes varied between 500-600  $\mu\text{m}$ , Franka and Heindel (Franka & Heindel, 2009) found that fluidization among the different materials had similar behaviors with some notable differences. They applied X-ray computed tomography (CT) in order to determine the effects of side air injection, superficial gas velocity, and bed material on fluidization behavior and local time-averaged gas holdup. Of the three bed materials examined, ground corncob fluidization was the least affected by side air injection and showed the highest overall gas holdup while glass bead fluidization was much more affected by side air injection and had the lowest overall gas holdup. Escudero and Heindel (Escudero & Heindel, 2011) showed also that for these materials, the gas holdup in the bed increased by decreasing the bed density. In a similar work performed in cold flow fluidized beds of 10.2 cm and 15.2 cm in diameter, Drake and Heindel (Drake & Heindel, 2012) concluded that bed mixing and uniformity were enhanced in both reactors when a lighter material was fluidized.

Zhang et al. (Yong Zhang, Jin, & Zhong, 2009) studied the bubbling fluidization of mixtures whose biomass-to-sand ratios varied from 1 to 3%. They used nearly cylindrical cotton stalk particles as the test biomass material, whose size and density are comparable to the particles used in the present study. By comparing pressure fluctuation amplitudes, they concluded that increasing biomass concentration led to a decreased probability for the growth and coalescence of bubbles (Y. Zhang et al., 2010). In other words, they envisaged that thin-long biomass particles had a positive influence on the eruption of bubbles, a fact that became more pronounced when the concentration of biomass increased (Yong Zhang, Jin, Zhong, et al., 2009).

It is worth noting that, in a hot gas-solid fluidized bed, in-bed emission of volatile materials during combustion or gasification is responsible for the formation of “endogenous” volatile bubbles around the fuel particles. Endogenous bubbles enhance axial segregation of fuel particles at the bed surface (Solimene, Chirone, & Salatino, 2012; Solimene, Marzocchella, & Salatino, 2003) and may influence the dynamic gas-solid distribution of the bed. The present study has been done under cold conditions and, thus, cannot assess this effect.

The present work aims to provide clear insight into the possible effects of large/light objects immersed in a bed of fine/dense particles on the gas distribution pattern in the bed. The gas fraction and gas holdup of the dilute (bubble) and dense (emulsion) phase profiles are studied at a given height of the bed in the presence of different quantities of biomass. Moreover, the dilute phase characteristics are measured using optical fiber probes for variable biomass loadings. The degree of bed expansion as a result of increasing gas velocity is used as a measure of the global gas holdup in the bed. All results are compared to baseline values of a pure-sand bed to determine the influence of irregularly-shaped, low-density particles on the multiphase flow features of a bubbling bed.

## **3.2 Experimental**

All experiments are conducted in a cold fluidized bed consisting of a Plexiglas column with an internal diameter of 152 mm. The distributor plate is perforated with 1 mm diameter holes arranged in a triangular pitch. The flow rate of air is measured by a bench of rotameters and is introduced into the bed through a conical windbox. The bed material used in the experiments is

sand with a particle size distribution (PSD) ranging from 300 to 500  $\mu\text{m}$ . Synthetic biomass particles are fabricated from cylindrical wood rods cut into identical lengths. Table 3.1 contains more details of all materials used in this study. To investigate the effect of biomass weight fraction, four mixtures of different weight fractions of biomass in sand are studied, as detailed in Table 3.2. The mixture voidage of two solids differing in size exhibits a minimum at intermediate composition (Formisani, Girimonte, & Longo, 2008b; Formisani et al., 2011; A. Yu & Standish, 1987). The porosity of sand is partially filled by the large biomass particles to a certain extent. Further increase in the volume fraction of biomass results in increasing the total voidage of the mixture because of the dominance of biomass particles having a much higher voidage than sand alone.

In all experiments, the static bed height is set to 228 mm ( $H_0/D=1.5$ ). In order to start from a well-mixed condition, the sand and biomass measures are each equally divided into eight batches. Each batch of sand is mixed with a single batch of biomass. Finally, the content of all mixtures is sequentially added to the fluidization column.

The dynamic pressure fluctuations are monitored along the bed via several differential pressure transducers (OMEGA PX 272) mounted flush with the wall of the bed. A pressure transducer (PT1) is applied to measure the pressure drop fluctuations across the whole bed (10-2000 mm above the distributor). Local pressure signals are acquired at low and high levels within the bed using two pairs of differential pressure transducers (PT2 and PT3). The mean distance of these pressure transducers from the distributor is 85 and 235 mm, respectively, while their probes are vertically spaced 50 mm. Fig. 3.1 exhibits the schematic of the experimental set-up equipped with various measurement probes.

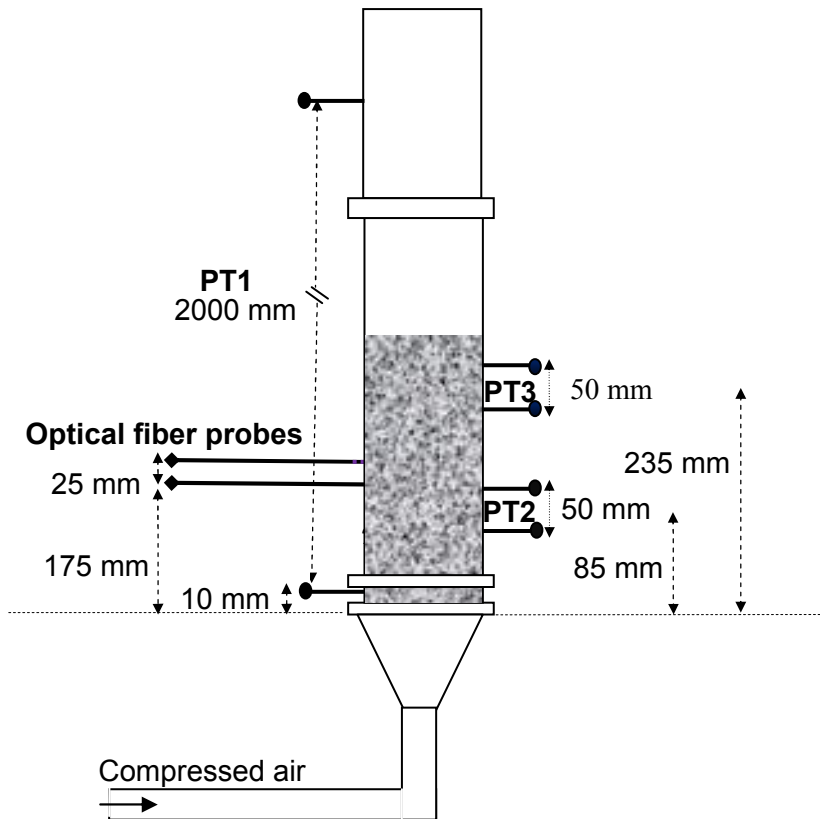


Fig. 3.1: Sketch of the fluidization column equipped with pressure transducers and optical fiber probes

Table 3.1: Properties of materials used

Material	Shape	$D_p$ (mm)	$L_p$ (mm)	$\rho_p$ (kg/m <sup>3</sup> )	$\rho_b$ (kg/m <sup>3</sup> )
Sand	Spherical	0.38	-	2650	1520
Biomass	Cylindrical	6.35	12.70	824	342

Table 3.2: Properties of systems studied

Wt.% of biomass	Vol.% of biomass	Bulk density of sand-biomass mixture (10 <sup>-3</sup> kg/m <sup>3</sup> )	Voidage of the fixed bed (-)
0	0.0	1.52	0.43
2	6.2	1.46	0.42
4	11.8	1.42	0.41
8	21.9	1.35	0.40
16	38.0	1.22	0.37

The local distribution pattern of gas, between the bubble and emulsion phases of the mixture is explored using an optical fiber particle concentration measurement device (PC-4 Powder Voidmeter) manufactured by the Institute of Process Engineering of the Chinese Academy of Science. The probe measures local voidage fraction and consists of a bundle of light-emitting/receiving optical fibers. Light projected by the light-emitting fibers is reflected by particles and the reflected light is collected by light-receiving fibers and converted to electric signals by a photomultiplier. The probe is placed at an axial position 175 mm above the distributor and over a range of radial positions between  $0 < r/R < 0.87$ . The calibration curve of normalized voltages developed by Cui et al. (Heping Cui, Navid Mostoufi, & Jamal Chaouki, 2001a) (Eq. (3.1)) is used to calibrate the optical fiber probe.

$$\frac{1 - \varepsilon}{1 - \varepsilon_{mf}} = \frac{0.4u}{1.4 - u} \quad (3.1)$$

where

$$u = \frac{V - V_0}{V_{mf} - V_0} \quad (3.2)$$

Before and after each experimental run, the voidmeter is calibrated against a black box ( $V_0=1$ ), representing the no-solid circumstance, and a packed bed of sand alone ( $V_{mf}=4$ ). It should be noted that Eq. (3.1) could be deployed as the calibration curve of the studied binary mixtures since the maximum solid holdups reaches under the fluidization conditions are lower than the solid holdup of pure-sand under the minimum fluidization conditions ( $1 - \varepsilon_{mf}$ ). It was verified experimentally by inserting the probe in a fixed bed of well-mixed mixture, composed of sand and 16% wt. biomass, (the maximum weight percentage of biomass used in this study) and measuring the local solid holdup. Moreover, a biomass particle was situated adjacent to the tip of the probe to fill the entire measurement volume of the probe as an extreme condition, which might take place during recording of the local voidage of a mixture. As depicted in Fig. 3.2, the corresponding voltage and the relevant solid holdup values of these two cases are lower than those of a bed of sand alone. The values shown in the figure are an average of 10 repetitions.

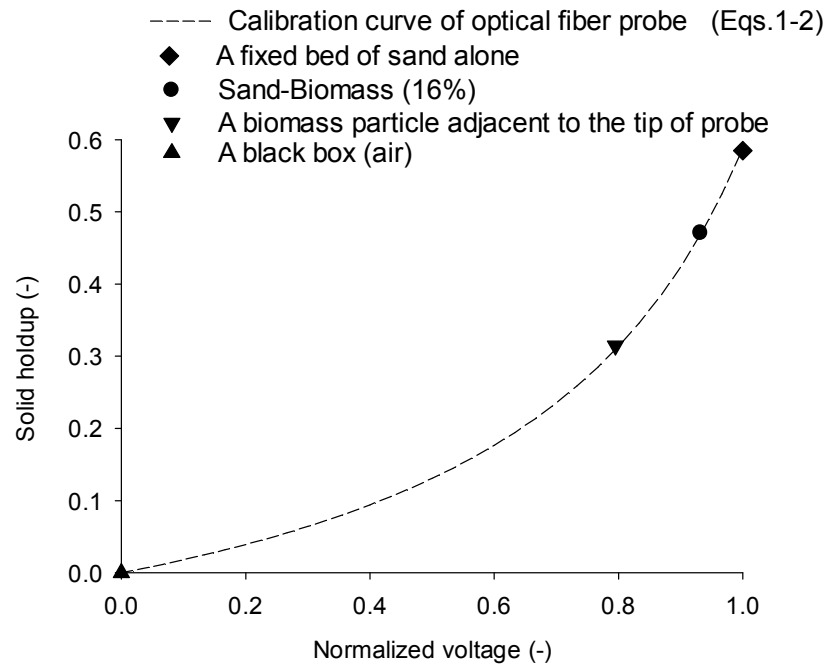


Fig. 3.2: The calibration curve used to calibrate the optical fiber probe and the mean values of solid holdup obtained using the calibration equation

In the second series of experiments, bubbling characteristics of the bed are studied by placing two identical reflective optical probes at bed heights of 175 and 200 mm above the distributor. Both vertically aligned probes are inserted horizontally into the axis of the column. The superficial gas velocity of each series of experiments varies from 0.2 to 1 m/s. The pressure and voidage data are acquired at a sampling frequency of 512 Hz through a 16 bit A/D data acquisition board with the help of the Labview 9.0.1® program. To evaluate the bubble size, an in-house code was developed following the algorithm introduced by Ruedisueli et al. (Ruedisueli, Schildhauer, Biollaz, & van Ommen, 2012)

### 3.3 Results and discussion

#### 3.3.1 Characteristic fluidization velocities

Three characteristic velocities are recognized when gas flow rate increases gradually, i.e., the initial fluidization velocity ( $U_{if}$ ), the initial bubbling velocity ( $U_{ib}$ ), and the final or complete

fluidization velocity ( $U_{ff}$ ).  $U_{if}$  is known as the superficial gas velocity in which the onset of deviation of the bed pressure drop from the initial linear fixed-bed condition occurs.  $U_{ff}$  corresponds to the lowest velocity for which the weight of the bed contents is fully counterbalanced with the gas flow drag force (Formisani et al., 2008b).  $U_{if}$  and  $U_{ff}$  were determined through plotting a time-averaged profile of whole bed pressure drop ( $\Delta P$ ) vs. gas velocity. The onset of bubble formation along the bed takes place at  $U_{ib}$ , which is usually higher than  $U_{if}$  but lower than  $U_{ff}$ . It is worth mentioning that the occurrence of a non-bubbling fluidization interval ( $U_{if} < U < U_{ib}$ ) is a characteristic of large particle fluidization (Cranfield & Geldart, 1974). As shown previously, the emergence of bubbles in the bed at  $U_{ib}$  is recognizable through the sudden change of the dominant frequency of pressure fluctuations determined through the FFT (Fast Fourier transform) technique (Fotovat, Shabanian, Chaouki, & Bergthorson, 2011). The effect of biomass load on the characteristic velocities of different mixtures is shown in Fig. 3.3. The initial fluidization velocity,  $U_{if}$ , of all systems is the same as for pure sand. On the other hand,  $U_{ib}$  and  $U_{ff}$  increase with increasing biomass concentration; however, increasing biomass load causes a larger variation in  $U_{ff}$ .

Paudel and Feng (Paudel & Feng, 2013) have recently proposed a correlation between the Reynolds number at minimum fluidization state ( $Re_{ff}$ , Eq.(3.3)), Archimedes number ( $Ar$ , Eq. (3.4)) and the weight percentage of biomass particles (Eq. (3.5)).

$$Re_{ff} = \frac{U_{ff} d_p \rho_g}{\mu} \quad (3.3)$$

$$Ar = \frac{d_p^3 \rho_g (\rho_p - \rho_g) g}{\mu^2} \quad (3.4)$$

$$Re_{ff} = \{30.28^2 + [0.046(1 - x_{Bm}) + 0.108x_{Bm}^{0.5}]Ar\}^{0.5} - 30.28 \quad (3.5)$$

As shown in Fig. 3.3, the experimental data could be satisfactorily correlated with Eq. (3.5). The relevant correlation coefficient is 0.98.

The upper limit of the bubbling regime, i.e., the onset of transition from a bubbling to turbulent regime ( $U_c$ ) is also elucidated in Fig. 3.3 for the systems studied. It is generally accepted that the maximum bubble size occurs at  $U_c$  which is recognizable through the maximum standard deviation of the pressure fluctuations along the bed (Chehbouni, Chaouki, Guy, & Klvana, 1994).

Hence, the corresponding gas velocity of the maximum standard deviation of pressure fluctuations measured by PT1 was considered as  $U_c$  of the studied system. By increasing the fraction of biomass in the bed,  $U_c$  decreases. This is ascribed to the shrinkage of bubbles as a consequence of increasing the biomass ratio in the mixture, which is discussed later (see Section 3.3.2). In other words, by increasing the biomass in the bed, the maximum growth of bubbles owing to raising the excess gas velocity occurs at relatively lower values. Such a behavior has also been observed by Zhang et al. (Yong Zhang, Jin, Zhong, et al., 2009). Note that a considerable gap is observed between  $U_{if}$  and  $U_{ff}$  ( $U_{mf}$ ) of a pure-sand bed due to the large particle size distribution of sand used in experiments.

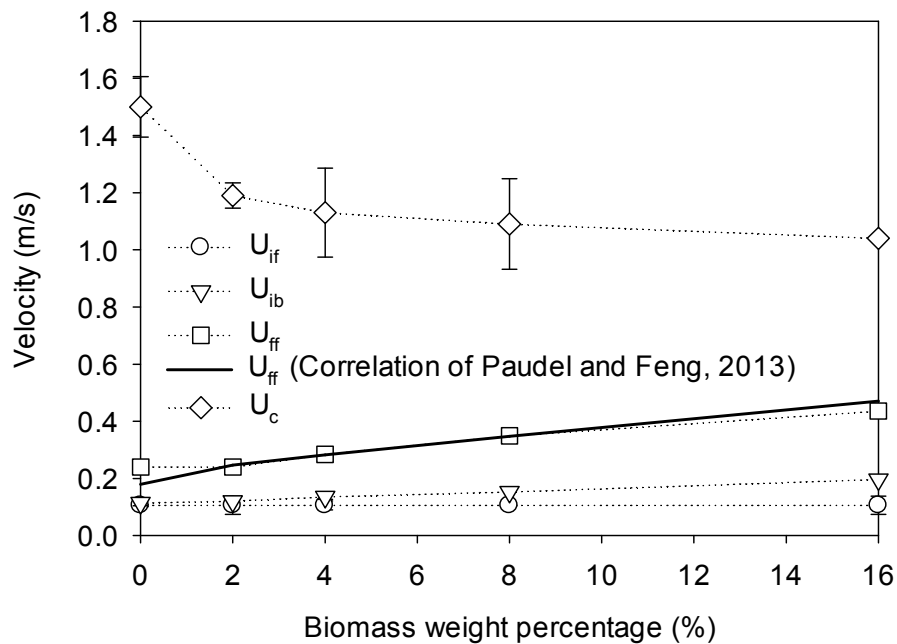


Fig. 3.3: Variation of  $U_{if}$ ,  $U_{ib}$ ,  $U_{ff}$ , and  $U_c$  with the load of biomass

### 3.3.2 Gas distribution pattern and bubble characterization

Bai et al. (B. Bai, Gheorghiu, van Ommen, Nijenhuis, & Coppens, 2005) have shown that the pressure statistics encode information about the bubble size distribution. Based on their findings, the power-law tail shape of the pressure probability density function (PDF) can be described by the Student's distribution and it is intimately related to the statistics of bubble size. Accordingly, they developed a method to extract the shape of the void size distribution in bubbling beds from a

time-measurement of pressure. This method has been employed in the present study to shed light on the bubble characteristics for mixtures containing biomass. Pressure increments were calculated for a certain time delay (10 ms) and the PDF of these increments was computed after removing their mean value and normalizing them to their standard deviation. Student's distribution (Eq. (3.6)) was fit to the PDF using a least-squares technique to obtain the two fitting parameters ( $\alpha$ ,  $\beta$ ). The lowest correlation coefficient to fit the experimental distribution of pressure fluctuations to Eq. (3.6) was 0.97, while it was 0.99 in most cases.

$$\rho_s(x) = N(\alpha, \beta)[1 + \alpha x^2]^{-\beta} \quad (3.6)$$

As shown by Bai et al. (B. Bai et al., 2005), parameter  $\beta$  is related to the shape of the void size distribution around the pressure measurement probe. Fig. 3.4 illustrates the values of parameter  $\beta$  obtained through fitting the PDF of pressure signals registered at the top of the bed with Student's distribution. As seen, at the low bubbling velocity studied,  $\beta$  values are relatively high denoting the undeveloped size distribution of voids. By increasing gas velocity, bubbles evolve and the  $\beta$  value drops. Comparing the trend of  $\beta$  values for different biomass loadings reveals that, at relatively low bubbling velocities, the formation and development of bubbles are significantly affected by the weight fraction of biomass. In other words, increasing biomass content suppresses bubble development. By increasing the gas velocity, the  $\beta$  value of systems containing a higher amount of biomass drops more steeply compared to other systems. After a certain velocity ( $U=0.60$  m/s), the  $\beta$  values are comparably low for all mixtures, which is a sign of a similarly broad distribution of bubble size. These observations imply that the formation and growth of bubbles is markedly influenced by the biomass content at modest bubbling velocities, plausibly due to the severe segregation of biomass particles influencing the bubble breakage and coalescence.

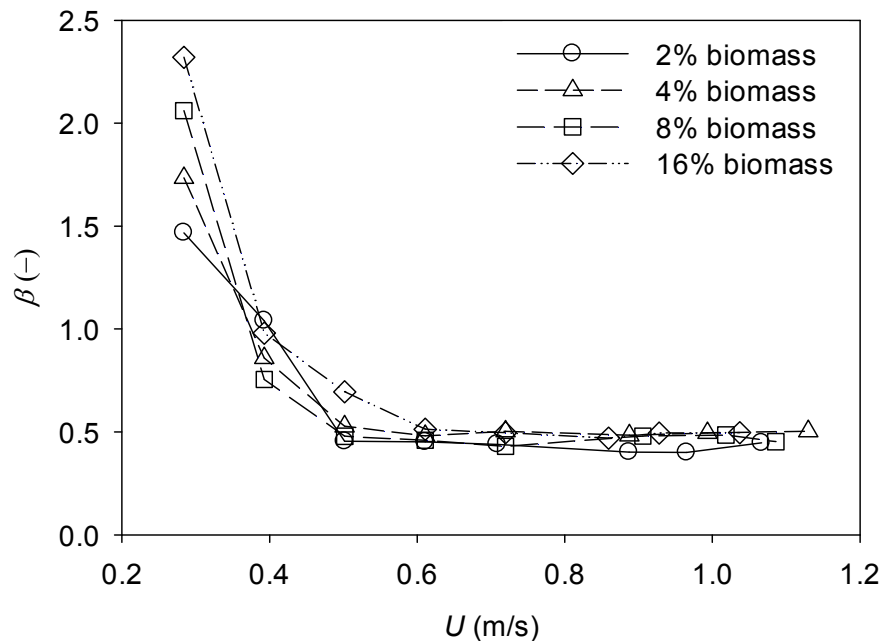


Fig. 3.4: Variation of parameter  $\beta$  as one of the two curve fitting parameters of Student's distribution

The local gas distribution between the bubble and emulsion phases is investigated by means of the optical fiber probes. Optical fiber signals are statistically analyzed and the respective voidage probability density is obtained. A continuous double-peak probability density function (PDF) from  $\varepsilon_{mf}$  to 1 denotes the entity of two distinct phases, i.e., solid (emulsion) and dilute (bubble) phases (Cui et al., 2001b). Accordingly, the corresponding voidage and the intensity of each peak represent the properties of each phase. Fig. 3.5 elucidates the PDF of the local voidages of mixtures containing 2 and 16% biomass at relatively low and high bubbling velocities at the center of the bed ( $r/R=0$ ) as well as the wall region ( $r/R=0.87$ ). As expected, the bubble phase is prevailing at the center of the bed, which is deduced from the higher intensity of the peaks appearing at  $0.9 < \varepsilon < 1$ . On the other hand, the emulsion phase prevails at the wall region. At  $U=0.30$  m/s, the probability distribution of voidage at the center of the bed is comparable for systems containing 2 and 16% biomass. However, the dense phase is comparatively more prevalent at the wall region. The content of biomass in the mixture could markedly influence the gas distribution pattern at higher superficial gas velocities. As inferred from the peaks corresponding to the dilute phase, by increasing fluidization velocity, gas is more prone to appear

in the dilute phase in the presence of higher quantities of biomass. It is particularly notable at  $U=0.80$  m/s close to the wall, where the particulate phase is normally predominant.

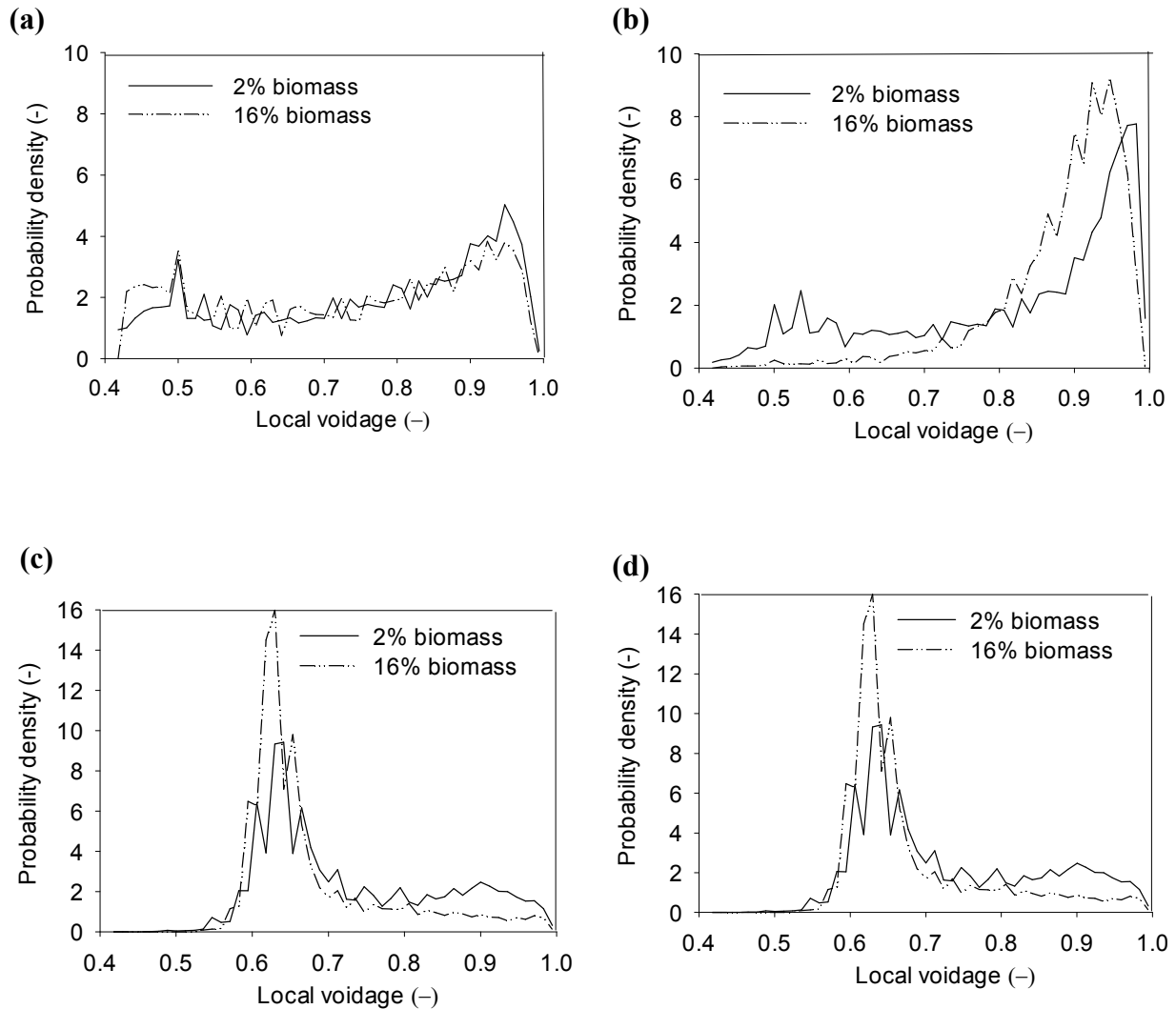
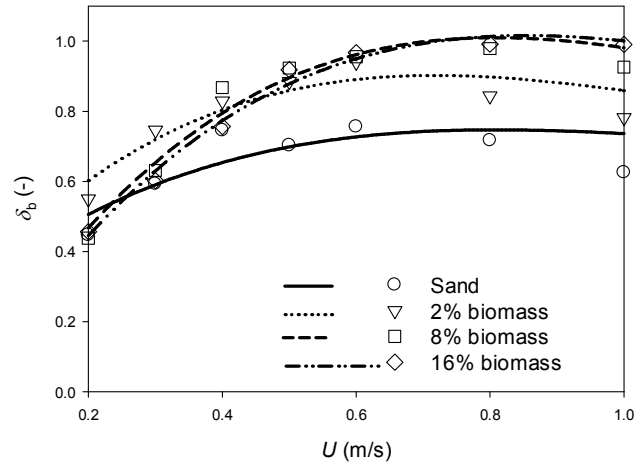


Fig. 3.5: The probability density function of the local voidages registered at  $h=175$  mm at a)  $U=0.30$  m/s,  $r/R=0$ , b)  $U=0.80$  m/s,  $r/R=0$ , c)  $U=0.30$  m/s,  $r/R=0.87$ , d)  $U=0.80$  m/s,  $r/R=0.87$

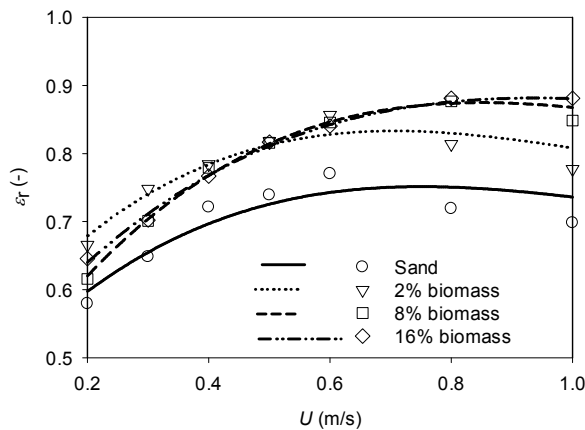
In order to compare the dynamic two-phase structure in systems differing in the load of biomass, the dilute phase fraction ( $\delta_b$ ), gas holdup ( $\varepsilon_r$ ), and the mean voidage of dilute ( $\varepsilon_b$ ) and dense ( $\varepsilon_e$ ) phases are calculated by analyzing the local optical probe signals. Fig. 3.6 shows the corresponding values of these parameters at  $h=175$  mm and  $r/R=0$  for the whole range of the bubbling fluidization regime, i.e.,  $U=0.2-1.0$  m/s. As illustrated, the addition of biomass to a bed of sand alone increases  $\delta_b$ ,  $\varepsilon_r$ , and  $\varepsilon_e$  but it does not change  $\varepsilon_b$  at the center of the bed. At high gas

velocities, systems comprised of 8 and 16% biomass show a more substantial enhancement in  $\delta_b$  and  $\varepsilon_r$  while  $\varepsilon_c$  values are almost comparable at corresponding velocities for all mixtures.

(a)



(b)



(c)

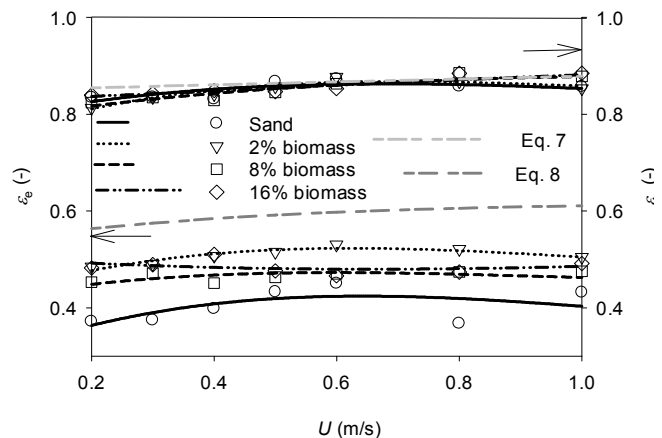


Fig. 3.6: a) The time-mean dilute phase fraction, b) the mean gas holdup, and c) the mean voidage of dilute and dense phases of beds comprising sand and biomass in a bubbling fluidization regime. ( $r/R=0$ ,  $h=175$  mm)

A change in the abovementioned parameters owing to the different loads of biomass at the wall region is more complicated. As depicted in Fig. 3.7a, the addition of biomass up to 8% wt. brought about a decrease in the dilute phase fraction; however, it is enhanced when the biomass fraction is increased further to 16%. On the other hand, the increase in gas holdup is proportional to the quantity of biomass in the mixture. As observed at the center of the bed, the dense phase is more dilute in the case of mixtures of sand and biomass compared to that of sand alone. In

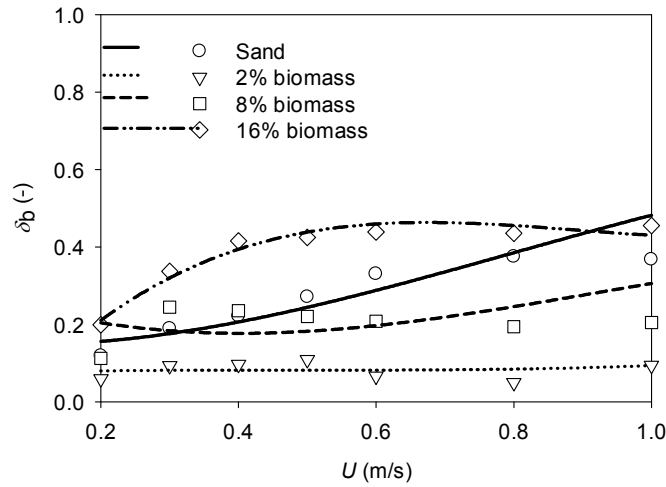
addition, the dilute phase voidage slightly increases in this region due to the presence of biomass particles. In other words, as a consequence of biomass addition to the sand, bubbles rising in the wall proximity lift up the lower quantities of sand. It should be noted, however, that raising the biomass content does not affect  $\varepsilon_b$  and  $\varepsilon_e$  in the mixtures studied. This confirms that the inherent characteristics of each phase are mainly governed by the fluidization medium and the irregular particles existing in the bed mostly influence the extensive properties of each phase. This observation is important for modeling the mass and heat transfer and kinetic phenomena in fluidized beds involving biomass. Data from pure-sand beds can be used to estimate model terms required these input parameters. For instance, the following correlations developed by Cui et al. (Cui, Mostoufi, et al., 2000) for pure-sand beds may be usable for beds containing mixture of sand and biomass.

$$\varepsilon_b = 1 - 0.146 \exp \left[ \frac{-(U - U_{mf})}{4.439} \right] \quad (3.7)$$

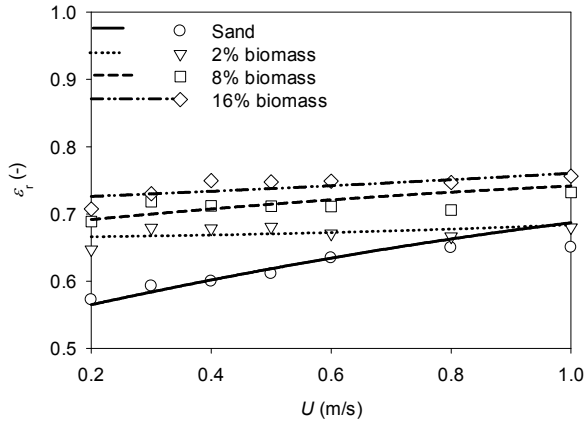
$$\varepsilon_e = \varepsilon_{mf} + 0.2 - 0.059 \exp \left[ \frac{-(U - U_{mf})}{0.429} \right] \quad (3.8)$$

The values obtained by these correlations for sand alone have been shown in Fig. 3.6c. While  $\varepsilon_b$  is in excellent agreement with the corresponding experimental data, the predicted  $\varepsilon_e$  is considerably higher. The typical correlation coefficients of equations (3.7) and (3.8) are 0.94 and 0.74, respectively. This discrepancy is presumably arises due to the smaller size distribution of sand particles used in this study as well as the smaller height of the static bed (PSD=300-500  $\mu\text{m}$ ,  $H_0=228$  mm) compared to those of Cui et al. experiments (PSD=100-1000  $\mu\text{m}$ ,  $H_0=300$  mm). As shown by (Tanfara, Pugsley, & Winters, 2002), for the wide PSD of particles at a fixed gas velocity, the gas tends to spread more uniformly over the bed cross section as static bed height increases, while the opposite is true in the case of narrow PSD, i.e., the gas flow becomes more centralized with increasing bed height.

(a)



(b)



(c)

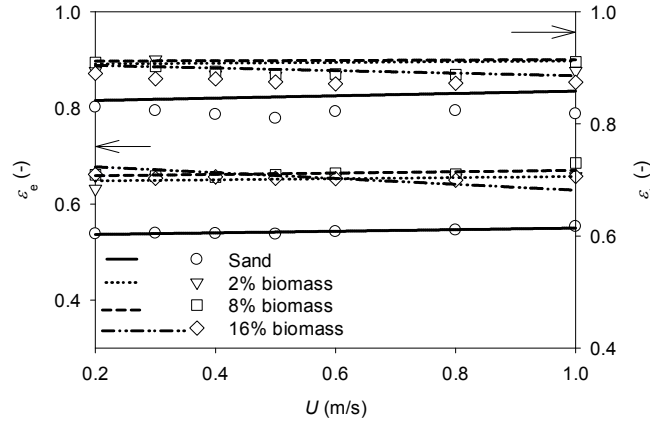


Fig. 3.7: a) The time-averaged dilute phase fraction, b) the mean gas holdup, and c) the mean voidage of dilute and dense phases of beds comprised of sand and biomass in a bubbling fluidization regime. ( $r/R=0.87$ ,  $h=175$  mm)

The distribution of gas between two phases is studied quantitatively by determining the ratio of the bed voidage of the dense phase to that of the dilute phase ( $\beta_g$ ) at different radii of a given height of the bed, i.e.,  $h=175$  mm (Eq. (3.9)).

$$\beta_g = \frac{(1 - \delta_b)\epsilon_e}{\delta_b\epsilon_b} \quad (3.9)$$

The  $\beta_g$  values of a bed of sand alone and mixtures consisting of 2, 8, and 16% biomass have been compared at  $U=0.30$  and  $0.80$  m/s in Fig. 3.8. As seen, the value of  $\beta_g$  increases by approaching

the wall primarily because of the restriction on bubble development in the wall region leading to a core-annulus structure in the bed (Cui et al., 2001b).

As demonstrated, adding limited quantities of biomass to the sand particles when it was fluidized at  $U=0.30$  m/s notably reduces the likelihood of the void (bubble) presence at the wall region. Consequently, a more explicit core-annulus structure forms in the bed; a fact which is not favorable to the actual operating processes. By raising the biomass weight fraction, however, the portion of gas in the dilute phase at the outer region of the bed ( $r/R>0.5$ ) become appreciable. An increase in fluidization velocity to  $U=0.8$  m/s dramatically intensifies the core-annulus structure in the case of the mixture containing 2% biomass whereas it improves the uniformity of gas distribution between two phases across the bed for higher biomass loading.

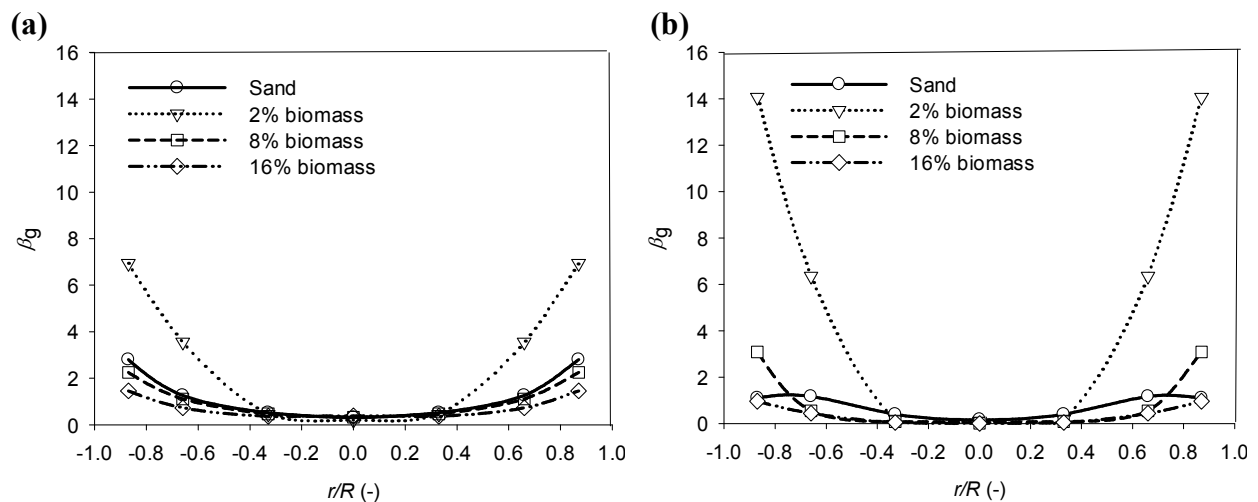


Fig. 3.8: The ratio of the bed voidage of the dense phase to that of the dilute phase at  $h=175$  mm at a)  $U=0.30$  m/s, b)  $U=0.80$  m/s

The mean size of bubbles ( $d_b$ ) in a bed of sand alone, as well as for the sand-biomass mixtures, is also determined at  $h=175$  mm through experiments conducted by using two optical probes inserted parallel to each other into the center of the bed ( $r/R=0$ ). It should be pointed out that what is measured in this way is more likely the pierced chord length of the bubble which is usually smaller than the actual bubble size. However, it is shown that the mean of the measured chord lengths can be taken as a representative bubble size in the bed ( $\pm 10\%$ ) (Ruedisueli et al., 2012). The respective values of the mean bubble size have been compared in Fig. 3.9. As depicted, bubbles are smaller on average in mixtures of sand-biomass compared to the bed of

sand alone and they nearly plateau at a certain gas velocity. Furthermore, the higher loading of biomass in the system is, the smaller bubbles form in the mixture. This finding is in agreement with those of Zhang et al. (Yong Zhang et al., 2008).

As discussed in another work (Fotovat, Chaouki, & Bergthorson, 2013a), in comparison with the other predictive correlations, those of Darton et al. (Darton, LaNauze, Davidson, & Harrison, 1977), i.e. Eq. (3.10), and Davidson and Harrison (Davidson & Harrison, 1963), i.e. Eq. (3.11), respectively, provide the most accurate predictions of the bubble size,  $d_b$ , and velocity,  $U_b$ , for the present measurements. It should be stressed that the bubble chord length is overestimated by the optical probe since very small bubbles tend to skirt the probes rather than pass through them (Liu, Zhang, Bi, Grace, & Zhu, 2010). Accordingly, the average bubble size obtained experimentally is usually greater than the average value predicted by the Darton et al. correlation. It is the case particularly at low bubbling gas velocities, as seen in Fig. 3.9. Moreover, it should be noted that compared to the experimental values, correlation of Darton et al. predicts a lower degree of reduction in the bubble size in the presence of higher quantities of the biomass particles. It is because the effect of biomass on the bubble break-up is not considered in this correlation and the different predicted sizes of bubble solely come from the different  $U_{ib}$  values of the studied systems. This shows the necessity of developing predictive correlations describing the bubble properties in beds containing irregular materials.

$$d_b = 0.54g^{-0.2}(U - U_{ib})^{0.4}(h + 4A_c^{0.5})^{0.8} \quad (3.10)$$

$$U_b = 0.711\sqrt{gd_b} + (U - U_{ib}) \quad (3.11)$$

The frequency of bubble (void) passage in front of the tip of the optical probe is also acquired at different radii (Fig. 3.10). At the center of the bed, bubble frequency increases by increasing the fraction of biomass in the mixture. An increase in the bubble frequency implies that the emergence of smaller bubbles, in the presence of biomass particles, is mainly caused by the breakage of large bubbles. On the other hand, adding 2% wt. biomass to the sand reduces the rate of bubble passage at the wall region, while further increasing the biomass quantity enhances it. The similarity between the profiles of bubble frequency and the dilute phase fraction demonstrates that the dynamics of the two phases is primarily governed by the change in the equilibrium of the bubble break-up and coalescence phenomena.

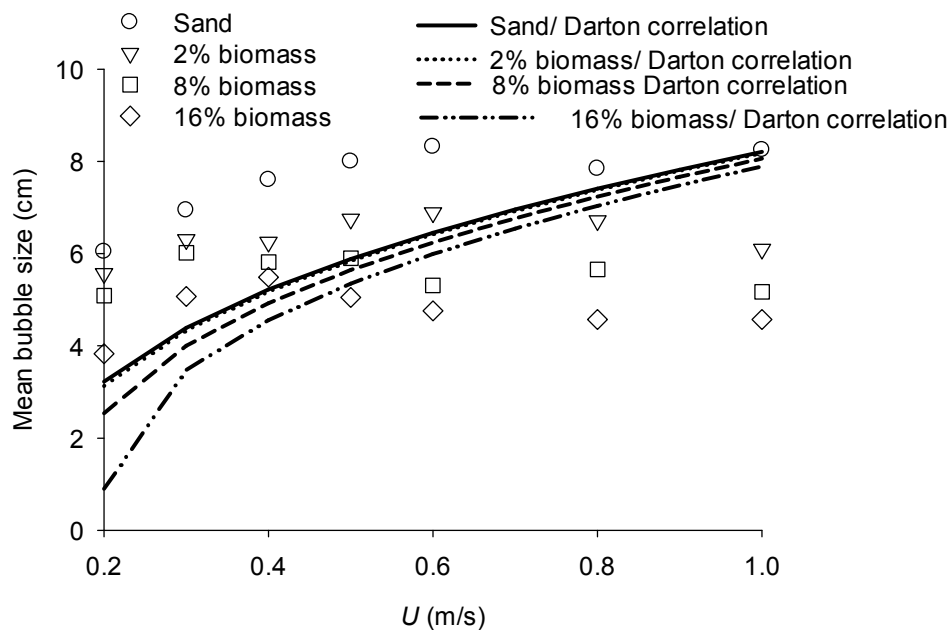


Fig. 3.9: A comparison of mean bubble size for a bed of sand alone and mixtures containing biomass at different fluidization velocities at  $r/R=0$

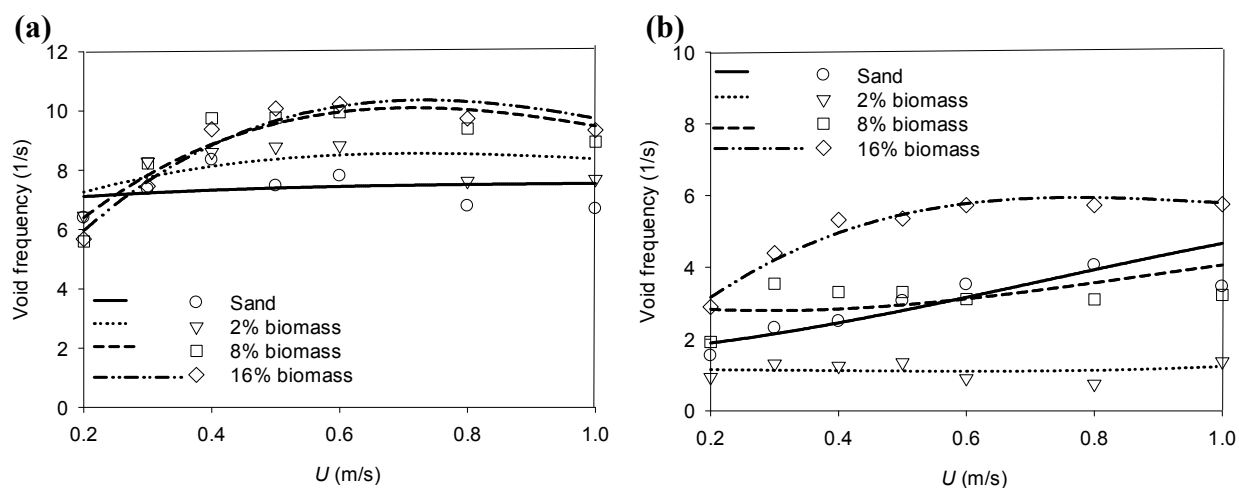


Fig. 3.10: Void frequency at  $h=175$  mm and a)  $r/R=0$ , b)  $r/R=0.87$

### 3.3.3 Visual bed expansion and mixing/segregation patterns

The impact of biomass content on the overall gas distribution pattern within the bed is assessed by comparing the bed expansion of all cases. The height of the bed is measured by averaging direct readings on three graduated scales spaced  $120^\circ$  around the column wall. Starting from an initially well-mixed state, the bed height slightly drops at the onset of fluidization ( $U_{if}$ ) because the sand particles rearrange to minimize the gas flow resistance. Correspondingly, this effect is more noticeable for low biomass loadings. The mechanism of segregation before the formation of bubbles is called the percolation of the fluidization medium (Yong Zhang, Jin, & Zhong, 2009). As observed in the experiments, sand particles surrounding each biomass particle come loose as they vibrate because of the passage of air. Consequently, they fall under the biomass particle and the over-layer sand sinks slightly. As fluidization progresses by increasing gas velocity, the fluidizing medium, i.e., sand, behaves as a liquid and the light biomass particles rise in the bed due to the buoyancy force. Additionally, the emergence of small bubbles enhances the segregation of bed components. The voids created beneath the bubbles are filled by sand causing the ascent of biomass in the bed. In general, at low bubbling velocities, i.e.,  $U_{if} < U < U_{ff}$ , the bed is subject to intensive segregation and its expansion with increasing gas velocity is proportional to the biomass loading. Under these conditions, a stratum of biomass particles forms at the top of a bed rich in sand. Considering the high voidage of this stratum compared to the sand beneath, its height determines the overall height of the bed. Therefore, higher biomass content gives rise to larger bed expansion. This trend, however, reverses by further increasing gas velocity. Visual observations of the bed confirm that the large bubbles reaching the bed surface burst at the splash zone and a substantial amount of sand, which is carried in the bubble wake, is depleted. The biomass particles therefore are buried below a layer of sand. By accumulating the sand at the top of the bed, biomass particles are effectively involved in a “gulf stream” pattern of solid circulation in the bed and sink at the wall region giving rise to the enhanced mixing of bed components.

It is generally accepted that under vigorous bubbling conditions, bed expansion is apparently largely due to the bubble volume, and there is comparatively little expansion in the particulate phase (Hilal & Gunn, 2002). As discussed above, with increasing biomass loading, the size of bubbles decreases and the resulting small bubbles disperses more uniformly across the bed cross section, which results in more modest bed expansion. Fig. 3.11 compares the extent of expansion

at corresponding velocities for the systems studied. Note that the bed height has been normalized to the  $H_{mf}$  in order to show clearly the different degrees of bed expansion caused by the change in bubbling behavior. The normalized bed height can be predicted at  $U > U_{mf}$  through an iterative procedure using the bubble volumetric flow per bed cross section area, i.e.,  $\dot{V}_b/A = Y(U - U_{mf})$ , and bubble velocity at the middle height of the bed (Crowe, 2010) which is calculated using Eq. (3.11).

The lines shown in Fig. 3.11 represent the degree of bed expansion as obtained from the iterative procedure and are fairly consistent with the experimental measurements. It should be pointed out that at low gas velocities ( $U < U_{ff}$ ), the bed height is mainly determined by the intensity of accumulation of biomass particles at the top of the bed which is proportional to the weight fraction of biomass.

The effects of increased biomass loading on the bed characteristics have been summarized in Table 3.3. It should be kept in mind that, due to the local nature of the optical fiber technique, the trends detected by this method may not be extrapolated to the entire bed. Regarding the vertical position of the probe located in the upper half of the bed, however, it can be stated that the relevant values represent the local behavior of the fluidized mixtures where the biomass particles are more prevalent.

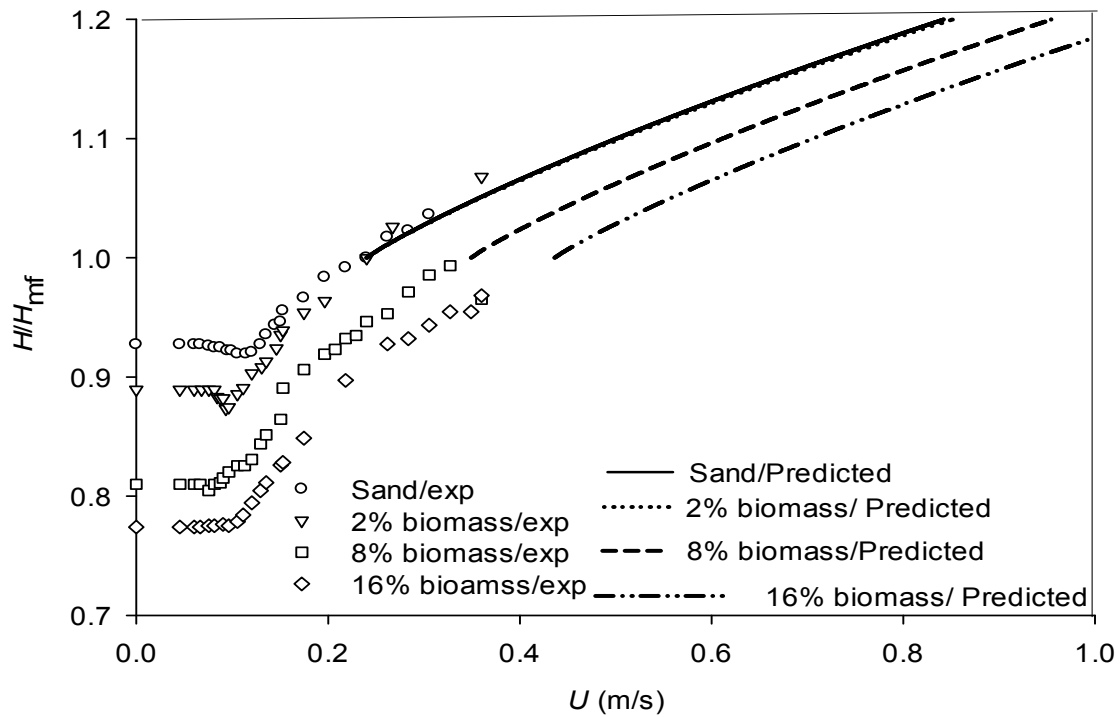


Fig. 3.11: Experimental and estimated values of  $H/H_{mf}$  vs. superficial gas velocity

Table 3.3: Summary of the effect of increasing the mass fraction of biomass on bed characteristics

Characteristic	$U_{if}$	$U_{ib}$	$U_{ff}$	$U_c$	$\delta_b$	$\varepsilon_r$	$\varepsilon_b$	$\varepsilon_e$	$d_b$	Void frequency
Trends	$\leftrightarrow^a$	$\uparrow^b$	$\uparrow$	$\downarrow^c$	$\uparrow$	$\uparrow$	$\leftrightarrow$	$\leftrightarrow$	$\downarrow$	$\uparrow$

<sup>a</sup> $\leftrightarrow$ =Unchanged, <sup>b</sup> $\uparrow$ =Increasing, <sup>c</sup> $\downarrow$ =Decreasing

### 3.4 Conclusion

The influence of biomass concentration on the gas distribution pattern and the bubble phase characteristics was explored by examining the pressure and voidage signals acquired by pressure transducers and optical fiber probes. While  $U_{if}$  of the systems studied is almost identical to  $U_{mf}$  of sand alone,  $U_{ib}$  and  $U_{ff}$  rise with increasing biomass loading. On the other hand,  $U_c$  shows a decreasing trend with increased biomass loading.

Statistical analysis of the local pressure signals revealed that the fluidization of mixtures containing higher quantities of biomass at relatively low superficial gas velocities leads to an undeveloped bubble size distribution, which is mitigated by raising the gas velocity. On the basis of the local voidage fluctuations recorded by the optical probes, gas holdup across the bed cross section rises primarily because of dilution of the dense phase. By increasing the load of biomass, the dilute phase fraction increases at the center of the bed; however, at the wall region, it increases and then decreases by raising the biomass fraction from 2 to 16%. Such behavior is in accordance with the variation of local bubble passage frequency. The breakage of bubbles triggered by the large biomass particles is the main cause of the alteration in the dynamic two-phase structure of the bed. The lower bed expansion rate for higher biomass loading is consistent with a reduction in mean bubble size through the bed. In view of the more uniform distribution of small bubbles across the bed cross section, the fluidization quality is enhanced by increasing the weight fraction of biomass for high enough bubbling velocities.

These findings corroborate that the design and operation of fluidized beds involving biomass cannot be based solely on the fluidization behavior of conventional bed materials. As shown in the present study, the presence of biomass particles, which are typically extreme in size and density, affects some critical characteristics of the bubble and emulsion phases. Understanding such effects is pivotal for successful design, operation, and modeling of biomass combustors and gasifiers.

## CHAPTER 4

### **ARTICLE 2: DISTRIBUTION OF LARGE BIOMASS PARTICLES IN A SAND-BIOMASS FLUIDIZED BED: EXPERIMENTS AND MODELING**

Farzam Fotovat<sup>1</sup>, Jamal Chaouki<sup>1</sup>, Jeffrey Berghorson<sup>2</sup>

<sup>1</sup>Department of Chemical Engineering, École Polytechnique de Montréal, C.P. 6079, Succursale Centre Ville, Montreal, QC, Canada, H3C 3A7

<sup>2</sup>Department of Mechanical Engineering, McGill University, Macdonald Engineering Building, 817 Sherbrooke Street West, Montreal, QC, Canada, H3A 2K6

**Abstract**

The axial distribution of large biomass particles in bubbling fluidized beds comprised of sand and biomass is investigated in this study. The global and local pressure drop profiles are analyzed in mixtures fluidized at superficial gas velocities ranging from 0.2 to 1 m/s. In addition, the Radioactive Particle Tracking (RPT) technique is employed to track the trajectory of a tracer mimicking the behavior of biomass particles in systems consisting of 2, 8 and 16% of biomass mass ratio. The effects of superficial gas velocity and the mixture composition on the mixing/segregation of the bed components are explored by analyzing the circulatory motion of the active tracer. Contrary to low fluidization velocity ( $U=0.36$  m/s), biomass circulation and distribution are enhanced at  $U=0.64$  m/s with increasing the load of biomass particles. The axial profile of volume fraction of biomass along the bed is modeled on the basis of the experimental findings.

**Topical Heading:** Particle Technology and Fluidization

**Keywords:** Fluidization, Mixing, Biomass, Particle tracking, Pressure analysis

## 4.1 Introduction

Producing energy from biomass provides a key substitution for fossil fuel sources which results in the mitigation of greenhouse gas emissions. Additionally, use of biomass in forms of municipal and agricultural waste as an energy resource relieves the problem of waste management in favor of developing localized plants of energy production.

Thermo-chemical and bio-chemical processes are known as the most widespread technologies to convert biomass into energy or value-added synthetic fuels. The main processes employed within the thermo-chemical conversion process are the following: combustion, pyrolysis, gasification, and liquefaction. Several unique operational advantages, like fuel flexibility, intense solids mixing and efficient heat transfer, have made the fluidized bed the most efficient reactor for all of these processes. Nonetheless, fluidization of biomass particles is a cumbersome or even impossible task owing to their irregular size, density, and shape. Generally, an inert material, like silica sand, alumina, calcite, etc., is added to biomass to assist its fluidization and improve the heat transfer; however some new multiphase flow complexities arise as a consequence of the fluidization of dissimilar components. Understanding and managing multiphase flows are critical for the successful design of biomass conversion units and for improving the existing biomass processes (Cui & Grace, 2007). One of the most undesirable multiphase flow phenomena in fluidization units comprising dissimilar components is the tendency of particles to be segregated along the bed. In general, particles which are larger in size or higher in density, tend to sink to the bottom of the bed (jetsam particles), while those that are smaller in size or lower in density move up to the bed surface (flotsam particles). Possessing very low densities, biomass particles behave regularly like flotsam in mixtures composed of sand and biomass and are likely to accumulate at the top of the bed.

The mass content of fuel, e.g., coal or biomass, as a percentage of the total bed mass in bubbling bed combustion or gasification conditions is typically about 1-5%, depending on the fuel type, size and reactivity. Considering the relatively low fraction of biomass in the mixture, the impact of biomass particles on the hydrodynamic characteristics of the fluidization medium has generally been neglected. Assuming insignificant interaction between multiple large objects, the common approach to studying the motion of fuel particles in fluidization conditions is immersing a single large/light object in a bed of relatively small/dense particles (Rees, Davidson, Dennis, &

Hayhurst, 2005; Soria-Verdugo, Garcia-Gutierrez, Garcia-Hernando, & Ruiz-Rivas, 2011; Soria-Verdugo, Garcia-Gutierrez, Sanchez-Delgado, & Ruiz-Rivas, 2011).

Fuel particles are subject to thermal fragmentation as they are fed into the reactor. However, it can be shown that the time needed to reach the bed temperature increases dramatically with the size of fuel particles. For instance, on the basis of the energy balance for a single particle, a 10 mm wood particle, which is comparable to the materials used in the present study, takes tens of seconds to reach 800 °C under bubbling fluidization conditions (Radmanesh, Chaouki, & Guy, 2006). During this considerable period of time, the mixing/segregation pattern of the bed can fully be established.

A few researchers have deployed particle tracking techniques to study the motion and mixing mechanisms of the objects possessing a larger size and lower density than the bed material. Using cinematographic recording and a radioactive tracer, Rios et al. (Rios, Dang Tran, & Masson, 1986) investigated the characteristic motions and the velocity of such particles as a function of superficial gas velocity, characteristics of bed material, and bed height in 2-D and 3-D columns. Lim and Agarwal (Kok S. Lim & Agarwal, 1994) utilized the automated image analysis methods to characterize the circulation pattern and measure the velocity of a light sphere 7 mm in diameter immersed in a 2-D bubbling fluidized bed of 0.7 mm glass ballotini. Pallares and Johnsson (Pallares & Johnsson, 2006) tracked phosphorescent tracers varying in size and density in a 2-D riser to obtain the concentration, velocity and dispersion field of the fuel-like particles. Employing digital image analysis in a 2-D bubbling fluidized bed, Soria-Verdugo et al. (Soria-Verdugo, Garcia-Gutierrez, Garcia-Hernando, et al., 2011; Soria-Verdugo, Garcia-Gutierrez, Sanchez-Delgado, et al., 2011) studied circulation of a large cylindrical object with the same density of the bed material and explored the effect of buoyant forces on the motion of objects with different sizes and densities.

Use of the radioactive particle tracking (RPT) technique for studying the solid circulation patterns in binary mixtures was initially introduced by Larachi et al. (Larachi, Cassanello, Marie, Chaouki, & Guy, 1995). Cassanello et al. (Cassanello, Larachi, Guy, & Chaouki, 1996) adopted this technique to investigate solids mixing in gas-liquid-solid fluidized beds. More recently, Upadhyay and Roy (Upadhyay & Roy, 2010) employed this method to explore the mixing and

hydrodynamic behavior in a bed consisting of equal weight percentages of the same size particles differing in density.

Zhang et al. (Yong Zhang, Jin, & Zhong, 2009) studied the effect of biomass ratio on the fluidization behavior of mixtures composed of 1 to 3% biomass. They found that the composition of mixtures had a quantitative impact on the ultimate distribution of biomass particles, i.e. increasing the ratio of biomass to sand at  $U > U_{ff}$  led to the occurrence of a greater maximum of mixing index at higher gas velocities. They have also reported that when mixing prevailed against segregation, increasing the biomass load exerted an adverse influence on the mixing; in contrast, as the increase of gas velocity enhanced particle segregation, increasing biomass load improved particle mixing (Yong Zhang et al., 2008).

Despite the widespread application for fluidization of a bulk of large and light Geldart D particles (D. Geldart, 1973) mixed with a fluidization medium of Geldart B, the phenomenological knowledge about their mixing pattern is still scarce. Accordingly, this work is aimed at deploying the powerful, non-intrusive RPT technique to shed some light on the distribution profile and circulatory motion of biomass particles fluidized with the help of sand. Moreover, the experimental findings have been used to develop a model predicting the volume concentration of biomass along the bed.

It is well known that at high temperature endogenous bubbles of volatile matter form around devolatilizing fuel particles (Bruni et al., 2002). Consequently, the density of biomass particles decreases and segregation is enhanced. Since the density of the tracer used in this study was constant during the experiment, such a phenomenon could not be mimicked. However, an approach to investigate this effect through the RPT is using a tracer with lower density compared to the conventional biomass. Since the experiments have been performed in a cold system, gas properties, such as density and viscosity, are different from a practical system where hot gas has a much lower density and higher viscosity. These differences should be taken into consideration before applying the results of this work to the practical units operating under extreme conditions.

It should be noted that since the fluidization of binary systems consisting of common bed materials and irregular particles is not limited to biomass processing, the range of weight fractions investigated in the present study extends beyond the typical maximum biomass loads in industrial units.

## 4.2 Experimental

A cylindrical Plexiglas column 152 mm in diameter is used as the main facility of all experiments performed in the present study. Air is injected into the column through 163 holes, 1 mm in diameter, arranged in a triangular pitch on a stainless steel distributor plate. The percentage of open area of the perforated plate is less than 1. It is worth pointing out that the cross section of the commercial biomass combustors or gasifiers may be as large as a few square meters, while the column diameter used in this study is quite limited. Such a small column diameter may affect the motion and mixing of the bed inventory particles and deviate from the reality in the industrial units.

The bed material utilized in the experiments is sand whose size distribution ranges from 100 to 1000  $\mu\text{m}$ . Since only one tracer can be tracked in the RPT technique, no variety of size and shape of biomass particles could be considered in the experiments and identical biomass particles are used in the system represented well by an active tracer. Accordingly, wood rods are carefully cut into similar cylindrical pieces in order to make identical biomass particles.

It should be kept in mind that, in reality, a broad range of biomass particles in terms of size and shape is fed into the thermal processing unit complicating the hydrodynamic and reaction phenomena. Moreover, biomass degrades into fine char (in pyrolysis and gasification) or ash (in combustion) particles and its proportion and properties change depending on their location in the bed. These deviations from the practical systems have not been addressed in this work. Nonetheless, as mentioned earlier, large biomass particles remain for a relatively long period of time at their original size before they reach the high temperatures which is needed for thermal degradation. This period is long enough to form the distribution pattern of particles in the bed.

Properties of materials used in the present study have been listed in Table 4.1. Measured quantities of these materials are mixed in order to obtain the desired weight fraction of the biomass in the mixture. Table 4.2 contains more details of the mixtures studied.

Table 4.1: Properties of materials used

Material	Shape	$D_p$ (mm)	$L_p$ (mm)	$\rho_p$ (kg/m <sup>3</sup> )	$\rho_b$ (kg/m <sup>3</sup> )
Sand	Spherical	0.38	-	2650	1520
Biomass	Cylindrical	6.35	12.70	824	342

Table 4.2: Properties of systems studied

Wt.% of biomass	Vol.% of biomass	Bulk density of sand-biomass mixture (10 <sup>-3</sup> kg/m <sup>3</sup> )	Voidage of the fixed bed (-)
0	0.0	1.52	0.43
2	6.2	1.46	0.42
4	11.8	1.42	0.41
8	21.9	1.35	0.40
16	38.0	1.22	0.37

In all experiments, the static bed height is set to 228 mm ( $H/D=1.5$ ). In order to start from a well-mixed condition, the sand and biomass measures are each equally divided into eight batches. Each batch of sand is mixed with a single batch of biomass. Finally, the content of all mixtures sequentially is added to the fluidization column.

Two differential pressure transducers (OMEGA PX 272) are deployed to measure the pressure fluctuations of the lower and upper sections of the dense bed. The mean distance of these pressure transducers from the distributor is 85 and 235 mm, respectively, while their respective probes are vertically spaced 50 mm. In addition, the time-averaged pressure drop along the whole bed (5-2000 mm above the distributor) is acquired through another pressure transducer (MODUS Instruments R32-100).

The tracer used for the RPT experiments is fabricated by embedding a tiny amount of a mixture of Scandium oxide and epoxy resin in a hole made in one of the biomass particles so that the size and density of the final tracer are almost identical to those of the original particle. Such a tracer could successfully mimic the motion of biomass particles while being fluidized. The tracer is then activated in the SLOWPOKE nuclear reactor of École Polytechnique up to an activity of 70  $\mu\text{Ci}$ . The produced isotope  $^{46}\text{Sc}$  emits  $\gamma$ -rays, which are counted by 12 NaI scintillation detectors. To maximize accuracy of the RPT results, detectors are distributed on three planes such that each plane is configured 100 mm apart from the adjacent one and staggered 45° to keep the farthest

distance between detectors on alternate planes. The spatial angle between two neighboring detectors in each plane is set to 90°. The horizontal distance between the column and detectors is set according to their saturation lengths measured beforehand.

A high speed data acquisition system counts the number of  $\gamma$ -rays detected by each detector. These counts are analyzed later to calculate the coordinates of the tracer. Details of the system calibration and the inverse reconstruction strategy for determining tracer position can be found elsewhere (Larachi, Chaouki, & Kennedy, 1995; Larachi, Kennedy, & Chaouki, 1994). In each experiment, the location of the tracer is tracked every 10 ms for about 6 hours until finally more than two million points are acquired. RPT experiments are conducted at low ( $U= 0.36$  m/s) and high ( $U= 0.64$  m/s) superficial gas velocities for systems containing 2, 8 and 16 wt. % biomass. It is important to note that the velocity range studied is similar to that of fluidized bed gasifier but lower than the superficial gas velocity adopted typically in fluidized bed combustors (1-3 m/s).

## 4.3 Results and discussion

### 4.3.1 Characterization of biomass fluidization

#### 4.3.1.1 Analysis of the local pressure drop

It is generally accepted that solids mixing in fluidized beds comprising dissimilar components is a function of the gas velocity. The local concentration of each substance therefore varies along the bed by changing the superficial gas velocity. These variations can be analyzed through the local time-averaged values of the signals of the pressure drop. In order to study the trend of mixing/segregation with gas velocity, the gradients of the local pressure drop versus gas velocity are obtained at bottom and top of the bed. Any change in these gradients arises due to the change in the fraction of sand, biomass, and the associated voidage. The fractions pertaining to sand and voidage (gas phase) are excluded by subtracting the corresponding experimental pressure drop gradients of a bed of sand alone which is fluidized under the similar operational conditions.

The resultant parameter, i.e.  $\left( \left[ \frac{d\Delta P}{dU} \right]_{mix} - \left[ \frac{d\Delta P}{dU} \right]_{sand} \right)$  reflects changing in the fraction of biomass in the intended section with the superficial gas velocity, on the assumption that the presence of

biomass does not change the void fraction of the bed of sand. Fig. 4.1a represents variations of this parameter at the top of the bed for mixtures containing different loads of biomass. The descending trend of profiles at  $U < 0.65$  m/s, indicates that the amount of biomass declines by increasing gas velocity. In other words, biomass particles which are initially accumulated on the surface of the bed at low gas velocity ( $U \sim U_{ff}$ ) sink to the lower parts and the mixing extent of sand and biomass is enhanced along the bed. It is noteworthy that the positive effect of increasing gas velocity on the mixing of the bed components is more pronounced when the load of biomass is higher. In other words, an identical increase in gas velocity brings about a greater decrease in the content of biomass when the total quantity of biomass in the mixture is higher. The values of the investigated parameter at velocities higher than  $U = 0.65$  m/s are relatively small and almost identical, regardless of the composition of the mixture. It denotes that compared to the low bubbling gas velocities, no significant change in the fraction of biomass at the top of the bed is expected when the superficial gas velocity exceeds a certain range.

This behavior is in total agreement with observations of Zhang et al. (Yong Zhang, Jin, & Zhong, 2009) who studied the mixing and segregation of biomass particles in a wide range of superficial gas velocities. They reported that the biomass concentration at the top layer of the bed decreases significantly with increasing gas velocity, and at a certain velocity, it reaches a minimum, then it increases gradually. They emphasized that enhancement of mixing as a consequence of increasing gas velocity is only limited to the top part of the bed. This is the case also in the present study, since plotting  $\left( \left[ \frac{d\Delta P}{dU} \right]_{mix} - \left[ \frac{d\Delta P}{dU} \right]_{sand} \right)$  vs.  $U$  for the bottom part of the bed brings no meaningful results.

The trend of evolution of void size distribution at the top of the bed is shown in Fig1b. As explained in our previous work (Fotovat, Chaouki, & Bergthorson, 2013b), this graph was obtained by analysis of the pressure statistics. In this regard, pressure increments were initially calculated for a certain time delay (10 ms). The probability density function (PDF) of these increments was then computed and normalized to the respective standard deviation value of the pressure signal. Finally, Student's distribution (Eq. (4.1)) was fit to the PDF to obtain two fitting parameters ( $\alpha$ ,  $\beta$ ). It has been shown that the parameter  $\beta$  is related to the shape of the void size distribution around the pressure measurement probe (B. Bai et al., 2005).

$$\rho_s(z) = N(\alpha, \beta)[1 + \alpha z^2]^{-\beta} \quad (4.1)$$

As seen, the remarkable similarity between the trend of change in  $\left(\left[\frac{d\Delta P}{dU}\right]_{mix} - \left[\frac{d\Delta P}{dU}\right]_{sand}\right)$  in Fig. 4.1a and  $\beta$  values in Fig. 4.1b with gas velocity signifies the existence of a linkage between the segregation pattern of biomass particles and evolution of size and shape of voidage at the top of the bed. It indicates that in systems composed of irregular particles like biomass, the local concentration of the non-conventional material governs the properties of bubbles in the bed at relatively low gas velocities.

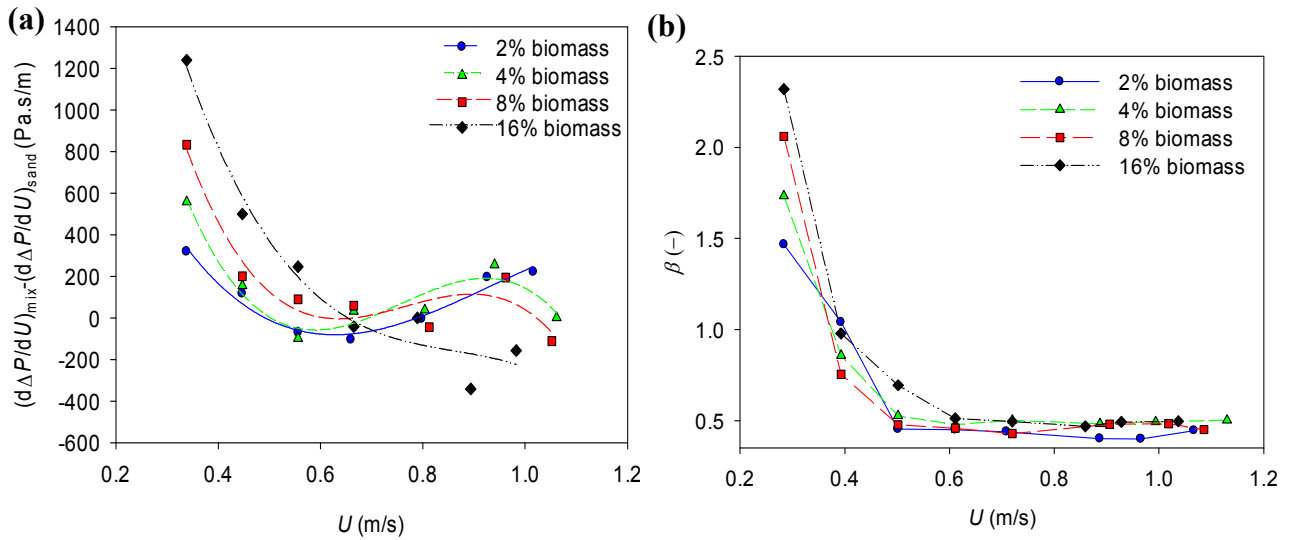


Fig. 4.1: a) Profile of the difference between the local pressure drop gradients of mixtures of sand and biomass and that of a similar bed composed of sand alone in a bubbling regime b) Variation of parameter  $\beta$  as one of the two curve fitting parameters of Student's distribution used to fit the PDF of pressure increments.

#### 4.3.1.2 Time-averaged concentration of biomass particles

The time-averaged concentration profile of biomass particles is obtained non-invasively by the Radioactive Particle Tracking (RPT) method. For this purpose, the bed space is imaginarily compartmentalized by means of azimuthal slices of several radial and axial cuts. The ratio of occurrence of the tracer in a specific compartment to the total number of occurrences, i.e., total fraction of recorded instantaneous positions, is considered as the corresponding concentration of that compartment.

The schematic concentration profile of biomass particles in systems containing 2 and 16% wt. biomass and fluidized at  $U=0.64$  m/s is depicted in Fig. 4.2. Formation of a biomass-rich layer at the top, as well as a region nearly devoid of biomass at the bottom, of the bed is a common feature observed for all fluidized systems regardless of the fluidization velocity studied. Such a feature denotes the flotsam behavior of biomass particles. The expansion extent of biomass particles as a consequence of increasing the gas velocity from 0.36 to 0.64 m/s is inversely proportional to the load of biomass. In other words, the higher weight fraction of biomass is, the lower extent of biomass expansion is expected.

A very low concentration of biomass particles in the core of the bed is ascribed to the dominance of bubbles in this region. Moreover, owing to the large size of biomass particles, it is unlikely that they are lifted in the wake of bubbles. Thus, it is not surprising that the biomass concentration is substantially higher at the bed annulus compared to the bed core.

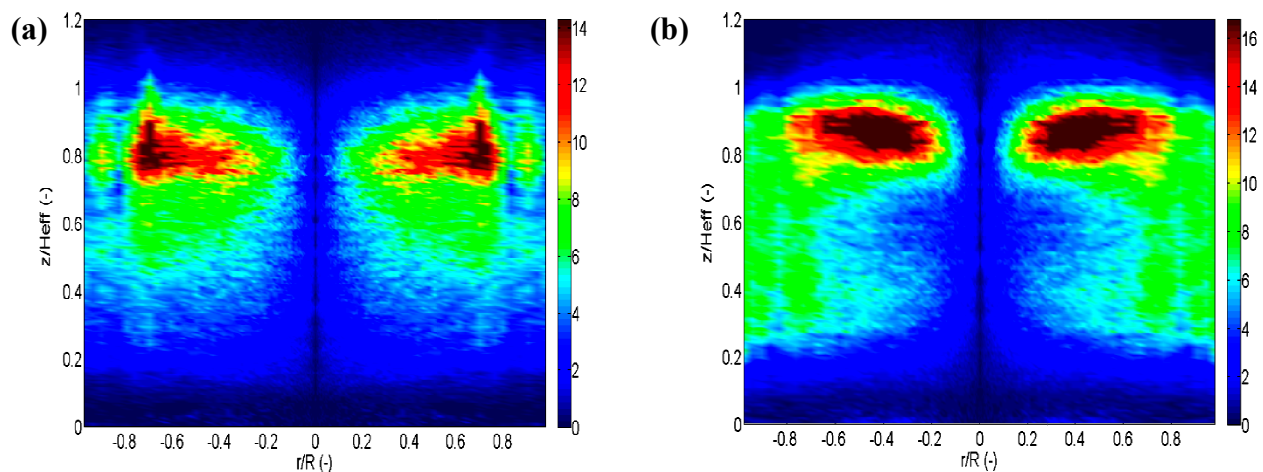


Fig. 4.2: Time-averaged concentration (occupancy) profile of biomass particles of mixtures containing a) 2%, b) 16% biomass, fluidized at  $U=0.64$  m/s

#### 4.3.1.3 Characteristics of biomass circulation

The axial trajectory of the tracer consists of several ascending and descending segments representing the rising and sinking paths. Gross circulation, i.e., upward movement of solids as a consequence of bubble rise and their offsetting downward flow in the dense phase is known as the main mechanism of solids mixing along the whole height of the bed. As explained by Stein et al. (Stein, Martin, Seville, McNeil, & Parker, 1997), the cycle time, i.e., the period of tracer

circulation from below 30% to higher than 70% of the bed height and back, correlates with the axial mixing rate of solids. However, Stein et al. determined these boundaries based on the circulation of Geldart-B particles. Our studies showed that they are also appropriate to delineate the circulation path of biomass particles in the mixtures used in the present work.

The gross circulation length is defined as the maximum vertical displacement traversed by the tracer in a gross cycle. Due to the lower degree of expansion of large particles in the bed, the effective dense height ( $H_{\text{eff}}$ ) decreases with increasing biomass loading and the gross cycle lengths drop proportionally.  $H_{\text{eff}}$  is defined as the height up to which 95% of all tracer occurrences took place. The probability distribution of gross circulation lengths normalized by the  $H_{\text{eff}}$  is shown in Fig. 4.3 for systems fluidized at low and high bubbling velocities.

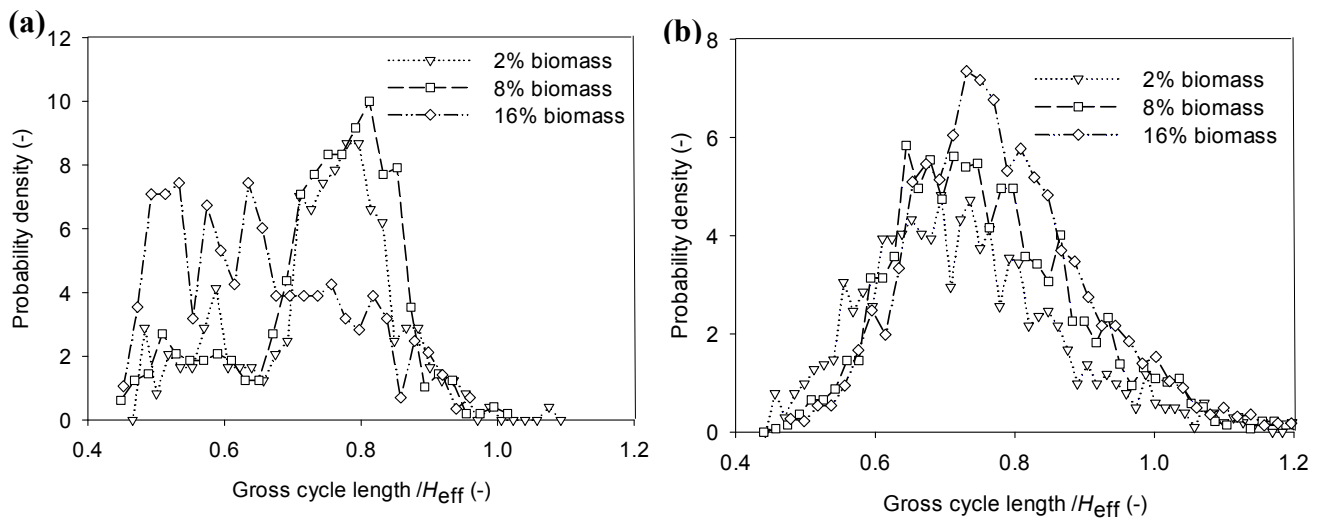


Fig. 4.3: Probability density function of the normalized gross cycle length for systems fluidized at a)  $U=0.36$  m/s b)  $U=0.64$  m/s

As inferred from the relatively short lengths of the most probable gross cycles and the wide distribution of the probability density profile, fluidization of the mixture containing 16% biomass at  $U=0.36$  m/s does not result in the adequate circulation of particles in the bed. On the other hand, at  $U=0.64$  m/s, the most frequent normalized gross cycle length is almost identical for all systems, whereas the corresponding frequencies rise by increasing the load of biomass. These variations signify the occurrence of more uniform cycles in the presence of larger quantities of biomass at a high enough superficial gas velocity.

The circulation pattern of an object immersed in a bubbling fluidized bed is characterized by the number of jumps occurring during its upward path as well as the maximum depth attained by the object (Soria-Verdugo, Garcia-Gutierrez, Sanchez-Delgado, et al., 2011). Fig. 4.4 shows the distribution of the number of jumps, which take place during rise of the tracer in the different systems studied. At  $U=0.36$  m/s, in spite of the shorter length of the most frequent gross cycles, a larger number of jumps occurs in the case of 16% biomass. This is ascribed to the feeble bubbles inducing the jumps, which are not capable of establishing a uniform circulatory motion of biomass particles. At  $U=0.64$  m/s, however, a lower number of jumps is required to vertically lift the biomass particles for beds with higher biomass fractions.

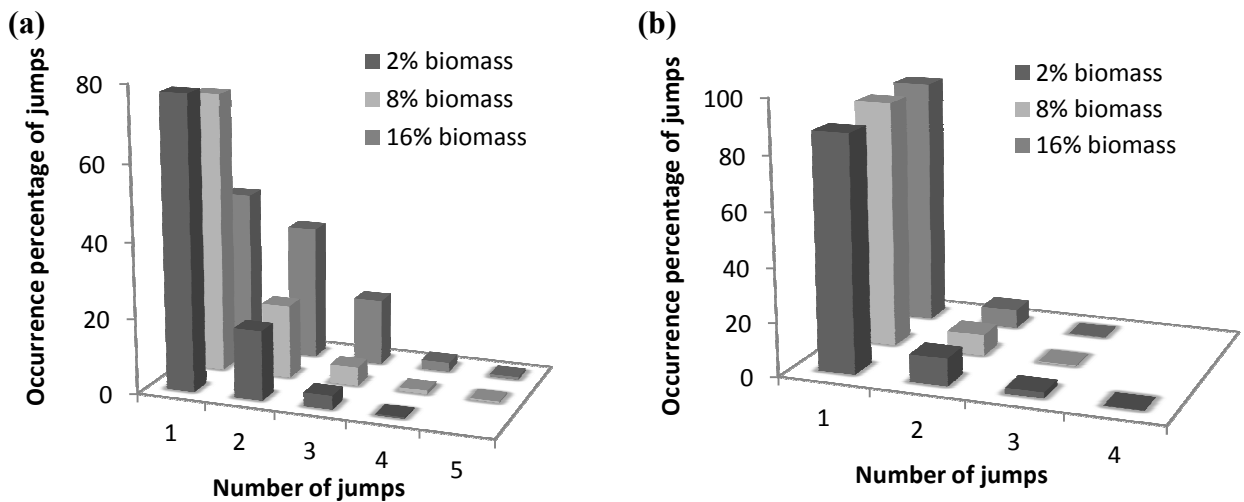


Fig. 4.4: Occurrence percentage of jumps in gross cycles of systems fluidized at a)  $U=0.36$  m/s, b)  $U=0.64$  m/s

As reported previously, at high superficial gas velocities, the dense phase fraction decreases at the center of the bed with increasing biomass loadings (Fotovat et al., 2013b). Thus, lift of biomass particles induced by bubbles is boosted since they are subject to less resistance during their upward paths which is caused by the dense phase. The similar pattern of change in the profiles of the normalized gross cycle length and the occurrence percentage of jumps implies the pivotal role of the bubbling characteristics of the bed in governing the circulatory motion of biomass particles.

The axial loci of valleys of the tracer trajectory are analyzed to explore the extent of penetration of biomass particles within the bed. The probability density profile of the normalized maximum attainable depth ( $L_{\max}/H_{\text{eff}}$ ) of mixtures fluidized at  $U=0.64$  m/s is plotted in Fig. 4.5. As defined above,  $H_{\text{eff}}$  is the height up to which 95% of all tracer occurrences take place. It was found that this limit (95%) delineates well the height of the dense bed beyond which biomass particles splash. Therefore, the zone over the dense bed height is not involved in the biomass circulation path and not shown in the graph.

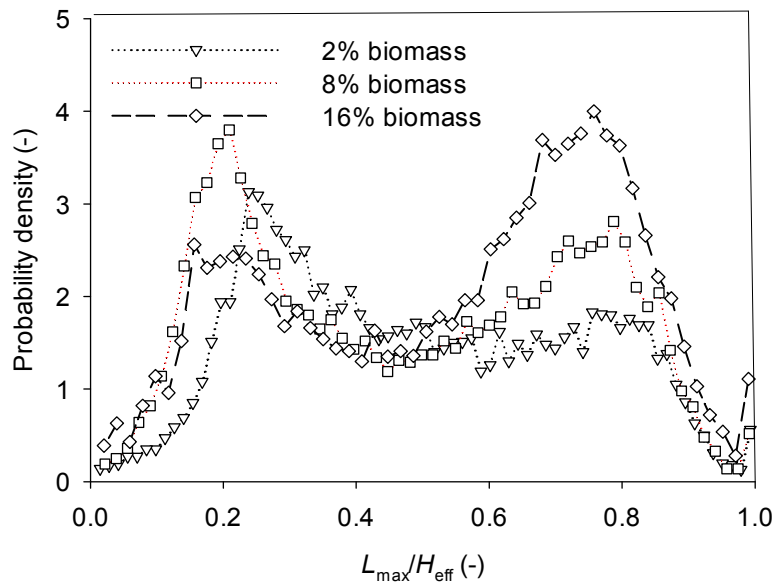


Fig. 4.5: Probability density profile of the maximum attainable depth of biomass particles for systems fluidized at  $U=0.64$  m/s.

As illustrated, the plots encompass two peaks. The first set of peaks signifies the downward motions disturbed by the rising bubbles impeding the sinking process. The second set corresponds to the deep penetration of biomass particles achieved in the gross cycles. It is observed that the probability that biomass particles will sink to the lower level of the bed is enhanced with increasing biomass fraction in the mixture. This behavior can be explained in light of recent findings by Soria-Verdugo et al. (Soria-Verdugo, Garcia-Gutierrez, Garcia-Hernando, et al., 2011), who found that the difference between the density of a large object immersed in a bubbling fluidized bed and the bulk density of the surrounding medium governs the sinking behavior of the object. Since the bulk density of the systems studied in the present study is

reduced by increasing the fraction of biomass, the net buoyant force exerted on the particles weakens proportionally. Additionally, studies of the gas distribution pattern between the dilute and dense phases show that increasing the quantity of biomass in the mixture leads to increased gas holdup and a dilution of the dense phase at the wall region (Fotovat et al., 2013b). Consequently, the sinking process at this zone is improved due to the higher permeability of the surrounding medium, which causes less resistance against the downward motion of the larger flotsam particles. As a result, the gross circulation of biomass particles in the bed is boosted with larger biomass loadings at high superficial gas velocities, and more successful gross cycles are observed in the bed per unit time.

Fig. 4.6 shows the mean cycle time (the mean duration of gross cycles) and the cycle frequency (number of cycles per given period of time) in mixtures differing in the quantity of biomass fluidized at  $U=0.36$  and  $0.64$  m/s. As expected, increasing gas velocity reduces the mean cycling time and raises the cycle frequency. The opposite effect of biomass fraction on the cycle characteristics at low and high superficial gas velocities is clearly seen in the figure. Unlike  $U=0.36$  m/s, the mean cycle time decreases and the cycle frequency increases at  $U=0.64$  m/s with increasing the quantity of biomass. It should be noted that the mean rising and sinking velocities of biomass particles do not change meaningfully by changing the load of biomass. Therefore, the increase in the cycle frequency is solely ascribed to the increase in the number of gross cycles that come to pass during a given period of time.

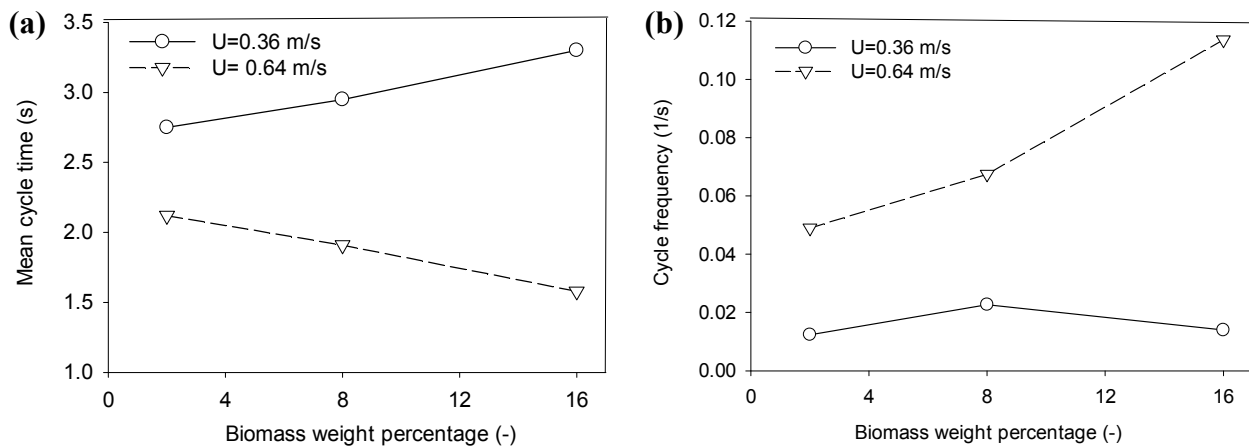


Fig. 4.6: a) The mean cycle time and b) the cycle frequency of systems fluidized at  $U=0.36$  and  $U=0.64$  m/s

The time-averaged concentration (occupancy) profiles of the biomass particles involved in gross cycles are illustrated in Fig. 4.7 for mixtures containing 2 and 16% biomass. Increasing the number of gross cycles with the load of biomass is inferred from the higher range of the corresponding legend of Fig. 4.7b compared to that of Fig. 4.7a. The cross-sectional distribution of biomass particles differs also for these systems. As inferred from the position of the red spots in the figure, in the case of 2% biomass, most of the gross cycles are demarcated between the center of the lower, and the wall region of the upper, bed sections. By raising the biomass fraction to 16%, however, particles start their ascent from the wall region and move towards the center of the column as they rise. The gross cycles are completed by sinking particles from the center of the bed towards the wall.

Mabrouk et al. (Mabrouk, Radmanesh, Chaouki, & Guy, 2005) studied the solid holdup profile in a column 15.2 cm in diameter filled with sand up to  $h/D=2$ . They found that at a given height the radial solid holdup is generally high close to the wall and declines moving towards the center of the column. In addition, it was shown that the cross-sectional averaged solid holdup increased by descending in the bed. In view of the direct correlation between the solid holdup and the local bulk density (Escudero & Heindel, 2011), it is expected that the local bulk density will increase by going down in the bed, particularly at the wall region. As discussed above, the higher bulk density of the sinking medium impedes the descent of biomass particles. As a consequence, the downward pathway of the flotsam particle is dragged to the core of the bed where the particle is exposed to the less buoyant force due to the more dilute state of the bed. In light of the bubble dominance at the core of the bed, however, biomass particles are prone to be involved in a rising process before a thorough sinking thus reducing overall mixing. When the biomass load is increased, the bulk mixture density decreases and it has been shown that, when the biomass fraction increased from 2 to 16%, the mean bubble size became smaller and the dense phase fraction at the wall region fell remarkably (Fotovat et al., 2013b). Hence, the sinking process could be carried out in the annular region of the bed and flotsam particles penetrate more effectively into the lowermost sections without being disturbed by the passage of large bubbles. In view of these phenomena, the most probable pathway of biomass gross cycles has been plotted in Fig. 4.7. It is worth pointing out that these differences matter from the practical point of view for considering an adequate choice for the feeding locations. In other words, the optimal feeding point can depend on the composition of the bed inventory. Radmanesh et al. (Radmanesh et al.,

2006) showed that the feeding location could significantly affect distribution of gas products in the bed. In bottom feeding, the product gases from the pyrolysis step enter directly into the region of the bed where the concentration of oxygen is high. As a result, light gases, such as  $H_2$  and  $CO$ , as well as tar, are prone to combustion in the bed. On the other hand, in top feeding, the gas product from the pyrolysis step enters in a region that has already become depleted of oxygen, mainly through the char combustion in the bed. Consequently, concentrations of  $H_2$  and  $CO$  are higher and cracking and combustion of tar is less prone.

In view of the influence of the composition of the bed inventory on the locus of the most probable circulation pathway of the biomass particles, it is inferred that the inward ascent (from the wall towards the central region) and the outward descent (from the center towards the wall of the bed) are the favored paths for occurrence of a higher degree of the axial mixing. This fact is a matter of importance in designing the feeding points of biomass combustors/gasifiers. In addition, the effectiveness of top or bottom feeding can be changed by changing the composition of the mixture fluidized in the bed. For instance, in the case of bottom feeding for the mixture composed of 16% biomass, particles are prone to being drawn into the rise path of the gross cycles as soon as being fed into the bed, whereas for the mixture containing 2% biomass, particles can rest longer in the lower part of the bed since the loci of gross cycles are far from the wall proximity in this region. Thus, it is expected that in the case of bottom feeding, contact of the pyrolysis products and oxygen takes place more effectively when the load of biomass is lower. On the other hand, since biomass particles are subject to descend in the wall region when the load of biomass in the bed is high, it is more likely that they will react effectively with the interstitial oxygen of the dense phase, thereby improving the reactor performance.

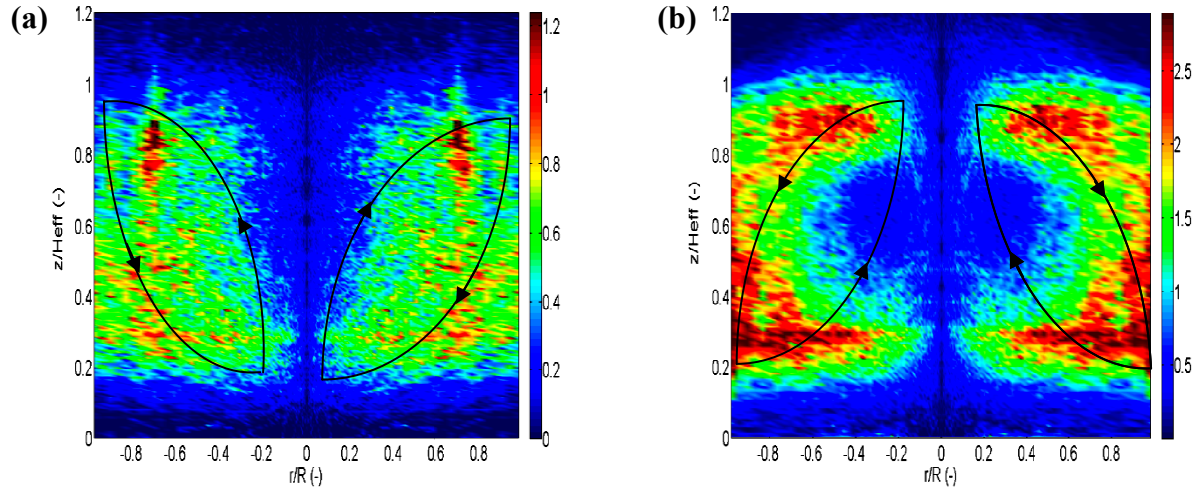


Fig. 4.7: The time-averaged concentration (occupancy) profiles of the biomass particles involved in gross cycles at  $U=0.64$  m/s for mixtures composed of (a) 2% (b) 16% biomass. The most probable pathway of the biomass gross cycle has been illustrated by the black curves.

### 4.3.2 Quantification and modeling the axial distribution of the volume fraction of biomass

Distribution of bed components along the bed is usually quantified through obtaining the axial profile of the volume fraction of jetsam or flotsam particles. In the present study, the volume fraction of biomass ( $X_B$ ) is obtained by post-processing of the RPT data through the virtual slicing of the bed and computing the ratio of occurrence of the tracer in a specific slice to the total number of occurrences, i.e. the total number of recorded instantaneous positions. These values are then related to the volume fractions of biomass in each slice knowing the quantities of sand and biomass mixed initially and the respective densities.

To compare the degree of uniformity of biomass distribution in mixtures differing in biomass fractions,  $X_B$  is normalized to the total volume fraction of biomass in the bed ( $X_{B,\text{total}}$ ). As depicted in Fig. 4.8, increasing gas velocity gives rise to a shift in the normalized  $X_B$  values, particularly at the middle height of the bed, to the dashed line indicating a perfectly mixed state. This improvement in the mixing state is more pronounced for systems containing 8 and 16% biomass, signifying the positive effect of the higher load of biomass particles on their even distribution along the bed.

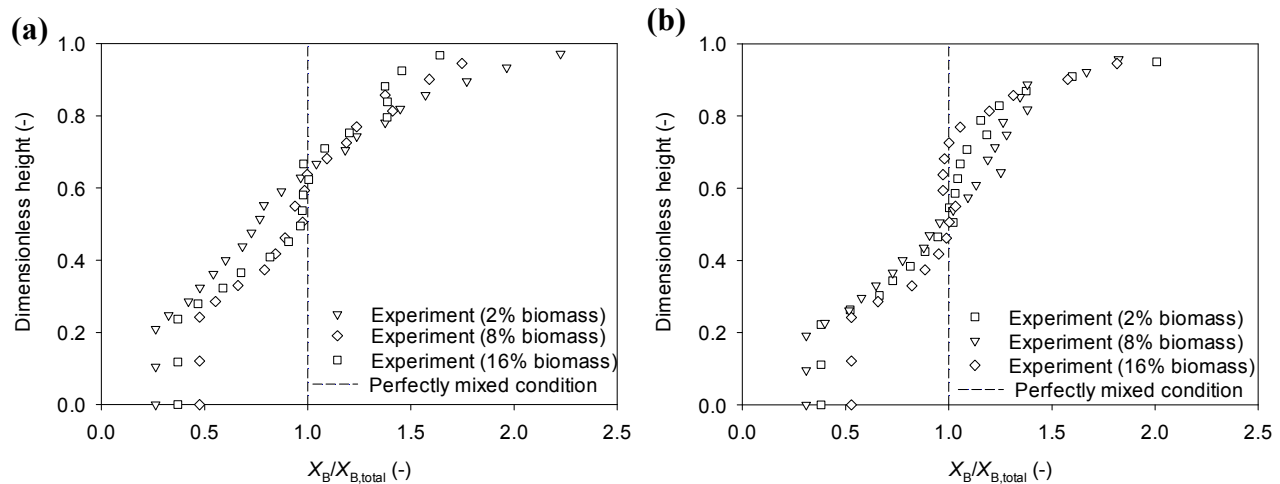


Fig. 4.8: The experimental normalized volume fraction of biomass ( $X_B/X_{B,\text{total}}$ ) vs. the dimensionless height at a)  $U=0.36$  m/s b)  $U=0.64$  m/s

In order to model the axial distribution of biomass, the principles of the Gibilaro and Rowe (G-R) model (Gibilaro & Rowe, 1974) are applied, however, unlike the G-R and other common models in which the jetsam profile is studied, the concentration profile of the flotsam component is described in the current model.

Since the bed is composed of dense and dilute phases, it has been assumed that the dilute phase is devoid of biomass particles because of their extreme size. The rise of biomass particles mainly occurs due to the intermittent jerks produced by a drift mechanism as a consequence of successive bubble passes. In addition, since bubbles travel preferentially in the central region of the bed, a large scale circulation is also felt by the flotsam particles. Jetsam particles, however, rise in the dilute phase and descend in the dense phase. Therefore, they can be exchanged between dilute and bubble phases. As reported by other researchers (R. Bilbao, Lezaun, Menendez, & Abanades, 1988; A. W. Nienow, 1985; Pallares & Johnsson, 2006), contribution of the jetsam axial mixing and segregation propensity to the material balances for solids mixing is negligible under the conditions of biomass fluidization, thus they have not been considered in the proposed model. Fig. 4.9 depicts a diagram of a horizontal layer of the bed of  $dZ$  thickness to which the mass balances of both phases have been applied. The mathematical expression of each term is as follows:

Fluidization medium (sand in our experimental systems) rises along the bed in the wake of bubbles and sinks in the dense (emulsion) phase. Thus, the flow of rising sand, i.e.,  $\Psi_F^b$  ( $\text{m}^3/\text{s}$ ), is formulated as below.

$$\Psi_F^b = U_b \delta_b F_w (1 - \varepsilon_F) A \quad (4.2)$$

where  $\varepsilon_F$  is the voidage of the emulsion phase of a bed containing sand only. It has been calculated by the Cui et al. correlation (Cui, Mostoufi, et al., 2000) taking into consideration the effect of gas velocity (Eq. (4.3)).

$$\varepsilon_F = \varepsilon_{mf} + 0.2 - 0.059 \exp \left[ -\frac{(U - U_{ib})}{0.429} \right] \quad (4.3)$$

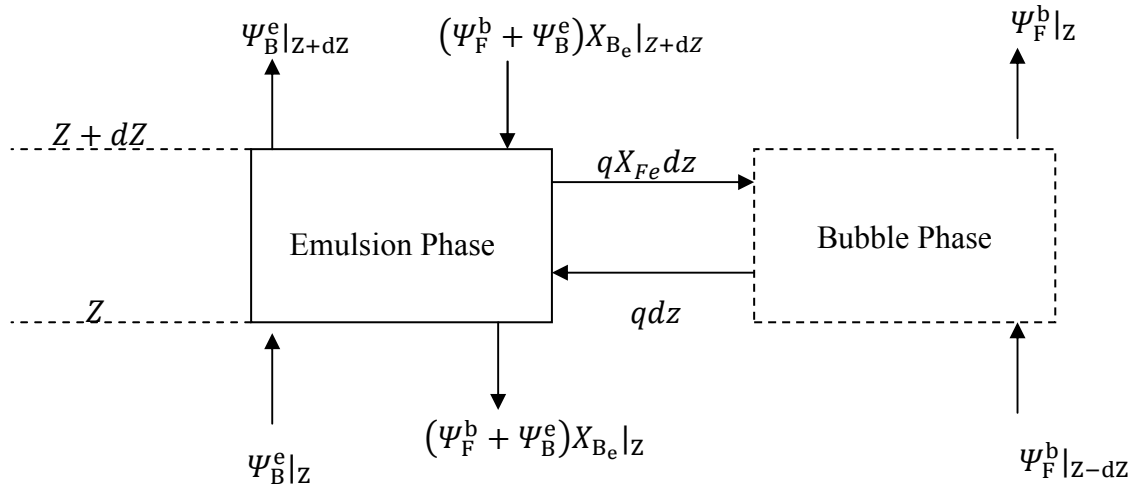


Fig. 4.9: Diagram of the model

The volume fraction occupied by bubbles has been calculated using Eq. (4.4).  $Y$  indicates the degree of deviation of the bed from the “two-phase theory”. Since sand is the dominant component in the investigated mixtures in terms of weight and volume,  $Y=0.7$  is chosen as a typical assumption for the Geldart B particles. As reported in another work (Fotovat et al., 2013b), the presence of biomass particles could delay the onset of bubbling compared to the bed of sand alone. Thus, it is reasonable to use the initial bubbling velocity ( $U_{ib}$ ) instead of  $U_{mf}$  of sand in order to evaluate the excess gas velocity.

$$\delta_b = \frac{Y(U - U_{ib})}{U_b} \quad (4.4)$$

On the basis of the analysis of the biomass rise velocity realized through post-processing of the RPT data, it was found that the average rise velocity of biomass particles is around 0.2 times the average bubble rise velocity (Fig. 4.10), consistent with the findings of Soria-Verdugo et al. (Soria-Verdugo, Garcia-Gutierrez, Sanchez-Delgado, et al., 2011). As discussed below, bubble size and velocity are calculated by using Darton et al. (Darton et al., 1977) and Davidson and Harrison (Davidson & Harrison, 1963) equations (Eqs. (4.9) and (4.10)), respectively. To calculate the mean bubble rise velocity, the latter equation is integrated and averaged along the bed height. Thus, the ratio of biomass to bubble velocity (0.2) is a height-averaged value.

In view of the rise of biomass particles in the emulsion phase, the rising flow of biomass, i.e.,  $\Psi_B^e$  ( $\text{m}^3/\text{s}$ ) is obtained by Eq. (4.5).

$$\Psi_B^e = 0.2U_b(1 - \delta_b)(1 - \varepsilon_e)X_{B_e}A \quad (4.5)$$

$\varepsilon_e$  is the voidage of the emulsion phase in a mixture containing fluidization medium and biomass particles and, as proposed by Bilbao et al. (R. Bilbao et al., 1988), it can be calculated using Eq. (4.6) based on the fact that the fluidization medium occupies the voidage between biomass particles.

$$\varepsilon_e = 1 - \frac{1 - \varepsilon_B}{1 - X_{F_e}} \quad (4.6)$$

Eq. (4.6) is valid when  $X_{B_e} > \frac{1 - \varepsilon_B}{1 - \varepsilon_F}$ . For lower values of  $X_{B_e}$ , it is assumed that the voidage of the mixture emulsion phase ( $\varepsilon_e$ ) equals to the voidage of a bed of fluidization medium alone ( $\varepsilon_F$ ).

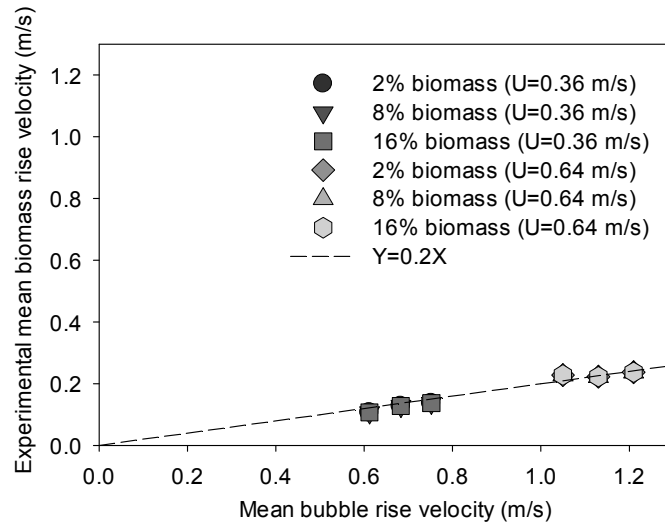


Fig. 4.10: Mean rising velocities of biomass particles along the bed compared with the mean velocity of bubbles

The exchange rate of the fluidization medium between bubble and emulsion phases per unit of bed height can be described by Eq. (4.7).

$$q = K_w \delta_b (1 - \varepsilon_F) A \quad (4.7)$$

Assuming that the exchange coefficient between the constitutive phases ( $K_w$ ) is not affected by the biomass particles, the correlation introduced by Hoffmann et al. (Hoffmann et al., 1993) (Eq. (4.8)) is chosen to calculate  $K_w$  from properties of the bed as pointed out by Radmanesh et al. (Radmanesh et al., 2006).

$$K_w = \frac{0.081}{2\varepsilon_{mf}d_b} \quad (4.8)$$

One of the common assumptions in modeling binary mixtures is that the bubbling characteristics of the system are those of a bed of pure fluidization medium. However, it was revealed that the presence of biomass particles led to the breakage of bubbles (Fotovvat et al., 2013b). From a holistic point of view, the mean bubble size and velocity in all systems could be fairly predicted by correlations of Darton et al. (Darton et al., 1977) (Eq. (4.9)), and Davidson and Harison (Davidson & Harrison, 1963) (Eq. (4.10)), respectively, regardless of the biomass fraction. It should be noted that other correlations, such as those developed by Choi et al. (Choi, Jae E, &

Sang Done, 1988), Cai et al. (Cai, Schiavetti, Demichele, Grazzini, & Miccio, 1994), and Horio and Nonaka (Horio & Nonaka, 1987), predict smaller values than the bubble size measured experimentally and their use in the model leads to predictions not in agreement with the present data.

$$d_b = 0.54g^{-0.2}(U - U_{ib})^{0.4}(Z + 4A_c^{0.5})^{0.8} \quad (4.9)$$

$$U_b = 0.711\sqrt{gd_b} + (U - U_{ib}) \quad (4.10)$$

A mass balance on a slice of the bed for both bubble and emulsion phases can be summarized as follows:

$$\frac{dX_{Be}}{dz} = \frac{qX_{Be}}{(\psi_F^b + \psi_B^e)} \text{ B.C. } X_{Be} = X_{Be0} \text{ } Z=0 \quad (4.11)$$

The axial volume fraction of biomass ( $X_B$ ) is derived from  $X_{Be}$  values through the following equation.

$$X_B = \frac{(1 - \delta_b)(1 - \varepsilon_e)X_{Be}}{(1 - \delta_b)(1 - \varepsilon_e) + F_w\delta_b(1 - \varepsilon_F)} \quad (4.12)$$

A computer program was developed to fit the experimental data with the above equations. To do so, the bed was virtually discretized into successive layers. Eq. (4.11) was then converted into the linear equations using a finite difference scheme and solved numerically for each layer. The boundary value ( $X_{Be0}$ ) was the only adjustable parameter. It should be noted that as exhibited in Fig. 4.2, the lowermost 50 mm of the bed in all studied cases is almost devoid of biomass and this layer is not involved in the circulatory motion of biomass particles presumably because of the ineffective bubbling conditions in this zone. Hence, the volume fraction of biomass in this part was considered as the boundary condition of the model.

Fig. 4.11 shows the experimental profile of biomass concentration along the bed compared to the proposed model at two different fluidization velocities. In general, the model could satisfactorily estimate the experimental data, particularly when the load of biomass is low. By increasing the weight fraction of biomass, however, the fitting quality slightly declines mainly because of the considerable deviation of the actual bubble size from what is predicted by the correlation of

Darton et al. Indeed, it is expected that the prediction capacity of the model would improve significantly if the effect of biomass on the bubbling behavior of systems could be taken into account more accurately. In order to keep the proposed model free of any adjustable parameter, it is reasonable to relate  $X_{B_{e0}}$  to the fluidization velocity ( $U$ ) and the weight fraction of biomass in the mixture ( $x_{Bm}$ ). Applying a multivariable data fitting reveals that  $X_{B_{e0}}$  is related to  $x_{Bm}$  and  $U$  as below.

$$X_{B_{e0}} = kx_{Bm}^{1.2}U^{1.6} \quad (4.13)$$

Since Eq. (4.13) has been obtained for the lowermost part of the bed, adjacent to the distributor, dependency of the volume fraction of biomass on superficial gas velocity can be linked to the parameters governing the multiple gas inlet jets. It has been shown that the minimum moving zone diameter ( $d_m$ ) around the jetting zone is correlated to  $U^{1.5}$  (Horio, Kiyota, & Muchi, 1980). As indicated by Agarwal et al. (Agarwal, Lattimer, Ekkad, & Vandsburger, 2011), this zone contains slow moving emulsion particles entraining into the jets and its demarcation is pivotal in determining the particle circulation volume in the region above the distributor base and below the jet penetration height. By enlarging this zone as a consequence of increasing gas velocity, the likelihood of biomass penetration from the upper layers to the distributor region is enhanced.

Table 4.3 compares the values of the  $X_{B_{e0}}$  obtained from the fitting of experimental data and Eq. (4.13). Furthermore, experimental data and a model in which Eq. (4.13) is considered as the boundary condition have been compared in Fig. 4.12. As seen, use of Eq. (4.13) in the suggested model for estimating  $X_{B_{e0}}$  brings about the acceptable prediction of the biomass distribution profile along the bed.

Table 4.3: Comparing the values of  $X_{B_{e0}}$  obtained from the fitting of experimental data and Eq. (4.13) ( $k=2$ )

Load of biomass	Gas velocity (m/s)	$X_{B_{e0}}$ (Fitting)	$X_{B_{e0}}$ (Eq. (4.13))
2%	0.36	0.0041	0.0036
	0.64	0.0089	0.009
8%	0.36	0.0237	0.0188
	0.64	0.0459	0.0473
16%	0.36	0.0431	0.0433
	0.64	0.1119	0.1086

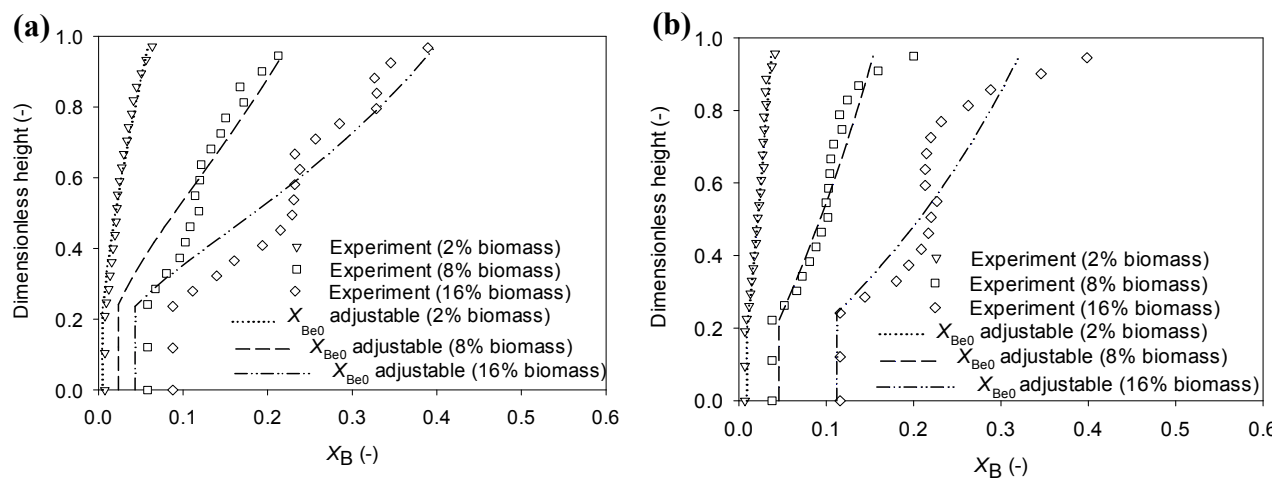


Fig. 4.11: The experimental and modeled volume fraction of biomass ( $X_B$ ) vs. the dimensionless height of the mixtures containing 2, 8, and 16% biomass fluidized at a)  $U=0.36$  m/s b)  $U=0.64$  m/s.  $X_{Be0}$  is the single adjustable parameter in the model used determined by data fitting.

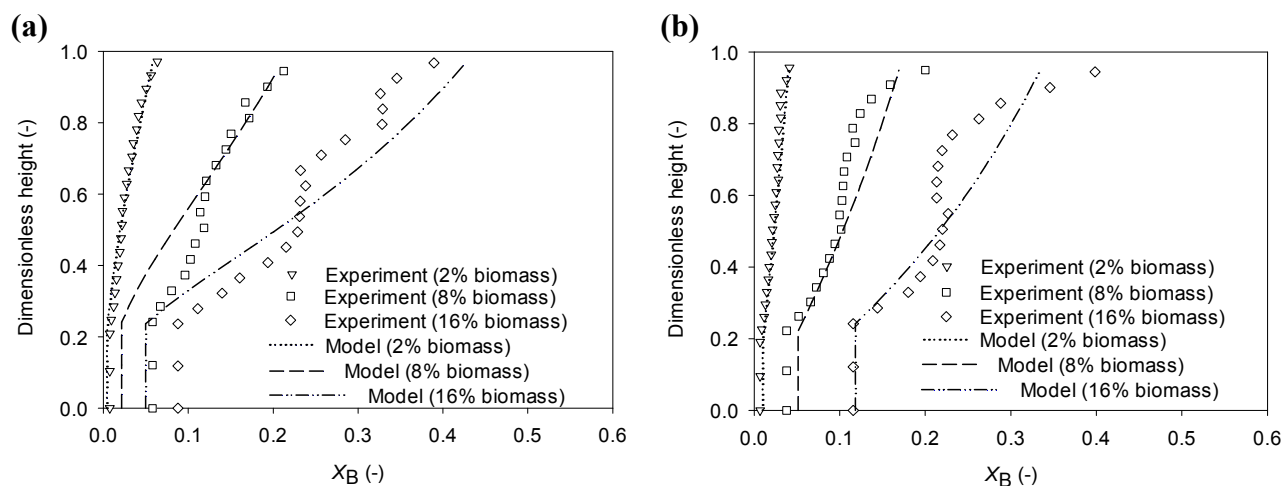


Fig. 4.12: The experimental and modeled volume fraction of biomass ( $X_B$ ) vs. the dimensionless height of the mixtures containing 2, 8, and 16% biomass fluidized at a)  $U=0.36$  m/s b)  $U=0.64$  m/s when Eq. (4.13) is used to estimate  $X_{Be0}$ .

Carrying out sensitivity analysis reveals that the sensitivity of the profile of biomass volume fraction to the load of biomass increases by increasing the superficial gas velocity. In other words, at high gas velocities, a slight change in the load of biomass could significantly impact biomass distribution along the bed. It is consistent with the above discussion considering the improvement in the circulation of large particles by increasing their fraction in the bed at  $U=0.64$  m/s.

To verify the suitability of the proposed model to predict the distribution of biomass in other experimental systems, it was applied to the experimental data of Bilbao et al. (R. Bilbao et al., 1988), who obtained the axial volume fraction profile of straw particles mixed with sand in a small fluidization column (I.D.=8 cm). To extract the volume fraction of sand along the bed, Bilbao et al. followed the “freezing bed” technique, i.e. they suddenly stopped the air flow and extracted 1 cm thick bed layers. It should be noted that this method does not allow for considering the real voidage of the bed under fluidization conditions; therefore the reported values may not be representative of the real axial distribution of the particles.

Considering the different properties of straw from those of the biomass particles used in our experiments, a sensitivity analysis was performed with respect to the ratio of the average rise velocity of biomass particles to that of bubbles in the bed ( $\frac{\bar{U}_{bm}}{\bar{U}_b}$ ). As shown in Fig. 4.13,  $\frac{\bar{U}_{bm}}{\bar{U}_b} = 0.3$  is the optimal ratio resulting in the predicted values representing the experimental data. Increase in  $\frac{\bar{U}_{bm}}{\bar{U}_b}$ , respecting the ratio used in the present study (0.2), is justifiable in light of the smaller size and the lower density of the straw particles compared with the large wood pieces fluidized with sand.

As demonstrated in Fig. 4.14 and Fig. 4.15, the error between the experimental and the corresponding model values for systems differing in composition and fluidization velocity decreases slightly when  $\frac{\bar{U}_{bm}}{\bar{U}_b}$  changes from 0.2 to 0.3.

The above discussion indicates that further experimental work is required to improve the developed model (with no adjustable parameter) in order to make it fully applicable to the fluidized beds involving various types of inert and biomass particles in terms of size, density and shape.

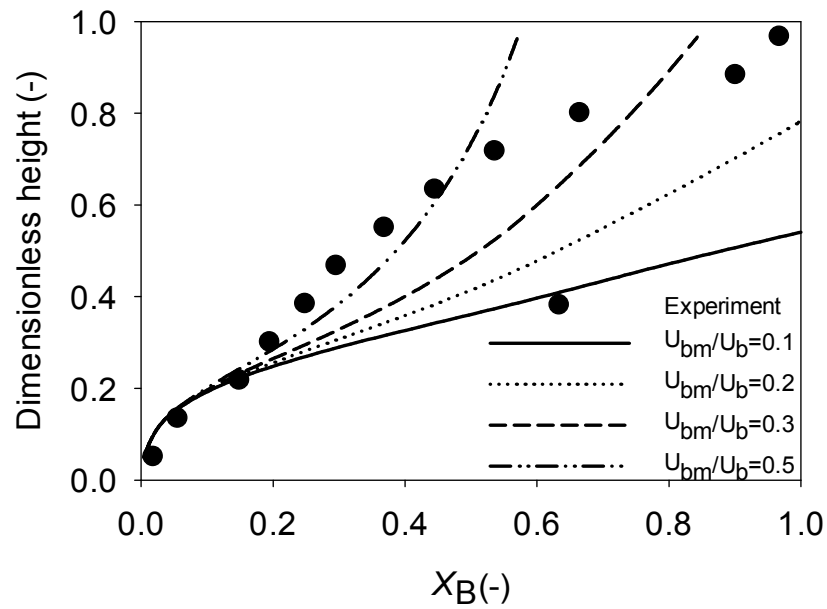


Fig. 4.13: Sensitivity of the model proposed with respect to  $\frac{\bar{U}_{bm}}{\bar{U}_b}$ , as applied to the experimental data of Bilbao et al. (R. Bilbao et al., 1988), (fluidization of straw-sand mixtures at  $U=0.14$  m/s, ( $x_{\text{straw}}=0.08$ ,  $d_{\text{sand}}=158 \mu\text{m}$ ,  $d_{\text{straw}}=794 \mu\text{m}$ ,  $\rho_{\text{sand}}=2000 \text{ kg/m}^3$ ,  $\rho_{\text{straw}}=350 \text{ kg/m}^3$ ))

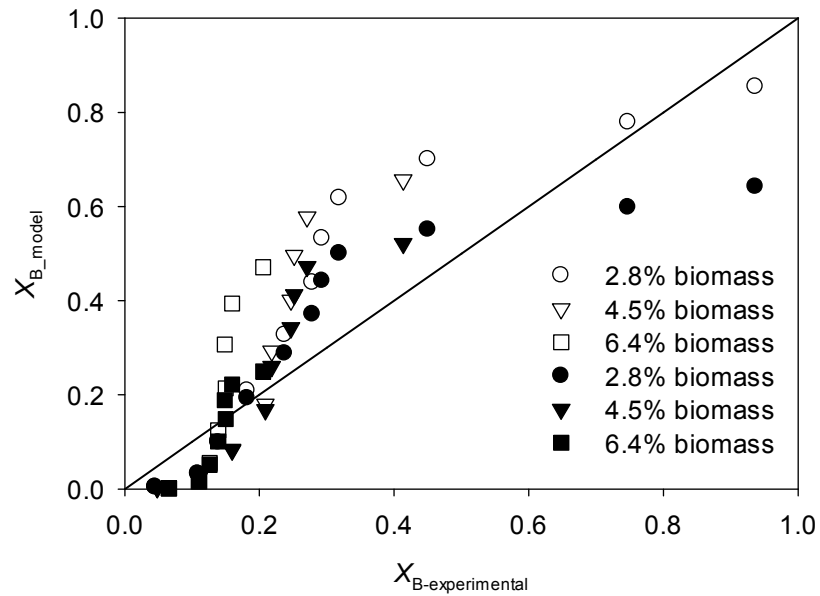


Fig. 4.14: The values predicted by the proposed model when  $\frac{\bar{U}_{bm}}{\bar{U}_b} = 0.2$  (white symbols) and  $\frac{\bar{U}_{bm}}{\bar{U}_b} = 0.3$  (black symbols) vs. the corresponding experimental data reported by Bilbao et al. (R. Bilbao et al., 1988), ( $U = 0.17$  m/s,  $d_{sand} = 158$   $\mu\text{m}$ ,  $d_{straw} = 1265$   $\mu\text{m}$ ,  $\rho_{sand} = 2000$   $\text{kg/m}^3$ ,  $\rho_{straw} = 350$   $\text{kg/m}^3$ )

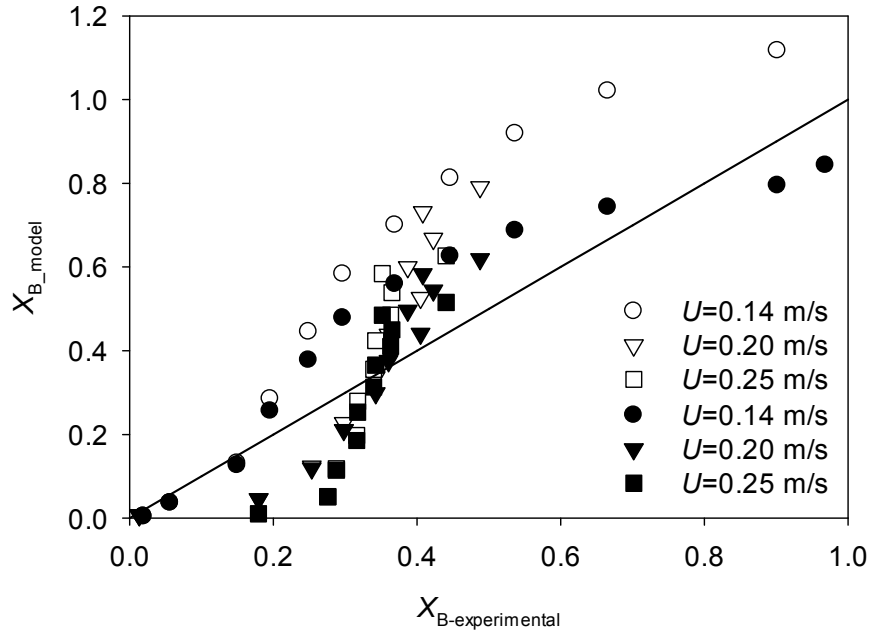


Fig. 4.15: The values predicted by the proposed model when  $\frac{\bar{U}_{bm}}{\bar{U}_b} = 0.2$  (white symbols) and  $\frac{\bar{U}_{bm}}{\bar{U}_b} = 0.3$  (black symbols) vs. the corresponding experimental data reported by Bilbao et al. (R. Bilbao et al., 1988), ( $x_{straw} = 0.08$ ,  $d_{sand} = 158 \mu\text{m}$ ,  $d_{straw} = 794 \mu\text{m}$ ,  $\rho_{sand} = 2000 \text{ kg/m}^3$ ,  $\rho_{straw} = 350 \text{ kg/m}^3$ )

## 4.4 Conclusion

The distribution of large biomass particles along a bubbling fluidized bed was studied experimentally through analysis of the local pressure fluctuations and inference of the biomass particle circulation patterns. The axial particle dispersion in the bed was explored by tracing the trajectory of an active tracer in mixtures containing different weight fractions of biomass. The occurrence of segregation in the bed was qualitatively perceived through the local time-averaged pressure drops as well as the time-averaged occupancy profile obtained by the RPT technique. Increasing the biomass fraction at  $U=0.36$  m/s leads to the imperfect circulation and severe segregation of biomass particles. However, at  $U=0.64$  m/s higher quantities of biomass in the bed improve the sinking process of biomass and bring about a more uniform distribution of biomass throughout the bed. Considering the enhanced mixing state and the loci of the most probable pathway of biomass circulation, it is expected that the impact of the feeding location (top or bottom feeding) on the distribution of gas products in the bed diminishes by increasing the biomass fraction under vigorous bubbling conditions.

The parameters relating terms of the G-R model to the operating conditions were improved on the basis of the experimental findings describing the motion of the flotsam particle and the characteristics of bubbling. Analysis of the experimental data acquired by the RPT technique revealed that the averaged rise velocity of biomass particles is around 0.2 times the bubble velocity in the bed regardless of the biomass load or fluidization velocity. A model has been proposed that could successfully predict the volume fraction of biomass along the bed. It was shown that the biomass volume fraction in the grid-zone region of the fluidized bed is correlated to the superficial gas velocity and the load of biomass.

## CHAPTER 5

### **BUBBLE BEHAVIOR IN A BIOMASS-SAND FLUIDIZED BED: VALIDATION OF CFPD-BASED MODEL**

Farzam Fotovat<sup>1</sup>, Alireza Abbasi<sup>2,3</sup>, Raymond Spiteri<sup>3</sup>, Hugo de Lasa<sup>2</sup>, Jamal Chaouki<sup>1</sup>

<sup>1</sup>Department of Chemical Engineering, École Polytechnique de Montréal, C.P. 6079, Succursale  
Centre Ville, Montreal, QC, Canada, H3C 3A7

<sup>2</sup>Department of Chemical and Biochemical Engineering, University of Western Ontario, London,  
ON, Canada

<sup>3</sup> Department of Computer Science, University of Saskatchewan, Saskatoon SK, Canada

## 5.1 Introduction

Biomass has great potential to become one of the major global primary energy sources during the next century. The clean nature of biomass-based energy systems mitigating emissions of greenhouse gases, make biomass an essential contributor to sustainable development in industrialized as well as developing countries (Berndes et al., 2003). Many of the biomass processing units require the use of fluidized beds where the irregular biomass particles are co-fluidized with much denser and more regular particles such as sand enhancing the fluidizability of fuel particles and heat transfer in the bed. The resulting multiphase flow is complex due to the heterogeneous nature of the particles, turbulence of the fluidizing fluid, complex geometries, simultaneous heat and mass transfer, and rapid gas release during devolatilization.

In spite of considerable progress in utilizing biomass in bubbling and circulating fluidized bed reactors, characterization of the multiphase flow aspects is still weak, leading to trial and error ad hoc solutions (Cui & Grace, 2007). Bubble phase characteristics in bubbling fluidization regime significantly impact the fluidization hydrodynamics and process efficiency by governing the heat and mass transfer in the bed (Franka & Heindel, 2009; Kiared et al., 1997). Bubble activity also dominates the particle mixing and segregation phenomena which are crucially important for controlling the performance of biomass combustors or gasifiers (Cooper & Coronella, 2005). Due to the relatively low fraction of fuel particles in fluidized beds handling mixtures of sand and biomass, the bubble characteristics are usually assumed the same as those of a bed of sand alone.

However, recent studies have confirmed the impact of irregular large particles on the bubbling behavior of inert material fluidization. Zhang et al. (Yong Zhang, Jin, & Zhong, 2009; Yong Zhang, Jin, Zhong, et al., 2009; Y. Zhang et al., 2010) have shown that increasing the size and fraction of biomass particles in sand-assisted fluidized beds leads to a decreased probability of bubble growth giving rise to smaller bubbles in the bed compared to a fluidized bed of pure sand. Fotovat et al. (Fotovat et al., 2013b) observed that the mean voidage of the bed is raised at higher biomass loadings. Fotovat et al. have also shown that the core-annulus bed structure is increased at low biomass loadings, while increasing the biomass leads to a more uniform distribution of small bubbles across the bed improving fluidization quality. Bubble properties in multi-component systems, where segregation of substances matters, are also influenced by the local

concentration of irregular particles, particularly at low fluidization velocities (Fotovat et al., 2013a).

It is accepted that the complex pressure signal measured along a fluidized bed is a result of local fluctuations caused mainly by traveling gas bubbles. Pressure waves due to bubble formation, coalescence and eruption. Therefore pressure time series and pressure fluctuations are significant parameters in understanding bubble dynamic behaviors. However, measurements of pressure signals are still dependent on expensive pilot scale experiments along with empirical or semi empirical models obtained from laboratory studies. Thus, the use of optical fiber probes is another method to locally describe rising bubbles. Unlike the pressure fluctuation measurements which provide only an average characteristic length scale of the bubble size, optical fibers allows assessing the entire distribution of the bubble properties (Ruedisueli et al., 2012). Optical probes, however, may have some disadvantages such as their potential intrusive nature which may disturb the fluidized bed hydrodynamics and the difficulty of discriminating the exact number of bubbles passing the probes (van Ommen & Mudde, 2008). While these issues have been effectively addressed with the CREC Optiprobe (S. Nova, Krol, & de Lasa, 2004; S. R. Nova, Krol, & de Lasa, 2007), optical fiber measurements may still not be easily implemented under the high temperatures and harsh conditions of large scale fluidized reactor.

In view of this, CFD (computational fluid dynamics) providing valuable tools to model fluidized bed dynamics (M. J. V. Goldschmidt et al., 2003) will play a central role in the future design and operation of large scale fluidized beds (M. Goldschmidt et al., 2001). The two common CFD approaches for modeling gas-solid fluidized beds are Eulerian-Lagrangian and Eulerian-Eulerian models. In the Eulerian-Lagrangian model the gas is treated as the continuous phase and the solid as the discrete phase. The particle trajectory is obtained by solving the Newton's equation of motion taking into account the collision between the particles and the force exerted on the particles by the gas. In the Eulerian-Eulerian model, the two phases are treated as interpenetrating continua. Since the volume of a phase cannot be occupied by the other phases and as a result the concept of phasic volume fraction is introduced (M. J. V. Goldschmidt et al., 2003). These volume fractions are assumed to be continuous functions of space and time and their sum is equal to one. Conservation equations for each phase are then derived obtaining a set of equations, which have similar structure for all phases. Eulerian-Eulerian model has been partially successful in simulating multiphase flow phenomena in risers in which gas and solids move concurrently

upwards. This model however presents major limitations in describing the physical model of the gas–particle, particle–particle and particle–wall interactions in bed (Gera et al., 2004). Thus, the challenge is of providing closure equations for the averaged quantities. This closure becomes even more difficult to achieve for complex systems such as polydisperse solids. The Eulerian-Lagrangian has two approaches in solving the discrete phase. These two approaches are Discrete Element Method (DEM) and Hybrid model. DEM models the solid phase by tracking a finite number of discrete semi-rigid particles interacting through contact forces and transferring momentum to and from the fluid through a drag closure model. The advantage of this approach is that it can accommodate complexities such as polydispersity. DEM has however, the disadvantage of (1) computational complexities when the particles population in the system surpasses a quantity (e.g.  $2 \times 10^5$  particles) and (2) extensive computational time requirement even for the two dimensional solutions (Abbasi, Islam, Ege, & de Lasa, 2012). As a result, DEM shows limited abilities for relevant calculations in fluidized beds either at the industrial or at laboratory-scale. Unlike traditional DEM method, the hybrid method models the collision of particles by a solid-phase stress gradient applied to discrete particles as opposed to calculating individual contacts between particles. In this approach, the numerical particle approximation is considered within a numerical control volume (domain) where the properties of the fluid are considered constant.

The focus of the present study is to validate the bubbling behavior of the biomass-sand mixtures fluidized in a bubbling regime as predicted with computational approaches using experimental data. With this end, the BARRACUDA CPFDP software was used to for the numerical studies. BARRACUDA CPFDP software employs a hybrid description of the solid phase. Specifically, particles are modeled by means of individually-tracked clouds (which represent many identical particles) and the particle–particle collisions are modeled by a solid-phase stress gradient rather than calculating individual contacts.

## 5.2 Experimental

Fluidization of sand-biomass mixtures were considered to take place under room temperature conditions in a Plexiglas column with a height of 3000 mm and an internal diameter of 152 mm

(Fig. 5.1). After adjusting the gas flow rate using a bench of rotameters, air is injected into the column through a conical windbox and a perforated plate with 1 mm diameter holes arranged in a triangular pitch. An external cyclone is installed at the outlet of the column in order to separate airborne particles and return them into the bed through a recycle path. Silica sand with a particle size distribution ranging from 100 to 1000  $\mu\text{m}$  is used as the inert material mixed with biomass. Synthetic biomass particles are fabricated from cylindrical wood rods cut into identical lengths.

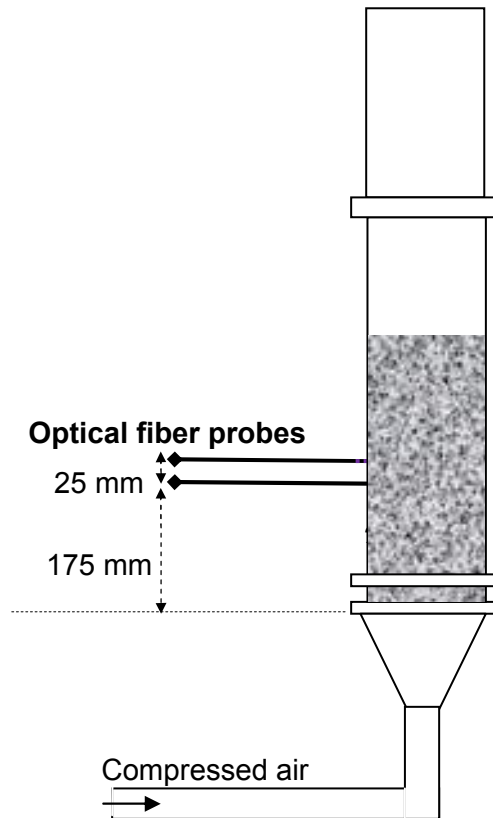


Fig. 5.1: Sketch of the fluidization column equipped with optical fiber probes used for the experiments.

Table 5.1 reports the properties of materials used in this study. The bed aspect ( $H_0/D$ ) ratio is set to 1.5 in all experiments. Accordingly, the required mass of sand and biomass are calculated, knowing the bulk density of each studied mixture obtained experimentally (Table 5.2). The weight percentage of biomass used in the experiments is 8% and 16%. The filling procedure followed in all experiment to start from a well-mixed initial condition is dividing the whole bed inventory into eight batches composed of a manually mixed sand and biomass mixture. The

content of each batch is then poured into the bed one by one in a way to form nearly eight homogenous strata of the bed components.

The local bubble properties are obtained using two optical fiber probes placed horizontally 175 and 200 mm above the distributor and inserted parallel to each other into the center of the bed ( $r/R=0$ ). Each probe consists of a bundle of light-emitting/receiving optical fibers. Light projected by the light-emitting fibers is reflected by particles and the reflected light is collected by light-receiving fibers and converted to electric signals by a photomultiplier. The method and the curves used for calibration of probes have been discussed in details in another work (Fotovvat et al., 2013b). The voidage data are acquired at a sampling frequency of 512 Hz through a 16 bit A/D data acquisition board with the help of the Labview 9.0.1 ® program. Based on the algorithm introduced by Ruedisueli et al. (Ruedisueli et al., 2012), an in-house code was developed to assess bubble size and velocity distribution.

Table 5.1: Properties of materials used

Material	Shape	$D_p(\text{mm})$	$L_p(\text{mm})$	$\rho_p(\text{kg/m}^3)$	$\rho_b(\text{kg/m}^3)$	Sphericity (-)
Sand	Spherical	0.38	-	2650	1520	1
Biomass	Cylindrical	6.35	12.70	824	342	0.84

Table 5.2: Properties of systems studied

Wt.% of biomass	Vol.% of biomass	Bulk density of sand-biomass mixture ( $10^{-3} \text{ kg/m}^3$ )	Voidage of the fixed bed (-)	Mass of sand used (kg)	Mass of biomass used (kg)
8	21.9	1.35	0.40	5.10	0.44
16	38.0	1.22	0.37	4.30	0.82

### 5.3 The Hybrid Mathematical Model

The motion of the fluid and dispersed phases is governed by their respective mass and momentum conservation equations. The volume-averaged fluid conservation of mass and momentum equations are given by Eqs. (5.1) and (5.2) as recommended by Abbasi et al (Abbasi et al., 2012):

$$\frac{\partial}{\partial t}(\rho_f \theta_f) + \nabla \cdot (\rho_f \theta_f \mathbf{v}_f) = 0 \quad (5.1)$$

$$\frac{\partial}{\partial t}(\rho_f \theta_f \mathbf{v}_f) + \nabla \cdot (\rho_f \theta_f \mathbf{v}_f \mathbf{v}_f) = -\nabla P + \nabla \cdot \boldsymbol{\tau} + \rho_f \theta_f \mathbf{g} - F \quad (5.2)$$

where  $\theta_f$  is the fluid volume fraction,  $\mathbf{v}_f$  is the fluid velocity,  $\rho_f$  is the fluid density,  $P$  is the fluid pressure,  $\boldsymbol{\tau}$  is the fluid stress tensor, and  $\mathbf{g}$  is the gravitational acceleration.  $F$  represents the momentum exchange rate per unit volume between the fluid and particle phases.

Furthermore, the trajectory calculation of the discrete phase is made by integrating the force balance on the particles. As a result, the particle motion is governed by the following Eq. (5.3).

$$\frac{d}{dt}(\mathbf{v}_p) = D_p (\mathbf{v}_f - \mathbf{v}_p) - \frac{\nabla P}{\rho_p} - \frac{\nabla \cdot \boldsymbol{\tau}_p}{\theta_p \rho_p} + \mathbf{g} \quad (5.3)$$

where  $\mathbf{v}_p$  is the particle velocity,  $\rho_p$  is the particle density,  $\theta_p$  is the particle volume fraction, and  $\boldsymbol{\tau}_p$  is the particle normal stress. One should notice that the interphase drag coefficient  $D_p$  is defined as with Eq. (5.4) (Dale Snider & Banerjee, 2010):

$$D_p = C_d \frac{3 \rho_f}{8 \rho_p} \frac{|\mathbf{v}_f - \mathbf{v}_p|}{\left(\frac{3V_p}{4\pi}\right)^{1/3}} \quad (5.4)$$

where  $C_d$  represents the drag coefficients and  $V_p$  is the particle volume.

Furthermore, the momentum exchange rate  $F$  is defined using Eq. (5.5) as recommended by Snider (DM Snider, 2001):

$$F = \frac{1}{V} \sum_{k=1}^{N_c} \left[ D_p (\mathbf{v}_{fc} - \mathbf{v}_{pc}) - \frac{\nabla P_{ck}}{\rho_{pk}} \right] n_{ck} m_{pk} \quad (5.5)$$

where  $V$  is the volume of the computational cell,  $N_c$  is the number of the clouds in the computational cell,  $n_c$  is the number of the particles in the clouds, and  $m_p$  is the mass of an individual particle in the cloud. The fluid stress tensor of a Newtonian fluid is described by:

$$\tau_{ij} = 2\mu_f S_{ij} - \frac{2}{3}\mu_f \delta_{ij} \frac{\partial u_i}{\partial u_j} \quad (5.6)$$

where  $\mu_f$  is the fluid viscosity coefficient,  $S_{ij}$  is the rate of fluid deformation, and  $\delta_{ij}$  is the Kronecker delta (i.e.,  $\delta_{ij}=1$  if  $i=j$  and  $\delta_{ij}=0$  otherwise). The rate of deformation,  $S_{ij}$ , defines the constitutive equation for the non-hydrostatic part of the stress as follows:

$$S_{ij} = \frac{1}{2} \left( \frac{\partial u_i}{\partial x_j} + \frac{\partial u_j}{\partial x_i} \right) \quad (5.7)$$

The drag coefficient used in the calculation was proposed by Ganser (Ganser, 1993). This is a drag coefficient specifically developed for non-spherical particles. This is particularly relevant in the present research given the cylindrical truncated form of the biomass particles and the irregular spherical shape of sand of the present study.

$$C_d = \left( \frac{24}{Re K_1 K_2} \left[ 1 + 0.1118 (Re K_1 K_2)^{0.6567} \right] + \frac{0.4305}{1 + \frac{3305}{Re K_1 K_2}} \right) \theta_f^{-2.65} K_2 \quad (5.8)$$

$$Re = \frac{2\rho_f |v_f - v_p| \left( \frac{3V_p}{4\pi} \right)^{1/3}}{\mu_f} \quad (5.9)$$

$$K_1 = \frac{3}{1 + \frac{2}{\sqrt{\phi}}} \quad (5.10)$$

$$K_2 = 10^{1.8148(-\log \phi)^{0.5743}} \quad (5.11)$$

where  $\varphi$  is the sphericity. The sphericity of a particle is defined as the ratio of the surface area of a sphere with the same volume as the given particle to the surface area of the particle. The sphericity parameter is of significant value given the dissimilar shape of the biomass particles with a truncated cylinder like and the sand particles with an irregular close to spherical shape.

Furthermore, particle-to-particle collisions are modeled by the particle normal stress,  $\tau_p$ . The particle normal stress model used here is from Abbasi et al. (Abbasi et al., 2012):

$$\tau_p = \frac{P_s \theta_p^\beta}{\max[\theta_{cp} - \theta_p, \varepsilon(1 - \theta_p)]} \quad (5.12)$$

where  $P_s$  is a positive constant that has units of pressure,  $\theta_p$  is solid volume fraction,  $\theta_{cp}$  is the particle volume fraction at close packing, and  $\varepsilon$  and  $\beta$  are dimensionless constants. Recommended values for  $\beta$  are in the  $2 \leq \beta \leq 5$  range (Dale Snider & Banerjee, 2010). The  $\varepsilon$  parameter is a small number on the order of  $1e-8$  is used to avoid singularity when the solid volume approaches closest packing (Leboreiro et al., 2008).

## 5.4 Simulation Parameters

To proceed with the CFPD simulations, computational domains were defined in the fluidized bed unit of Fig. 5.1 using a  $10 \times 10 \times 92$  ( $10 \times 10$  in radial and 92 axial dimensions) mesh arrangement. Dimension of cells in the mesh were selected in order to allow at least one biomass particle to fit in a truncated cell located at the wall region or alternatively to have the same cell filled with sand particles. Thus, Barracuda software dealt in the calculation with cells either filled with biomass particles or with an ensemble of sand particles called the numerical particle. Regarding the simulation model used in the present study, the moving particles are represented with moving “clouds”. A moving “cloud” designates a large number of moving particles having the same attributes. As a result, biomass and sand particles were treated as separate entities with different number of moving “clouds” and dissimilar number of particles. For biomass, 2448 moving clouds were identified in the entire bed having 1 particle per cloud. For sand 40256 moving

clouds were selected in the entire bed having  $5.93 \times 10^{10}$  particles per cloud. The outlet bed pressure is set at 101325 Pa.

The input parameters for the simulations are reported in Table 5.3. The diffuse bounce,  $D_f$ , represents the random post-collision normal and tangential “cloud” velocities with the unit wall. This parameter emulates surface roughness effect (Leboreiro et al., 2008). Collisions of clouds with the walls are calculated using normal,  $e_n$ , and tangential,  $e_t$ , particle restitution coefficients. The values of restitution coefficients considered are the ones suggested by Zhao et al. (Y. Zhao, Ding, Wu, & Cheng, 2010) The  $\xi$  parameter represents an elastic restitution factor that limits the velocity of particles that bounce off of a region at close packing.  $\beta$  and  $P_s$  represent the dimensionless constants for the solid-phase stress model. These parameters are set at  $\beta=3$  and  $P_s=10$  Pa as recommended by Snider (DM Snider, 2001). Large eddy turbulence model was used in the simulations. This is an expected fluid dynamic pattern in fluidized beds. As well, a partial donor cell differencing scheme was applied for convection terms. This scheme is a weighted average of central difference and upwind convection (Amsden, Orourke, & Butler, 1989). The numerical solution of the linearized governing equations is performed using an iterative method. The iterations continue until a selected number of variables satisfy conditions assigned to the summation of residuals. These computational control variables are as follows: i) maximum iterations for volume calculations,  $I_v$ ; ii) residuals for volume,  $r_v$ ; iii) maximum iterations for pressure,  $I_p$ ; iv) residuals for pressure,  $r_p$ ; v) maximum iterations for velocity,  $I_u$ ; and vi) residuals for velocity,  $r_u$ .

Table 5.3: The input parameters for the simulation

Time step, $\Delta t$	$25 \times 10^{-4} \text{s}$
Particle–wall normal restitution coefficient, $e_n$	0.95
Particle–wall tangential restitution coefficient, $e_t$	0.95
Diffuse bounce, $D_f$	0
Dimensionless constant of the solid-phase stress model, $\beta$	3
Dimensionless constant of the solid-phase stress model, $\varepsilon$	$10^{-8}$
Pressure constant of the solid-phase stress model, $P_s$	10 Pa
Solid volume fraction at closest packing, $\theta_{cp}$	0.55
Gravitational acceleration, $g$	$-9.8 \text{ m/s}^2$
Maximum volume iterations, $I_v$	1
Volume residual, $r_v$	$10^{-6}$
Maximum pressure iterations, $I_p$	2000
Pressure residual, $r_p$	$10^{-8}$
Maximum velocity iterations, $I_u$	50
Velocity residual, $r_u$	$10^{-7}$
Maximum momentum redirection from collision, $\xi$	40%

## 5.5 Results and Discussion

Fig. 5.2 shows the simulated evolution of particle volume fraction or solid holdup once simulation starts. The load of biomass and superficial gas velocity are set to 8% wt. and  $U=0.64$  m/s, respectively. The height of the bed expands up to 0.65 m in 0.5 s. Some lifted particles rain down during this period and those that could rise further (up to 0.6 m) drop later. The bed height gets stable at 0.4 m in 0.8 s after starting the simulation. The different tendency of particles to be raised by the air is believed to trigger segregation in the column. The non-uniformity of the solid holdup after 1 s fluidization is evident.

Fig. 5.3 and Fig. 5.4 demonstrate the evolution of the fluidization pattern of sand and biomass particles of the abovementioned mixture during 10 seconds after initiation of simulation. Results obtained show that simulations require approximately 3 s of computational time to reach a stable state numerical solution. It is also apparent that particle distribution fluctuates over time. Their average value or solid hold up remains at any given axial position quite stable. The extent of solid expansion is noticeably greater with respect to sand compared to biomass particles. As seen in Fig. 5.4, the lowermost 5 cm of the bed becomes almost devoid of biomass particles, just 1 s after starting fluidization while a mild accumulation of biomass particles is discernible at the top of the bed. All of these observations are in total agreement with the experimental results as discussed in previous chapters.

Fig. 5.5 and Fig. 5.6 compare bubble size distributions and bubble rise velocity measured experimentally using the optical fiber technique and calculated numerically employing Barracuda software. Results show fairly good correspondence between distributions displaying in all cases a quite asymmetric shape distribution with a long tail. In order to be able to make a better comparison between the corresponding values, the statistical parameters of the bubble size and bubble rise velocity distribution have been reported in Table 5.4 and Table 5.5, respectively.

Fig. 5.7, Fig. 5.8 and Fig. 5.9 respectively compare the mean, standard deviation and skewness of the bubble size and the bubble rise velocity of the systems studied as obtained from the experiments and the numerical approach for gas velocities ranging from 0.3 to 0.8 m/s. The dashed lines in these figures demarcate the extent of errors between the experimental and corresponding simulation data. The simulated mean and standard deviation values of the bubble size and rise velocity distributions are generally lower than the corresponding values obtained

experimentally for both of the studied mixtures. This trend is, however, opposite for the skewness values. The magnitude of error is much more considerable for the skewness values compared to that of the mean and standard deviation errors.

In view of the smaller errors relating to the mixture composed of 16% wt. compared to those of the mixture composed of 8% wt. biomass, it can be stated that the simulation is more successful to predict the bubble behavior of the mixture when the biomass fraction is higher. This conclusion can be linked to the size of the computational cell (mesh) used in this study. It is worth pointing out that the CPFD method presupposes that a statistically significant number of computational particles fit within a computational cell. Accordingly and in view of the large size of biomass particles used in this study, the size of the computational cell chosen for performing the simulations was set relatively large to embody a significant number of biomass particles. Adopting such a large cell could result in accurate results when the biomass concentration is relatively high, e.g. 16% wt.; however, a smaller computational cell is preferable to proceed with the numerical simulation of mixtures containing lower loads of biomass, where the dominance of the small sand particles are more pronounced. Use of large computational cells for simulating fluidization of the mixtures with very low amount of biomass, e.g. 2% wt. or less, brought about poor results which were not comparable with the corresponding experimental values and therefore were not discussed in this work.

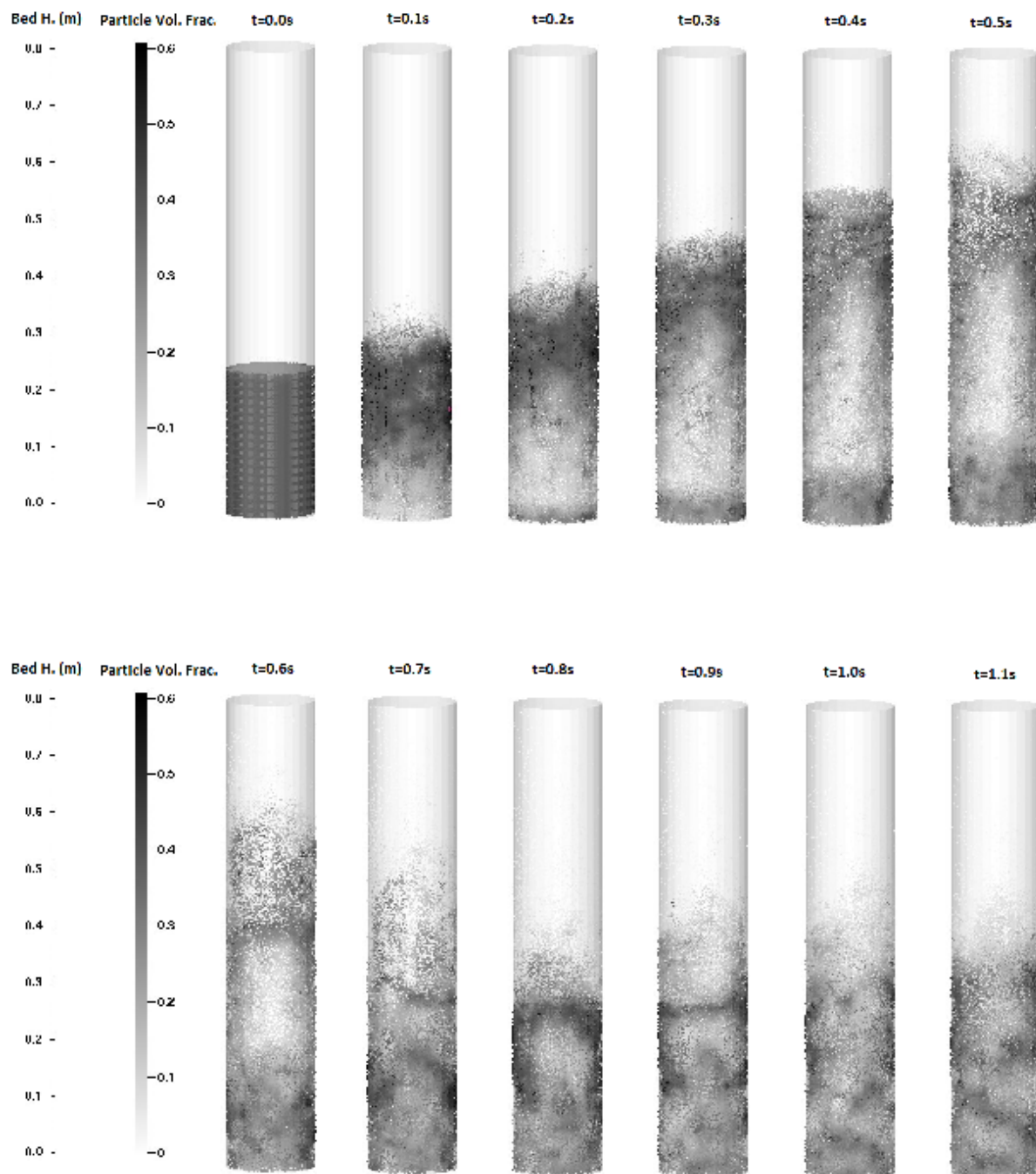


Fig. 5.2: Particles volume fraction during the first 1s fluidization of a sand-biomass mixture at  $U = 0.64$  m/s, (biomass load= 8% wt., initially well-mixed mixture)

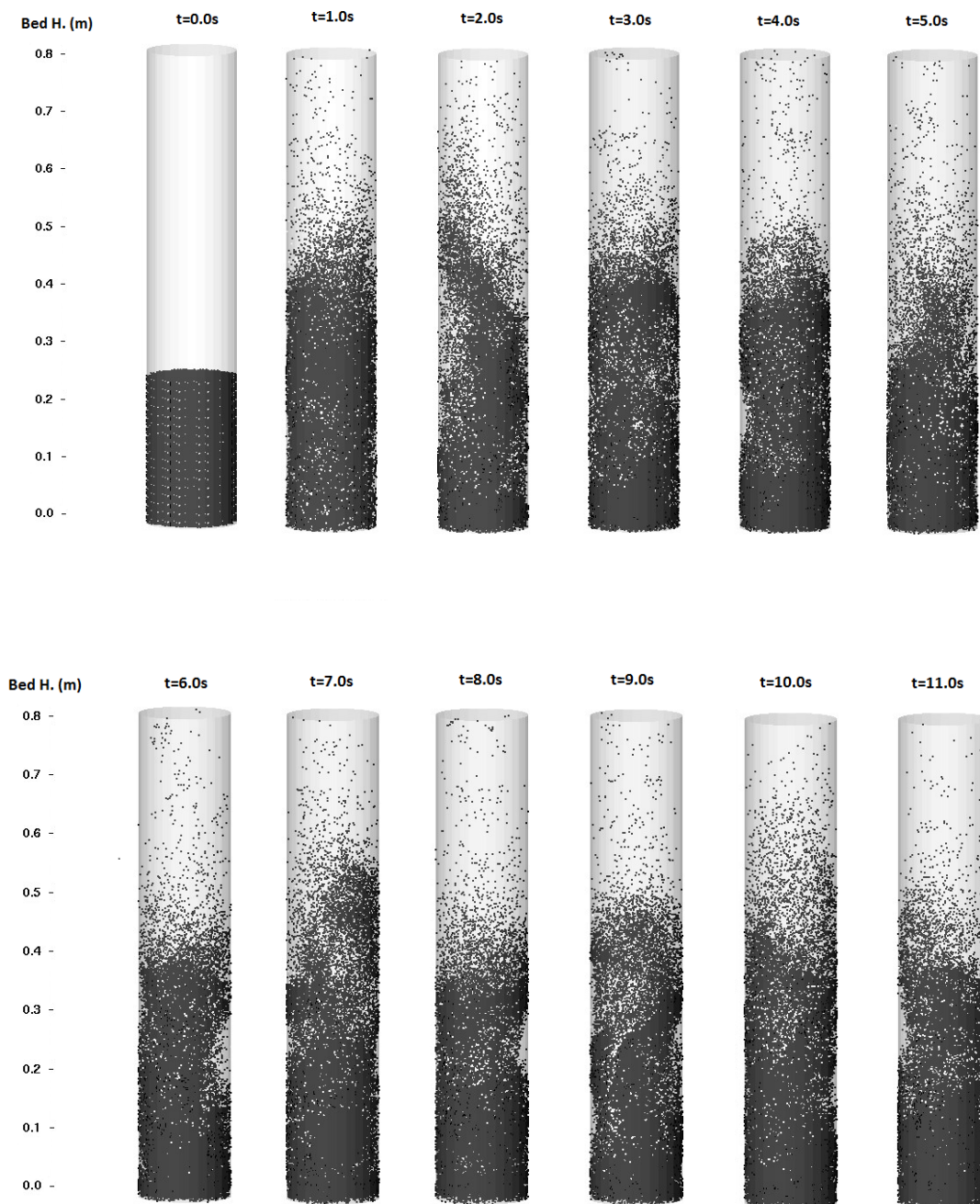


Fig. 5.3: Simulation of sand fluidization in a bed constituted by sand and biomass particles.  $U=0.64$  m/s, (biomass load= 8% wt., initially well-mixed mixture)

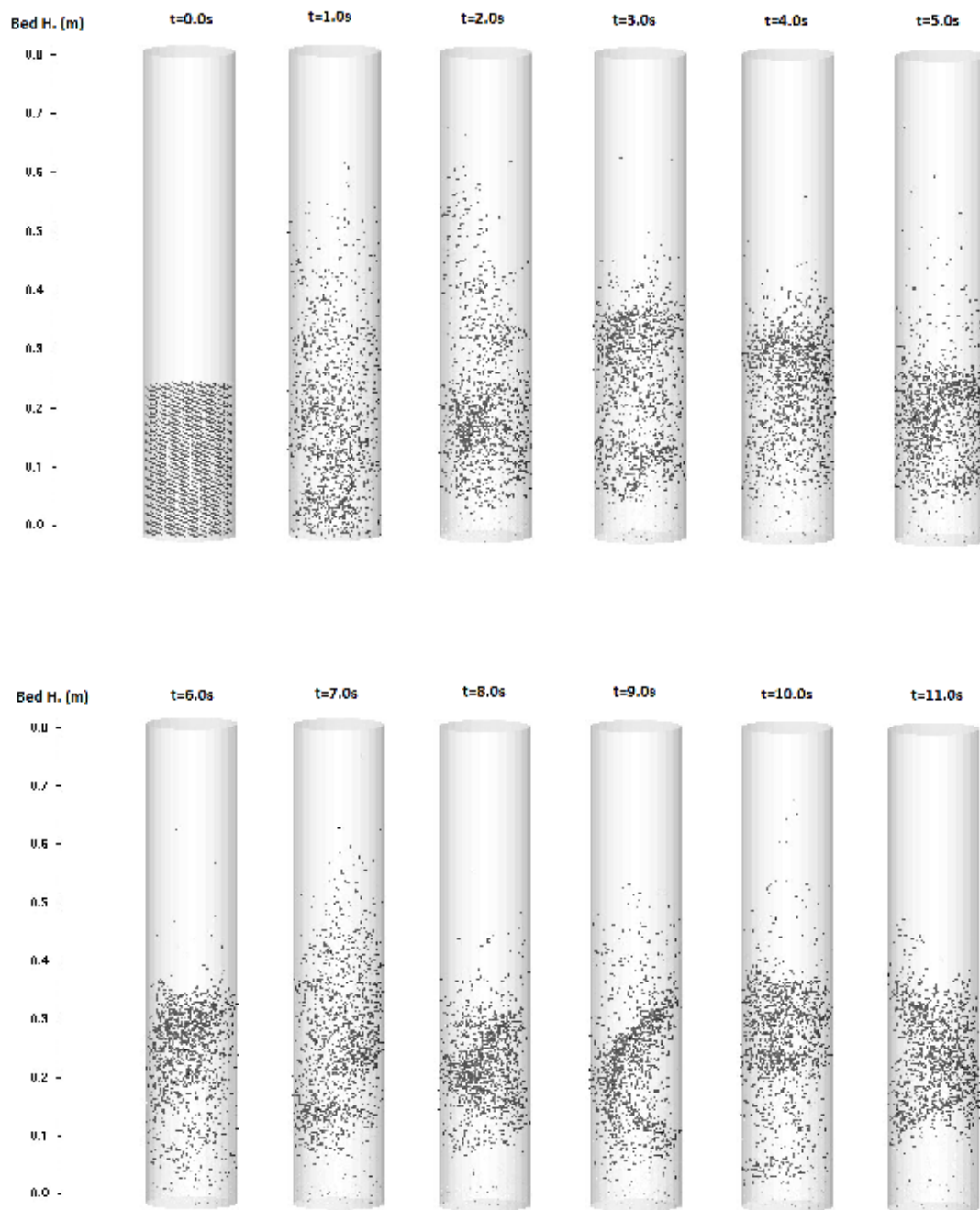


Fig. 5.4: Simulation of biomass fluidization in a bed constituted by sand and biomass particles.  $U = 0.64$  m/s, (biomass load= 8% wt., initially well-mixed mixture)

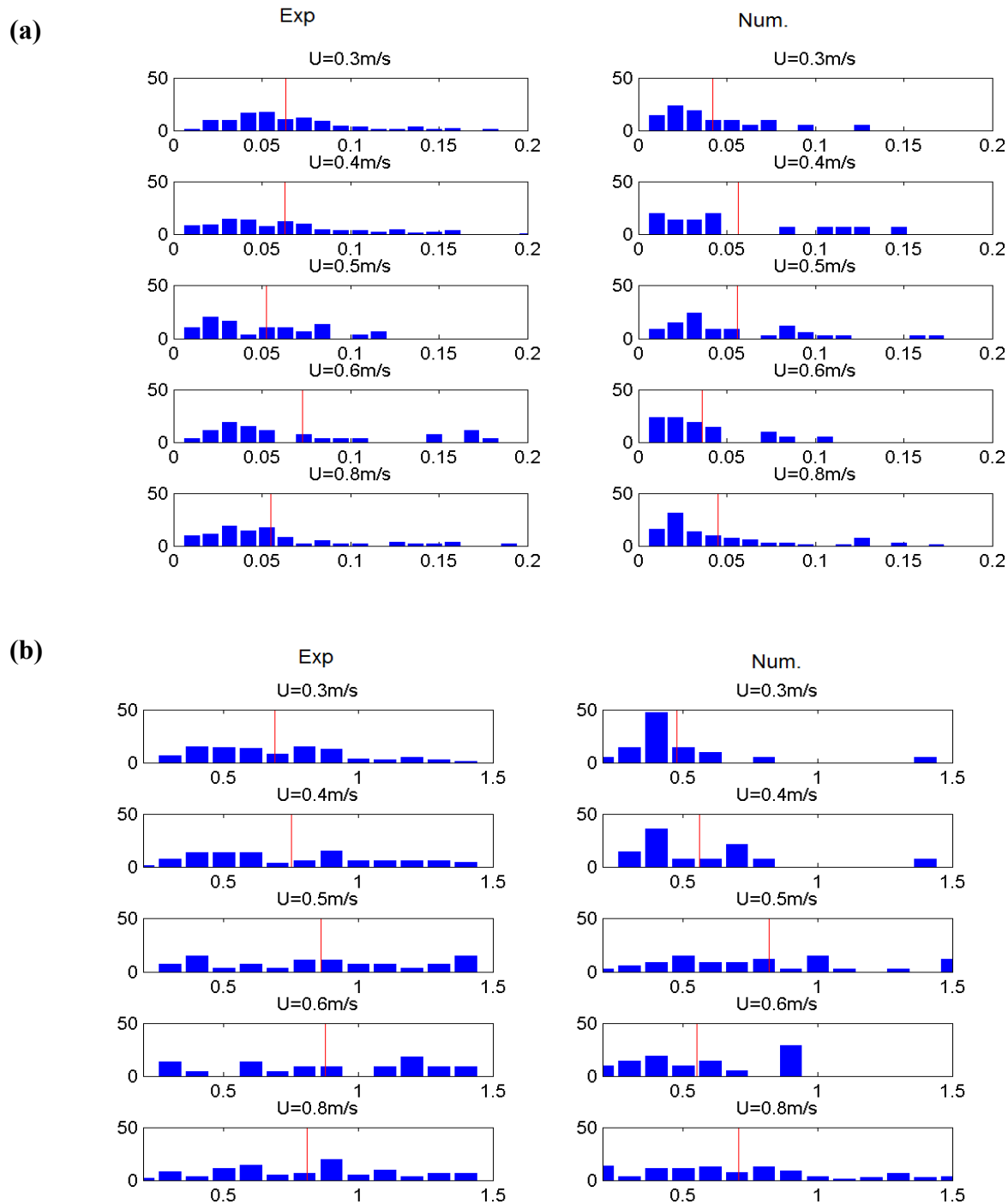


Fig. 5.5: Comparison of the experimentally measured and numerically calculated a) bubble size distribution b) bubble rise velocity distribution as a function of superficial gas velocity for a mixture containing 8% wt biomass. Red lines indicate the mean value of each graph.

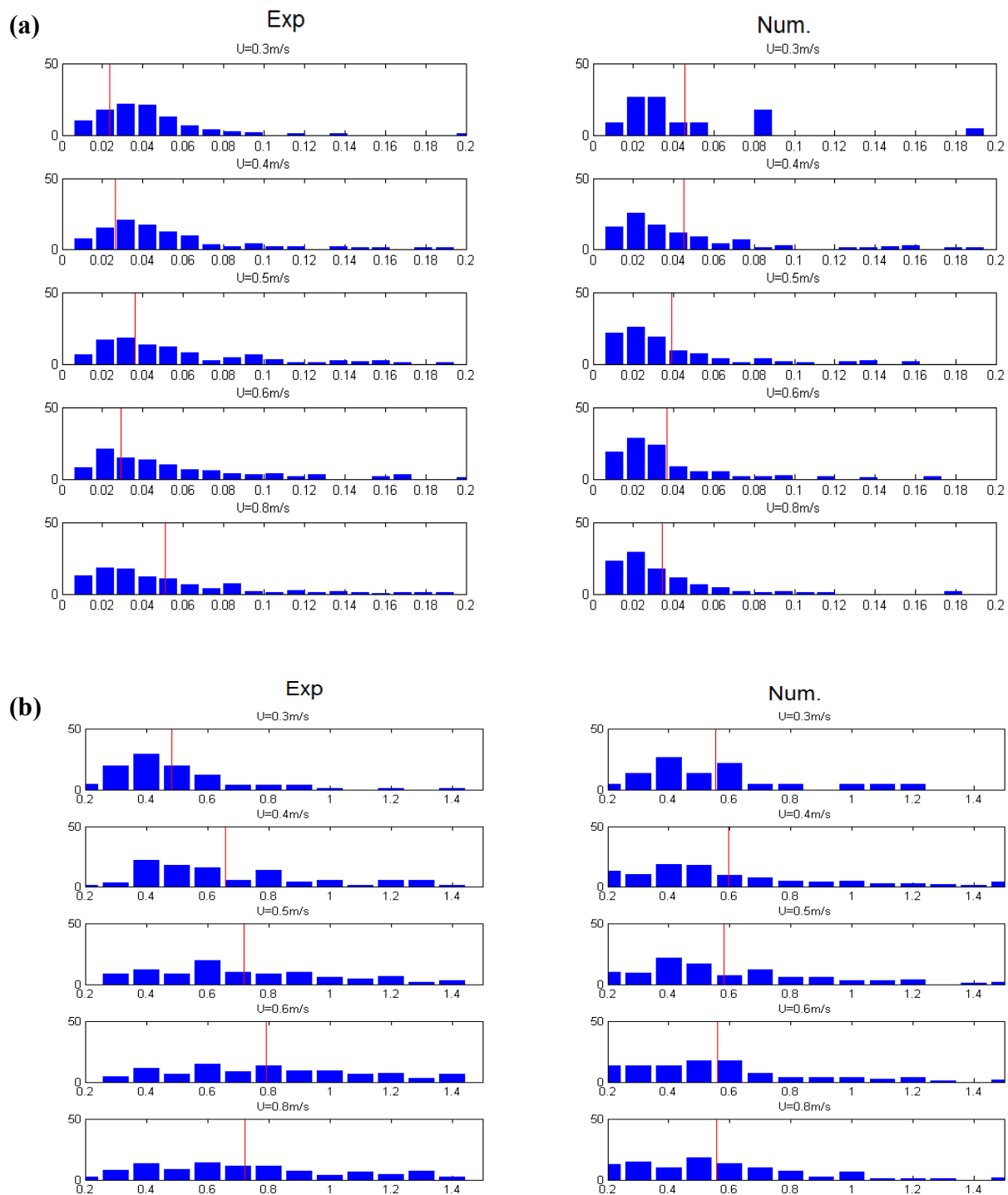


Fig. 5.6: Comparison of the experimentally measured and numerically calculated a) bubble size distribution b) bubble rise velocity distribution as a function of superficial gas velocity for a mixture containing 16% wt biomass. Red lines indicate the mean value of each graph.

Table 5.4: Comparisons of the mean, standard deviation and skewness of the experimentally and corresponding numerically obtained bubble size distributions.

Wt% of biomass	8						16					
Parameter/ Gas velocity (m/s)	$\bar{d}_b$ (cm)		$\sigma(d_b)$ (cm)		$\gamma(d_b)$ (-)		$\bar{d}_b$ (cm)		$\sigma(d_b)$ (cm)		$\gamma(d_b)$ (-)	
	Exp	Num	Exp	Num	Exp	Num	Exp	Num	Exp	Num	Exp	Num
0.3	6.0	4.1	3.6	2.9	1.3	1.8	5.1	4.6	3.2	3.9	2.0	2.2
0.4	5.8	4.3	3.7	3.7	0.9	2.0	5.5	4.5	3.9	3.9	1.4	2.0
0.5	5.9	4.1	4.1	3.4	1.2	1.9	5.1	3.9	3.5	3.3	1.7	1.9
0.6	5.3	3.6	3.8	2.8	1.6	2.4	4.8	3.7	3.6	3.0	1.6	2.4
0.8	5.7	4.2	4.2	3.9	1.3	1.8	4.6	3.4	3.5	2.9	1.9	2.8

Table 5.5: Comparisons of the mean, standard deviation and skewness of the experimentally and corresponding numerically obtained bubble velocity distributions.

Wt% of biomass	8						16					
Parameter/ Gas velocity (m/s)	$\bar{U}_b$ (cm/s)		$\sigma(U_b)$ (cm/s)		$\gamma(U_b)$ (-)		$\bar{U}_b$ (cm/s)		$\sigma(U_b)$ (cm/s)		$\gamma(U_b)$ (-)	
	Exp	Num	Exp	Num	Exp	Num	Exp	Num	Exp	Num	Exp	Num
0.3	71.5	50.6	33.0	27.6	1.4	1.4	64.9	55.4	26.5	26.5	1.3	1.1
0.4	79.9	57.1	40.4	35.3	0.9	1.3	72.4	59.7	33.6	35.6	1.1	1.3
0.5	88.8	60.4	41.5	35.6	0.6	1.1	79.4	58.2	37.2	31.0	0.9	1.1
0.6	85.6	63.0	40.6	35.7	0.7	1.1	79.2	56.1	40.3	31.2	0.9	1.5
0.8	84.5	57.9	41.8	36.9	0.7	1.0	78.8	55.7	34.3	29.8	0.6	1.2

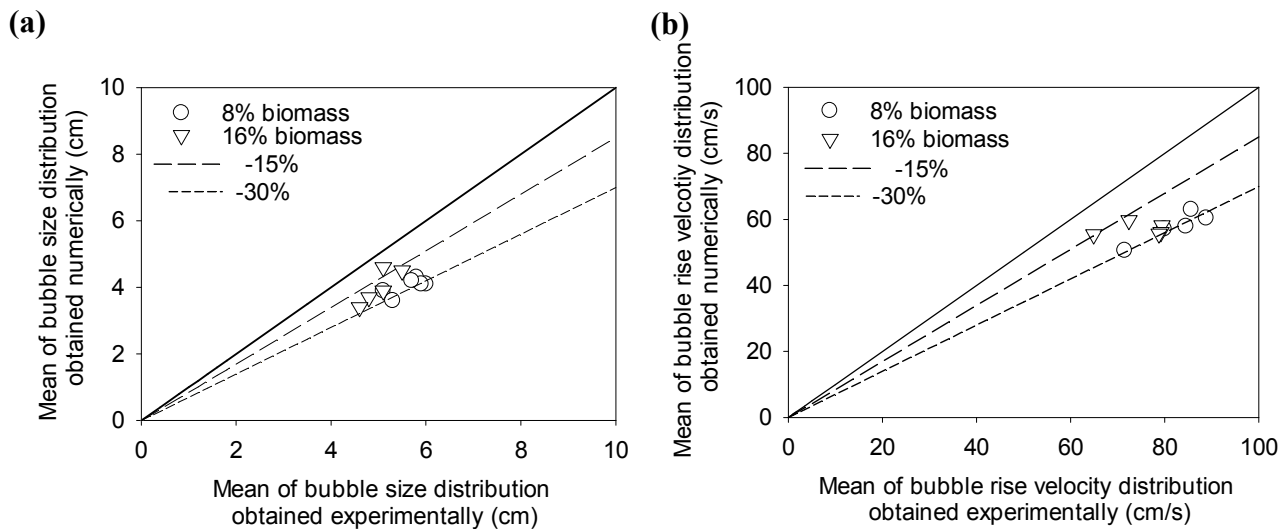


Fig. 5.7: Comparison of the experimentally obtained and corresponding numerical values of the mean a) bubble size, b) bubble velocity distribution

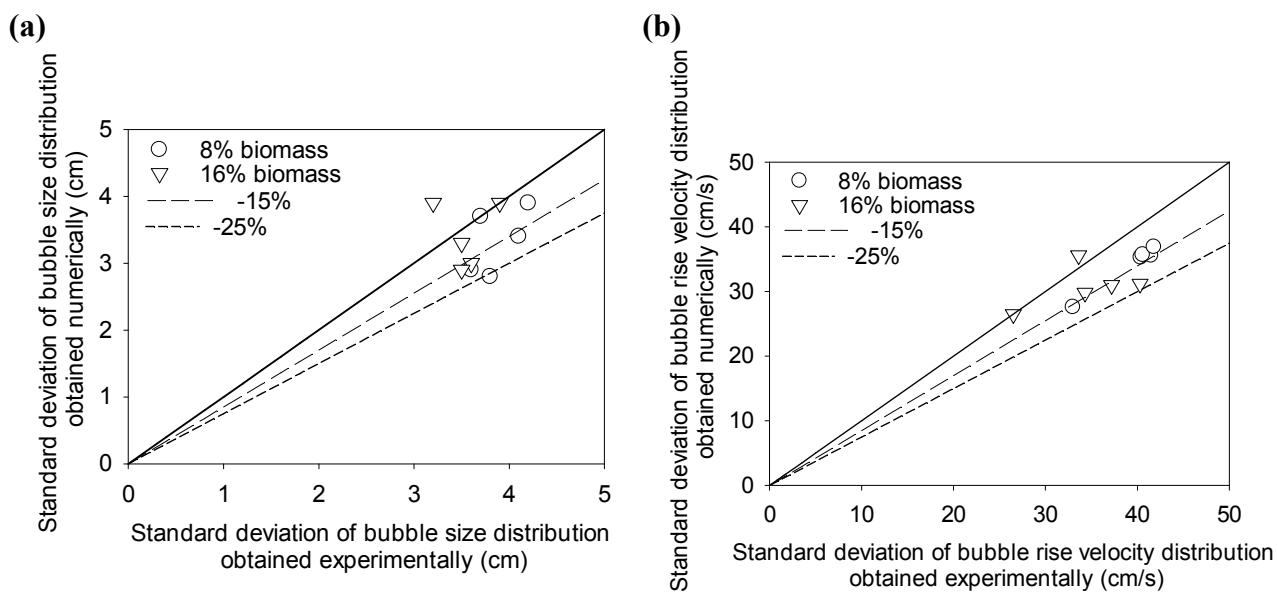


Fig. 5.8: Comparison of the experimentally obtained and corresponding numerical values of the standard deviation of a) bubble size, b) bubble velocity distribution

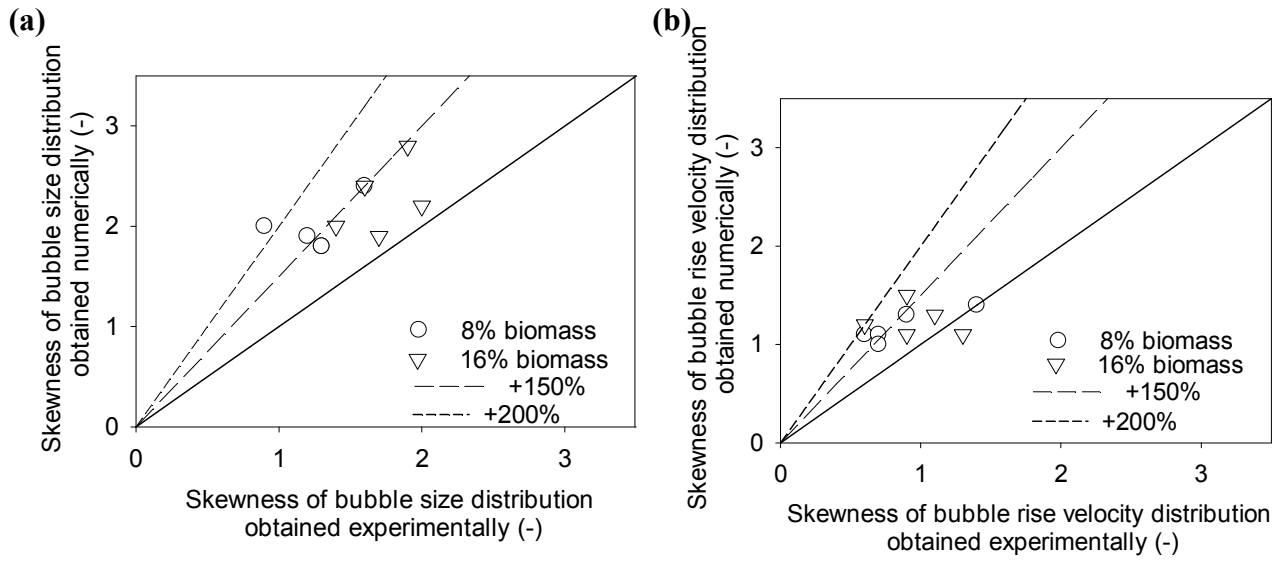


Fig. 5.9: Comparison of the experimentally obtained and corresponding numerical values of the skewness of a) bubble size, b) bubble velocity distribution

## 5.6 Conclusion

The characteristics of the bubbles in the presence of biomass particles were numerically investigated through the BARRACUDA CPFD software that is based on the Lagrangian-Eulerian approach. The dynamics of fluidization after injection of gas in the column was in agreement with the phenomena observed visually or inferred from the RPT data. For instance, simulation could successfully predict the degree of bed expansion with respect to sand and biomass particles as well as the qualitative distribution of biomass particles along the bed. The distribution of bubble size and bubble rise velocity at a specific height of the bed ( $17.5 \text{ cm} < h < 20 \text{ cm}$ ) obtained by processing the simulated voidage signals was compared with the voidage signals measured experimentally using optical fiber probes. In general, the bubble size and rise velocity distribution profiles of the experimental and numerical attempts were reasonably comparable in mean and standard deviation and to a lower extent in skewness values. The discrepancy between the experimental and the corresponding numerical results diminished as the load of biomass rose. It was attributed to the large size of the computational cell adopted for the simulations, which lowered the accuracy of the simulation results when the portion of the small sand particles was larger in the mixture and consequently in each computational cell.

## CHAPTER 6

### **ARTICLE 3: THE SEPARATION OF THE MAIN COMBUSTIBLE COMPONENTS OF MUNICIPAL SOLID WASTE THROUGH A DRY STEP-WISE PROCESS**

Farzam Fotovat, Jamal Chaouki

Department of Chemical Engineering, École Polytechnique de Montréal, C.P. 6079, Succursale  
Centre Ville, Montreal, QC, Canada, H3C 3A7

**Abstract**

Tailoring the solid waste-based fuels composition is essential to improve the combustion efficiency and control the resultant emissions. In the present study, a dry step-wise process has been developed in a pilot-scale setup to recover the main combustible elements of shredded bulky waste (SBW) consisting of 72% fiber, 12% soft plastic and 8% hard plastic. For this purpose, the SBW is initially elutriated to enhance the processability of the feedstock and separate its lightest components. Elutriation of SBW at  $U_e=1.5$  m/s for 15 minutes could result in the effective separation of light components, i.e., fiber and soft plastic. These components are then separated from each other in a second elutriation column at  $U_e=0.2$  m/s for 2-3 minutes.

By means of a fluidization medium, which prompts density segregation of the feedstock components under fluidization conditions, the non-elutriated fraction of the SBW is further separated into non-combustible and undesirable combustible components as well as hard plastic through two consecutive steps. The fluidization media chosen for the first and second dry density separation columns are Polypropylene (PP) and glass beads, respectively. The optimum fluidization velocity to maximize the overall separation of each step is slightly higher than the respective  $U_{mf}$  of the corresponding fluidization medium. Size and density of the bed medium as well as the initial configuration of the bed inventory are the parameters governing the recovery and purity percentage of the bed.

**Keywords:** Municipal waste, Separation, Elutriation, Fluidization, Fiber, Plastic

## 6.1 Introduction

Around the world researchers explore other reliable energy resources to replace fossil fuels, as they are slowly depleted. It is expected that the global energy market will continue to depend on fossil fuels for only another few decades. Coal constitutes approximately 65% of the fossil fuel reserves in the world. Unlike the oil and gas reservoirs, which are concentrated in a few regions of the world, coal remains abundant and broadly distributed throughout the world. Economically recoverable reserves of coal are available in more than 70 countries worldwide, and in each major world region. These two geological reasons support the fact that coal reserves have the potential to become the dominant fossil fuel in the future (Shafiee & Topal, 2009). Coal is projected to have the biggest increase in demand in absolute terms, jumping by 73% between 2005 and 2030. It is the largest source of electricity generation in China and the United States, i.e., 68.7% and 46% of total power generated in these countries, respectively. Coal power stations, however, are the least carbon efficient power stations in terms of the level of carbon dioxide produced per unit of electricity generated (Calabrese & Bai, 2010). In addition, the combustion of fossil fuels, including coal, contributes to acid rain, global warming, accelerated soil acidification, forest degradation and air pollution due to the impurities and chemical composition of the fuel (Alvarez-Ayuso, Querol, & Tomás, 2006). Combustion of fossil fuels is the main cause of significant amounts of pollutants, such as  $\text{NO}_x$  and  $\text{SO}_2$ . Fig. 6.1 demonstrates the rate of  $\text{NO}_x$  and  $\text{SO}_2$  emissions of a variety of American coal-based power plants.

Management of municipal solid waste (MSW) is one of the major issues facing the world (Dunnu, Maier, & Gerhardt, 2009). Both landfills and the resulting emission of greenhouse gases (GHG) present serious health and environmental threats. Due to the significant portion of combustible materials, such as paper, and soft and hard plastic in MSW, it can be incinerated or used as feedstock to produce fuel, such as refuse-derived fuel (RDF), solid recovery fuel (SRF) or other types.

MSW generally undergoes pre-treatment processes, including metals separation and the removal of other recyclable material: paper (referred to as fiber), plastics, metals and glass). The MSW can be further processed to remove waste with low calorific value (food waste, yard trimmings, rubber, leather, textiles and other waste) and then shredded (in the range of a mesh 4, hole size of approximately 4.75 mm) for the production of fuels. The resulting waste stream, referred to as

shredded bulky waste (SBW), is composed of combustible materials (plastic, fiber, wood and others) and small amounts of non-combustible materials (glass, metals, sand and others).

Fig. 6.2 shows the composition of the total amount (250 million tons) of MSW generated in the United States in 2011. As illustrated, the total percentage of paper, paperboard, and plastic, which are the main combustible materials, reaches 40.7% or the equivalent of 102 million tons. With a US recycling rate of about 34%, the potential for SBW production in the US is in the range of 67 million tons.

The incineration process produces large quantities of GHG, e.g., CO<sub>2</sub>. Typically, the amount of energy produced per equivalent CO<sub>2</sub> expelled during incineration is very low, thus making incineration of MSW for energy production one of the worst offenders in producing GHG released into the atmosphere (Calabrese & Bai, 2010).

Typically, RDF refers to the segregated high calorific fraction of processed MSW. The term SRF is used to describe a fuel with tight quality specifications required by the customer (Hernandez-Atonal et al., 2007). In spite of processing MSW to produce RDF or SRF, the final streams include a variety of different combustible materials whose composition is prone to change due to the alteration of the waste source composition and variation of the MSW processing efficiency. On the other hand, it is vital to control the composition of the solid waste-based fuel in order to avoid technical problems and harmful emissions. For instance, the combustion of waste paper and paperboard, known as fiber materials, leads to the production of a significant ash content, which may disturb combustor operation. In addition, burning chlorine-contained plastics, such as Polyvinyl chloride (PVC), included in hard plastic waste causes serious corrosion in the furnace or kiln (M. Yoshida et al., 2010); however, the presence of a low level of chlorine may be useful to mitigate mercury emissions by transforming them to mercuric chloride, which is more readily captured either in scrubbers or by collection in the particulate form (Senior, Helble, & Sarofim, 2000). In view of these facts, it is crucially important to develop a novel solid waste-based fuel with customized characteristics. Such a fuel, which has been patented as “Engineered Fuel (EF),” aims at offsetting or replacing coal as the feedstock in coal fired power generation plants to mitigate the detrimental effects of coal combustion (Calabrese & Bai, 2010). EF contains specific chemical molecular characteristics, such as carbon, hydrogen, oxygen, sulfur ash and moisture content, and HHV for thermal-conversion of carbon-containing materials, such as coal. Thus, it

can serve both the needs of alternative clean fuels and efficient waste management systems devised for reducing GHG emissions.

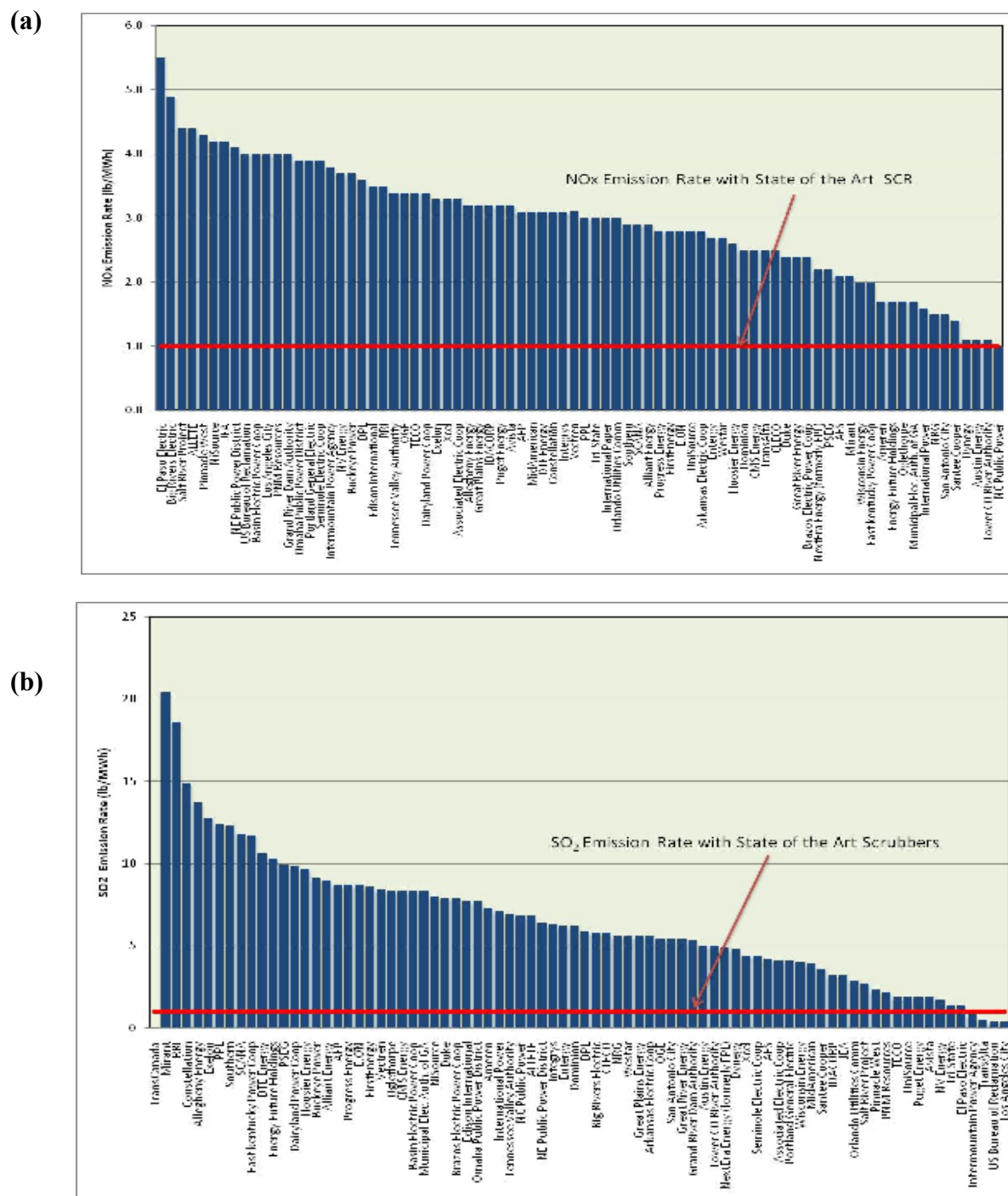


Fig. 6.1: a) NO<sub>x</sub> b) SO<sub>2</sub> emission rate of some of the US power plants combusting coal

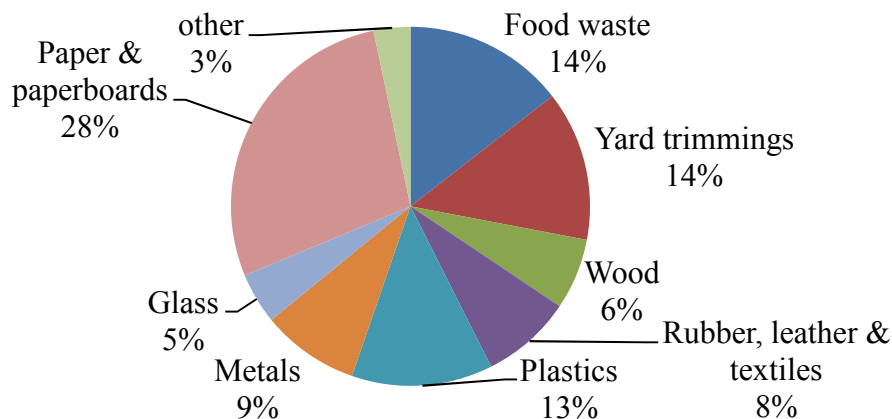


Fig. 6.2: Total MSW generation (by material), 2011 (Agency, 2013)

In order to produce EF, processes are required to efficiently separate the individual desired combustible components of MSW whose properties are reported in Table 6.1. A combination of predetermined fractions of pure combustible components derived from an efficient separation process makes EF tailoring feasible. This tailoring can aim at enhancing the efficiency of combustion as well as mitigating the pollutant emissions.

Table 6.1: High heating value (HHV), elemental analysis and moisture content of the main combustible components of SBW used in this study

Parameter/element	Fiber	Soft plastic	Hard plastic
HHV (kJ/g)	14.1	39.6	34.2
C (% wt)	40.2	70.3	79.8
H (% wt)	5.4	11.5	12.0
O (% wt)	42.0	14.5	2.7
N (% wt)	1.0	1.1	1.0
Ash (% wt)	11.4	2.6	4.5
Moisture (% wt)	5.4	1.5	0.5

Various techniques are currently used to separate SBW into combustible, noncombustible, and individual fractions. One technique involves separation via vibrations and trommel screens to separate a SBW stream into an overflow and an underflow, assumed to be composed of combustible and non-combustible materials, respectively. However, it was shown that the loss up on ignition of the underflow (assumed as non-combustible material) may reach 50% due to the high percentage of wood, fiber, and plastics (Tomoo Sekito, Tanaka, & Matsuto, 2006). Another technique exploits the difference in SBW components' density and hydrodynamic properties to promote separation via elutriation. Elutriation, air classification or air tabling can lead to significant costs due to the high gas velocities required. In addition, as demonstrated by Vesilind et al. (Vesilind, Peirce, & McNabb, 1982) the shape and characteristic sizes of particles of a material can significantly affect their terminal settling velocities (TSV) resulting in a diminution of separation performance, thus a precise control of these parameters is required for efficient separation. Studies have reported that pulsed flow air classification based on the TSV of components can comparatively improve the separation performance (Stessel & Peirce, 1986). Nonetheless, since TSV is highly dependent on the particle size, it is likely that the TSV of plastics, metals, rubber, and glass pieces having a broad size distribution overlaps regardless of their different densities. This limits the efficiency of separation in air classifiers and therefore density separation has been proposed as a more suitable technique (T. Sekito, Tanaka, & Matsuto, 2003).

Differences in density and surface wettability are usually exploited in the liquid separation technique; the mixed SBW particles are fed into a separation liquid so that the particles with a lower density than that of the liquid float and are removed, while particles that are denser than the liquid sink to the bottom of the vessel. However, high separation efficiency may be difficult to attain since most plastics are hydrophobic by nature, which may result in air bubbles attaching onto the particle surface and lowering the effective density. Furthermore, the effect of surface tension may be increased, which holds the plastic at the air-water interface. To overcome these issues, flotation may require wetting the plastic particles or using increased shear forces to dislodge attached air bubbles (H. T. Shen, Forssberg, & Pugh, 2002). The liquid separation technique also suffers from the requirement of a drying process and wastewater treatment, which are costly.

Density separation can also be performed dry through the fluidization of the material in a gas-solid fluidized bed. Under this condition, the use of a suitable fluidization medium is required so that the objects having a smaller density than the apparent density of the fluidized bed float, while those with a larger specific gravity sink (M. Yoshida, Oshitani, Ono, Ishizashi, & Gotoh, 2008). Dry density separation requires lower gas velocities compared to the elutriation technique (reduced energy costs) and reduces post-treatments compared to wet density separation techniques (no drying required). This technique was originally developed for coal cleaning (Fraser & Yancey, 1926) and then employed in ore processing technology (Douglas, Walsh, & Whitehead, 1968) as well as the separation of agriculture products (Zaltzman, Feller, Mizrach, & Schmilovitch, 1983). A few researchers have reported the successful use of the gas-solid fluidized bed technology for the separation of real or simulated SBW materials. Beekmans and Yu (Beekmans & Yu, 1992) used a rotating screen fluidized bed to separate scrap plastics. The technique was also successfully applied to separate CI-contained and CI-free plastics (M. Yoshida et al., 2010) as well as plastics and copper wire of automobile shredded residues (Oshitani, Kiyoshima, & Tanaka, 2003).

Using glass beads as the bed material, Sekito et al. (Tomoo Sekito et al., 2006) could separate SBW into combustibles, such as wood, paper, plastics and incombustibles, such as metals and glass, with the overall efficiency of 0.93. They also used a mixture of 80% nylon shots and 20% glass beads as the bed material to adjust the apparent density of the bed, so that wood and paper components were recovered while plastics remained in the bed to achieve a final overall efficiency of 0.88. They observed that the accumulation of SBW at the bottom of the bed significantly reduced the separation efficiency. Thus, in another work, they tried to separate fractions of 5.6-50 mm SBW into combustible and non-combustible components via density segregation experiments performed in a stirred fluidized bed (T. Sekito, Matsuto, & Tanaka, 2006). Stirring was shown to be effective in preventing the above-mentioned accumulation; however, the flexible sheet materials, such as paper and film plastics, still decreased significantly the separation efficiency. Excluding flexible materials from the SBW feed enhanced the overall efficiency of batch-scale tests to 0.90, while it decreased to 0.79 when the untreated feedstock was fed to the bed in the continuous feeding tests.

In the present study, a process has been developed to (1) separate combustible and non-combustible materials from residential and commercial SBW and (2) perform a partial separation

of the individual combustible components. The proposed original process includes two main separation steps: (1) an elutriation approach is first adopted to remove and separate lighter components (fiber and soft plastic) from the main SBW feed and (2) a fluidization medium is then introduced in order to separate undesirable combustible components and hard plastic from non-combustible materials on the basis of the dry density segregation technique realized under fluidization conditions.

## **6.2 Experimental**

### **6.2.1 Characteristics of SBW**

The SBW used in the experiments was obtained from residential and commercial waste collected by the Chittenden county Vermont (USA) recycling facility and the Maine (USA) Energy Recycling Company (MERC). These two facilities process waste collected from recycle bins: the waste is sorted to separate contaminants (organics, for example) and recyclable components (metals, glass and plastics). At the end of the sorting process, a certain mass of waste remain either because it could not be sorted or it has no value as a recyclable material. This mixed waste is generally sent to landfills or sold for the production of RDF or EF. To produce RDF or EF, this mixed waste is generally shredded to obtain a more uniform size distribution for further treatment: densification, sorting, addition of components, etc. The SBW used in the present study corresponds to waste shredded for the production of EF: it was shredded to a mesh 4, which is typical for RDF or EF production processes. The SBW was used as provided and its size distribution and moisture content were not altered for the present study. Individual SBW components (fiber, soft plastic and hard plastic) were also provided: these components were separated manually.

The SBW contained fiber, soft plastics (PE), hard plastics (PP, PVC, PC, PS and ABS) and non-combustible materials (mainly glass, metals and non-recyclables such as stony material). The characteristics of the fiber, soft plastic and hard plastic samples are detailed in Table 6.1. The SBW composition is specified in Table 6.2 along with the true and bulk density of the fiber, soft plastic and hard plastic. The true density is measured with a gas pycnometer (Micromeritics, AccuPyc II 1340) while the bulk density is measured with a graduated cylinder. Because of the

highly porous and non-homogenous characteristics of ingredients, the values of true (skeleton) densities obtained with the gas pycnometer are much higher than the typical particle density of fiber (paper) and soft or hard plastics. Bulk densities, which are the mean values of five repetitions, however, reflect well the relative heaviness of the main components of the SBW.

The particle size distribution of the fiber, soft plastic and hard plastic is measured using ASTM sieves and the average results from 5 measurements are shown in Fig. 6.3. The errors bars shown in Fig. 6.3 correspond to the variability in the 5 measurements.

Table 6.2: True and bulk densities of the waste, its main constituents and their respective weight fractions

Material	$\rho_{\text{true}}$ (kg/m <sup>3</sup> )	$\rho_{\text{bulk}}$ (kg/m <sup>3</sup> )	Weight fraction in SBW (%)
SBW	1504±2.5	70±1.4	-
Fiber	1642±0.1	48±4.2	72.18
Soft plastic	1025±2.1	18±3.6	12.06
Hard plastic	1094±0.3	209±8.5	7.86
Other combustible materials	n/a	n/a	7.35
Non-combustible materials	n/a	n/a	0.55

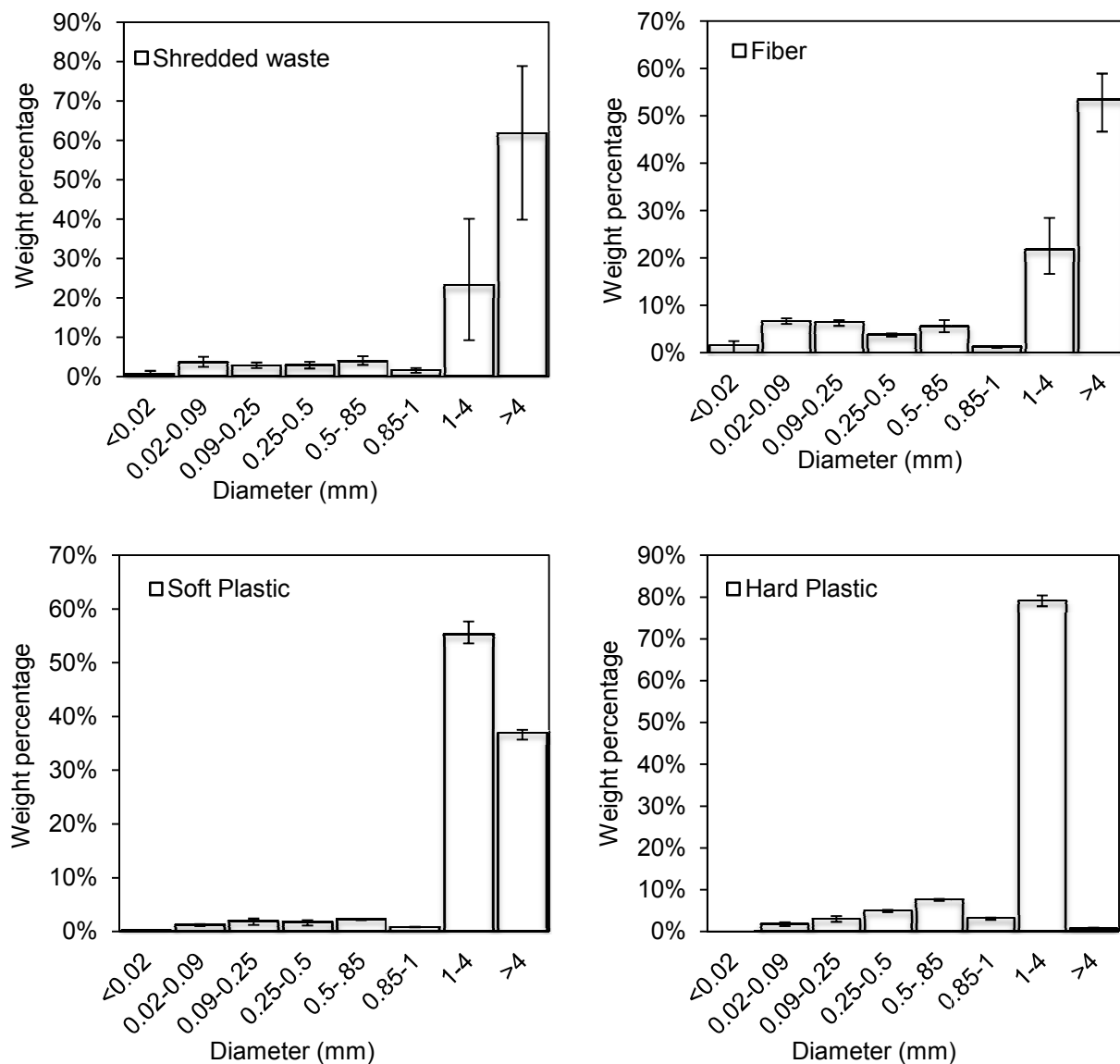


Fig. 6.3: Particle size distribution of the SBW used in the experiments and its main constituents

## 6.2.2 Experimental apparatus and procedure

Pretreatment of SBW (the first elutriation step) is performed in a cylindrical fluidization column with an internal diameter of 152 mm, connected to an external cyclone at its top outlet. Prior to each experiment, the column is filled with a specific mass of waste through a feeding window. The initial waste bed mass is kept below 150 g to avoid an upward drift of the whole mass in the column because of the highly entwined nature of the SBW. Air is then injected into the column (below the bed) through a perforated plate with an opening area ratio below 1% (163 orifices of 1

mm in diameter). Superficial gas velocity is adjusted to a specific value through an assemblage of two rotameters and an orifice flow-meter: the elutriation velocity varies between 0.5 m/s and 2 m/s. The drag force exerted by the upward moving air entrains waste particles upward. The cyclone recovers the elutriated materials, which are finally collected in a bag. The duration of each run varies between 15 and 45 min and the gas flow is then cut off. At the end of an experiment, the contents of the bag filter and the waste remaining in the bed is collected, hand sorted and weighed. The elutriation behavior of each individual component, i.e., fiber, soft plastic and hard plastic are studied in separate experiments. The second elutriation and the density segregation experiments are performed in a 75 mm I.D. column equipped with a porous plate distributor. To make the separation of interwoven feedstock possible in the second elutriation step, it is manually agitated using a normal rod during the elutriation process. The mass of waste material used for all experiments was 150 g and 5 g for the first and second elutriation step, respectively.

Separation of the target components in the density segregation experiments is realized by fluidization of the feedstock with the help of a granular substance called “bed material” or “fluidization medium”. This substance primarily facilitates independent fluidization of the feedstock components, which are not normally fluidized well alone owing to the significant irregularity in size and density. In addition, in the presence of a proper bed material whose density lies between that of the light and heavy components of the feedstock, density segregation can take place during the fluidization, which results in separation. Accordingly, the lighter components tend to accumulate at the top of the fluidization medium, whereas the heavier material moves underneath.

Prior to each density segregation experiment, given quantities of the feedstock and the fluidization medium (glass beads, polymeric or wood beads) is fed inside the fluidized bed vessel in three possible configurations: feedstock on top of the bed, feedstock at the bottom of the bed and feedstock uniformly mixed with the medium. As discussed later, these bed materials are chosen in view of the densities of the target components, which should be separated. Air is then injected through the distributor of the column and fluidization velocity ( $U_f$ ) is kept equal or slightly higher than the minimum superficial fluidization velocity ( $U_{mf}$ ) of the bed material, which governs the fluidization process in view of its much higher quantity in the bed compared with the feedstock. The components that accumulate at the top of the bed are collected carefully

at the end of each run by using a suction device, hand sorted and weighed. The rest of the bed content is emptied afterwards in a similar way and the waste is separated from the bed materials by sieving. Target components of each run are manually separated from the associated impurities in order to measure the purity percentage of each experiment. The average particle diameter, true density, bulk density and minimum fluidization velocity of the different beads used are specified in Table 6.3. True and bulk densities are measured using the same methods mentioned in section 6.2.1. The  $U_{mf}$  of each material is obtained through the following correlation (Crowe, 2010). Note that the mass of waste material used for all density segregation experiments was 10 g and 30 g for the first and second step, respectively.

$$Re_{mf} = \frac{\rho_g d_p U_{mf}}{\mu_g} = \sqrt{33.7^2 + 0.0408 Ar} - 33.7 \quad (6.1)$$

$$Ar = \frac{g \rho_g (\rho_p - \rho_g) d_p^3}{\mu_g^2} \quad (6.2)$$

Table 6.3: Properties of bed materials used in density segregation experiments

Material	Abbreviated name	Particle diameter (mm)	True density (kg/m <sup>3</sup> )	Bulk density (kg/m <sup>3</sup> )	$U_{mf}$ (m/s)
Glass bead	GB1	1.00	2536	1480	0.59
Glass bead	GB1.15	1.15	2536	1210	0.69
Glass bead	GB3.2	3.17	2536	932	1.51
Polypropylene (PP)	PP3.2	3.17	892	529	0.85
Polypropylene (PP)	PP6.3	6.35	886	535	1.30
Polyvinylidene fluoride (PVDF)	PVDF	2.00	1780	1098	0.90
Wood balls	WB9.5	9.53	644	381	1.38

## 6.3 Results and discussion

### 6.3.1 The overall process

Considering the SBW characteristics, a four step process is proposed as follows to separate combustible and non-combustible materials as well the individual combustible components: fiber, soft plastic and hard plastic. The process is represented in Fig. 6.9, where the target streams for each step are identified:

Step 1: Elutriation of fiber and soft plastic from the SBW;

Step 2: Separation of soft plastic from other elutriated combustible materials via elutriation;

Step 3: Dry density separation of non-elutriated combustible materials from hard plastic and non-combustible materials (target components);

Step 4: Dry density separation of hard plastic (target component) from non-combustible materials;

It should be noted that the number and arrangement of these steps are primarily governed by the properties of the SBW and the number of desired combustible components, which should be recovered. To quantify the separation performance of each step, the percentage of recovery ( $R$ ) and purity ( $P$ ) of the target components are calculated based on weight measurements using the following equations:

$$R = \frac{W_{it}}{W_{if}} \times 100 \quad (6.3)$$

$$P = \frac{W_{it}}{W_{Tt}} \times 100 \quad (6.4)$$

Moreover, the overall separation efficiency, known also as Newton separation efficiency, of each density segregation step is calculated using Eq. (6.5). This parameter reflects the overall efficiency of the separation unit since it returns the fraction of the recovered target components after excluding the fraction of the non-target components which are recovered, but undesirable and considered as impurity.

$$e = \frac{R}{100} - \frac{W_{jt}}{W_{jf}} \quad (6.5)$$

### 6.3.2 Shredded bulky waste (SBW) elutriation

Due to the high content of fluffy fiber materials in the SBW feedstock, the SBW components are strongly interwoven and could not be fluidized independently even at high superficial gas velocities. Therefore, a dry density separation could not be successfully performed on the SBW. This effect is mainly caused by the fibrous materials and soft plastic being abundantly present in the SBW feedstock. This issue has also been addressed in other similar investigations (T. Sekito et al., 2006). The fiber and soft plastic materials are characterized by a relatively low density (see Table 6.2) and low terminal velocity in comparison with the other SBW constituents, such as hard plastic and non-combustible components. These characteristics are therefore exploited to perform a first separation of fiber and soft plastic from other components in an elutriation column. In order to determine the most appropriate operating conditions for the elutriation step, several parameters detailed below are investigated.

#### 6.3.2.1 First elutriation column (step 1)

Fig. 6.4 shows the elutriation yield as a function of time for four superficial gas velocities, i.e.,  $U_e = 0.5$  m/s, 1.0 m/s, 1.2 m/s and 1.5 m/s. The elutriation yield is defined as the ratio of the elutriated mass to the total mass of the SBW initially fed into the bed. It is observed that the superficial gas velocity has a significant effect on the elutriation yield at a given time: the elutriation yield increases from less than 0.1 to 0.5 - 0.6 as  $U_e$  increases from 0.5 m/s to 1 m/s. The elutriation yield further increases, but more mildly, as  $U_e$  increases to 1.2 m/s. On the other hand, increasing  $U_e$  to 1.5 m/s raises the yield significantly. It is the case particularly at relatively shorter periods of elutriation, i.e.,  $t_e = 15$  and 30 minutes.

For relatively low elutriation velocities, i.e.,  $U_e < 1$  m/s, increasing the elutriation period could slightly enhance the elutriation yield. Longer elutriation of the feedstock is favorable for increasing the elutriation yield when  $U_e$  increases to 1.2 m/s. As inferred from Fig. 6.4, a further increase in  $U_e$  to 1.5 m/s results in the elutriation of the majority of the SBW components during 15 minutes, improving only 7% after a lapse of an additional 15 or 30 minutes.

A period of 30 minutes is generally sufficient to reach the steady state conditions at all gas velocities, except at  $U_e = 1.2$  m/s where steady state is not reached even after 45 minutes.

It is noteworthy that since the elutriated fraction is mainly composed of fiber and soft plastic, the ordinate of Fig. 6.4 also provides an indication of the degree of separation of these two materials from the SBW. Hence, the dashed line in Fig. 6.4 denotes the sum of the fiber and soft plastic weight fractions of the SBW (0.84). As inferred from the graphs, elutriation of the SBW at  $U_e = 1.2$  m/s for 45 minutes or at  $U_e = 1.5$  m/s for at least 15 minutes could lead to the full separation of the fiber and soft plastic. However, this is not observed in practice and a small quantity of these components remains non-elutriated. It mainly occurs because of the large size of some fiber and soft plastic particles, which cannot be elutriated under the operating conditions examined. Furthermore, there are some light undesirable combustible materials (mainly textile) in the SBW samples, which are elutriated even at low velocities and reduce the purity of the elutriated fiber and soft plastic.

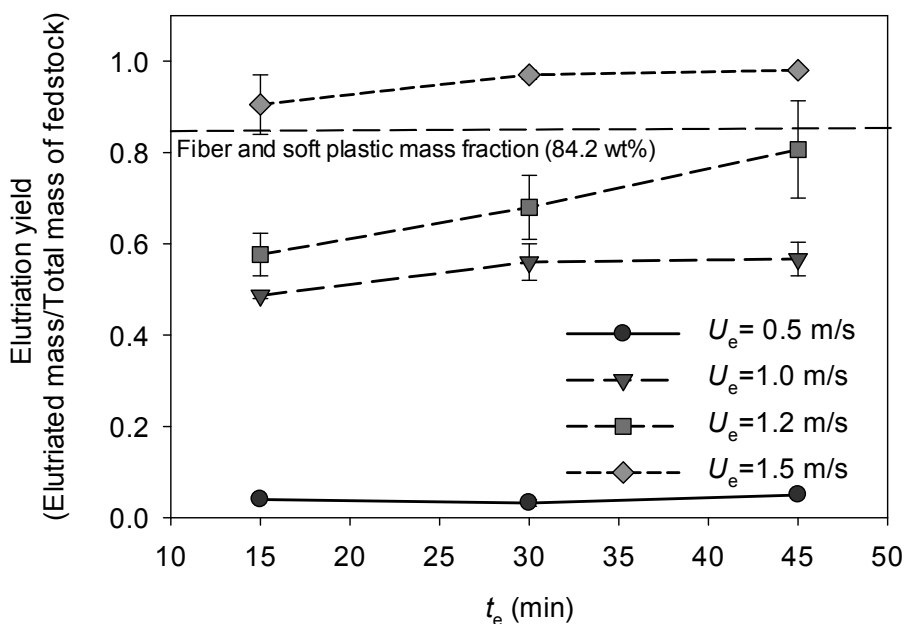


Fig. 6.4: Elutriation yield vs. time for four different gas velocities

The light components of the SBW, which are subject to elutriation in the experiments, are composed of diverse and entwined substances, which are not easy to differentiate. Thus, quantification and analysis of the elutriated fraction of SBW are not accurate. Accordingly, to

investigate the elutriation behavior of each combustible material (fiber, soft plastic and hard plastic) and determine the respective portions in the elutriated mass, each material is individually elutriated for 45 minutes in velocities ranging from 0.7 m/s to 1.9 m/s. The elutriated mass of each component is measured and then added to the corresponding value of others. An effectiveness factor ( $\eta_i$ ) is accordingly defined as below:

$$\eta_i = \frac{\text{Weight fraction of component "i" in the total elutriated mass}}{\text{Weight fraction of component "i" in the SBW}} \quad (6.6)$$

The elutriation technique can be qualified as a helpful method for separating component  $i$  when  $\eta_i > 1$ . As observed in Fig. 6.5,  $\eta_{\text{fiber}}$  is higher than 1 and  $\eta_{\text{hard plastic}}$  is lower than 1 regardless of  $U_e$ , whereas  $\eta_{\text{soft plastic}} > 1$  is satisfied only when  $U_e > 1$  m/s and it reaches a steady value at  $U_e = 1.5$  m/s. It is worth pointing out that  $\eta_{\text{fiber}}$  increases by velocity up to 1.0 m/s. Further increase in gas velocity, however, gives rise to a reduction of the fiber effectiveness factor. This trend is ascribed to the wide size distribution of fiber. As elucidated in Fig. 6.3, compared to other combustible components, a more considerable fraction of fiber material is very small in size (<0.25 mm), which is elutriated in relatively low velocities. In view of the lower density of soft plastic compared to fiber, its elutriation overtakes that of large pieces of fiber at high gas velocities leading to reduced  $\eta_{\text{fiber}}$ . It should be pointed out that the presence of other materials, such as undesirable combustible components, which are relatively very small in amount and heavier than fiber and soft plastic, slightly diminishes the respective effectiveness of fiber and soft plastic when the SBW is used as the feedstock. Thus, the results obtained can be attributed to the real SBW used in the experiments.

Weight fractions of fiber, soft plastic, hard plastic and other combustible and non-combustible materials in the non-elutriated fraction are shown in Fig. 6.6 for elutriation experiments performed on the SBW at 4 different velocities for 45 minutes. It is observed that the fraction of fiber drops drastically when  $U_e$  is increased above 0.5 m/s due to the relatively easier elutriation of small pieces of fiber discussed above. It should be noted that as inferred from Fig. 6.4, with increasing  $U_e$ , the total mass of non-elutriated material decreases. Moreover, the weight fraction of hard plastic and other unwanted combustibles, such as pieces of textile and wood splinters in the non-elutriated substances, rises by velocity because of the enhanced elutriation state of fiber and soft plastic at higher velocities.

Considering all of the abovementioned findings, it can be concluded that elutriation of SBW at  $U_e = 1.5$  m/s could result in the highest elutriation yield and separation efficiency of fiber and soft plastic, which is achievable during a comparatively short period of time (15 minutes). It is worth pointing out that the moisture content of the SBW was relatively low as shown in Table 6.1. The effect of higher moisture content was not investigated in the present study, but it can be assumed that it would increase the mass of the fiber particles. As such, the results from the present study suggest that this would result in a higher processing period for the first elutriation step: the moisture content of fiber particle would decrease with time until it is sufficiently low for the fiber particles to be elutriated.

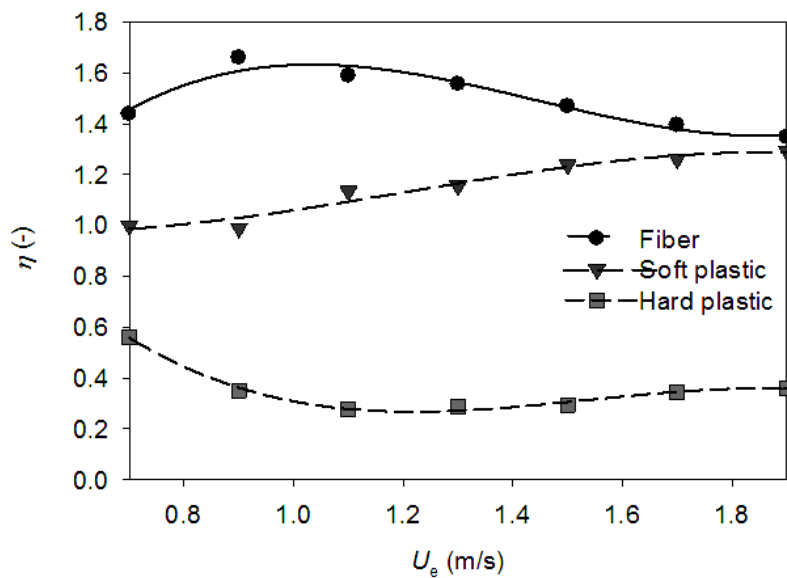


Fig. 6.5: Effectiveness of the separation of fiber, soft plastic and hard plastic via the elutriation technique in step 1.

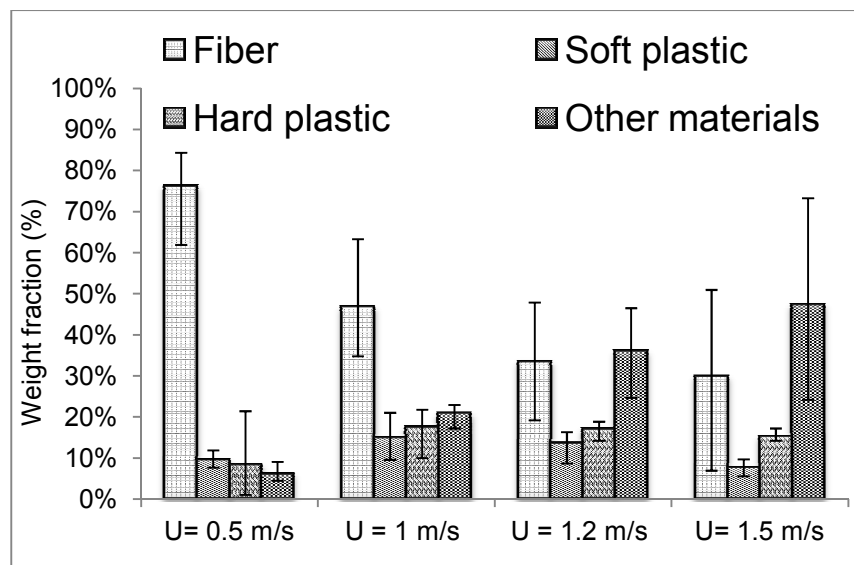


Fig. 6.6: Weight fraction of main constituents of waste in the non-elutriated materials of step 1

### 6.3.2.2 Second elutriation column (step 2)

The main constitutive components of the overflow of the first elutriation column are fiber and soft plastic. In view of the very low density of these materials, a second elutriation column is considered as the best approach for further separation of fiber and soft plastic. In this regard, the elutriated fraction of the first elutriation step ( $U_e=1.5$  m/s,  $t_e=15-30$  min.) is used as the feedstock of this step. Highly interwoven characteristics of this fraction, however, entail agitating the feedstock while being elutriated, in order to break the strong linkage between components. The feedstock is therefore stirred manually using a metal rod. The lowest gas velocity required to trigger the elutriation under these conditions is around 0.22 m/s. Being lower in density than fiber, almost all soft plastic flakes are prone to fast elutriation leading to a very high recovery percentage with respect to soft plastic (97%). However, the relevant purity is low because, as mentioned above, a significant fraction of fiber is very small in size and could be elutriated comparably to soft plastic pieces. Sieving the elutriated fraction, however, could partly settle the issue and enhance the ultimate purity because of the relatively larger size of the plastic flakes compared to the elutriated fiber particles. The aperture size of the sieve used for this purpose is 2.8 mm. The recovery and purity percentages of the second elutriation step are averaged for 8 repetitions and reported in Table 6.7.

### 6.3.3 Dry density separation

The elutriation technique results in a significant separation of the fluffy fiber materials and soft plastic from the SBW. Additionally, the granular properties of the non-elutriated SBW are noticeably improved. Thus, unlike the SBW, the materials remaining in the first elutriation column as the non-elutriated fraction can be handled as a mixture of discrete particles of different materials. This feature is essential for further processing of this fraction in the following dry density separation steps.

As discussed above, in the presence of an appropriate fluidization medium feedstock particles are subject to segregation while being fluidized so that the components, which are lighter than the fluidization medium move upward to the top of the bed (flotsam behavior), while the heavier components sink to the bed bottom (jetsam behavior). One of the most advantageous aspects of this method is that the separation efficiency is not as sensitive to the size of the particles as the other techniques, like elutriation (T. Sekito et al., 2003).

The non-elutriated SBW is mainly composed of non-combustible materials, hard plastic, and remnants of fiber and soft plastic. It also contains particles of wood and textile. The first density separation step is aimed at removing all combustible matters (overflow) from the non-elutriated SBW except for the hard plastic, which remains with the non-combustible materials in the underflow. In a second dry density segregation step, hard plastic is separated from the non-combustible materials. It should be stressed that the early removal of undesirable combustibles in the first step is necessary to enhance the efficiency and purity of hard plastic separation in the subsequent step.

In the current study and in both fluidization density separation steps, the optimal fluidization velocity to separate light and heavy materials is slightly higher than the  $U_{mf}$  of the corresponding fluidization medium reported in Table 6.3. As found experimentally, further increase in gas velocity unfavorably boosts the axial mixing of the constitutive components of the waste. It is in agreement with the findings of some other works, where the maximum extent of segregation occurred at  $U_{mf}$  of the bed inventory, particularly when the size and density of the bed components differed greatly (Noda et al., 1986; Yong Zhang, Jin, Zhong, et al., 2009).

### 6.3.3.1 First density segregation step (step 3)

As mentioned above, the feedstock used for this step is the non-elutriated fraction of the first elutriation column composed of 41% hard plastic, 36% undesirable combustible components, 15% fiber, 4% soft plastic, and 3% non-combustible materials. Several experiments are carried out using a variety of fluidization media, such as glass beads, polymeric, and wood balls.

*Effect of the initial arrangement of feedstock and bed material:* Three initial configurations of non-elutriated materials and bed material are studied: feedstock on top, feedstock at the bottom and the initially well-mixed condition, representing possible feeding strategies in continuous industrial units.

When the waste is on top, fluidization of the bed content does not result in the separation of the intended components since the waste remains almost intact without interacting with the fluidization medium. On the other hand, a much higher gas velocity than  $U_{mf}$  of the bed material is required to initiate fluidization when the waste is at the bottom. This prompts the crumbs of the waste to rise to the bed surface in the bubbles' wake without having interacted with the bed material. Furthermore, some large pieces of waste are trapped in the fluidization medium. Both of these events negatively affect the efficiency and purity percentage of this step (see Table 6.4). Pre-mixing of bed inventories before feeding into the column brings about acceptable recovery and purity percentages and therefore is adopted for other experiments.

*Effect of bed material density:* An appropriate bed material in terms of density provides the conditions under which the target component can behave as flotsam or jetsam making its recovery achievable. Accordingly, the bulk density of fluidization material should be between of those of light and heavy components of the feedstock under the fluidization conditions. To this purpose, glass beads and polymeric (PP) spheres are selected as potentially proper fluidization media of the first density separation step in which hard plastic and non-combustible matter should be separated from undesirable combustible components.

Table 6.4: Details of experiments conducted to examine the effect of some operating conditions on the performance of the fluidization column I

Elutriation conditions of the feedstock		Bed material used-size (mm)	Bed material to feed mass ratio (-)	$L/D$ (-)	Recovery (%)	Purity (%)	Overall efficiency (-)	Initial mixing state of the waste	
$U_e$ (m/s)	$t_e$ (min)								
<i>Non-elutriated materials</i>	1.5	15	GB-1.15	60	1	75	35.1	0.54	Unmixed (Bottom)
	1.5	15	GB-1.15	60	1	87	63.8	0.83	Well mixed
	1.5	15	PP-3.2	40	2	100	70.0	0.94	Well mixed
	1	30	PP-3.2	20	1	100	65.2	0.84	Well mixed
	1	30	PP-3.2	40	2	100	51.1	0.88	Well mixed
	1	30	PP-6.3	20	1	100	2.5	0.61	Well mixed
	1	30	WB-9.5	15	1	100	32.2	0.78	Well mixed

It is observed that in the case of using glass beads, hard plastic particles congregate beneath the flotsam species (the combustible components) which gives rise to reduction in the recovery percentage. This issue, which is more pronounced when the larger glass beads are used, is ascribed to the comparable apparent densities of the glass beads and hard plastic particles in the fluidized mode leading to the undesirable flotation of hard plastic. PP beads are utilized as the bed material of this step since their use brings about a higher recovery and purity percentage of the target components (Table 6.4).

#### 6.3.3.2 Second density segregation step (step 4)

Underflow of the first density segregation step is considered as the feedstock of the second density separation column. Working with this stream, however, is difficult in the scale of our experimental setup because of its very low content of non-combustible materials lowering the accuracy of experiments. Thus, the feedstock used in the experiments is simulated by mixing equal amounts of hard plastic particles, glass splinters, and small pieces of metal wire (Table 6.5). Therefore, it should be noted that the recovery and purity values reported in Table 6.5 are obtained without considering any undesirable combustible materials in the feedstock, which may

remain untreated from the previous step. On the basis of the experimental observations, it is unlikely that the presence of such materials would reduce the recovery of hard plastic particles. However, since they are subject to behave as flotsam; the purity of hard plastic particles in the overflow stream is prone to decrease. The purity percentage of the density segregation column II is reported in Table 6.7, with and without considering the presence of undesirable combustible materials in the overflow stream. In the latter case, it is assumed that all quantities of undesirable combustible matter appear as flotsam in the second separation step.

*Effect of the initial arrangement of the feedstock and bed material:* Contrary to the first density segregation step, pre-mixing of the feedstock and bed material favors mixing of the bed inventory instead of prompting segregation of the intended components. The dissimilarity between the optimal initial conditions of two density segregation steps stems from the difference in the size range of the target components in each step. As elucidated in Fig. 6.3, a substantially smaller size of hard plastic particles in comparison with other combustible substances leads to a more facilitated mixing of the fluidization medium and hard plastic while being fluidized, which is unfavorable. Hence, unlike the first density segregation step, fluidization medium and feedstock should be fed separately into the bed in the second step so that the feedstock lies at the top of the fluidization medium. Under these conditions, heavy non-combustible materials associated with hard plastic sink to the bottom whereas the hard plastic remains at the top of the bed.

*Effect of bed material density:* Regarding the true densities of PVDF and glass beads, they are tested as the tentative fluidization media of the second density segregation step. Compared to glass beads, the use of PVDF beads improves the purity of the target components, i.e., hard plastic at the expense of reducing the recovery percentage and the overall efficiency (Table 6.5). These differences can be explained in light of the lower density of PVDF than that of the glass beads. As shown in Fig. 6.7, when the bed material is glass beads, because of the comparable densities of the fluidization medium and glass splinters existing in the non-combustible materials, there is a low quantity of glass at the top layer of the bed decreasing the separation purity. On the other hand, due to the smaller difference between the densities of hard plastic and PVDF beads,

hard plastic particles could penetrate into the middle heights of the bed, a phenomenon that lowers the separation efficiency.

Table 6.5: Details of experiments conducted to examine the effect of the fluidization medium properties on the performance of the fluidization column II

Feedstock properties			Bed material used	Bed material to feed mass ratio (-)	Recovery (%)	Purity (%)	Overall efficiency (-)	Initial mixing state of the waste
Mass of hard plastic (g)	Mass of glass pieces (g)	Mass of metal pieces (g)						
10	10	10	GB3.2	20	96.5	92.0	0.72	Unmixed (Top)
10	10	10	PVDF	14	80	97.9	0.64	Unmixed (Top)

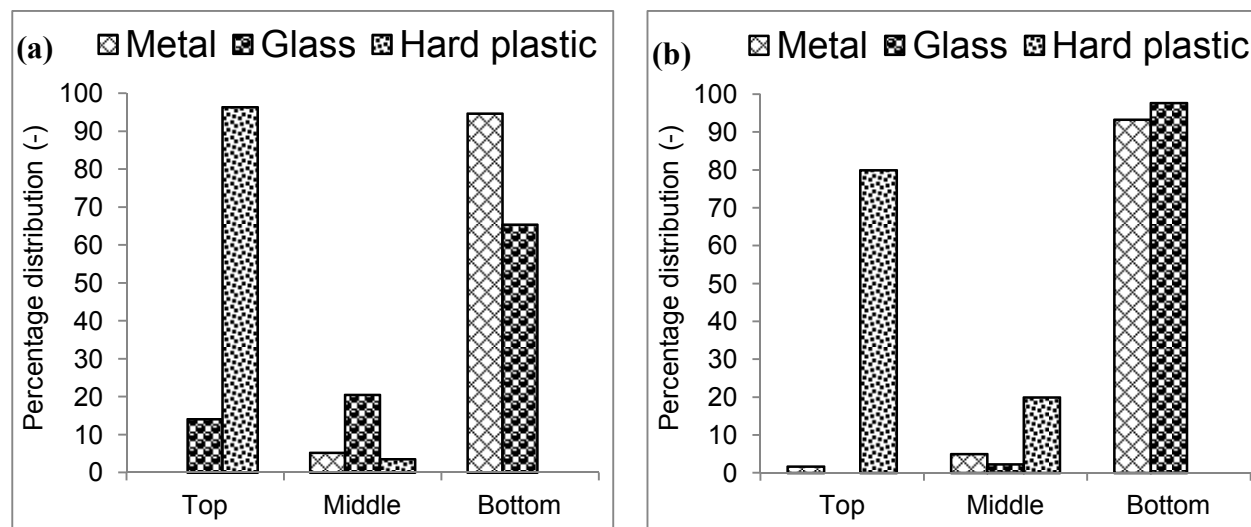


Fig. 6.7: Percentage distribution of feed components along the bed in the second density segregation step when the fluidization medium is a) glass beads b) PVDF beads

### 6.3.4 Effect of bed material size

As observed experimentally, segregation of the non-elutriated SBW components is more sensitive to the size of the bed materials compared to their densities. In the case of small glass

beads ( $d_p < 1$  mm), the emergence of bubbles, even at the onset of fluidization ( $U_f \approx U_{mf}$ ), notably enhances the mixing of various components along the bed, reducing separation efficiency. By increasing the size of the bed material particles ( $d_p = 1.15$  or  $3.2$  mm), full segregation of light and heavy components takes place at respective  $U_{mf}$  and no significant axial mixing occurs. As examined by using the large PP beads ( $d_p = 6.3$  mm), a further increase in the size of the bed material, however, leads to trapping of the non-combustible impurities, which drastically reduces the purity and overall separation efficiency of the target components (Table 6.4). Compared to the large PP beads, the use of large wood balls ( $d_p = 9.5$  mm) results in higher purity and overall separation efficiency, presumably because of the lower density of wood.

### 6.3.5 Effect of bed dimensions

To study the probable effect of bed dimensions on the performance of density segregation experiments, a few experiments are conducted in a column with a double-size diameter ( $D = 15.2$  cm). The similarity of the results obtained from the experiments conducted in two columns confirms that the wall effects have not meaningfully influenced the separation efficiency or purity percentage of the experiments performed in the small column. It is worth noting that changing the aspect ratio of the dense bed ( $L/D$ ) from 1 to 2 does not significantly affect the recovery or purity of the target components (Table 6.4).

### 6.3.6 Effect of feed (non-elutriated SBW) properties

As reported in Table 6.4, the overall efficiency of the first density separation step (fluidization column I) is greater for the feedstocks obtained from the higher elutriation velocities, primarily because of the lower quantity of the non-target components associated with hard plastic and non-combustible materials. In other words, the higher the quantity of these materials in the feedstock is, the higher the degree of disturbance is caused to the fluidization process. The most noticeable impurity observed in the first density segregation step is splinters of wood. Consistent with the observations of Sekito et al. (Tomoo Sekito et al., 2006), bar or needle shape splinters are more prone to be trapped at the wall region of the bed, compared to the other irregular particles. In fact, these materials remain unfluidized in the dense bed under the moderate fluidization conditions.

### 6.3.7 Kinetics of segregation in dry density separation

The dynamics of segregation in both density separation steps are also studied in order to determine the residence time required for achieving the maximum attainable separation. Studying the kinetics of segregation is crucial for designing the scaled up units operating continuously on the basis of the proposed process.

As discussed by Leaper et al. (M. C. Leaper et al., 2004), density segregation can be represented by a simplified first-order process in which the local rate of change of jetsam mass concentration at the top of the bed  $x$  is proportional to the difference between the local current value and an equilibrium value  $x_{\infty}$  (Eq. (6.7)).

$$\frac{dx}{dt} = -k(x - x_{\infty}) \quad (6.7)$$

which can be integrated to give the following solution:

$$x = x_{\infty} + (x_0 - x_{\infty})e^{-kt} \quad (6.8)$$

A similar approach can be considered for the concentration of flotsam mass at the bottom of the bed. Accordingly, concentrations of the intended components are measured at different time intervals after initiation of the experiments. The *segregation rate constant* ( $k$ ) can then be found by fitting the resultant values to Eq. (6.8).

In the case of the first density separation step, the flotsam components, i.e., undesirable combustible materials congregate at top of the bed over time. Thus, assessing the concentration of the flotsam species is more accurate in comparison with jetsam spread out in the bed. On the other hand, in the case of the second density separation step, jetsam materials, i.e., metal and glass, show a more explicit segregating behavior compared to the rest of the components of the feedstock and their accumulation at the bottom of the bed is pronounced. Accordingly, in order to drive the equation of segregation kinetics, variation of the flotsam concentration is measured at the bottom of the bed in the case of first density separation step. In the second step, however, concentration of jetsam at top of the bed is recorded over time.

Fig. 6.8a exhibits the local concentration of undesirable combustible materials (flotsam) at the bottom of the first density separation column vs. time, which is fitted with Eq. (6.7). Fig. 6.8b

and Fig. 6.8c show the local concentration of metal and glass vs. time in the top layer of the second density separation column, respectively. The exponential equation captures the segregation kinetics of metal, however, the glass concentration at the top layer declines linearly with time (Eq. (6.9) ).

$$x = x_0 - kt \quad (6.9)$$

It is plausibly because of the comparable density of the fluidization medium and glass. It is believed that the primary cause of segregation in the case of glass splinters is their different size from the particles of the fluidization medium (glass beads). In general, relatively fast segregation of the intended materials in both separation steps is a promising operational feature corroborating the suitability of corresponding large scale units, which should operate continuously. Table 6.6 contains the equations describing the segregation kinetics as well as their respective parameters obtained by fitting the experimental data.

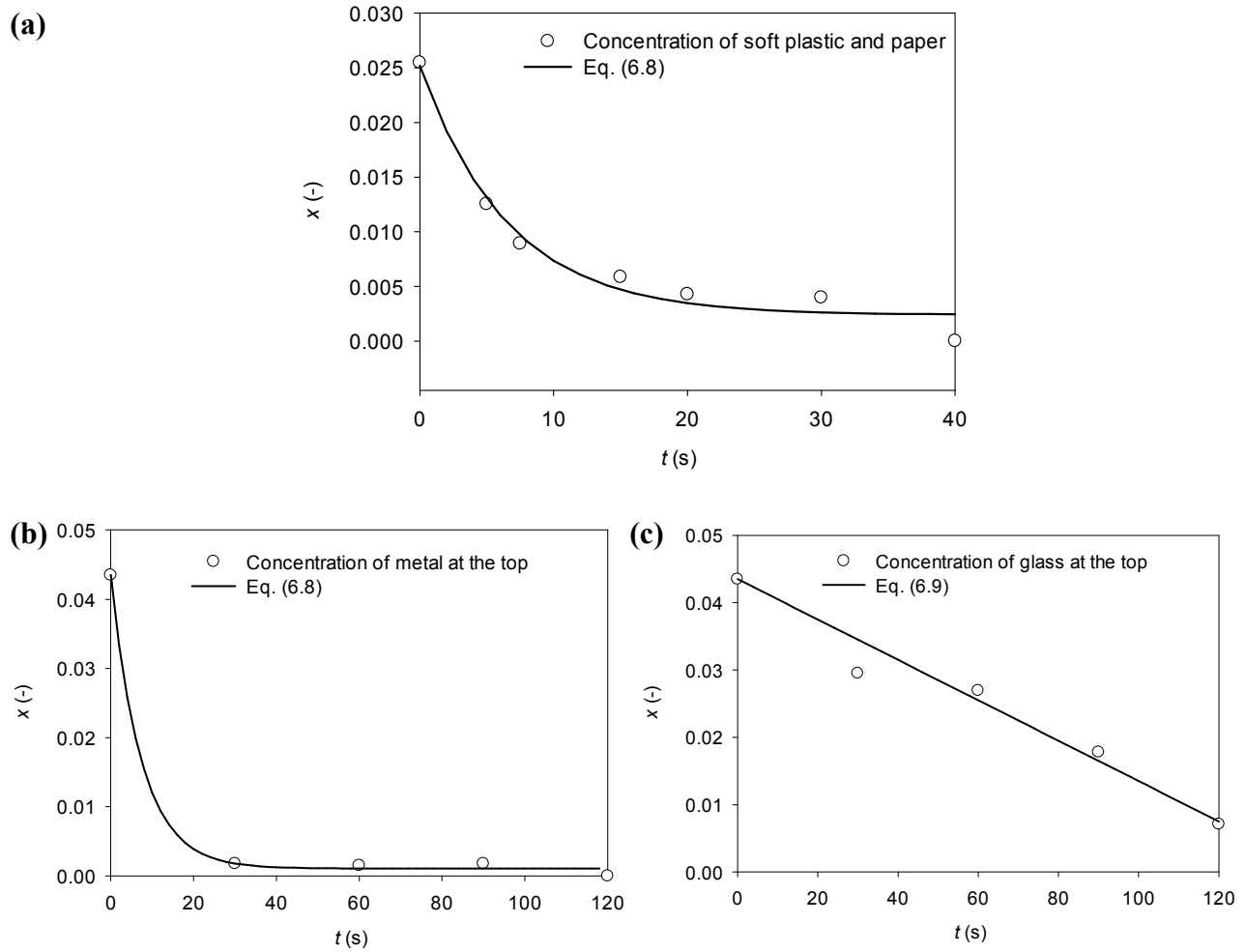


Fig. 6.8: Concentration of the intended components vs. time for the density separation step a) I b, c) II

Table 6.6: List of components whose segregation kinetics are studied in the density separation steps and the equations and respective parameters describing the kinetics

Density separation Step/studied material(s)	Fitting equation	$k$	$x_0$	$x_\infty$
1- Soft plastic/fiber	$x = x_\infty + (x_0 - x_\infty)e^{-kt}$ (6.7)	0.152	0.025	0.002
2- Metal	$x = x_\infty + (x_0 - x_\infty)e^{-kt}$ (6.8)	0.135	0.043	0.001
2-Glass	$x = x_0 - kt$ (6.9)	0.0003	0.043	-

## 6.4 Conclusion

In order to separate combustible and non-combustible materials from residential and commercial SBW, a step-wise process was developed based on elutriation and dry density separation techniques. Effective separation of the light individual combustible components, i.e., fiber and soft plastic, was achieved by elutriating the SBW in two consecutive steps. The non-elutriated fraction was then subjected to density segregation in the presence of a fluidization medium to separate non-combustible components and hard plastic particles. Size and density of the bed material could significantly affect the degree of recovery and purity of the target components. Accordingly, the most adequate bed media for attaining the highest recovery and purity percentages in density segregation columns I and II were polypropylene and glass beads ( $d_p=3.2$  mm), respectively. The optimal fluidization velocity is slightly higher than  $U_{mf}$  of the fluidization medium. Properties of the feedstock determine the most effective initial arrangement of the bed inventory.

Table 6.7 summarizes the function and target components of each separation step. In addition, it contains the recovery and purity percentages based on the composition of the target stream under optimal operating conditions. The target stream is one of the over or under flow streams in which the target components are dominant. Fig. 6.9 illustrates the overall process as well as the mass balance of each unit calculated on the basis of the corresponding purity and recovery percentages.

Process scale-up calculations for higher throughputs can be performed by assuming that the ratio of the bed height over the diameter ( $H/D$ ) is kept constant for higher fluidized bed diameters and that the elutriation rate remains constant. The required fluidized bed diameters for a throughput of 1 ton per hour are estimated as 1.8 m, 1.5 m, 0.5 m and 0.4 m for steps 1, 2, 3 and 4, respectively. On the other hand, the required diameters for a throughput of 10 tons per hour are estimated as 3.9 m, 3.3 m, 1.1 m and 0.8 m for steps 1, 2, 3 and 4, respectively. This shows that the scale-up of this 4-step process is realistic. This calculation is based on a fluidized bed continuous process (continuous injection and removal of mass), which are common in many industries.

The dotted section in Fig. 6.10 demonstrates the phase diagram of the EF, which can be produced by mixing streams containing primarily fiber, soft and hard plastic as recovered from the proposed process. The purity percentage of each stream has been indicated in the figure. It should

be recalled that the associated impurities are undesirable combustible or non-combustible components.

Table 6.7: Specifications of each separation unit

Step	Function(s)	Target component (s)	Recovery (%)	Purity (%)
Elutriation I	Removal of fluffy and entwined materials. Separation of light components.	Fiber and soft plastic	95.6	99.4
Elutriation II	Separation of fiber and soft plastic	Soft plastic	97	38.0 (47.3 <sup>*</sup> )
Fluidization I	Recovery of fiber and soft plastic	Hard plastic and non-combustible components	100	93.1
Fluidization II	Recovery of hard plastic	Hard plastic	96.5	92.0 (67.3 <sup>**</sup> )

<sup>\*</sup> After sieving

<sup>\*\*</sup> Assuming all undesirable components accumulate at the top of the bed.

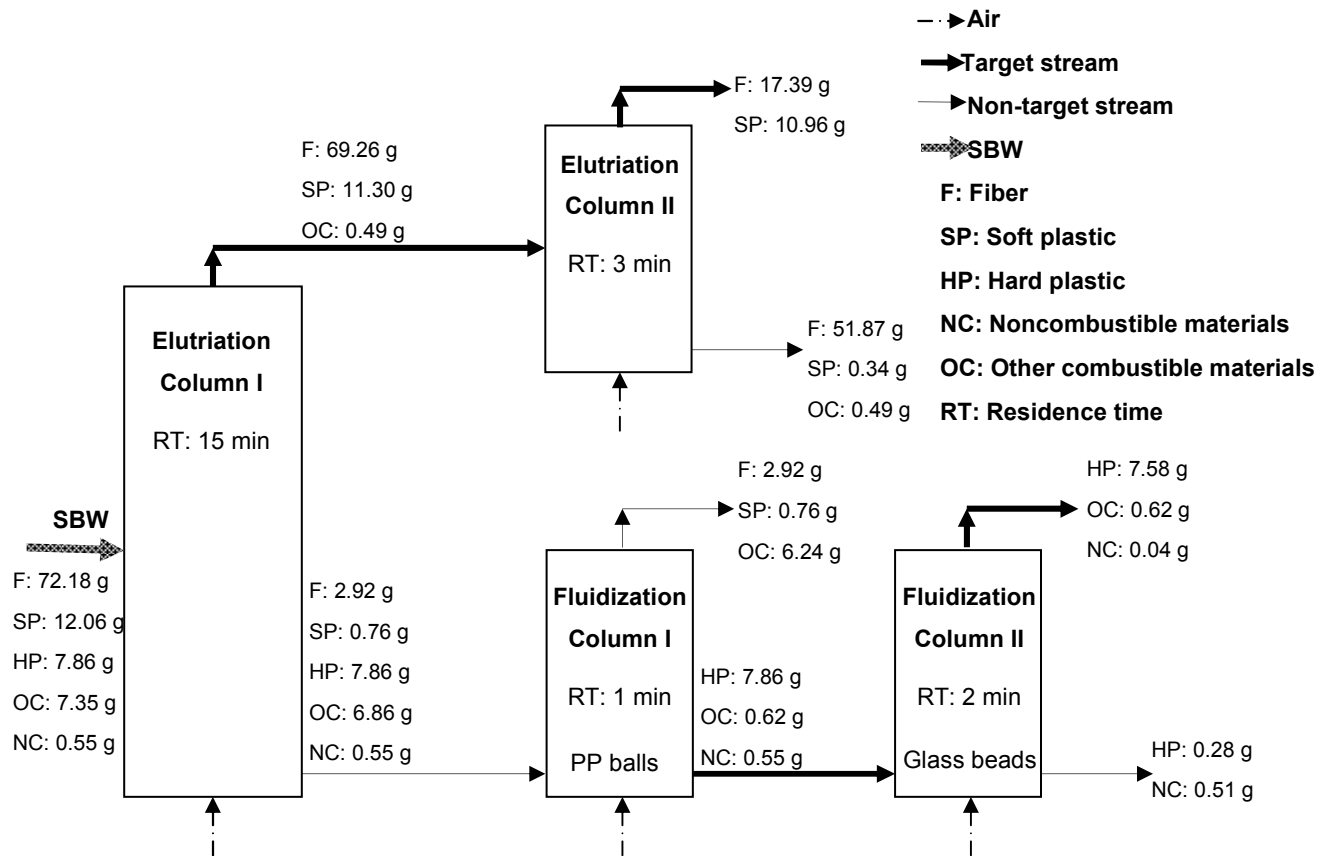


Fig. 6.9: Schematic presentation of the whole process proposed for the separation of the MSW components and mass balance calculated for 100 g of the SBW based on the separation efficiency of each unit.

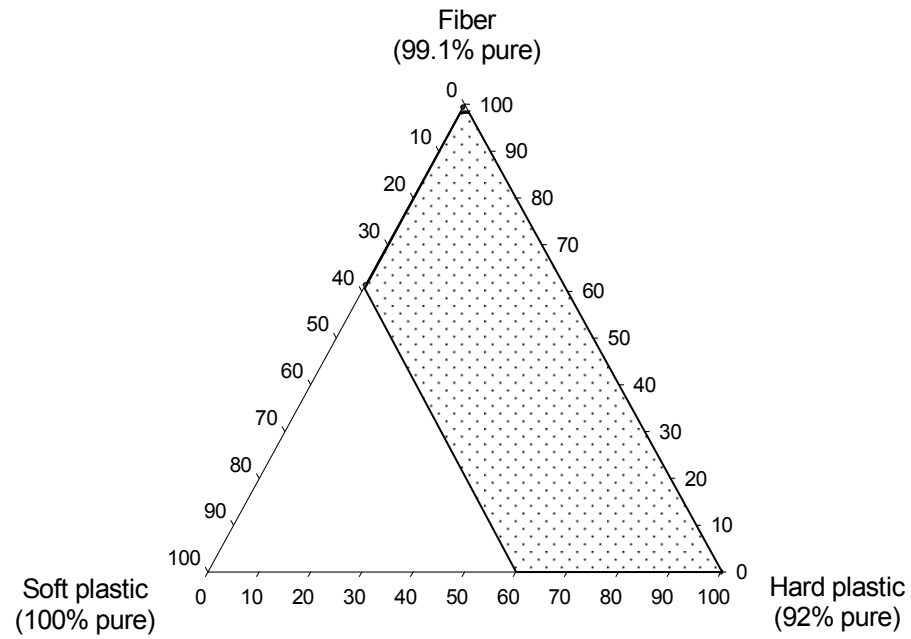


Fig. 6.10: Ternary diagram of the EF composition, which can be produced by mixing fiber, soft and hard plastic on the basis of the separation efficiencies of the proposed process.

## CHAPTER 7

### GENERAL DISCUSSION

Optimizing the design and operation of biomass processing units, which are based on fluidization, requires extensive knowledge of the multiphase flow aspects of gas-solid mixtures. The peculiar nature and the irregular properties of the biomass particles bring about some hydrodynamic complexities that are not observed in conventional fluidized beds. In addition, the fluidization of dissimilar components, i.e., inert material and biomass particles, gives rise to segregation that adversely affects the thermal processes. Understanding segregation-related phenomena would be valuable to control the resulting effects, whether segregation is detrimental, like in combustors or gasifiers, or beneficial, as in fluidized bed classifiers or separators.

The influence of large biomass particles on the characteristics of the dilute phase of fluidization and the gas distribution pattern in the bed was addressed in CHAPTER 3 when the weight fraction of biomass varied from 2 to 16%. Increasing the load of biomass resulted in raising the characteristic fluidization velocities, including  $U_{ib}$ ,  $U_{ff}$ ,  $U_c$ ; however,  $U_{if}$  was found to be independent of the mixture composition, at least for the systems studied. In general, the bubbling trend at low superficial gas velocities ( $U < 0.6$  m/s) was affected by the load of biomass, while it was not the case at higher velocities. This was inferred from the undeveloped bubble size distribution at low gas velocity on the basis of the statistical analysis of the pressure signals. The local exploration of the dilute (bubble) and dense (emulsion) fluidization phases by optical probes revealed that the presence of biomass particles in a bed of sand leads to the dilution of the dense bed and an increase in the gas holdup. A lower degree of bed expansion was observed when the biomass content was increased in the bed. The local examination of the bubble phase confirmed that the biomass particles triggered bubble breakage resulting in the emergence of smaller bubbles. This phenomenon, which was intensified by increasing the load of biomass, led to the local variations in the dilute phase fraction and bubble frequency. It was noticed that the voidage of the bubble and emulsion phases remained unaffected in the presence of biomass particles. These observations imply an improvement in the fluidization quality of the systems studied at a high enough gas velocity as a result of increasing the biomass ratio in the bed.

The hydrodynamics of biomass fluidization was studied in CHAPTER 4 by analyzing pressure fluctuations and employing the Radioactive Particle Tracking (RPT) technique in mixtures differing in composition. In the RPT experiments, the instantaneous position of a tracer mimicking the motion of biomass particles was acquired for about 6 hours in a Lagrangian framework. Changing the biomass fraction at the top of the bed as a result of increasing the gas velocity was reflected in the variation of the local time-averaged pressure drops after excluding the corresponding values of a bed of pure sand, i.e.,  $\left(\left[\frac{d\Delta P}{dU}\right]_{\text{mix}} - \left[\frac{d\Delta P}{dU}\right]_{\text{sand}}\right)$ . The time-averaged occupancy (concentration) profile of biomass along the bed that was obtained from the RPT data clearly demonstrated the flotsam behavior of the biomass particles. This behavior was mitigated by increasing fluidization velocity.

The segregation propensity of biomass particles was studied through their circulatory motion pattern. Comparing the probability density function of the normalized gross cycle length of biomass particles revealed that increasing the load of biomass at a low bubbling gas velocity ( $U=0.36$  m/s) prompted their imperfect circulation of biomass particles. This was ascribed to the feeble small bubbles that were not capable of inducing a jump similar to large particles. However, the cycling trait of the systems composed of 2%, 8% and 16% biomass became comparable by raising the gas velocity to  $U=0.64$  m/s. It was recognized that under intense bubbling conditions, increasing the weight fraction of biomass in the mixture smoothed the sinking process of the flotsam particles. Consequently, a larger number of the biomass particles penetrated into the lower parts of the bed, giving rise to an enhanced mixing state.

As discussed in CHAPTER 4, the biomass-sand ratio of the bed inventory could also govern the loci of gross cycles. Accordingly, it is expected that in the case of bottom feeding, contact between the pyrolysis products and oxygen takes place more effectively in systems containing a low fraction of biomass, i.e., 2%. On the other hand, the improved mixing of the bed components when the load of biomass is high, i.e., 16%, promotes the interaction of the interstitial oxygen of the dense bed and the fuel particles, boosting the reactor performance.

The axial distribution of large biomass particles was modeled based on the Gibilaro-Rowe (G-R) model (Gibilaro & Rowe, 1974) adapted for the irregular flotsam particles. Moreover, some terms of the G-R model were linked to the measurable hydrodynamic phenomena scrutinized by the RPT technique. For example, the height-averaged rise velocity of biomass particles was

found to be 0.2 times that of bubble velocity, thus the upward flux of biomass particles in the bed was correlated to the bubble rise velocity. The model could satisfactorily predict the volume fraction of biomass along the bed. The discrepancy between the experimental results and the corresponding modeled values increased slightly by raising the load of biomass, mainly because of the deviation of the real bubble properties from the corresponding values obtained from the Darton et al. (Darton et al., 1977) and Davidson and Harrison (Davidson & Harrison, 1963) correlations. It was shown that the biomass volume fraction in the lowermost section of the bed is governed by the superficial gas velocity and the load of biomass.

In CHAPTER 5 the characteristics of the bubbles in the presence of biomass particles were numerically investigated through the BARRACUDA CPFD software that is based on the Lagrangian-Eulerian approach. The dynamics of fluidization after injection of gas in the column was in agreement with the phenomena observed visually or inferred from the RPT data. For instance, simulation could successfully predict the degree of bed expansion with respect to sand and biomass particles as well as the qualitative distribution of biomass particles along the bed. The distribution of bubble size and bubble rise velocity was also obtained by processing the simulated voidage signals recorded at  $h=17.5$  and 20 cm, similar to the experimental procedure followed to measure the local voidage fluctuations using optical fiber probes. In general, the bubble size and rise velocity distribution profiles of the experimental and numerical attempts were reasonably comparable in mean and standard deviation and to a lower extent in skewness values. The discrepancy between the experimental and the corresponding numerical results diminished as the load of biomass rose. It was attributed to the large size of the computational cell adopted for the simulations, which lowered the accuracy of the simulation results when the portion of the small sand particles was larger in the mixture and consequently in each computational cell.

Studying the phenomena controlling the segregation of dissimilar particles, the parameters that could enhance segregation were recognized and exploited in a novel dry step-wise process devised for the separation of the combustible components of shredded bulky waste (SBW), i.e., fiber, and soft and hard plastic. Providing pure streams of combustible materials derived from the waste is vital for tailoring the proper solid waste-based fuels with a low level of emissions, which are used in the existing fluidized or pulverized coal combustors. As detailed in CHAPTER 6, the proposed process was composed of two elutriation and two density segregation steps. Most of the

fiber and soft plastic in SBW (95.6%) were recovered from the first elutriation column and partially separated from each other in the second elutriation column. The non-elutriated materials were further separated in a fluidization column because of their different densities. Using an adequate fluidization medium made the segregation of the target and non-target substances possible under incipient fluidization conditions. Thus, hard plastic and non-combustible components were totally recovered in the first fluidization column by utilizing Polypropylene (PP) beads as the fluidization medium. Hard plastic was then separated with the help of glass beads in the second fluidization column. The recovery and purity percentages of this step were 96.5 and 92.0, respectively. The impact of some operating conditions, such as gas velocity, the properties of the bed material particles and the initial arrangement of the bed inventory on the recovery and purity of the streams, was investigated. The segregation kinetics was also determined for both fluidization steps.

## CHAPTER 8

### CONCLUSIONS AND RECOMMENDATIONS

#### 8.1 Conclusions

Hydrodynamics and solids mixing of bubbling fluidized beds involving mixtures of sand and large biomass particles have been explored in this dissertation. In this regard, some light has been shed to the hydrodynamic parameters which are matter of importance in terms of design, operation and control of the fluidized bed combustors or gasifiers. In CHAPTER 3, it was shown that  $U_{ff}$  and  $U_c$  are those characteristic velocities which change with the mixture composition. Moreover, based on the optical fiber results, it was illustrated that changing the fraction of biomass could considerably affect the properties of the bubble and emulsion phases. Emergence of smaller bubbles and more uniform distribution of gas across the bed as a result of higher biomass loads in the mixture are two instances of these effects giving rise to enhanced fluidization quality. Deploying the non-intrusive RPT technique, it was explored in CHAPTER 4 that the mechanisms governing the extent of mixing of sand-biomass particles are linked to the properties of the bubble and emulsion phases which are subject to change in the presence of different quantities of biomass particles. It was found that increasing the biomass fraction at low gas velocity ( $U=0.36$  m/s) leads to the imperfect circulation and severe segregation of biomass particles, however, raising the load of biomass at high enough bubbling gas velocity ( $U=0.64$  m/s) results in the enhanced sinking process of biomass particles mainly due to a) the lower difference between the density of the light biomass particles and the bulk density of the surrounding medium and b) the looser structure of the emulsion phase. Under these conditions, the problem of choosing the most suitable feeding position (top or bottom feeding) becomes less tricky due to the more uniform distribution of the gas products in the bed. The RPT results were also processed to relate the terms of the G-R model to the hydrodynamic phenomena in the bed. In this regard, a model with no adjustable parameter could be developed, which predicts the axial distribution of biomass particles along the bed as a function of the superficial gas velocity, bed material and biomass properties and the composition of the bed inventory.

The bubbling behavior of the investigated systems was numerically simulated in CHAPTER 5 through the BARRACUDA CPFDF software that is based on the Lagrangian-Eulerian approach. The proposed CPFDF model could reproduce the asymmetric character of both bubble size and bubble velocity distributions. In addition, the simulated and experimental bubble size and bubble velocity distributions yielded close first-, second-, and third-order statistical moments in the case of systems with high fractions of biomass (8 and 16 wt%). The degree of accuracy of the proposed model to predict the bubble characteristics declined with decreasing the biomass fraction. It was ascribed to the large size of the computational cell adopted for the simulations of all systems, which brought about feeble results in the case of 0 and 2 wt% biomass for which the portion of the sand particles was considerable in each computational cell.

In CHAPTER 6 segregation phenomena were exploited to separate the combustible components of the municipal solid waste, i.e., fiber, soft and hard plastic. In this regard, a step-wise process was proposed in order to treat the shredded bulky waste (SBW). Early elutriation of the light fluffy constituents of the SBW was vital to facilitate separation of the species in the subsequent density segregation steps. Effective separation of dissimilar materials in density segregation steps was achieved by choosing an appropriate fluidization medium in terms of size and density. Moreover, fluidization velocity and the initial configuration of the bed materials determined the recovery and purity percentages of each step.

## **8.2 Original contributions**

The novel aspects of this study are as follow:

- a) Detailed study of the impact of large biomass particles belonging to Geldart D on the distribution of gas and bubbling characteristics of sand fluidized beds.
- b) Phenomenological investigation of mixing and segregation of sand-biomass particles under bubbling fluidization conditions by means of the non-intrusive RPT technique.
- c) Developing a model with no adjustable parameter, which predicts the extent of axial segregation of biomass particles fluidized with the help of a bed material in bubbling regime.

- d) Developing an Eulerian-Lagrangian (CPFD) model for the numerical simulation of a sand-biomass fluidized bed and validating the simulation results by experimental data.
- e) Scrutinizing the impact of the bed inventory composition on the fluidization and mixing behavior of bubbling fluidized beds involving biomass.
- f) Developing a step-wise process based on elutriation and segregation phenomena in order to recover the main combustible components of the shredded bulky waste.

### **8.3 Future work and recommendations**

This research shed light on the impact of the irregular particles on the typical characteristics of fluidized beds containing conventional inert materials, like sand. In addition to the insight gained about the characteristics, such as velocities, bubbling features and the segregation affinity of biomass-sand mixtures, it is now clearer which hydrodynamic aspects call for a more in-depth study as discussed below.

#### **Driving correlations predicting bubble size and velocity in the presence of biomass**

The correlations used in this study for describing the bubble behavior were those developed for pure Geldart B particles, like sand. It was realized that the main cause of the deviation between the results of the predictive model developed in this study and the experimental work stemmed from the incapability of these correlations to capture the real size and velocity profile of bubbles in the bed. Hence, new correlations should be developed that take into consideration the effect of large irregular particles on the bubbling behavior of the bed material.

#### **Determining the hydrodynamics of the biomass containing beds under real (hot) conditions**

It is well known that at high temperature endogenous bubbles of volatile matter form around devolatilizing fuel particles (Bruni et al., 2002). Under this condition, solid circulation is established around the gas-emitting fuel particle resulting in an upflow of solids around the gas source. It has been shown that non-buoyant particles can turn their behavior into a buoyant one under the effect of gas emission. Inherently buoyant particles can display augmented buoyancy

under the action of the lift force. Overall, segregation turns out to be enhanced by gas emission according to mechanisms different from those that apply to classical flotsam/jetsam segregation (Solimene et al., 2003). This evidence illustrates that some experimental measures should be considered to determine the gas and solid holdup, bubble properties and particle trajectory at elevated temperatures. This is a matter of significance to evaluate the distribution of reactants and products in the bed and understand the segregation phenomena under real operating conditions.

### **Exploring the effect of biomass size and shape on the bubbling and mixing features**

Investigating the effect of biomass particle properties was initially considered in the proposal of this work; however, due to several experimental hurdles it was not finally achieved. It is believed that size and shape play a key role in determining the upward and downward motion of biomass particles, especially when the drag force and the relevant coefficient matter. The impact of these parameters is lacking mainly because of the incapability of the usual experimental techniques. RPT is a powerful method to discover valuable facts with respect to these parameters, particularly when the more advanced approaches, like multiple particle tracking, are adopted.

### **Finding the critical load of biomass in terms of the impact on the fluidization properties of the mixture**

The highest weight percentage of biomass investigated in this study was 16%. Increasing the biomass load up to this amount could in general improve the fluidization quality and the mixing state. Nonetheless, since by further increasing the ratio of biomass to sand in the mixture, the hydrodynamic aspects of pure biomass fluidization prevail over those of sand. It is believed that there is a critical load of biomass beyond which the fluidization properties deteriorate. This load, however, depends on the operating conditions, i.e., superficial gas velocity and the properties of biomass and inert material particles. Conducting research on this topic provides a more comprehensive picture of the effect of the bed inventory composition on the function of the biomass combustors/gasifiers.

### **Studying the multiphase flow aspects of the turbulent fluidization of biomass-inert materials**

It is worth pointing out that the majority of the high capacity thermal biomass units (over 100 MW<sub>th</sub>) are based on circulating fluidization. Circulating fluidized bed (CFB) combustors and gasifiers have a high market attractiveness and are technically well proven (Bridgwater, 2003). In view of the predominance of the turbulent fluidization regime in CFBs, the multiphase flow aspects of biomass fluidization should also be explored in this regime. It is expected that the critical parameters, such as the gas and solid distribution pattern, the extent of mixing/segregation and the flow structure of biomass particles in this regime, differ markedly from the corresponding features of the bubbling regime.

### **Assessing a scaled-up continuous waste separation process**

The next step to industrialize the step-wise process proposed in this work for waste separation is evaluating the feasibility of performing each step in a continuous mode. In addition, the scale up issues should also be addressed. The optimal residence time of the waste components in the elutriation columns, the continuous procedure of removing segregated materials at the top and bottom of the bed, purification of the bed media and replacing them with less expensive materials as well as the economic assessment of the entire process, are the typical subjects that need to be examined in detail.

## BIBLIOGRAPHY

- Abbasi, A., Ege, P. E., & De Lasa, H. I. (2011). CFB simulation of a fast fluidized bed steam coal gasifier feeding section. *Chemical Engineering Journal*, 174(1), 341-350.
- Abbasi, A., Islam, M. A., Ege, P. E., & de Lasa, H. I. (2012). Downer reactor flow measurements using CREC-GS-Optiprobes. *Powder Technology*, 224, 1-11.
- Abbasi, A., Islam, M. A., Ege, P. E., & de Lasa, H. I. (2013). CFB flow pattern simulation in downer reactors. *Aiche Journal*, 59(5), 1635-1647.
- Abdullah, M. Z., Husain, Z., & Pong, S. L. Y. (2003). Analysis of cold flow fluidization test results for various biomass fuels. *Biomass & Bioenergy*, 24(6), 487-494.
- Agarwal, G., Lattimer, B., Ekkad, S., & Vandsburger, U. (2011). Influence of multiple gas inlet jets on fluidized bed hydrodynamics using Particle Image Velocimetry and Digital Image Analysis. *Powder Technology*, 214(1), 122-134.
- Agency, U. S. E. P. (2013, May 2013). Municipal solid waste generation, recycling, and disposal in the United States: facts and figures for 2011, from [http://www.epa.gov/osw/nonhaz/municipal/pubs/MSWcharacterization\\_508\\_053113\\_fs.pdf](http://www.epa.gov/osw/nonhaz/municipal/pubs/MSWcharacterization_508_053113_fs.pdf)
- Alvarez-Ayuso, E., Querol, X., & Tomás, A. (2006). Environmental impact of a coal combustion-desulphurisation plant: Abatement capacity of desulphurisation process and environmental characterisation of combustion by-products. *Chemosphere*, 65(11), 2009-2017.
- Amsden, A. A., Orourke, P., & Butler, T. (1989). KIVA-2: A computer program for chemically reactive flows with sprays. *NASA STI/recon technical report N*, 89, 27975.
- Arena, U. (2012). Process and technological aspects of municipal solid waste gasification. A review. *Waste Management*, 32(4), 625-639.
- Aznar, M. P., Gracia-Gorria, F., & Corella, J. (1992). Minimum and maximum velocities for fluidization for mixtures of agricultural and forest residues with a second fluidized solid. I. Preliminary data and results with sand-sawdust mixtures. *Int. Chem. Eng*, 32(1), 95-102.
- Bai, B., Gheorghiu, S., van Ommen, J. R., Nijenhuis, J., & Coppens, M. O. (2005). Characterization of the void size distribution in fluidized beds using statistics of pressure fluctuations. *Powder Technology*, 160(2), 81-92.
- Bai, D., Issangya, A. S., & Grace, J. R. (1999). Characteristics of Gas-Fluidized Beds in Different Flow Regimes. *Industrial & Engineering Chemistry Research*, 38(3), 803-811.
- Bai, W., Keller, N. K., Heindel, T. J., & Fox, R. O. (2012). Numerical study of mixing and segregation in a biomass fluidized bed. *Powder Technology*.
- Beeckmans, J. M., & Yu, Z. (1992). Continuous separation of mixed solids using a rotating-screen fluidized-bed. *Canadian Journal of Chemical Engineering*, 70(6).

- Berndes, G., Hoogwijk, M., & van den Broek, R. (2003). The contribution of biomass in the future global energy supply: a review of 17 studies. *Biomass and Bioenergy*, 25(1), 1-28.
- Berruti, F., Liden, A. G., & Scott, D. S. (1988). Measuring and modelling residence time distribution of low density solids in a fluidized bed reactor of sand particles. *Chemical Engineering Science*, 43(4), 739-748.
- Bilbao, R., Lezaun, J., & Abanades, J. (1987). Fluidization velocities of sand/straw binary mixtures. *Powder Technology*, 52(1), 1-6.
- Bilbao, R., Lezaun, J., Menendez, M., & Abanades, J. C. (1988). Model of mixing segregation for straw/sand mixtures in fluidized beds. *Powder Technology*, 56(3), 149-155.
- Bokkers, G., van Sint Annaland, M., & Kuipers, J. (2004). Mixing and segregation in a bidisperse gas–solid fluidised bed: a numerical and experimental study. *Powder Technology*, 140(3), 176-186.
- Bridgwater, A. (2003). Renewable fuels and chemicals by thermal processing of biomass. *Chemical Engineering Journal*, 91(2), 87-102.
- Bruni, G., Solimene, R., Marzocchella, A., Salatino, P., Yates, J., Lettieri, P., & Fiorentino, M. (2002). Self-segregation of high-volatile fuel particles during devolatilization in a fluidized bed reactor. *Powder Technology*, 128(1), 11-21.
- Buyevich, Y. A., & Kapbasov, S. K. (1994). Random fluctuations in a fluidized bed. *Chemical Engineering Science*, 49(8), 1229-1243.
- Cai, P., Schiavetti, M., Demichele, G., Grazzini, G. C., & Miccio, M. (1994). Quantitative estimation of bubble-size in PFBC. *Powder Technology*, 80(2), 99-109.
- Calabrese, P. A., & Bai, D. (2010). USA Patent No. US 20100031560 A1.
- Cassanello, M., Larachi, F., Guy, C., & Chaouki, J. (1996). Solids mixing in gas-liquid-solid fluidized beds: Experiments and modelling. *Chemical Engineering Science*, 51(10), 2011-2020.
- Chehbouni, A., Chaouki, J., Guy, C., & Klvana, D. (1994). Characterization of the flow transition between bubbling and turbulent fluidization. *Industrial & Engineering Chemistry Research*, 33(8), 1889-1896.
- Chen, C., Werther, J., Heinrich, S., Qi, H.-Y., & Hartge, E.-U. (2012). CPFD simulation of circulating fluidized bed risers. *Powder Technology*.
- Chiba, S., Nienow, A., Chiba, T., & Kobayashi, H. (1980). Fluidised binary mixtures in which the denser component may be flotsam. *Powder Technology*, 26(1), 1-10.
- Chiba, T., Chiba, S., & Nienow, A. (1986). *Prediction of the steady-state segregation pattern in gas fluidised beds with particles in throughflow*. Paper presented at the Proc. Eng. Found. Conf. Fluidisation.
- Chiesa, M., Mathiesen, V., Melheim, J. A., & Halvorsen, B. (2005). Numerical simulation of particulate flow by the Eulerian–Lagrangian and the Eulerian–Eulerian approach with application to a fluidized bed. *Computers & chemical engineering*, 29(2), 291-304.
- Choi, J. H., Jae E, S., & Sang Done, K. (1988). Bubble size and frequency in gas fluidized beds. *Journal of Chemical Engineering of Japan*, 21, 171-178.

- Clarke, K., Pugsley, T., & Hill, G. (2005). Fluidization of moist sawdust in binary particle systems in a gas–solid fluidized bed. *Chemical Engineering Science*, 60(24), 6909-6918.
- Cooper, S., & Coronella, C. J. (2005). CFD simulations of particle mixing in a binary fluidized bed. *Powder Technology*, 151(1), 27-36.
- Cranfield, R. R., & Geldart, D. (1974). Large particle fluidisation. *Chemical Engineering Science*, 29(4), 935-947.
- Crowe, C. T. (2010). *Multiphase Flow Handbook* (pp. 5-1:5-93). Florida, USA: Taylor & Francis.
- Cui, H., & Grace, J. R. (2007). Fluidization of biomass particles: A review of experimental multiphase flow aspects. *Chemical Engineering Science*, 62(Compendex), 45-55.
- Cui, H., Li, J., Kwauk, M., An, H., Chen, M., Ma, Z., & Wu, G. (2000). Dynamic behaviors of heterogeneous flow structure in gas–solid fluidization. *Powder Technology*, 112(1), 7-23.
- Cui, H., Mostoufi, N., & Chaouki, J. (2000). Characterization of dynamic gas-solid distribution in fluidized beds. *Chemical Engineering Journal*, 79(2), 133-143.
- Cui, H., Mostoufi, N., & Chaouki, J. (2001a). *Comparison of measurement techniques of local particle concentration for gas-solid fluidization*. Paper presented at the The 10th International Conference on Fluidization, Beijing.
- Cui, H., Mostoufi, N., & Chaouki, J. (2001b). Gas and solids between dynamic bubble and emulsion in gas-fluidized beds. *Powder Technology*, 120(1-2), 12-20.
- Cundall, P. A., & Strack, O. D. (1979). A discrete numerical model for granular assemblies. *Geotechnique*, 29(1), 47-65.
- Dahl, S., & Hrenya, C. (2005). Size segregation in gas–solid fluidized beds with continuous size distributions. *Chemical engineering science*, 60(23), 6658-6673.
- Darton, R. C., LaNauze, R. D., Davidson, J. F., & Harrison, D. (1977). BUBBLE GROWTH DUE TO COALESCENCE IN FLUIDISED BEDS. *Trans Inst Chem Eng*, 55(4), 274-280.
- Davidson, J. F., & Harrison, D. (1963). *Fluidised Particles*. Cambridge: Cambridge University Press.
- Deen, N. G., Van Sint Annaland, M., Van der Hoef, M. A., & Kuipers, J. A. M. (2007). Review of discrete particle modeling of fluidized beds. *Chemical Engineering Science*, 62(1–2), 28-44.
- Demirbas, A. (2000). Biomass resources for energy and chemical industry. *Energy Edu. Sci. Technol*, 5(1), 21-45.
- Demirbas, A. (2005). Potential applications of renewable energy sources, biomass combustion problems in boiler power systems and combustion related environmental issues. *Progress in energy and combustion science*, 31(2), 171-192.
- Detournay, M. (2011). *Vapogazéification de la biomasse en Lit Fluidisé Circulant : Élaboration des outils théoriques et expérimentaux*. Doctorat, Université de Toulouse, Université de Toulouse.

- Deza, M., Franka, N. P., Heindel, T. J., & Battaglia, F. (2009). CFD modeling and X-ray imaging of biomass in a fluidized bed. *Journal of fluids engineering*, 131(11).
- Di Renzo, A., Di Maio, F. P., Girimonte, R., & Formisani, B. (2008). DEM simulation of the mixing equilibrium in fluidized beds of two solids differing in density. *Powder Technology*, 184(2).
- Dos Santos, F. J., & Goldstein, L., Jr. (2008). Experimental aspects of biomass fuels in a bubbling fluidized bed combustor. *Chemical Engineering and Processing*, 47(9-10), 1541-1549.
- Douglas, E., Walsh, T., & Whitehead, A. (1968). *The Development of Equipment for the Dry Concentration of Minerals*: Warren Spring Laboratory.
- Drake, J. B., & Heindel, T. J. (2012). Local time-average gas holdup comparisons in cold flow fluidized beds with side-air injection. *Chemical Engineering Science*, 68(1), 157-165.
- Dunnu, G., Maier, J., & Gerhardt, A. (2009). Thermal Utilization of Solid Recovered Fuels in Pulverized Coal Power Plants and Industrial Furnaces as Part of an Integrated Waste Management Concept *Appropriate Technologies for Environmental Protection in the Developing World* (pp. 83-91): Springer.
- Enwald, H., Peirano, E., & Almstedt, A.-E. (1996). Eulerian two-phase flow theory applied to fluidization. *International Journal of Multiphase Flow*, 22, 21-66.
- Escudero, D., & Heindel, T. J. (2011). Bed height and material density effects on fluidized bed hydrodynamics. *Chemical Engineering Science*, 66(16), 3648-3655.
- Fan, R., & Fox, R. O. (2008). Segregation in polydisperse fluidized beds: Validation of a multi-fluid model. *Chemical Engineering Science*, 63(1), 272-285.
- Fan, R., Marchisio, D. L., & Fox, R. O. (2004). Application of the direct quadrature method of moments to polydisperse gas–solid fluidized beds. *Powder Technology*, 139(1), 7-20.
- Feng, Y., Xu, B., Zhang, S., Yu, A., & Zulli, P. (2004). Discrete particle simulation of gas fluidization of particle mixtures. *Aiche Journal*, 50(8), 1713-1728.
- Feng, Y., & Yu, A. (2007). Microdynamic modelling and analysis of the mixing and segregation of binary mixtures of particles in gas fluidization. *Chemical engineering science*, 62(1), 256-268.
- Feng, Y., & Yu, A. (2008). An analysis of the chaotic motion of particles of different sizes in a gas fluidized bed. *Particuology*, 6(6), 549-556.
- Formisani, B., Cristofaro, G. D., & Girimonte, R. (2001). A fundamental approach to the phenomenology of fluidization of size segregating binary mixtures of solids. *Chemical Engineering Science*, 56(1), 109-119.
- Formisani, B., Girimonte, R., & Longo, T. (2008a). The fluidization pattern of density-segregating binary mixtures. *Chemical Engineering Research & Design*, 86(4A), 344-348.
- Formisani, B., Girimonte, R., & Longo, T. (2008b). The fluidization process of binary mixtures of solids: Development of the approach based on the fluidization velocity interval. *Powder Technology*, 185(2), 97-108.

- Formisani, B., Girimonte, R., & Vivacqua, V. (2011). Fluidization of mixtures of two solids differing in density or size. *Aiche Journal*, 57(9), 2325-2333.
- Fotovat, F., Chaouki, J., & Bergthorson, J. (2013a). Distribution of large biomass particles in a sand-biomass fluidized bed: experiments and modeling. *Accepted for publication in the AICHE Journal*.
- Fotovat, F., Chaouki, J., & Bergthorson, J. (2013b). The effect of biomass particles on the gas distribution and dilute phase characteristics of sand–biomass mixtures fluidized in the bubbling regime. *Chemical Engineering Science*, 102(0), 129-138.
- Fotovat, F., Shabaniyan, J., Chaouki, J., & Bergthorson, J. (2011). *Characterization of the fluidization and mixing of binary mixtures containing biomass at low gas velocities*. Paper presented at the Circulating fluidized bed 10, Oregon, USA.
- Franka, N. R., & Heindel, T. J. (2009). Local time-averaged gas holdup in a fluidized bed with side air injection using X-ray computed tomography. *Powder Technology*, 193(1), 69-78.
- Fraser, T., & Yancey, H. F. (1926). Artificial storm of air-sand floats coal on its upper surface, leaving refuse to sink. *Coal Age*, 29, 325-327.
- Gallucci, K. (2012). Biomass and Waste Gasification *Fuel Cells in the Waste-to-Energy Chain* (pp. 65-79): Springer.
- Ganser, G. H. (1993). A rational approach to drag prediction of spherical and nonspherical particles. *Powder Technology*, 77(2), 143-152.
- Gao, J., Chang, J., Lu, C., & Xu, C. (2008). Experimental and computational studies on flow behavior of gas–solid fluidized bed with disparately sized binary particles. *Particuology*, 6(2), 59-71.
- Geldart, D. (1973). Types of gas fluidization. *Powder Technology*, 7(5), 285-292.
- Geldart, D., Baeyens, J., Pope, D., & Van De Wijer, P. (1981). Segregation in beds of large particles at high velocities. *Powder Technology*, 30(2), 195-205.
- Gera, D., Syamlal, M., & O'Brien, T. J. (2004). Hydrodynamics of particle segregation in fluidized beds. *International Journal of Multiphase Flow*, 30(4), 419-428.
- Gibilaro, L. G., & Rowe, P. N. (1974). A model for a segregating gas fluidized bed. *Chemical Engineering Science*, 29(6), 1403-1412.
- Gidaspow, D. (1986). Hydrodynamics of Fluidization and Heat Transfer: Supercomputer Modeling. *Applied Mechanics Reviews*, 39(1), 1-23.
- Gidaspow, D. (1994). *Multiphase Flow and Fluidization: Continuum and Kinetic Theory Descriptions*: Academic Press.
- Goldschmidt, M., Kuipers, J., & Swaaij, v. W. (2001). *Segregation in dense gas-fluidised beds: validation of a multi-fluid continuum model with non-intrusive digital image analysis measurements*. Paper presented at the 10th Engineering Foundation Conference on Fluidization, Fluidization X Beijing, China.
- Goldschmidt, M. J. V., Link, J. M., Mellema, S., & Kuipers, J. A. M. (2003). Digital image analysis measurements of bed expansion and segregation dynamics in dense gas-fluidised beds. *Powder Technology*, 138(2-3), 135-159.

- Hemati, M., Spieker, K., Laguérie, C., Alvarez, R., & Riera, F. A. (1990). Experimental study of sawdust and coal particle mixing in sand or catalyst fluidized beds. *The Canadian Journal of Chemical Engineering*, 68(5), 768-772.
- Hernandez-Atonal, F. D., Ryu, C., Sharifi, V. N., & Swithenbank, J. (2007). Combustion of refuse-derived fuel in a fluidised bed. *Chemical Engineering Science*, 62(1), 627-635.
- Hilal, N., & Gunn, D. J. (2002). Solid hold up in gas fluidised beds. *Chemical Engineering and Processing*, 41(4), 373-379.
- Hoffert, M. I., Caldeira, K., Jain, A. K., Haites, E. F., Harvey, L. D., Potter, S. D., . . . Wigley, T. M. (1998). Energy implications of future stabilization of atmospheric CO<sub>2</sub> content. *Nature*, 395(6705), 881-884.
- Hoffmann, A. C., Janssen, L., & Prins, J. (1993). Particle segregation in fluidized binary-mixtures. *Chemical Engineering Science*, 48(9), 1583-1592.
- Hoomans, B. P. B., Kuipers, J. A. M., Briels, W. J., & van Swaaij, W. P. M. (1996). Discrete particle simulation of bubble and slug formation in a two-dimensional gas-fluidised bed: A hard-sphere approach. *Chemical Engineering Science*, 51(1), 99-118.
- Horio, M., Kiyota, H., & Muchi, I. (1980). Particle movement on a perforated plate distributor of fluidized bed. *Journal of Chemical Engineering of Japan*, 13(2), 137-142.
- Horio, M., & Nonaka, A. (1987). A generalized bubble diameter correlation for gas-solid fluidized beds. *Aiche Journal*, 33(11), 137-142.
- Huilin, L., Yurong, H., & Gidaspow, D. (2003). Hydrodynamic modelling of binary mixture in a gas bubbling fluidized bed using the kinetic theory of granular flow. *Chemical Engineering Science*, 58(7), 1197-1205.
- Huilin, L., Yurong, H., Gidaspow, D., Lidan, Y., & Yukun, Q. (2003). Size segregation of binary mixture of solids in bubbling fluidized beds. *Powder Technology*, 134(1-2), 86-97.
- Jenkins, J., & Savage, S. (1983). A theory for the rapid flow of identical, smooth, nearly elastic, spherical particles. *Journal of Fluid Mechanics*, 130(1), 187-202.
- Jenkins, J. T., & Mancini, F. (1987). Balance Laws and Constitutive Relations for Plane Flows of a Dense, Binary Mixture of Smooth, Nearly Elastic, Circular Disks. *Journal of Applied Mechanics*, 54(1), 27-34.
- Johansson, T. B., Kelly, H., Reddy, A. K., & Williams, R. H. (1993). Renewable fuels and electricity for a growing world economy: defining and achieving the potential. *Energy Studies Review*, 4(3), 6.
- Joseph, G. G., Leboireiro, J., Hrenya, C. M., & Stevens, A. R. (2007). Experimental segregation profiles in bubbling gas-fluidized beds. *AIChE Journal*, 53(11), 2804-2813.
- Kalogirou, S. A. (2004). Solar thermal collectors and applications. *Progress in energy and combustion science*, 30(3), 231-295.
- Kaneko, Y., Shiojima, T., & Horio, M. (1999). DEM simulation of fluidized beds for gas-phase olefin polymerization. *Chemical Engineering Science*, 54(24), 5809-5821.

- Karimipour, S., & Pugsley, T. (2012). Application of the particle in cell approach for the simulation of bubbling fluidized beds of Geldart A particles. *Powder Technology*, 220, 63-69.
- Keller, N. K. G., Bai, W., Fox, R. O., & Heindel, T. J. (2013). Quantifying mixing in 3D binary particulate systems. *Chemical Engineering Science*, 93(0), 412-422.
- Kiared, K., Larachi, F., Cassanello, M., & Chaouki, J. (1997). Flow structure of the solids in a three-dimensional liquid fluidized bed. *Industrial & Engineering Chemistry Research*, 36(11).
- Kuipers, J., Van Duin, K., Van Beckum, F., & Van Swaaij, W. (1992). A numerical model of gas-fluidized beds. *Chemical Engineering Science*, 47(8), 1913-1924.
- Kuipers, J. A. M., Prins, W., & Van Swaaij, W. P. M. (1992). Numerical calculation of wall-to-bed heat-transfer coefficients in gas-fluidized beds. *Aiche Journal*, 38(7), 1079-1091.
- Larachi, F., Cassanello, M., Marie, M., Chaouki, J., & Guy, C. (1995). Solids circulation pattern in 3-phase fluidized-beds containing binary-mixtures of particles as inferred from RPT *Chemical Engineering Research & Design*, 73(A3), 263-268.
- Larachi, F., Chaouki, J., & Kennedy, G. (1995). 3-D Mapping of solids flow-fields in multiphase reactors with RPT *Aiche Journal*, 41(2), 439-443.
- Larachi, F., Kennedy, G., & Chaouki, J. (1994). A gamma-ray detection system for 3-D particle tracking in multiphase reactors. *Nuclear Instruments & Methods in Physics Research Section a-Accelerators Spectrometers Detectors and Associated Equipment*, 338(2-3), 568-576.
- Leaper, M. C., King, A. C., & Burbidge, A. S. (2007). Total solution of the Gibilaro and Rowe model for a segregating fluidized bed. *Chemical Engineering & Technology*, 30(2).
- Leaper, M. C., Seville, J. P. K., Hilal, N., Kingman, S. W., & Burbidge, A. S. (2004). Investigating the dynamics of segregation of high jetsam binary batch fluidised bed systems. *Chemical Engineering and Processing*, 43(2), 187-192.
- Leboreiro, J., Joseph, G. G., Hrenya, C. M., Snider, D. M., Banerjee, S. S., & Galvin, J. E. (2008). The influence of binary drag laws on simulations of species segregation in gas-fluidized beds. *Powder Technology*, 184(3), 275-290.
- Li, J., Wen, L., Ge, W., Cui, H., & Ren, J. (1998). Dissipative structure in concurrent-up gas-solid flow. *Chemical Engineering Science*, 53(19), 3367-3379.
- Lim, K., Zhu, J., & Grace, J. (1995). Hydrodynamics of gas-solid fluidization. *International Journal of Multiphase Flow*, 21, 141-193.
- Lim, K. S., & Agarwal, P. K. (1994). Circulatory motion of a large and lighter sphere in a bubbling fluidized bed of smaller and heavier particles. *Chemical Engineering Science*, 49(3), 421-424.
- Lim, K. S., Gururajan, V. S., & Agarwal, P. K. (1993). Mixing of homogeneous solids in bubbling fluidized beds: theoretical modelling and experimental investigation using digital image analysis. *Chemical Engineering Science*, 48(12), 2251-2265.

- Lior, N. (2010). Sustainable energy development: The present (2009) situation and possible paths to the future. *Energy*, 35(10), 3976-3994.
- Liu, M., Zhang, Y., Bi, H., Grace, J. R., & Zhu, Y. (2010). Non-intrusive determination of bubble size in a gas–solid fluidized bed: An evaluation. *Chemical Engineering Science*, 65(11), 3485-3493.
- Lun, C. (1991). Kinetic theory for granular flow of dense, slightly inelastic, slightly rough spheres. *J. Fluid Mech*, 233, 539-559.
- Mabrouk, R., Radmanesh, R., Chaouki, J., & Guy, C. (2005). Scale Effects on Fluidized Bed Hydrodynamics. *International Journal of Chemical Reactor Engineering*, 3(1), 1-11.
- Marzocchella, A., Salatino, P., Di Pastena, V., & Lirer, L. (2000). Transient fluidization and segregation of binary mixtures of particles. *Aiche Journal*, 46(11), 2175-2182.
- Marzocchella, A., Zijerveld, R. C., Schouten, J. C., & van den Bleek, C. M. (1997). Chaotic behavior of gas-solids flow in the riser of a laboratory-scale circulating fluidized bed. *Aiche Journal*, 43(6), 1458-1468.
- Mathiesen, V., Solberg, T., & Hjertager, B. H. (2000). An experimental and computational study of multiphase flow behavior in a circulating fluidized bed. *International Journal of Multiphase Flow*, 26(3), 387-419.
- Mathiesen, V., Solberg, T., & Hjertager, B. H. (2000). Predictions of gas/particle flow with an Eulerian model including a realistic particle size distribution. *Powder Technology*, 112(1), 34-45.
- Mazzei, L. (2011). Limitations of quadrature-based moment methods for modeling inhomogeneous polydisperse fluidized powders. *Chemical Engineering Science*, 66(16), 3628-3640.
- Mazzei, L., Marchisio, D. L., & Lettieri, P. (2009). Direct Quadrature Method of Moments for the Mixing of Inert Polydisperse Fluidized Powders and the Role of Numerical Diffusion. *Industrial & Engineering Chemistry Research*, 49(11), 5141-5152.
- Miccio, F., Russo, S., & Silvestri, N. (2013). Assessment of the devolatilization behavior of fuel pellets in fluidized bed. *Fuel Processing Technology*, 115, 122-129.
- Min, J., Drake, J. B., Heindel, T. J., & Fox, R. O. (2010). Experimental validation of CFD simulations of a lab-scale fluidized-bed reactor with and without side-gas injection. *Aiche Journal*, 56(6), 1434-1446.
- Mourad, M., Hemati, M., & Laguerie, C. (1994). Hydrodynamique d'un séchoir à lit fluidisé a flottation: Détermination des vitesses caractéristiques de fluidisation de mélanges de maïs et de sable. *Powder Technology*, 80(1), 45-54.
- Musmarra, D., Poletto, M., Vaccaro, S., & Clift, R. (1995). Dynamic waves in fluidized beds. *Powder Technology*, 82(3), 255-268.
- Naimer, N. S., Chiba, T., & Nienow, A. W. (1982). Parameter-estimation for a solids mixing segregation model for gas-fluidized beds. *Chemical Engineering Science*, 37(7).
- Nienow, A., & Naimer, N. (2011). Continuous mixing of two particulate species of different density in a gas fluidised bed. *Transactions of the Institute of Chemical Engineers*, 58.

- Nienow, A., Naimer, N., & Chiba, T. (1987). Studies of segregation/mixing in fluidised beds of different size particles. *Chemical Engineering Communications*, 62(1-6), 53-66.
- Nienow, A., Rowe, P., & Cheung, L.-L. (1978). A quantitative analysis of the mixing of two segregating powders of different density in a gas-fluidised bed. *Powder Technology*, 20(1), 89-97.
- Nienow, A. W. (1985). Fluidization of dissimilar materials. *Fluidization*, 357-382.
- Noda, K., Uchida, S., Makino, T., & Kamo, H. (1986). Minimum fluidization velocity of binary mixture of particles with large size ratio. *Powder Technology*, 46(2), 149-154.
- Norouzi, H. R., Mostoufi, N., & Sotuddeh-Gharebagh, R. (2012). Effect of fines on segregation of binary mixtures in gas–solid fluidized beds. *Powder Technology*, 225(0), 7-20.
- Nova, S., Krol, S., & de Lasa, H. (2004). Particle velocity and particle clustering in down-flow reactors. *Powder Technology*, 148(2), 172-185.
- Nova, S. R., Krol, S., & de Lasa, H. I. (2007). *Radial distribution of particle clusters in down flow reactors*. Paper presented at the The 12th International Conference on Fluidization-New Horizons in Fluidization Engineering.
- Oka, S. (2010). *Fluidized Bed Combustion*: Taylor & Francis.
- Olivieri, G., Marzocchella, A., & Salatino, P. (2004). Segregation of fluidized binary mixtures of granular solids. *Aiche Journal*, 50(12), 3095-3106.
- Oshitani, J., Kiyoshima, K., & Tanaka, Z. (2003). Continuous dry material separation from automobile shredder residue. *Kagaku Kogaku Ronbunshu*, 29(1).
- Pain, C., Mansoorzadeh, S., & De Oliveira, C. (2001). A study of bubbling and slugging fluidised beds using the two-fluid granular temperature model. *International Journal of Multiphase Flow*, 27(3), 527-551.
- Pallares, D., & Johnsson, H. (2006). A novel technique for particle tracking in cold 2-dimensional fluidized beds - simulating fuel dispersion. *Chemical Engineering Science*, 61(8), 2710-2720.
- Paudel, B., & Feng, Z.-G. (2013). Prediction of Minimum Fluidization Velocity for Binary Mixtures of Biomass and Inert Particles. *Powder Technology*, 134-140.
- Psomopoulos, C., Bourka, A., & Themelis, N. J. (2009). Waste-to-energy: A review of the status and benefits in USA. *Waste Management*, 29(5), 1718-1724.
- Qiaoqun, S., Huilin, L., Wentie, L., Yurong, H., Lidan, Y., & Gidaspow, D. (2005). Simulation and experiment of segregating/mixing of rice husk–sand mixture in a bubbling fluidized bed. *Fuel*, 84(14–15), 1739-1748.
- Radmanesh, R. (2006). *Fluidized bed biomass gasification*. Ph.D., Ecole Polytechnique, Montreal (Canada), Ann Arbor. ProQuest Dissertations & Theses Full Text database.
- Radmanesh, R., Chaouki, J., & Guy, C. (2006). Biomass gasification in a bubbling fluidized bed reactor: Experiments and modeling. *Aiche Journal*, 52(12), 4258-4272.
- Ramakers, B. J., de Ridder, R., & Kerkhof, P. J. (2004). Fluidization behavior of wood/sand mixtures. *Maderas. Ciencia y tecnología*, 6(2), 145-153.

- Rao, K. V. N. S., & Reddy, G. V. (2010). Cold Flow Studies of Rice Husk, Saw Dust, and Groundnut Shell Fuels in a Fluidized Bed. *Energy Sources, Part A: Recovery, Utilization, and Environmental Effects*, 32(18), 1701-1711.
- Rao, T., & Ram Bheemarasetti, J. (2001). Minimum fluidization velocities of mixtures of biomass and sands. *Energy*, 26(6), 633-644.
- Rasul, M., & Rudolph, V. (2000). Fluidized bed combustion of Australian bagasse. *Fuel*, 79(2), 123-130.
- Rasul, M. G., Rudolph, V., & Carsky, M. (1999). Segregation potential in binary gas fluidized beds. *Powder Technology*, 103(2), 175-181.
- Rees, A. C., Davidson, J. F., Dennis, J. S., & Hayhurst, A. N. (2005). The rise of a buoyant sphere in a gas-fluidized bed. [Article]. *Chemical Engineering Science*, 60(4), 1143-1153.
- Rhodes, M., Wang, X., Nguyen, M., Stewart, P., & Liffman, K. (2001). Study of mixing in gas-fluidized beds using a DEM model. *Chemical Engineering Science*, 56(8), 2859-2866.
- Rios, G. M., Dang Tran, K., & Masson, H. (1986). Free object motion in a gas fluidized bed. *Chemical Engineering Communications*, 47(4-6), 247-272.
- Rowe, P. N., & Nienow, A. W. (1976). Particle mixing and segregation in gas fluidised beds. A review. *Powder Technology*, 15(2), 141-147.
- Rowe, P. N., Nienow, A. W., & Agbim, A. J. (1972). Preliminary quantitative study of particle segregation in gas-fluidized beds-binary systems of near-spherical particles. *Transactions of the Institution of Chemical Engineers*, 50, 324-333.
- Roy, S., Larachi, F., Al-Dahhan, M., & Duduković, M. (2002). Optimal design of radioactive particle tracking experiments for flow mapping in opaque multiphase reactors. *Applied Radiation and Isotopes*, 56(3), 485-503.
- Ruedisueli, M., Schildhauer, T. J., Biollaz, S. M. A., & van Ommen, J. R. (2012). Bubble characterization in a fluidized bed by means of optical probes. *International Journal of Multiphase Flow*, 41, 56-67.
- Sekito, T., Matsuto, T., & Tanaka, N. (2006). Application of a gas-solid fluidized bed separator for shredded municipal bulky solid waste separation. *Waste Management*, 26(12).
- Sekito, T., Tanaka, N., & Matsuto, T. (2003). Study on composition and particle characteristics of shredded municipal waste for the improvement of separation efficiency in a municipal bulky waste processing facility. *Waste Management & Research*, 21(4).
- Sekito, T., Tanaka, N., & Matsuto, T. (2006). Batch separation of shredded bulky waste by gas-solid fluidized bed at laboratory scale. *Waste Management*, 26(11), 1246-1252.
- Senior, C. L., Helble, J. J., & Sarofim, A. F. (2000). Emissions of mercury, trace elements, and fine particles from stationary combustion sources. *Fuel Processing Technology*, 65-66(0), 263-288.
- Shafiee, S., & Topal, E. (2009). When will fossil fuel reserves be diminished? *Energy Policy*, 37(1), 181-189.

- Shen, H. T., Forssberg, E., & Pugh, R. J. (2002). Selective flotation separation of plastics by chemical conditioning with methyl cellulose. *Resources Conservation and Recycling*, 35(4), 229-241.
- Shen, L., Xiao, J., Niklasson, F., & Johnsson, F. (2007). Biomass mixing in a fluidized bed biomass gasifier for hydrogen production. *Chemical Engineering Science*, 62(1-2), 636-643.
- Shoushtati, N. A., Hosseini, S. A., & Soleimani, R. (2013). Investigation of Segregation of Large Particles in a Pressurized Fluidized Bed with a High Velocity Gas: A Discrete Particle Simulation. *Powder Technology*.
- Si, C., & Guo, Q. (2008). Fluidization characteristics of binary mixtures of biomass and quartz sand in an acoustic fluidized bed. *Industrial & Engineering Chemistry Research*, 47(23), 9773-9782.
- Snider, D. (2001). An incompressible three-dimensional multiphase particle-in-cell model for dense particle flows. *Journal of Computational Physics*, 170(2), 523-549.
- Snider, D., & Banerjee, S. (2010). Heterogeneous gas chemistry in the CPFD Eulerian–Lagrangian numerical scheme (ozone decomposition). *Powder Technology*, 199(1), 100-106.
- Snider, D. M. (2007). Three fundamental granular flow experiments and CPFD predictions. *Powder Technology*, 176(1), 36-46.
- Solimene, R., Chirone, R., & Salatino, P. (2012). Characterization of the devolatilization rate of solid fuels in fluidized beds by time-resolved pressure measurements. *Aiche Journal*, 58(2), 632-645.
- Solimene, R., Marzocchella, A., & Salatino, P. (2003). Hydrodynamic interaction between a coarse gas-emitting particle and a gas fluidized bed of finer solids. *Powder Technology*, 133(1-3), 79-90.
- Soria-Verdugo, A., Garcia-Gutierrez, L. M., Garcia-Hernando, N., & Ruiz-Rivas, U. (2011). Buoyancy effects on objects moving in a bubbling fluidized bed. *Chemical Engineering Science*, 66(12), 2833-2841.
- Soria-Verdugo, A., Garcia-Gutierrez, L. M., Sanchez-Delgado, S., & Ruiz-Rivas, U. (2011). Circulation of an object immersed in a bubbling fluidized bed. *Chemical Engineering Science*, 66(1), 78-87.
- Stein, M., Martin, T. W., Seville, J. P. K., McNeil, P. A., & Parker, D. J. (1997). Chapter 10 - Positron emission particle tracking: Particle velocities in gas fluidised beds, mixers and other applications. In C. Jamal, L. Faïcal & P. D. Milorad (Eds.), *Non-Invasive Monitoring of Multiphase Flows* (pp. 309-333). Amsterdam: Elsevier Science B.V.
- Stessel, R. I., & Peirce, J. J. (1986). Comparing plusing classifiers for waste-to-energy. *Journal of Energy Engineering-Asce*, 112(1).
- Taghipour, F., Ellis, N., & Wong, C. (2005). Experimental and computational study of gas–solid fluidized bed hydrodynamics. *Chemical Engineering Science*, 60(24), 6857-6867.

- Tanfara, H., Pugsley, T., & Winters, C. (2002). Effect of particle size distribution on local voidage in a bench-scale conical fluidized bed dryer. *Drying Technology*, 20(6), 1273-1289.
- Tanimoto, H., Chiba, S., Chiba, T., & Kobayashi, H. (1980). Mechanism of solid segregation in gas fluidised beds *Fluidization* (pp. 381-388): Springer.
- Todes, O. M. (1965). Applications of fluidized beds in the chemical industry, Part II *Izd Znanie* (pp. 4-27). Leningrad.
- Tsuji, Y., Kawaguchi, T., & Tanaka, T. (1993). Discrete particle simulation of two-dimensional fluidized bed. *Powder Technology*, 77(1), 79-87.
- Upadhyay, R. K., & Roy, S. (2010). Investigatin of hydrodynamics of binary fluidized beds via radioactive particle tracking and dual-source densitometry *Canadian Journal of Chemical Engineering*, 88(4), 601-610.
- Van der Hoef, M., Ye, M., van Sint Annaland, M., Andrews, A., Sundaresan, S., & Kuipers, J. (2006). Multiscale modeling of gas-fluidized beds. *Advances in chemical engineering*, 31, 65-149.
- van Ommen, J. R., & Mudde, R. F. (2008). Measuring the Gas-Solids Distribution in Fluidized Beds--A Review. *International Journal of Chemical Reactor Engineering*, 6(1).
- Vesilind, P. A., Peirce, J. J., & McNabb, M. (1982). Predicting particle behavior in air classifiers. *Conservation & Recycling*, 5(4).
- Wirsum, M., Fett, F., Iwanowa, N., & Lukjanow, G. (2001). Particle mixing in bubbling fluidized beds of binary particle systems. *Powder Technology*, 120(1-2), 63-69.
- Wu, S., & Baeyens, J. (1998). Segregation by size difference in gas fluidized beds. *Powder Technology*, 98(2), 139-150.
- Yin, C., Rosendahl, L., K Kær, S., & J Condra, T. (2004). Use of numerical modeling in design for co-firing biomass in wall-fired burners. *Chemical Engineering Science*, 59(16), 3281-3292.
- Yoshida, K., Kameyana, H., & Shimizu, F. (1977). *Mechanism of particle mixing and segregation in gas fluidized bed*. Paper presented at the Proceedings PACHEC, Denver, Colorado.
- Yoshida, M., Nakatsukasa, S., Nanba, M., Gotoh, K., Zushi, T., Kubo, Y., & Oshitani, J. (2010). Decrease of Cl contents in waste plastics using a gas-solid fluidized bed separator. *Advanced Powder Technology*, 21(1).
- Yoshida, M., Oshitani, J., Ono, K., Ishizashi, M., & Gotoh, K. (2008). Control of Apparent Specific Gravity in Binary Particle Systems of Gas-Solid Fluidized Bed. *Kona Powder and Particle Journal*, 26.
- Yu, A., & Standish, N. (1987). Porosity calculations of multi-component mixtures of spherical particles. *Powder Technology*, 52(3), 233-241.
- Yu, A. B., & Xu, B. H. (2003). Particle-scale modelling of gas–solid flow in fluidisation. *Journal of Chemical Technology and Biotechnology*, 78(2-3), 111-121.

- Yu, Y. H., Oh, J. H., Lee, J. Y., & Choi, H. W. (2003). Mixing characteristics of large cylindrical particles (RDF) in a gas-solid fluidized bed. *Journal of Industrial and Engineering Chemistry*, 9(6), 798-803.
- Zaltzman, A., Feller, R., Mizrach, A., & Schmilovitch, Z. (1983). Separating potatoes from clods and stones in a fluidized-bed medium. *Transactions of the Asae*, 26(4).
- Zhang, D., & Rauenzahn, R. (2000). Stress relaxation in dense and slow granular flows. *Journal of Rheology*, 44, 1019.
- Zhang, Y., Jin, B., & Zhong, W. (2008). Fluidization, mixing and segregation of a biomass-sand mixture in a fluidized bed. *International Journal of Chemical Reactor Engineering*, 6, 1-29.
- Zhang, Y., Jin, B., & Zhong, W. (2009). Experimental investigation on mixing and segregation behavior of biomass particle in fluidized bed. *Chemical Engineering and Processing*, 48(3), 745-754.
- Zhang, Y., Jin, B., Zhong, W., Ren, B., & Xiao, R. (2009). Characterization of Fluidization and Segregation of Biomass Particles by Combining Image Processing and Pressure Fluctuations Analysis. *International Journal of Chemical Reactor Engineering*, 7, 1-19.
- Zhang, Y., Jin, B. S., & Zhong, W. Q. (2010). *Fluidization Characteristics of Stalk-Shaped Biomass in Binary Particle System*. Paper presented at the 20th International Conference on Fluidized Bed Combustion.
- Zhang, Y., Zhong, W., & Jin, B. (2011). Experimental and Theoretical Study on Fluidization of Stalk-Shaped Biomass Particle in a Fluidized Bed. *International Journal of Chemical Reactor Engineering*, 9, 1-23.
- Zhao, P., O'Rourke, P. J., & Snider, D. (2009). Three-dimensional simulation of liquid injection, film formation and transport, in fluidized beds. *Particuology*, 7(5), 337-346.
- Zhao, Y., Ding, Y., Wu, C., & Cheng, Y. (2010). Numerical simulation of hydrodynamics in downers using a CFD-DEM coupled approach. *Powder Technology*, 199(1), 2-12.
- Zhong, W., Jin, B., Zhang, Y., Wang, X., & Xiao, R. (2008). Fluidization of Biomass Particles in a Gas-Solid Fluidized Bed. *Energy & Fuels*, 22(6), 4170-4176.
- Zhu, H., Zhou, Z., Yang, R., & Yu, A. (2008). Discrete particle simulation of particulate systems: A review of major applications and findings. *Chemical Engineering Science*, 63(23), 5728-5770.